



Università degli Studi di Siena

Department of Biotechnology, Chemistry and Pharmacy

PhD in Chemical and Pharmaceutical Sciences

Cycle XXXIV

Coordinator: Prof. Maurizio Taddei

New bioconjugates for targeted anticancer therapy

Tutor: Prof. Maurizio Taddei

CHIM/06 – Organic Chemistry

PhD candidate: Francesca Migliorini

Academic Year 2020/2021

Abstract

The Antibody-Drug Conjugates (ADCs) is one of the novel therapeutic strategies with a great potential in many medicinal treatments.

ADCs are composed of a monoclonal antibody (mAb) connected to a drug (payload) through a properly designed linker. The mAb is responsible for the selective transport of the drug into target cells expressing the specific antigen; in this way, the off-target toxicity of the drug can be avoided. The linker plays an important role due to its dual features: stability in blood and ability to release the payload into the target cells thanks to its degradation. In this thesis, several different aspects of the ADC development are explored. Different ADCs charged with SMO inhibitors as payload are investigated for the treatment of melanoma, and novel multifunctional linkers with trigger groups are designed for the drug release in different environments in a very elegant and controlled way.

Besides the work on bioconjugates aforementioned, micellar catalysis is also investigated to perform catalytic transformations in water media avoiding the use of organic solvents. Micellar catalysis is applied in the presence of a proper rhodium salt to develop a suitable hydroformylation process with very good results.

Abstract

Gli *Antibody-Drug Conjugates* (ADCs) rappresentano una nuova terapia innovativa avendo un grande potenziale in diversi trattamenti clinici.

Gli ADCs sono composti da un anticorpo monoclonale (mAb) legato a molecole citotossiche (*payloads*) attraverso uno specifico spaziatore chimico (*linker*). L'mAb è responsabile del trasporto selettivo del farmaco all'interno delle cellule bersaglio che esprimono sulla loro superficie uno specifico antigene riconosciuto dall'anticorpo. In questo modo, gli effetti collaterali dovuti alla poca selettività degli agenti citotossici può essere elusa. Il *linker* possiede un ruolo chiave per la sua duplice funzionalità: conferisce stabilità al coniugato nel plasma e parallelamente, grazie alla sua degradazione, promuove il rilascio del farmaco all'interno delle cellule bersaglio. In questa tesi, sono stati studiati diversi aspetti riguardanti lo sviluppo di nuovi ADCs. È stata quindi investigata la possibilità di sviluppare ADCs che hanno come *payloads* inibitori del recettore SMO per il trattamento di tumori HH-dipendenti. Sono stati inoltre studiati nuovi *linkers* aventi specifici gruppi funzionali che promuovono, in determinate e specifiche condizioni, il rilascio del citotossico in modo elegante e controllato.

Oltre al lavoro riguardante lo sviluppo di bioconiugati sopracitato, è stata valutata la possibilità di poter sfruttare la catalisi micellare per rendere più sostenibile il processo di idroformilazione in presenza di uno specifico catalizzatore al rodio evitando, così, l'utilizzo di solventi organici.

Index

Index.....	I
List of abbreviations.....	VI
 SECTION A – Development of New Antibody-Drug Conjugates (ADCs).....	1
 CHAPTER 1 – INTRODUCTION.....	3
1.1 Targeted therapy.....	3
1.1.1 Kinase inhibitors.....	3
1.1.2 Monoclonal Antibody (mAb).....	4
1.1.3 Drug delivery systems.....	6
1.1.3.1 Antibody-Drug Conjugates.....	8
1.1.3.2 ADCs in the market.....	10
1.2 Evaluation of ADC components, properties and design.....	12
1.2.1 Antibody and antigen.....	12
1.2.2 Linker and self-immolative spacer.....	13
1.2.2.1 Metabolic sensitive linkers.....	13
1.2.2.2 Chemically labile linkers.....	14
1.2.2.2.1 pH sensitive linker.....	14
1.2.2.2.2 Reactive oxygen species (ROS) sensitive linkers.....	22
1.2.2.3 Enzymatic sensitive linkers.....	25
1.2.2.3.1 Protease-sensitive linkers.....	25
1.2.2.3.2 β -glucuronidase-sensitive linkers.....	27
1.2.2.4 Pre-targeting strategy-based linkers.....	28
1.2.2.5 Self-immolative spacer.....	30
1.2.2.6 Polarity.....	35
1.2.3 Payloads.....	35
1.2.3.1 Other payloads.....	41
1.2.3.1.1 Epigenetic modulators.....	41
1.2.3.1.2 Payloads for non-oncology indications.....	44
1.2.3.1.3 SMO inhibitors: unexplored payloads.....	44
1.2.4 Bystander effect.....	45
1.2.4.1 Non-internalizing ADCs.....	45

1.2.5 Bioconjugation strategies.....	46
1.2.5.1 Classical chemical conjugation.....	47
1.3 Hedgehog pathway.....	48
1.3.1 SMO receptor.....	52
1.3.2 SMO inhibitors.....	54
1.3.2.1 MRTs.....	56
1.4 Aim of this research work.....	61
1.4.1 A new pH responsive crosslinker platform for drug targeting delivery.....	61
1.4.2 A new reactive oxygen species (ROS) sensitive linker.....	61
1.4.3 ADCs armed with SMO inhibitors.....	62
 CHAPTER 2 – RESULTS AND DISCUSSION.....	 65
2.1 A new pH responsive crosslinker platform for drug targeting delivery.....	65
2.1.1 Synthesis of HMPO linker.....	66
2.1.2 Experiments to evaluate the HMPO hydrolysis profile.....	67
2.1.3 The hypothetical release mechanism of HMPO linker.....	69
2.1.4 ADCs based on HMPO linker.....	71
2.1.5 Hydrolysis profile experiments of the sequences Doxorubicin-HMPO and Combretastatin A-4-HMPO	73
2.1.6 MTT assay of Ctx-HMPO-Doxorubicin and Ctx-HMPO-Combretastatin A-4 ADCs....	75
2.2 A new reactive oxygen species (ROS) sensitive linker.....	76
2.2.1 First linker proposed.....	77
2.2.2 Second linker proposed.....	79
2.3 ADCs armed with SMO inhibitors.....	81
2.3.1 SMO inhibitors as potential payloads for the development of ADCs.....	81
2.3.2 ADCs armed with SMO inhibitors by using non-cleavable linkers.....	83
2.3.2.1 Synthesis of non-cleavable linkers.....	83
2.3.2.2 Synthesis of ADCs armed with MRT-86 through a non-cleavable linker using the guanidine as drug binding moiety.....	84
2.3.2.3 Synthesis of ADCs armed with FRM326 through a non-cleavable linker using the phenol group as drug binding moiety.....	87
2.3.2.4 Synthesis of ADCs armed with Vismodegib through a non-cleavable linker using the pyridine nitrogen as drug binding moiety.....	88

2.3.2.5 Synthesis of ADCs armed with Cyclopamine through a non-cleavable linker using the secondary amine as drug binding moiety.....	89
2.3.3 ADCs armed with SMO inhibitors using innovative cleavable linkers.....	90
2.3.3.1 Synthesis of ADCs armed with FRM326 through HMPO linker using the phenol group as drug binding moiety.....	90
2.3.3.2 Synthesis of ADCs armed with Vismodegib through HMPO linker using the pyridine nitrogen as drug binding moiety.....	91
2.3.3.3 Synthesis of ADCs armed with Cyclopamine through HMPO linker using the secondary amine as drug binding moiety.....	92
2.3.3.4 Synthesis of ADCs armed with Cyclopamine through borate cleavable linker using the secondary amine as drug binding moiety.....	93
CHAPTER 3 – CONCLUSIONS	96
CHAPTER 4 – EXPERIMENTAL PART	100
4.1 A new pH responsive crosslinker platform for drug targeting delivery.....	100
4.1.1 General experimental procedures, materials and instruments.....	100
4.1.2 Synthetic procedures	101
4.1.3 General procedure for preparation of ADCs. 53 (Ctx-NH- 50), 54 (Ctx-NH- 52).....	109
4.1.4 MALDI analysis of bioconjugates.....	109
4.1.5 HPLC method for hydrolysis.....	110
4.1.6 ¹ HNMR method to study the disassembling mechanism for HMPO conjugates.....	110
4.1.7 Stability in human plasma of HMPO derivatives.....	111
4.1.8 MTT assay of ADCs (ADC 53 and 54)	111
4.2 A new reactive oxygen species (ROS) sensitive linker.....	113
4.2.1 General experimental procedures, materials and instruments.....	113
4.2.2 Synthetic procedures	113
4.2.3 HPLC method for hydrolysis	121
4.3 ADCs armed with SMO inhibitors.....	122
4.3.1 General experimental procedures, materials and instruments.....	122
4.3.2 Synthetic procedures	123
4.3.3 General procedure for preparation of ADCs. ADCs 84 , 88 , 94 , 97 , 100 , 103 , 105	139
4.3.4 MALDI analysis of bioconjugates.....	139

SECTION B - Micellar catalysis for sustainable hydroformylation.....	142
CHAPTER 1 – INTRODUCTION.....	144
1.1 Green chemistry.....	144
1.1.1 Atom economy and E-Factor.....	144
1.1.2 Solvents.....	145
1.1.3 Catalysis.....	145
1.1.4 Use of alternative reaction medium and micellar catalysis.....	146
1.2 Hydroformylation.....	149
1.3 Microwave assisted reactions.....	154
1.4 Aim of this research work.....	157
CHAPTER 2 – RESULTS AND DISCUSSION.....	159
2.1 Optimization of reaction conditions.....	159
2.2 Evaluation of reaction conditions for a future application in industrial scale.....	162
2.3 Expedient of bisulfite adduct and catalyst and micelles recycle.....	163
2.4 TON, TOF and DLS, Z-potential and TEM analysis.....	165
2.5 Scope of reaction.....	168
2.6 Tandem reaction with intramolecular hemiacetalization.....	170
CHAPTER 3 – CONCLUSIONS.....	173
CHAPTER 4 – EXPERIMENTAL PART.....	175
4.1 General experimental procedures, materials and instruments.....	175
4.2 Synthetic procedures.....	175
4.2.1 Preparation of not commercially available starting alkenes.....	175
4.2.2 General methods for the hydroformylation reaction.....	186
4.2.3 General method for the synthesis of cyclic hemiacetals.....	195
SECTION C – Bibliography.....	203

List of abbreviations

5-FU	5-Fluorouracil
AAC	Antibody-Antibiotic Conjugate
ADC	Antibody-Drug Conjugate
ADCC	Antibody-Dependent Cell-mediated Cytotoxicity
Ala	alanine
AML	acute myeloid leukemia
API	Active Pharmaceutical Ingredient
Arg	arginine
ATP	adenosine triphosphate
BCC	basal cell carcinoma
BHQ-2	Black Hole Quencher 2
Biphephos	6,6'-[(3,3'-Di- <i>tert</i> -butyl-5,5'-dimethoxy-1,1'-biphenyl-2,2'-diyl)bis(oxy)]bis(dibenzo[<i>d,f</i>][1,3,2]dioxaphosphepin)
bs	broad singlet
CD22	cluster of differentiation 22
CDC	Complement-Dependent Cytotoxicity
CDK1	Cyclin Dependent Kinase-1
CDR	Complementarity Determining Region
CI	combination index
Cit	citrulline
CMC	Complement Mediated Cytotoxicity
CPT	Camptothecin
CRD	cysteine-rich domain
CTABr	cetyltrimethylammonium bromide
CTCL	cutaneous T-cell lymphoma
CTLA-4	cytotoxic T lymphocyte antigen 4
CCAA	Copper(I)-Catalyzed Azide-Alkyne Cycloaddition
Cys	cysteine
d	doublet
DAR	drug-to-antibody ratio
dd	doublet of doublets
ddd	doublet of doublets of doublets
dddd	doublet of doublets of doublets of doublets
DDS	Drug Delivery System
Dhh	Desert Hedgehog
DIPEA	<i>N,N</i> -diisopropylethylamine
DLS	dynamic light scattering
DM1	Mertansine or Emtansine
DM4	Ravtansine or Soravtansine
DMAC	dimethylacetamide

DMAP	4-dimethylaminopyridine
DMF	dimethylformamide
DMSO	dimethyl sulfoxide
DMSO- <i>d</i> ₆	deuterated dimethyl sulfoxide
DNA	deoxyribonucleic acid
DPEphos	oxydi-2,1-phenylene)bis(diphenylphosphine)
DPPA	diphenylphosphoryl azide
Dppf	1,1'-ferrocenediyl-bis(diphenylphosphine)
ECD	<i>N</i> -terminal extracellular domain
ECL	long extracellular loop
ECM	extracellular matrix
EDC	1-ethyl-3-(3-dimethylaminopropyl)carbodiimide
EDC	linker domain
EDS	energy-dispersive X-ray spectroscopy
EGFR	epidermal growth factor receptor
EPR	Enhanced Permeability and Retention effect
ESI	electrospray ionization
ETBE	ethyl- <i>tert</i> -butyl ether
EtOAc	ethyl acetate
Fab	fragment antigen-binding
FAP- α	fibroblast activation protein- α
Fc	fragment constant
FDA	Food and Drug Administration
GC-MS	gas chromatography-mass spectrometry
Glu	glutamic acid
Gly	glycine
GPCR	G-protein-coupled receptor
GSH	reduced glutathione
GVL	γ -valerolactone
HAT	histone acetyltransferase
HBA	hydrogen bond acceptor
HBL	hydrophilic-lipophilic balance
HDAC	histone deacetylase
HER1	human epidermal growth factor receptor 1
HER2	human epidermal growth factor receptor 2
HF	hydroformylation
HH	Hedgehog pathway
Hhip	human Hedgehog-interacting protein
HPLC	high-performance liquid chromatography
HY	hydrophobic interaction
IC ₅₀	half maximal inhibitory concentration
IFT	intraflagellar transport protein
IgG	immunoglobulin G

IGN	indolinobenzodiazepins
Ihh	Indian hedgehog
K _i	inhibitory constant
KI	kinase inhibitors
KIF	kinesin superfamily protein
Lys	lysine
m	multiplet
mAbs	monoclonal antibodies
MAC	methylene-alkoxy carbamate
MALDI	matrix-assisted laser desorption/ionization
MAOS	microwave assisted organic synthesis
MC	maleidocaproic acid
MDR1	multidrug resistance protein 1
MMAE	Monomethyl Auristatin-E
MMAF	Monomethyl Auristatin-F
MMP-2	extracellular matrix metalloproteinase-2
MPF	M-phase promoting factor
MS	mass spectroscopy
MTT	(3-[4,5-dimethylthiazol-2-yl]-2,5 diphenyl tetrazolium bromide)
MW	microwave
NBS	<i>N</i> -bromosuccinimide
NHS	<i>N</i> -hydroxysuccinimide
NMR	nuclear magnetic resonance
NPM	<i>N</i> -methyl pyrrolidone
PABA	<i>p</i> -aminobenzyl alcohol
PBS	phosphate-buffered saline
PDB	pyrrolobenzodiazepin
PE	petroleum ether
PEG	polyethylene glycol
PEG-750-M	hydrophilic poly(ethyleneglycol)methyl ether
Phe	phenylalanine
Pro	proline
PTCH	12-pass transmembrane receptor Patched
PTS	polyoxyethanyl- α -tocopherol sebacate
q	quartet
R _f	retention factor
RhCl(PPh ₃) ₃	chloridotris(triphenylphosphine)rhodium(I)
RhH(CO)(PPh ₃) ₃	tris(triphenylphosphine)rhodium(I) carbonyl hydride
ROS	reactive oxygen species
R _t	retention time
r.t.	room temperature
s	singlet

SAHA	Vorinostat, suberanilohydroxamic acid
SCLC	small cell lung cancer
SDS	sodium dodecyl sulfate
Shh	Sonic hedgehog
SMCC	succinimidyl-4-(<i>N</i> -maleimidomethyl)cyclohexane-1-carboxylate
SMDC	Small Molecule-Drug Conjugate
SMO	Smoothened receptor
S-NHS	<i>N</i> -hydroxysulfosuccinimide
SpiDO	Spiro-Di-Orthoester
STEM	scanning transmission electron microscopy
SUFU	suppressor of fused homolog
t	triplet
TAMRA	tetramethylrhodamine
TBAI	<i>N</i> -tetrabutylammonium iodide
TCO	<i>trans</i> -cyclooctene
TEA	triethylamine
TEM	transmission electron microscopy
THF	tetrahydrofuran
Thr	threonine
TLC	thin-layer chromatography
TMD	heptahelical membrane spanning domain
TOF	turnover frequency
TON	turnover number
TPGS-750-M	DL- α -tocopherol methoxypolyethylene glycol succinate
TPPTS	trisodium 3,3',3''-phosphanetriyltri(benzene-1-sulfonate)
Trp	tryptophan
Tyr	tyrosine
UV/Vis	ultraviolet-visible spectroscopy
Val	valine
VEGF	vascular endothelial growth factor
WT	wild type
Xantphos	4,5-bis(diphenylphosphino)-9,9-dimethylxanthene

SECTION A

Development of New Antibody-Drug Conjugates (ADCs)

Introduction

1.1 Targeted therapy

Classic anti-tumor therapy undergoes a lack of selectivity towards rapidly proliferating tissues (*i.e.* bone marrow, skin, gastrointestinal tract) generating in most cases drug resistance with a therapeutic ineffectiveness or a high systemic toxicity because of the need of higher therapeutic doses.

The drug's ability to reach the tumor site, especially in solid tumors characterized by irregular vasculature and high interstitial pressure, is a relevant issue due to a difficult and not optimal biodistribution. [1]

Despite the great improvement in the development of cytotoxic molecules, the interest in targeted therapy is rising day by day due to its competence in interfering only with a specific tumor pathway blocking both carcinogenesis and the tumor growth without affecting healthy cells. The outlook results very high for the resulting therapeutic efficacy and low adverse effects. [2]

The initial acclaim for targeted therapy as a “magic bullet” in oncology has weakened over time due to the slow progress in some metastatic cancer and still high off-target toxicity levels of the actually available chemotherapeutic drugs. Moreover, the development of targeted therapies selectively acting on tissues affected by tumors, still remains the main goal in cancer therapy towards personalized medicine. [4]

Knowing the cellular pathways responsible to pathological processes and tumors, few targeting strategies could be exploit. Four main types of targeted therapy are available for cancer treatment: [3]

- kinase inhibitors (both tyrosine and serine/threonine);
- monoclonal Antibody (mAbs);
- Antibody-Drug Conjugates (ADCs);
- Small Molecule-Drug Conjugates (SMDCs). [3]

1.1.1 Kinase inhibitors

The constitutive overexpression of specific kinases is responsible for the abnormal phosphorylation of serine, threonine or tyrosine residues of many powerful proteins that

activate the signaling pathways responsible for tumor cell growth, differentiation and inhibition of death regulation. Therefore, selective kinase inhibitors have been developed as anticancer agents by different pharmaceutical companies. These small molecules, able to interact with the cytoplasmic domain of transmembrane kinase receptors, block the activity of the catalytic domain by competing with ATP binding. [5] The first kinase inhibitor approved by the FDA in 2001 was Imatinib (Gleevec®) for the treatment of chronic myelogenous leukemia in patients expressing the BCR- ABL fusion protein. Nowadays, the FDA has approved more than 60 inhibitors, mainly represented by tyrosine-kinase inhibitors (*i.e.* Pemigatinib) and serine/threonine-kinase inhibitors (*i.e.* Vemurafenib) (Figure 1). [6, 7]

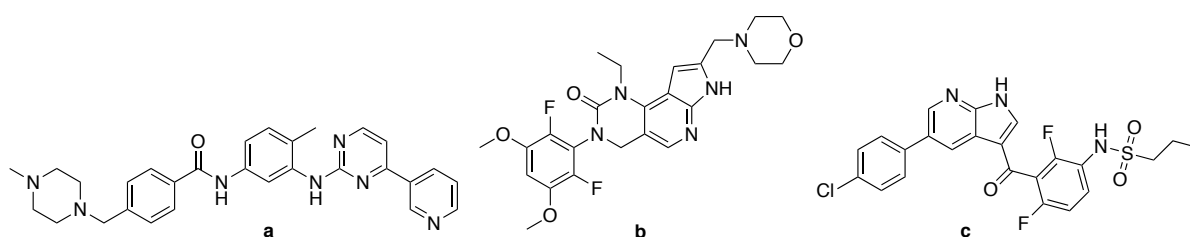


Figure 1. Structures of the kinase inhibitors: (a) Imatinib, (b) Pemigatinib, (c) Vemurafenib.

1.1.2 Monoclonal Antibody (mAb)

Most of the monoclonal antibodies (mAbs) used in medicine are immunoglobulin G (IgG), and they are one of the most successful tools to target antigens that are overexpressed or mutated in cancer cells. mAbs are most efficiently prepared by using immunizing nonhuman species (*i.e.* mice) to generate the desired specificity. On the other hands, they must not be recognized as foreign by the human immune system thanks to a process called humanization. Mice immunization with specific antigen is allowed by lymphocytes B isolation from the mice's spleen; these cells are immortalized by fusion with myeloma cells and diluted into plate-wells (one cell in each well). An *in vitro* screening of pure hybridoma cells provide mAbs, which bind single specific epitopes of the antigen of interest. [8]

mAbs can allow cancer cell death with different mechanisms: for example, through agonist effect or receptor inhibition leading to cancer cells apoptosis. Otherwise, their activity can exploit in tumor vasculature or stroma. mAbs promote also immune-mediated cell killing mechanisms as complement or antibody-dependent cytotoxicity or T cells regulation. [9]

The first generation of mAbs is the chimeric antibody where specific murine protein sequences are replaced by human sequences without modifying the affinity for its antigen. The second generation is the humanized antibody with higher human sequences, the murine part being only

limited to the essential antigen binding moiety called Complementarity Determining Region (CDR). The third generation is the human mAb in which all the sequences are human-derivatives and show a longer survival in blood than other ones: the Half-life ($T_{1/2}$) is up to three weeks instead of two/three days of murine mAb (Figure 2). [10]

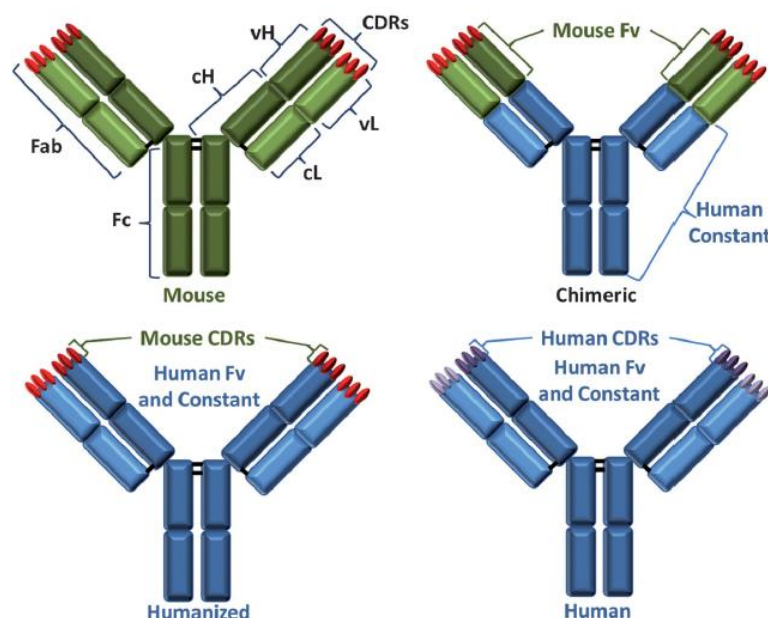


Figure 2. Representation of mouse (green), chimeric, humanized, and human (blue) antibodies. [21]

mAbs are used as single agents for different physiological targets to inhibit the development of harmful inflammations (*i.e.* psoriasis, rheumatoid arthritis, Crohn's disease) and to induce a cytotoxic response in different tumor types. For these purposes, the first best-seller mAbs were represented by Trastuzumab (Herceptin®), Rituximab (Rituxan®) and Bevacizumab (Avastin®) used in oncology since 2014. Nowadays, more than one hundred of mAbs have been approved by the FDA and many more are in clinical phases. [11]

The mechanisms of action can be indicated as independent and dependent immune effect. [12]

The first one does not directly involve immune system and just blocks a crucial activation signal for cell growth. The tumor cell death is related to:

- a direct cross-linking with a surface receptor on the target cells with an agonist activity (apoptosis);
- an interference with ligand inducing dimerization of the receptor with an antagonist activity (inhibit proliferation);
- removal of the ligand from the circulation.

An example of independent immune effector is represented by the Trastuzumab, an anti-EGFR mAb, that is able to block ErbB family of receptors (HER-1 and HER-2) as a competitive antagonist of EGF ligands by locking ligand-binding and by downregulating EGFR expression. The mechanisms that are dependent on the immune system can be divided in:

- Antibody-Dependent Cellular Cytotoxicity (ADCC). Many different effector cells of the immune system (*i.e.* NK cells, macrophages, monocytes, activated granulocytes) can be drafted by Fc γ R portion of a mAb already bound with its target antigen. The lyses of tumor cells thanks to an induction of phagocytosis and activation of T cells is the final result.
- Complement Mediated Cytotoxicity (CMC). mAbs with enhanced ability to activate complement based on improve or suppress other mechanisms of action essential for cells life. [13, 14]

In spite of the success of mAbs in targeted therapy, this approach is usually less active in solid tumor and must be associated with chemotherapy. This association has brought to the development of systems that take advantage of the mAb to deliver a classic cytotoxic molecule into tumor cells.

1.1.3 Drug delivery systems

During the years, several approaches have been explored for the selective delivery of cytotoxic agents into tumor cells avoiding their off-target toxicity. The nanoencapsulation of anticancer agents into nanoparticles (*i.e.* liposomes, polymers and micelles) is just an example of these attempts that try to take advantage of poorly differentiated vasculature in tumor. Solid tumor vasculature allows extravasation nanoparticles *phenomenum* resulting in a quantitative accumulation of the drug in the target tissues (Enhanced Permeability and Retention effect – EPR). [15] The EPR effect is one of the most used strategies to deliver a cytotoxic to the tumor and it is classified as passive drug targeting. Some examples of passively-targeted nanomedicines approved for clinical use are PEGylated (*i.e.* Caelyx® active substance: Doxorubicin) and non-PEGylated (*i.e.* Myocet® active substance: Doxorubicin) liposomal anthracyclines, and protein nanoparticles (*i.e.* Abraxane® albumin-based paclitaxel). [16]

Otherwise, the main focus is on the active drug targeting strategies developed by the evidence of the overexpression of receptors, enzymes or other cytoplasmic proteins in specific tumors. The identification of malignant cells is possible by targeting vehicles (*i.e.* mAbs, small molecules such vitamins, hormones, analogue peptides) covalently bond with cytotoxic

molecules and able to bind specific tumor antigens. These Drug Delivery Systems (DDS) are developed to release the active compound (cytotoxic payload) only after binding the target antigen. [14]

Based on the localization of different receptors, the active targeting can be defined as:

- active targeting to cancer cells: the antigen is expressed on the tumor cells membrane. It is commonly a transmembrane receptor that induces an internalization of DDS by endocytosis (Figure 3).
- Active targeting to endothelial cells: the antigen is overexpressed on the tumor vessels (*i.e.* endothelial cells) avoiding the extravasation and penetration requirements. Blocking tumor growth is supported by deprivation of oxygen, nutrients and growth factors. Moreover, the cytotoxic molecule can diffuse and penetrate into tumor tissues thanks to its low molecular weight (Figure 3). [14]

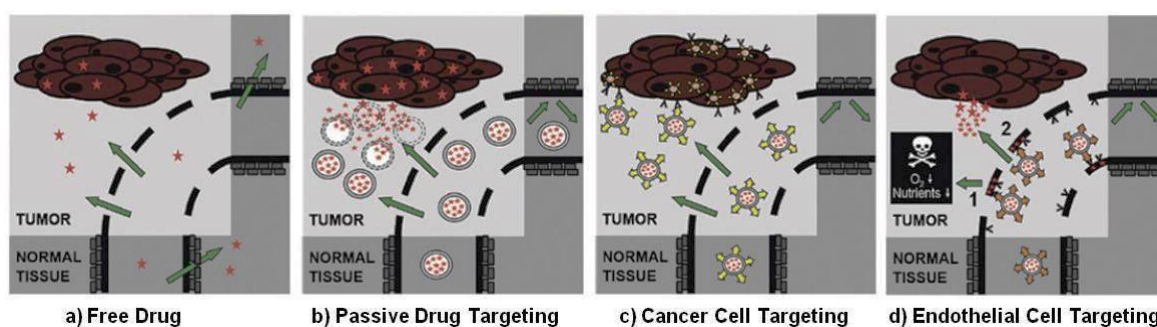


Figure 3. Representation of: a) traditional chemotherapy in which the drug accumulates in the tumor at low concentration and its localization in healthy tissues can be high; b) passive drug targeting by EPR effect; c) active drug targeting by recognized of specific receptors expressed on the tumor d) active drug targeting by recognized of specific receptors expressed on the endothelial cells. [14]

Another strategy for a selective tumor targeting is represented by a non-internalizing approach that is useful when the target is expressed in the ExtraCellular tumor Matrix (ECM) or it is represented by a transmembrane protein that does not induce the internalization of DDS. The cytotoxic molecule presents in the extracellular space is able to diffuse and penetrate in the surrounding various cells (*i.e.* tumor, endothelial cells) causing their death. This strategy called “bystander effect” can be exploited also with internalizing drug delivery system to promote an increase of the system efficacy (see paragraph 1.2.4). [17,18]

1.1.3.1 Antibody-Drug Conjugates

Antibody-Drug Conjugates (ADCs) actually are the most promising active drug delivery systems. This technology has been developed with the aim to selectively deliver a variety of known cytotoxic agents in diseased cells thus reducing their side effects. ADCs are composed of a mAb connected to a cytotoxic molecule (payload) through a properly designed linker that is responsible of ADC plasma stability and the drug release into the target cells (Figure 4). Even if the linker seems to be just a connection in between the antibody and the payload, it plays a crucial role on the efficacy of the final ADC. A poorly designed linker can lead to side toxicity effect in healthy tissue; so, it must be stable in blood at physiological pH and, at the same time, it should be easily and rapidly cleaved once inside the target cells. In this way, the cytotoxic drug is active only once it is released, while it is inactive, exactly as a prodrug, when is connected to the mAb. The design of a successful new Antibody-Drug Conjugate is a complex of knowledge that involves many disciplines such as organic chemistry, biochemistry and medicine. As Chudasama et al. said in their review: "Each ADC is being constructed in a tailor-made fashion for the specific antibody and drug combination in question." [19]

The target antigens should be present in high concentration in tumor cells and may be poorly expressed in healthy tissues.

The number of sequence linker-payload *per* antibody (drug-to-antibody ratio, DAR) must be as regular as possible, due to pharmacokinetic considerations. All these components must be cautiously assembled to achieve a successful ADC.

The sequence linker-payload has an electrophilic moiety (*i.e.* N-hydroxysuccinimidyl ester or a maleimide) that coupled to mAb nucleophilic residues (*i.e.* lysine and cysteine chains). All the small molecules used as payloads act in the nucleus of the cells by binding DNA or tubulin causing DNA damage ($IC_{50} = 0.1 \text{ nM} - 1 \text{ pM}$) or by modeling genic transcription as inhibitor of histone deacetylase 3 and 4 (HDAC 3-4). [20]

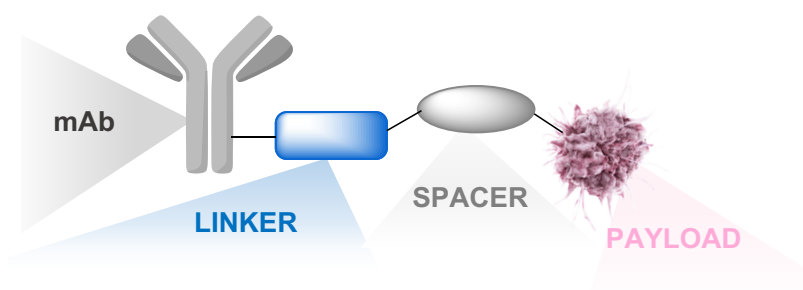


Figure 4. A generic ADC's structure.

The ADC must be designed to be internalized allowing the drug release inside the cell. The release mechanism is caused by mAbs binding with its antigen that promoting a receptor-mediated endocytosis of the ADC. The antigen-antibody interaction leads to the internalization of this complex through endocytosis with the formation of vesicles that merge with the lysosomes or proteasomes. The environmental conditions of these compartments as acid pH, high concentration of proteases and antioxidants are responsible of the degradation of the antibody and the linker and the following release of the drug in the cytoplasm (Figure 5). [21] Here the drug interacts with the target leading to the blockage of proliferation and apoptosis. Part of the released molecules that have a certain permeability across the plasmatic membrane can be accumulate in the extracellular environment thanks to a passive diffusion and can reach the neighbor tumor or vessel cells (bystander effect - Figure 5). [22]

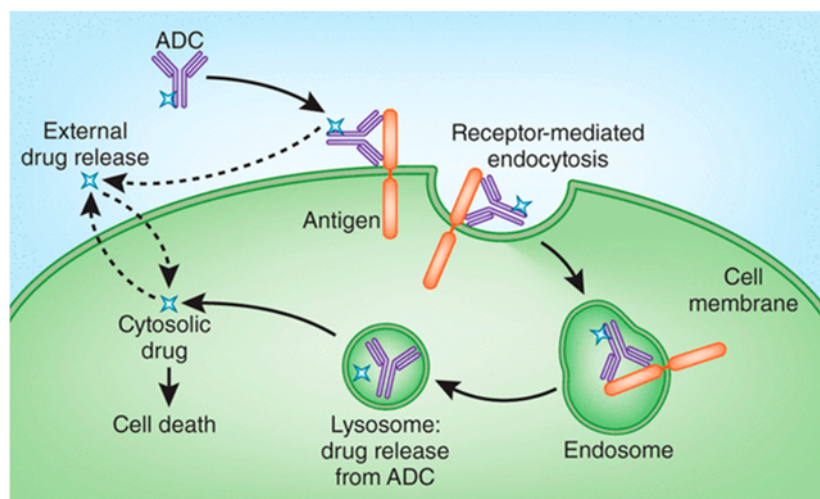


Figure 5. Release mechanism of an internalizing-ADC and bystander-effect. [23]

Otherwise, some antigens are non-internalizing and after the mAb-antigen binding, the ADC remains bound to the cell surface. After linker cleavage, the cytotoxic molecule can be released in the extracellular environment and passively diffused through the cell membrane (bystander effect). [24]

The difficulty stands in finding new suitable active molecules that would have low hydrophobicity, high potency, suitable moieties to be connected with the linker. ADCs charged with Doxorubicin and Methotrexate failed in clinical trial for their high off-target toxicity. The commonly used cytotoxic drugs are based on tubulin binding (*i.e.* Auristatins and Maytansinoids). On the other side, the engineering of monoclonal antibody allows a better and defined loading of the linker-payload system with an improvement of the homogeneity of the

conjugates thus impacting in the pharmacokinetic properties. The final result could be an ADC with a reproducible DAR with low deconjugation rate in blood, mild side effects and a very high selectivity and activity towards cancer cells. [22]

1.1.3.2 ADCs in the market

Food and Drug Administration (FDA) has already approved ten ADCs in 2021, namely respectively Adcetris®, Kadcyla®, Besponsa®, Mylotarg®, Polivy®, Padcev®, Enhertu®, Trodelvy®, Blenrep®, and Zynlonta® as monotherapy or used in combinational therapy, and more than eighty ADCs are being evaluating in about one hundred and fifty clinical trials (Figure 6). [25]

Adcetris® was approved in 2011 for the treatment of untreated stage III or IV Hodgkin's lymphoma and for systemic anaplastic large lymphoma. [26] The mAb used is Brentuximab Vedotin, a chimeric IgG1 anti-CD30 linked with Auristatin MMAE through a protease-cleavable valine-citrulline linker and a *p*-aminobenzyl self-immolative spacer (PABA). The sequence linker-payload is connected to the antibody by Cys residues with a DAR of 4 (Figure 6A). [27]

Kadcyla® was approved in 2013 for the treatment of metastatic breast cancer HER2-positive. Trastuzumab Emtansine is the humanized monoclonal antibody IgG1 anti-HER2 (an ErbB receptor) connected with a methabolic sensitive thioether linker to Maytansinoid DM1 (Figure 6B). The conjugation is allowed by mAb lysine (DAR=3.5). [28]

Besponsa® was approved in 2017 by the FDA for the treatment of acute and chronic lymphocytic leukemia; it is composed of Inotuzumab Ozogamicin as mAb (humanized IgG4) that recognized the antigen CD22 and Calicheamicin as a drug connected each other by a cleavable hydrazone linker (Figure 6A). [29]

Mylotarg® was reapproved in 2017 as single agent or in combinational therapy for the treatment of acute myeloid leukemia. The mAb used is Gemtuzumab Ozogamicin, a humanized IgG4 anti-CD33 as target which is connected to cytotoxic molecule Calicheamicin with a cleavable hydrazine linker (Figure 6A). [30]

Polivy® was approved by the FDA in 2019 for the treatment of refractory diffuse B-cell lymphoma (DBCL). The mAb used is Polatuzumab, a humanized IgG1 that recognized CD79b as target antigen and linked with MMAE through a cleavable valine-citrulline peptide (Figure 6A). [25]

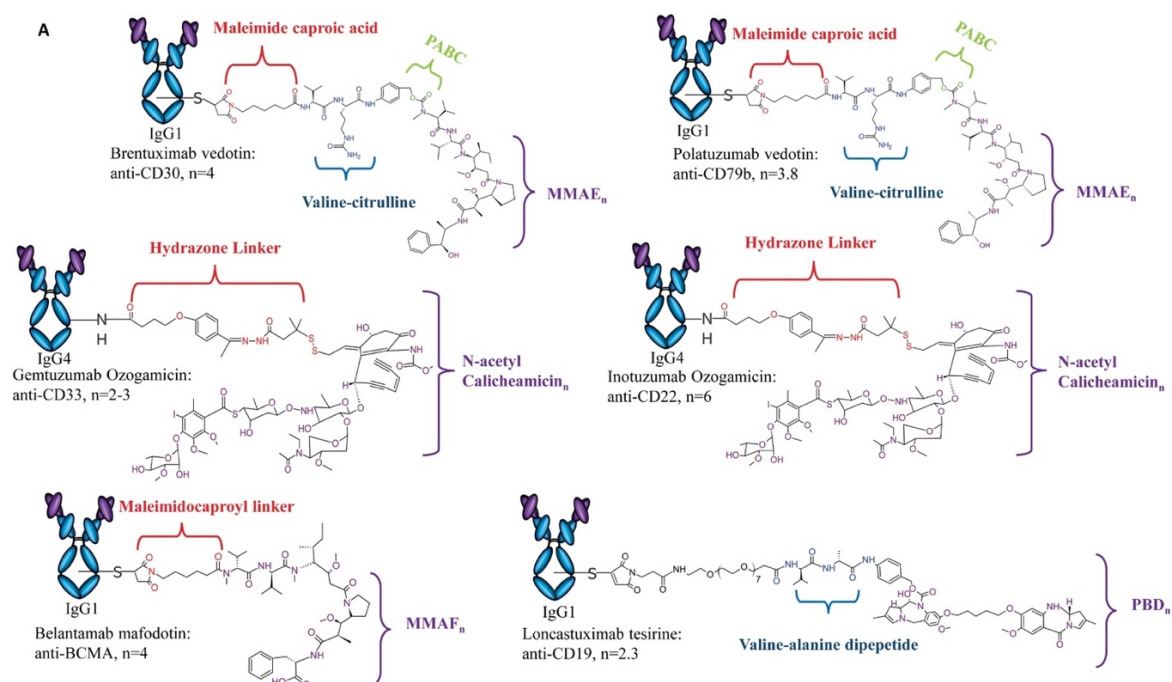
Padcev® was approved in 2019 for adult patients with advanced or metastatic urothelial cancer. The mAb is Enfortumab Vedotin a Human IgG1 that recognized Nectin-4 as target antigen and linked with MMAE through a cleavable valine-citrulline peptide (Figure 6B). [25]

Enhertu® was approved in 2019 for metastatic HER-2 positive breast cancer. Trastuzumab is the mAb used linker with a tetrapeptide to Deruxtecan a topoisomerase I inhibitor (Figure 6B). [25]

Trodelvy® was approved in 2020 for adult patients with metastatic triple-negative breast cancer who have already received other two therapies. This ADC is composed of a humanized IgG1 called Sacituzumab Govitecan, SN-38 as antineoplastic drug and a CL2A linker (Figure 6B). [25]

Blenrep® was approved by the FDA in 2020 in adult patients with refractory multiple myeloma who have received four other therapies before. It is composed of a humanized IgG1 Belantamab Mafodotin anti-BCMA connected with a maleimidocaproyl uncleavable linker to Auristatin MMAF. DAR = 4 (Figure 6A). [25]

Zynlonta® was approved by the FDA in 2021 for the treatment of refractory large B-cell lymphoma. The mAb used is a humanized IgG1 anti-CD19 called Loncastuximab Tesirine which is connected with a cleavable valine-alanine linker to a SG3249 PBD dimer. The conjugation is allowed by antibody cysteines; DAR=2.3 (Figure 6A). [25]



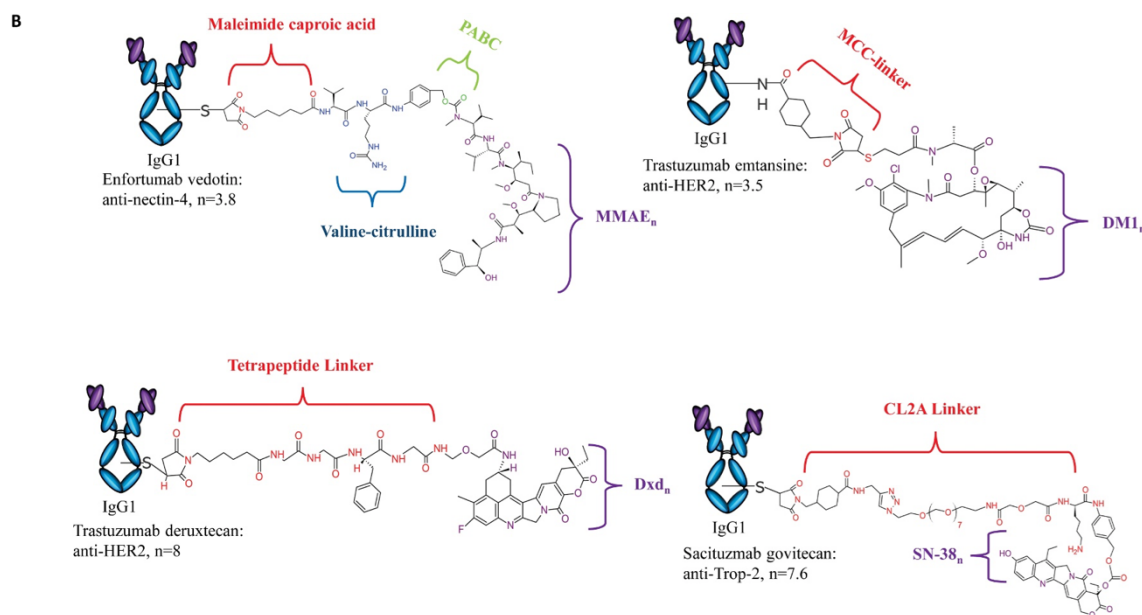


Figure 6. Structure of ADCs Approved by the FDA for Clinical Use. Design of each ADC: antibody isotype, linker chemistry, payload class and DAR. (a) ADCs approved for hematological malignancies: Adcetris®, Polivy®, Mylotarg®, Besponsa®, Blenrep®, and Zynlonta®. (b) ADCs approved for solid tumors: Padcev®, Kadcyla®, Enhertu® and Trodelvy®. [25]

1.2 Evaluation of ADC components, properties and design

1.2.1 Antibody and antigen

The identification of the target antigen is the key for the development of a suitable ADC. More than one hundred different targets, both intra- and extracellular, have been studied in order to design an appropriate and specific target delivery system. [31]

The fragment antigen-binding (Fab region) is responsible for the recognition and binding of the mAb to the antigen. The suitable target antigen could be specific towards cancer cells and low expressed on healthy tissues, even though different levels of the same antigen could be found not only in different patients but also in the same one. A lack of homogeneity, especially in solid tumors, brought to a minor activity and off-target toxicity. In this case, bystander effect may promote an equal diffusion of the drug in heterogeneous tumors. For the ADC efficacy, another important parameter is the ability of the antigen to induce the internalization of the ADC (if it's an internalizing one). [32] The fragment crystallizable region (Fc region) is responsible for binding with Fc receptors or some complement system proteins and regulates the ADC half-life. Fc region influences the immune responses by activating or inhibiting Fc receptors on the surface of immune cells or by interacting with complement system. This has an impact on triggering the secondary immune effector function when the antibody used is CDC

or ADCC. [33]

The common mAbs are Immunoglobulins G (IgGs) that are subdivided in IgG1, IgG2, IgG3 and IgG4. Apart from IgG3 that has low half-life, the other classes are used for ADC design. [34] IgG1 subclass is the most used one; it has a great profile regarding the activation of the immune system even if it has a lower half-life (21 days) than IgG2 and IgG4. IgG2 and IgG4 are used when the immune system activation is not required because of their low affinity. The number of disulfide bridges can influence the DAR if the conjugation is performed with Cysteine. IgG 1 and 4 have two bridges, while IgG2 has four ones. [35]

1.2.2 Linker and self-immolative spacer

As aforementioned, the linker has the function to connect the mAb to the payload and it must be stable in plasma while able to release the drug in the tumor environment. Even if the linker is seemingly used only to bind the antibody with the payload, it plays a crucial role on the design of a well-functioning drug conjugate. A non-well-designed chemical linker leads to off-target effects in healthy tissues and a low therapeutic window due to high instability in blood with aspecific drug release. [36] Linkers can be divided in three parts: the binding site, the trigger that is the cleavable part of it, and the self-immolative spacer, a moiety that after its own rearrangement promotes the drug release. The linkers could be divided in cleavable and non-cleavable linkers depending on whether a specific functional group is sensible to tumor microenvironment conditions or it is hydrolyzed by a lysosomal process. There is also another classification based on different external *stimuli* that bring to the cleavage. Linkers can be divided in: chemically labile, enzymatic or metabolic sensitive linkers. The choice of the correct one still remains a “trial-and-error” whenever you want develop an ADC. [37]

1.2.2.1 Metabolic sensitive linkers

The metabolic sensitive linkers known as non-cleavable linkers release the drug after a complete lysosomal proteolytic degradation after ADC internalization. The advantage is the great stability at physiological pH that provides a high therapeutic window. They require a good processing after internalization of the ADC if not the mechanism is not granted.

The most known metabolic sensitive linkers have a succinimide-thioether moiety which takes advantage from Michael reaction between thiols and maleimides. The release mechanism is based on a retro-Michael reaction occurring inside lysosomes, and generating cascade reaction

chains that lead to drug release into the target cells. The exact inner working is still not properly known, maybe also the proteolytic degradation of the antibody could involve reactions that promote linker rearrangement with drug release as a consequence. [38]

For example, Kadcyla® has the thioether linker succinimidyl-4-(*N*-maleimidomethyl) cyclohexane-1-carboxylate (SMCC – Figure 7a), one of the most common used metabolic sensitive linker. Moreover, cyclohexane ring gives stability due to its steric hindrance. Another well-known non-cleavable linker has a maleidocaproic acid moiety (MC – Figure 7b) and it is used in Blenrep® in which the drug (MMAF) is connected to it with a stable amide bond that does not guarantee the release of the drug. MMAF, as opposed of MMAE, remain active with the same potency also bound with small alkyl chain. [39] This MC linker is also used in Adcetris®, in Polivy® and in Padcev®.

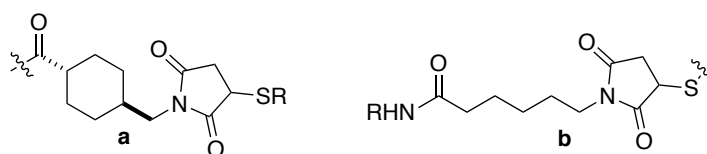


Figure 7. Metabolic sensitive linkers: SMCC (a) and MC (b). R= payload.

1.2.2.2 Chemically labile linkers

The release of the drug is related to the different pH and redox environments in plasma and target compartments. These linkers are more versatile than metabolic ones but with low plasma stability properties that can be hampered by introducing steric hindrance close to the sensitive part of the linker called trigger moiety. [40]

1.2.2.2.1 pH sensitive linker

pH sensitive linkers drug release efficiency depends on pH changes in the target tissue and undergo acid-catalyzed cleavage.

Hydrazones and oximes.

Hydrazone is the first chemical sensitive linker developed with a long half-life at pH 7.0 of several days and selectively cleavable in lysosomes acid conditions (pH 5.0). [41] In 2008 a study of oximes and hydrazones using NMR in deuterated buffer affirmed that water molecule attacks on C1 with an acid catalysis through a protonation of the N1. Electron-withdrawing X groups increase the possibility of protonate N1 with a lack of hydrolysis rate (Figure 8). [42]

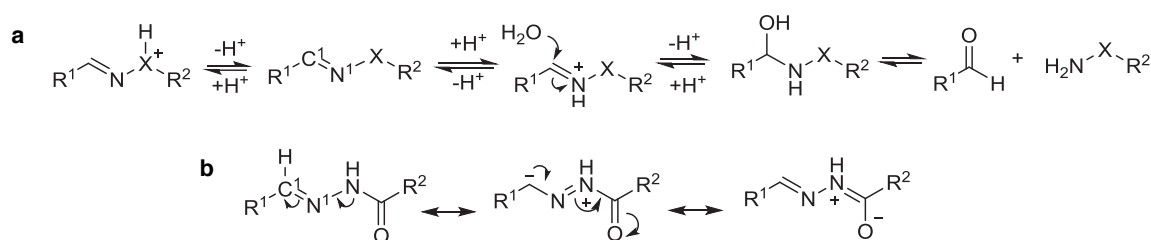


Figure 8. Hydrolytic cleavage mechanism of hydrazone/oxime (X=O, Oxime; X=NH, Hydrazone).

The stability at pH 7 is ranked in this order: trialkylhydrazonium ion (no detectable hydrolysis) >> oxime >> acyl hydrazone > primary hydrazone > secondary hydrazone > imine (Figure 9). The quaternary ammonium hydrazone (Figure 9a) is too stable at pH 5 and for this reason is not used as chemical sensitive linker. Among all these, the acyl hydrazone linker (Figure 9d) is the best one due to its resistance to hydrolysis plasma pH while it is more unstable at pH 5 than alkyl hydrazones. Such acyl hydrazone properties reflect a delicate balance between the imine carbon electrophilicity and the ability for acid environment to catalyze the hydrolysis reaction at pH 5 through protonation. The acyl hydrazone stability profile makes it an excellent chemically sensitive linker for anticancer drug delivery (Figure 9d). [43-45]

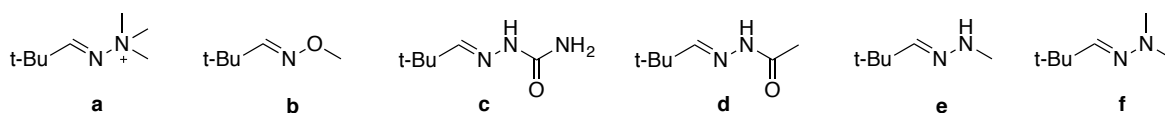


Figure 9. List of different Hydrazones.

For the development of ADCs, high cytotoxic payloads like Calicheamicin (sub-nM IC₅₀) are usually used. This design requires linkers with an excellent controlled stability at physiological pH to prevent the premature release of the drug. Therefore, using Mylotarg® as a model, many different aliphatic and aromatic aldehydes and ketones were added in the acyl hydrazone linker to increase the selectivity for the release in acid conditions. [46] The one formed by 4-(4-acetylphenoxy) butanoic acid (AcBut) and acylhydrazone (Figure 6a) showed the highest pH selectivity. The resulting ADCs obtained (Mylotarg®) shows stability with only 6% hydrolysis at pH 7.4 after 24 h at 37°C, with 97% of calicheamicin released after 24 h at 37 °C at pH 4.5 (lysosomal pH). These results are related to the stabilization of the acyl hydrazone linker by the p-alkyloxyphenyl group with an increase of electron density of the hydrazone carbon (C1 in Figure 8), making it less willing to be attacked by a nucleophilic water molecule. [46] Another

approved ADC in 2017 was Besponsa® (Figure 6a) that has the same AcBut-acylhydrazone linker with 12.3 days of half-life. [47]

The oxime linker was used in a PEG-Doxorubicin micelle drug delivery system showing a very slow release $T_{1/2} = 15$ h at pH 5 and a bad stability at plasma pH (drug release = 20% after 12 h) These results indicate that the oxime linker has a worse stability-release profile than the hydrazone one. [48]

With the aim of improving the hydrazone linker, Zheng et al. combined an acyl hydrazone linker with a proteolytic bridge to form a peptide-bridged twin-acylhydrazone (PTA) linker (Figure 10). The peptide is used to join two acyl hydrazone linkers connected together with a bis-aldehyde spacer. [49] The two peptides used are GGPLGLAGG, a substrate for extracellular matrix metalloproteinase-2 (MMP-2), and GGFLGG, a chymotrypsin substrate. A fluorophore (Oregon Green 488)-quencher (Dabcyl) pair was used as model to prove the efficiency of the protease-mediated cleavage. The cleavage of the peptide linker before, and the hydrolysis of the hydrazone moiety after, allow the separation of the quencher from the fluorophore, leading to an increase of fluorescence. When this model was incubated at both pH 7.4 and 4.0 for 24 h, there was not fluorescence, a signal of linker chemical stability. The chemical stability at pH 4 is due to the spatial proximity of the two hydrazone linkers, which facilitates the reformation of acylhydrazone immediately after its hydrolyses. On the other hand, this model was incubated with MMP-2 or chymotrypsin for 2 h followed by incubation in buffers (pH 7.4 and pH 4) for 24 h. 50% fluorescent was recovered at pH 4.0 and about 10% fluorescent was recovered at pH 7.4. The PTA linker with the same fluorescent model system was conjugated to integrin-targeted RGD-peptide and tested in U87 cells, which highly express the $\alpha v \beta 3$ integrin, a receptor for RGD; an increase of fluorescence was detected by confocal microscopy after 24 h of incubation. Then the system RGD-PTA linker with different peptide bridges were used with MMAE, a cytotoxic drug (MMAE $IC_{50} = 0.75$ nM in U87 cell), and studied in cancer cells testing separately MMP-2, chymotrypsin, and lysosomal cathepsin (Figure 10). The conjugates showed cytotoxicity (IC_{50}) in U87 cells of 61.9 nM (MMP-2 substrate bridge), 140.9 nM (chymotrypsin substrate bridge), and 623.1 nM (cathepsin substrate bridge) respectively. MMP-2 and chymotrypsin are extracellular enzymes and the cleavage of the peptide bridge has to happen before the target delivery system gets into the cells. The advantage of this mechanism is that the drug is released under the combined conditions of an acid environment (hydrazone moiety) and the presence of an appropriate protease. On the other hand, even if this system would be promising, the release rate is considerably slower than using a conventional acyl hydrazone linker. [49] However, this two-stage release mechanism should be more investigated

in animal models to understand its applicability.

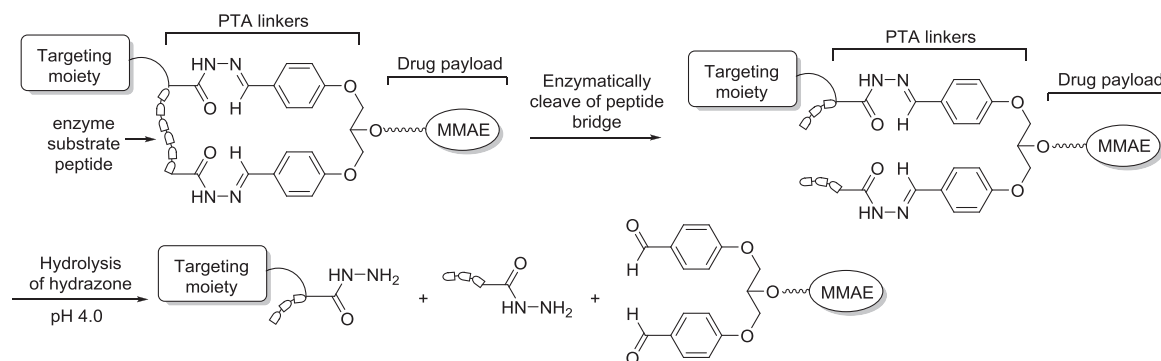


Figure 10. Proteolytic unlocking of twin-acylhydrazone linkers (PTA linker) for lysosomal acid-triggered release of anticancer drugs. [50]

Phosphoramidate linkers.

Phosphoramidate chemistry exploits the acid catalysis which promotes the protonation of a pyridinyl group (Figure 11). The pKa of a protonated pyridine stays under the physiological pH and the pyridine remains in the unprotonated form at pH 7.4. A lower pH, the acid catalysis allows pyridine nitrogen protonation and facilitates the hydrolytic cleavage of the phosphoramidate linker. The hydrolysis rate of the phosphoramidate analogs with $n = 2$ (Figure 11) at pH 5.5 was determined as follow: a ($T_{1/2}$: 1.64 h) > b ($T_{1/2}$: 2.13 h) > c ($T_{1/2}$: 16.2 h) > d ($T_{1/2}$: 31.5 h). If $n = 1$, for example the compound e in the Figure 11, the release is very fast at both pHs and the half-life $T_{1/2} = 0$ h due to the instantly hydrolysis in water. If $n = 2$, for example the compound a (Figure 11), the release profile becomes valuable: at pH 5.5 $T_{1/2} = 1.64$ h, and at pH 7.4 $T_{1/2} = 23.9$ h. The position of the neighbors of pyridinium nitrogen influences the hydrolysis because of their characteristic to form intramolecular hydrogen bond with the formation of a nine- or eight-membered rings in the transition state. The nine membered ring is more favorable in the process of accomplishing general-acid catalysis and leads to a non-selective rapid hydrolysis. The substituent R^1 and R^2 of phosphoramidate moiety influence the half-life: an aliphatic amine has a shorter $T_{1/2}$ than an aryl one (*i.e.*, a vs. b, c vs. d, e vs. f, Figure 11). Of course, the pyridine nitrogen must be in ortho-position (Figure 11). The amine pKa is inversely proportional to linker stability. [51]

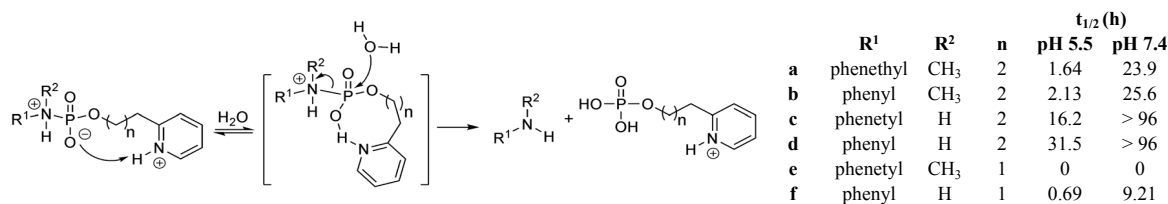


Figure 11. Phosphoramidate linkers and mechanism of drug release.

Acetal-, orthoester-based linkers.

Acetal is an acid-labile protecting group of the aldehyde group that can quickly undergo hydrolysis in acidic conditions (Figure 12).

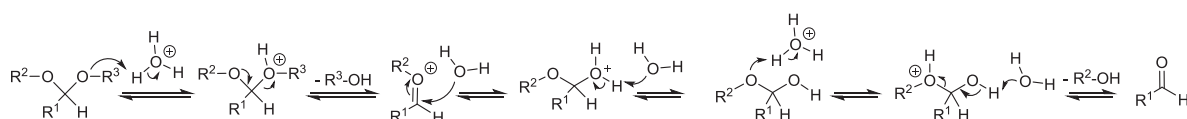


Figure 12. Acid-catalyzed hydrolysis of acetals.

Wagner et al. [52] identified several simple benzaldehyde acetals sensitive to acid pH and applicable as linkers. R₁ and R₃ could be modified with –H –OMe –OEt –imidazole moiety to prepare pH-sensitive linkers and ethoxybenzyl acetal derivatives had the best selectivity and efficiency (Table 1). The imidazole derivative represented is used to develop the *N*-ethoxybenzylimidazole (NEBI) linker (Table 1, Entry 4).

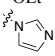
Entry	R ¹	R ²	R ³	t _{1/2} (h)		Ratio (K _{pH 5.5} /K _{pH 7.4})
				pH 5.5	pH 7.4	
1	H	H	OEt	0.8	12.2	15.3
2	OMe	H	OEt	0.1	5.3	53.3
3	H	OMe	OEt	0.1	19.9	199
4	H	OMe		1.1	28.8	31.7

Table 1. Hydrolysis kinetics of different acetal linkers.

Deslongchamps et al. in 2000 published an interesting article about the hydrolytic behavior of acyclic and cyclic acetals, ketals, orthoesters and ortho- carbonates. [53] Generally speaking, there is an increase of hydrolysis when the central carbon has the higher degree of substitution. If a hydrogen atom is replaced with an alkyl or alkoxy moiety, there is an acceleration of hydrolysis rate. This can happen due to the stability of the corresponding alkoxy carbenium ion intermediate while hydrolysis occurs. The more this intermediate is stable, the greater is the chance that it can be formed with the obtainment of final product hydrolyzed. Regarding the cyclic orthoester compounds, this rule is perfectly followed, and as for acyclic orthoformates,

and additional alkyl group in the central carbon (instead of –H) increase the kinetics of the process. Moreover, compared to acetals and ketals, orthoesters have two oxygen lone pairs that improve the basicity of leaving group aiding the hydrolysis. [53]

Wagner et al. [54] designed a Spiro-Di-Orthoester linker (SpiDO) linker and tested its release profile compared with acylalkylhydrazone linker, and non-hydrolysable linker. The studied system was based on a FRET-based fluorescent, composed of a tetramethylrhodamine (TAMRA) fluorophore, a black hole quencher (BHQ-2), and the linker that joins them together (Figure 13). Different pHs, especially pH 7.4 and 5.5, were tested on each type of linker and the fluorescent changes at different pH were monitored. The SpiDO conjugate in Figure 13a gave the highest pH-dependent selectivity and efficiency. The complete hydrolysis of SpiDO was immediate below pH 3.0, whereas the half-life was found to be 1.5 h and 7 h were needed to achieve complete hydrolysis at pH 5.5. At pH 6.0 and 7.0, it showed 65% and 24% of hydrolysis after 15 h. Therefore, the SpiDO linker seems to be more sensitive to lysosomal pH compared with the acylhydrazone linker. [54] This is an important aspect to keep in mind because in some cancers, the external solid tumor environment is more acidic than healthy tissues and the pH can drop down until 6-7 value still remaining different from lysosomal pH (4.5-5.5). pH-sensitive linkers could be tested also at pH slight acid (pH 6.5 for example) to be sure that the release of the drug happen only after internalization of the drug delivery system.

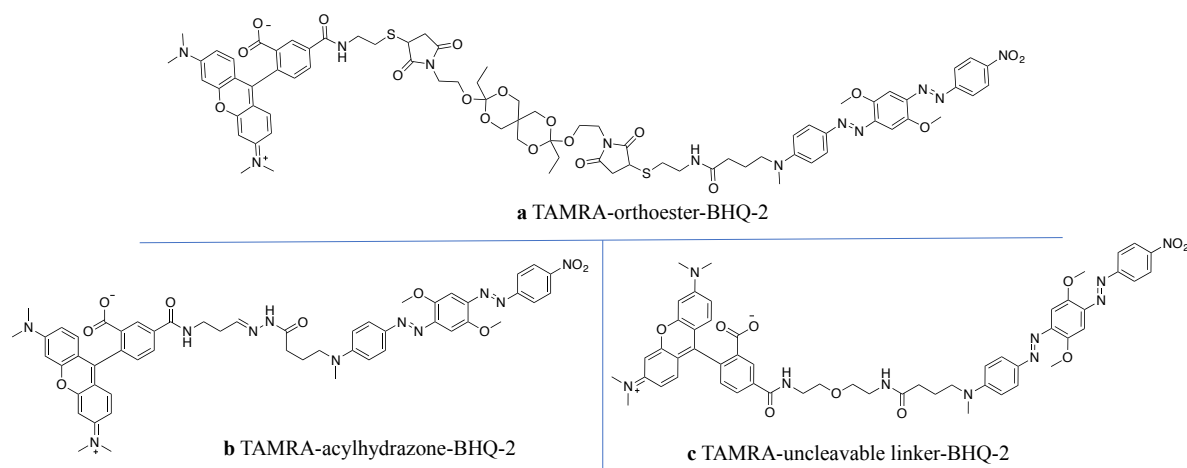


Figure 13. a) TAMRA-Orthoester-BHQ-2; b) TAMRA-acylhydrazone-BHQ-2; c) TAMRA-uncleavable linker-BHQ-2.

Maleic acid-derivative linkers.

Maleic acid derivatives are used as linkers thanks to the intramolecular cyclization of maleoyl amide at pH less than the pKa of the free carboxylic acid group (Figure 14). This system was first reported in 1981 with a highly desirable pH-sensitive release profile, providing the

complete release in 3 h at pH 4.0, while it remained stable at pH 7.0 up to 96 h. [55] Zhang et al. [56] tried to understand the release mechanism based on experimental findings and literature reports (Figure 14). At pH below the pKa of the acid moiety, compound **2** is the major species, and this compound leads to drug release with at least three possible routes. Pathway A is the main mechanism and involves the intramolecular proton transfer from the carboxylic acid to the amide group followed by ring closure. This mechanism caused the formation of the intermediate **5**. The subsequent degradation of this intermediate brought to the release of the drug and maleic anhydride as products (Figure 14). [56] At pH over the pKa of carboxylic acid, no detectable hydrolysis of the amide is observed. [57] The key of this mechanism is the intramolecular proton transfer with the obtainment of the tetrahedral intermediate **5**. The influence pH value indicates that this pathway is specific-acid catalyzed. [57] The double substitution on maleamic acid led to a 700- fold increase in the amide hydrolysis rate because of alkyl groups have entropic advantages for cyclization. [56, 57] On the other hand, the rate-limiting step is the breakdown of the intermediate **5**. [57] In Pathway B, the amide oxygen attack leads to the isomaleimide **9**, which hydrolyzes into the tetrahedral intermediate **5** releasing the drug in its free form and maleic anhydride as in pathway A (Figure 14). In the pathway C, the drug is not directly released (Figure 14). However, all reactions are reversible under the conditions used. [56]

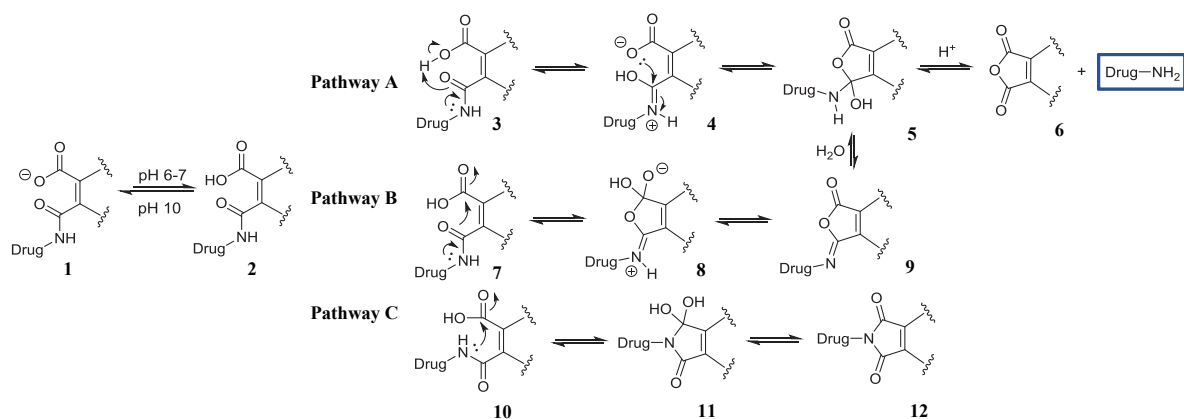


Figure 14. Three possible release mechanisms of maleic acid linkers.

At the end, it is clear that targeting endosome/lysosome with a low pH, acylhydrazone linkers can give a very fast and selective release. Otherwise, to target solid tumor with only a slight drop in pH (6.0–7.0), a high selective pH range sensible linker it would be desirable to use the SpiDO linker and/or a maleamic acid linker.

Thiol-sensitive linkers.

Thiol-sensitive linkers have a disulfide bridge which is reduced in presence of glutathione (GSH) and its intracellular concentration is in the range of 1–10mM, while in plasma and other extracellular fluids, the concentration is on μM range. Moreover, the tumor cells contain a higher level of GSH than normal tissues. [58] Disulfide bridges are reduced in the cytosol of cells and this brings many advantages: good biocompatibility, easy synthesis, high drug-release performance, thermodynamic stability at physiological pH, while it is unstable in the intracellular reducing environment. For these reasons, disulfide linkers have been developed in drug targeting field. [59] The stability of disulfide bridge can be improved by adding substituents adjacent the S-S bond. [60] This type of linker is also applied to link a mAb with various cytotoxic agents for the development of ADCs. For example, Sliwkowski et al. [61] synthesized and studied many of trastuzumab-maytansinoid (DM) conjugates, by using a disulfide or a thioether bond as the linkers (Figure 15). The disulfide linkers used had different numbers of methyl groups (a–d, Figure 15) and all conjugates showed a higher potency on HER-2 positive BT-474 and SK-BR-3 cells line than free DM. To understand the stability of these differently functionalized linkers, pharmacokinetic (PK) analyses of the various conjugates were conducted in nude mice. The less hindered disulfide conjugate (compound a) was more easily degraded in plasma and the ADC level was undetectable after 3 days. With the increase of steric hindrance, the ADC clearance time in plasma increased as thought. On day three, 60% of conjugate a (Figure 15) and 20% of conjugate c (Figure 15) were degraded. The most hindered disulfide-linker d (Figure 15) maintained 70% of the total conjugate concentration after seven days. In vivo efficacy studies on MMTV-HER2 Fo5 mammary tumor transplant (trastuzumab-resistant) model were done measuring the tumor size after treatment with ADCs developed with different linkers, an expected correlation between the stability of the linker and the antitumor activity was achieved. [61]

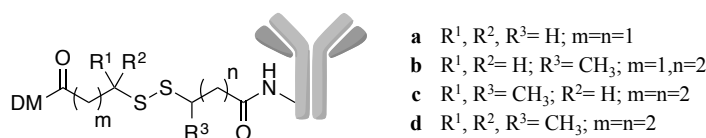


Figure 15. Disulfide linkers.

1.2.2.2.2 Reactive oxygen species (ROS) sensitive linkers

The reactive oxygen species (ROS) are free radicals as singlet oxygen ($^1\text{O}_2$), hydrogen peroxide (H_2O_2), and ions such as superoxide (O_2^-) or hypochlorite (OCl^-). ROS influence various cellular signaling processes responsible for proliferation, differentiation and regulation of immune responses. The oxidative environment generated by ROS is able to determinate post-translational modifications of various proteins due to the oxidation of the thiol group in reactive forms like sulfenic acid ($-\text{SOH}$). The following reaction of the $-\text{SOH}$ group with $-\text{SH}$ moiety of cysteines brought to disulfide bond formation with changing in the structure and in the function of various proteins. [62] In cancer cells and many other pathogenic conditions, high concentrations of ROS have been detected. [63] Drug delivery systems take advantage of this non-physiological condition to allow a targeting drugs release. [64] For this reason, linkers containing boronate/boronic ester, sulfide, selenide/telluride thioether and ferrocene are commonly used to take advantage of high concentration of ROS.

Aryl boronic acid and borate-based linkers.

Prodrugs developed starting from Vorinostat (SAHA), SN-38, NO donors, nitrogen mustards and 5-Fluorouracil (5-FU) take advantage of the selectivity of boronic acid and boronate groups towards oxygen free radical, and it represents a great chance for the development of a delivery drug system. [65] 5-FU is a potent cytotoxic drug that gives many side effects (*i.e.* myelosuppression, gastrointestinal toxicity, and central neurotoxicity) [66, 67] and it is metabolically unstable turning into the cardio- and neurotoxic α -fluoro- β -alanine. At the end, only the 3% of the injected dose reaches the tumor. To overcome these limitations, a *p*-boronate benzyl moiety is introduced to avoid the metabolic degradation and to be used as ROS-sensitive trigger for the drug activation, only in presence of H_2O_2 . In this case, the borate function is converted into phenol moiety, which spontaneously rearranges itself in a quinone species providing 5-FU as free drug. The quinone byproduct is quickly hydrolyzed by water to obtain nontoxic 4-(hydroxymethyl)phenol. Boronic ester is more efficient in terms of drug release than boronic acid. Thanks to a study using RP-UPLC-MS, compounds **13a** and **13b** (100 μM ; Figure 16) were tested in the presence of 5 equivalents of H_2O_2 and the boronic ester trigger moiety released 5-FU within 5 min, while **13b** took 250 min for a complete conversion into free drug. *In vitro* studies in more than 60 cancer cell lines were performed to claim prodrugs inhibition growth ability with very good results especially for the compound **13a**. Perhaps the difference

between boronic ester and acid is attributed to the major permeability of the borate prodrug. [68]

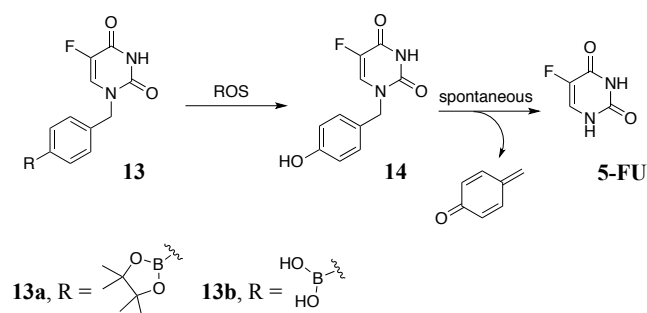


Figure 16. ROS activated prodrugs of 5-FU.

Boronic acids and the final product of boronic acid after oxidation are ingredients found in vegetables and plants. The boric acid and ester byproducts formed after the drug release are known to be well tolerated in humans. [69] Moreover, aryl boronic acids and esters are very stable and have a very selective reactivity toward H_2O_2 . For these characteristics, they are good moieties to use as ROS-sensitive trigger. [70]

Aryl boronate esters were also investigated as ROS sensitive trigger function by Phillips at al. for the development of *stimuli*-responsive reagents that should be capable of release small molecules that contain primary/secondary alcohols or phenols. This designed linker is able to bind two different types of alcohols and at the same time to indicate the release by forming a yellow color thanks to its transformation in *p*-aminobenzaldehyde that is a colorimetric indicator (Figure 17). [71]

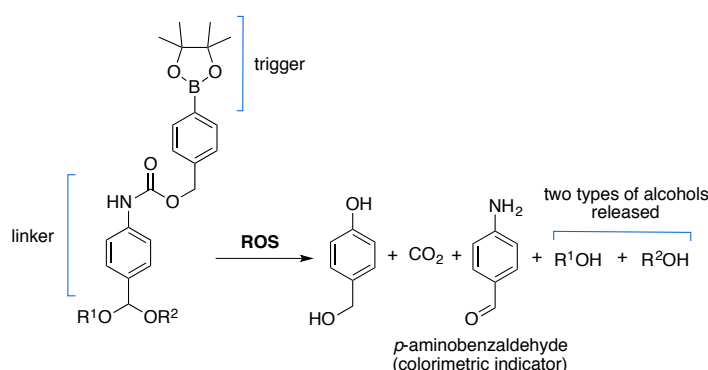


Figure 17. Aryl borate ester as ROS trigger moiety capable to release small molecule with primary/secondary alcohols or phenols.

The examples aboved are not linkers but prodrugs and maybe these promising triggers would be more investigated for the development of drug delivery systems.

Thioketal-based linkers (TKs).

Thioketal function can be used as ROS sensitive trigger moiety leading to another class of linkers, which can be cleaved by various ROS species to give the corresponding thiol and acetone (Figure 18). [72] A thioketal-based cationic polymer was designed in 2012 to deliver gene transfection in prostate tumor cells. The degradation kinetics of the polymeric system was studied by ^1H NMR studies in presence of H_2O_2 and a catalytic amount of CuCl_2 to induce radical production. The polymer degradation was found directly proportional to H_2O_2 concentration. [73]



Figure 18. Mechanism of release of thioketal based linkers in presence of ROS.

This type of linker gives a relatively slow degradation profile under physiological ROS concentration in tumor cells and an extra boost of ROS generation can be furnished to accelerate the kinetic release. Wang et al. [74] designed a nanoparticle called PPE-TK-DOX system using ROS-sensitive thioketal linker (TK) to link a polyphosphoester (PPE) with Doxorubin (DOX). This polymer was assembled with chlorin e6 (Ce6) that is a photosensitizer which can generate ROS red light irradiation.

The high stability in physiological conditions in addition to the selectivity of the delivery gives good hopes for the development of drug delivery system based on thioketal linker. Otherwise, the slow release rate under convention tumor conditions could represent a limit.

Thioether-based linkers.

The thioether function could be used for the development of a ROS sensitive linker due to its transformation in more hydrophilic sulfoxide or sulfone group in the presence of an oxidative species. [75] This type of targeting system is based on the solubility switch concept (from hydrophobic to hydrophilic) for the release of the drug.

Zhu et al. designed a polymeric micelle consisting of two parts. The external part is represented by a polymer HPG-2S-SN38 formed by tethering cytotoxic drug 7-ethyl-10-hydroxy-camptothecin (SN38) connected with a ROS-sensitive thioether linker to a hyperbranched polyglycerol (HPG). [76] This polymer was then self-assembled into nanomicelles with cinnamaldehyde (CA) encapsulated in the core. CA has antitumor effects by generating ROS in the mitochondria of cancer cells and facilitates the drug release from the nanomicelles. The

payload is released due to destabilization resulting from polymer properties changes in presence of ROS. [77]

The sensitivity to different types of ROS and the byproducts toxicity are crucial to design an efficient ROS-sensitive drug delivery system.

Linkers based on thioether moiety allow drugs release by a change in solubility due to its transformation in a more hydrophilic sulfoxide or sulfone group, while other linkers such as boronates and thioketals are cleavage-based ones. Since different disease states may involve various elevated levels of ROS, the ROS sensitive linkers could be used in many different medical applications. [50]

1.2.2.3 Enzymatic sensitive linkers

The enzymatic sensitive linkers are very popular because of their excellent stability in plasma and for their selective release delivery by specific intracellular enzymes.

1.2.2.3.1 Protease-sensitive linkers

Targeted delivery could take advantage of different concentrations of enzymes between the desired site of action and other tissues. Linkers with peptide sequence is considered a useful trigger with the chance to selective cleavage by, for example, proteases. [78] Cathepsin B is overexpressed in specific invasive and metastatic cancers [79] and aberrant levels of kallikrein peptidase family (KLK1~15) in other type of tumors. For example, some prodrugs for the treatment of prostate cancer used the isoform 3 of KLK also called PSA, to release the drug in its active form. [80]

In some cases, the drug delivery system used directly as a peptide even if linking the drug to a peptide may interfere with the proteolytic cleavage because of its steric hindrance. [81] In ADCs, a small self-immolative spacer like *p*-aminobenzyloxyl alcohol (PABA) is often added between the payload and the peptide linker (Figure 19). Adcetris® is an ADC approved by the FDA and it is composed of a valine-citrulline (Val-Cit) cleavable peptide as linker plus a PABA-like self-immolative spacer as a connection between the cytotoxic payload and the monoclonal antibody. [82] The cathepsin B is the protease that is able to recognize peptide-spacer bond and cleavage it.

The release mechanism for this ADC is that one: after antigen-targeted delivery and internalization, Cathepsin B hydrolyzes the amide bond between Cit and the PABA to promote the 1,6-elimination of the spacer with the release of cytotoxic MMAE, avoiding the formation of an inactive aminoacid-drug adduct. The removal of PABA decreases the release rate due to an improvement of steric hindrance effects within the enzyme pocket. To study the stability of Val-Cit-PABA linker (Figure 19b), MMAE was loaded in a cAC10 monoclonal antibody (a non-therapeutic biosimilar of the monoclonal antibody drug brentuximab anti-CD30, used only for research use). The *in vivo* linker $T_{1/2}$ was higher than the hydrazone linker: around 144 h in mice, 230 h in monkey and very stable also in humans. [83] In 2011 the clinical phase II produced very good results: 75% response rate in patients with Hodgkin lymphoma and 87% in patients with anaplastic large cell lymphoma. [82] Dubowchik et al. conducted a study about the enzymatic release profiles of activity of cathepsin B towards peptide linkers. The comparison was performed with ten different Doxorubicin conjugates with dipeptide linkers with/without PABA spacer. *In vitro* enzymatic release assay, Phe-Lys and Val-Lys with a PABA showed a fast release of around 8 minutes while the same dipeptide without the PABA spacer showed no hydrolysis over 6 h. [85] Different drugs were investigated and usually the amine-derivatives were used in order to obtain carbamate-PABA derivatives; also, alcohol groups would be exploited to prepare carbonate-PABA derivatives like in Trodelvy® in which SN-38 was connected to the antibody thanks to its alcohol moiety. [86]

The addition of a spacer can influence the drug release ratio but not always in a positive way. Several other self-immolative spacers would be employed for the development of prodrugs or delivery systems that involved the proteolytic cleavage of the peptide-immolative spacer amide bond with the cyclization or elimination rearrangement of the spacer. The design of peptide linker-spacer structure is important for a functional ADC; many different protease substrates should be examined to find the best pharmacokinetic profile. Careful in extrapolating from results that come from animal models: for example, the most known Val-Cit linker was found to be labile in the mouse plasma and more stable in the human one. [87]

Val-Cit dipeptide is the most used linker for the design of new ADCs even if, the importance of valine-alanine (Val-Ala) linker is growing especially in SMDCs. Val-Ala peptide is cleaved by cathepsin B too but it appears to have a higher plasma stability than Val-Cit, is easier to synthesize and leads a reduction of antibody aggregation phenomena. [88]

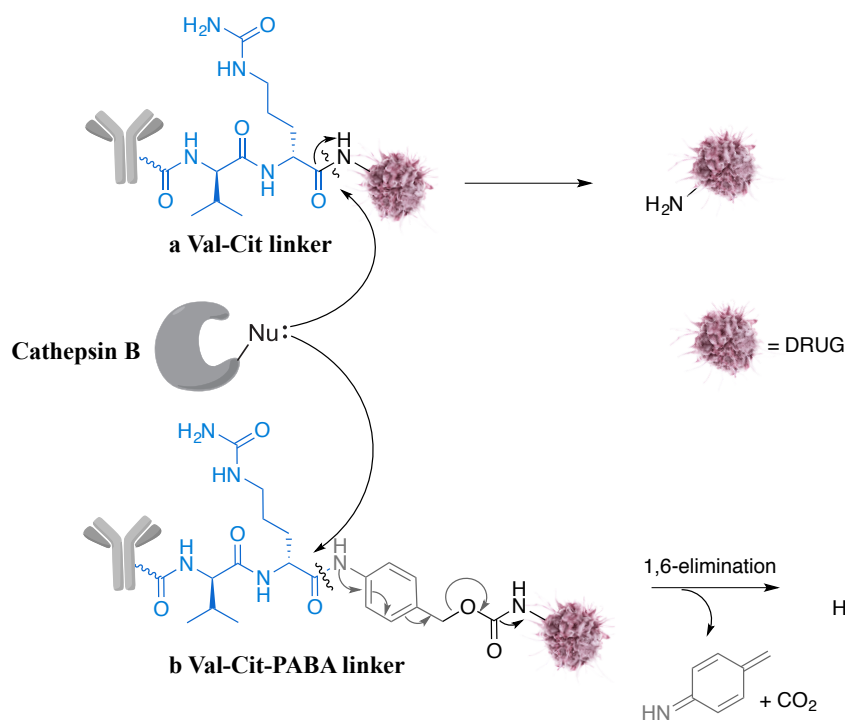


Figure 19. a) Val-Cit linker; b) Val-Cit-PABA linker and their mechanism of cleavage in presence of Cathepsine B.

1.2.2.3.2 β -glucuronidase-sensitive linkers

The glycosidic moiety is cleavage in its glycosidic bond in lysosomes by the available β -glucuronidase, a noncirtulating enzyme overexpressed in some specific tumors with a low concentration in the extracellular compartments. [89] This linker is usually combined with a self-immolative spacer PABA-like and the drugs often used are Auristatins (Figure20). [90] Compared with Val-Cit linkers, β -glucuronide linkers are highly hydrophilic with a reduction of aggregation phenomena (from 80 % to 5%) and better clearance and solubility in plasma. [91] The use of this water-soluble linker is an excellent strategy for the target delivery also for their great stability and desirable release profile. [92]

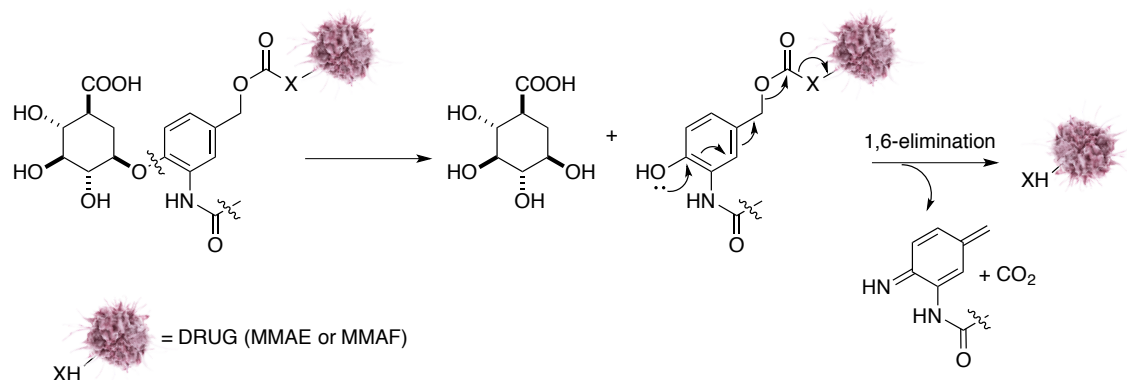


Figure 20. Mechanism of cleavage of β -glucuronidase linkers. X= O or NH.

1.2.2.4 Pre-targeting strategy-based linkers

There are some limits in the drug-conjugates techniques such as:

- the limited number of receptors on the cells surface;
- the low DAR of ADCs and so the low concentration of the cytotoxic drug that achieved the desired site;
- the difficult balance between stability and cleavability of the linker. [93, 94]

To overcome these problems, bioorthogonal chemistry pretargeting strategy (*i.e.* a click reaction to trigger release) can be used. In other words, the linker cleavage to allow the drug release depends on a biomolecular click reaction. The nontoxic targeting moiety as an azido group or a double bond can be added to the conjugates that are accumulated in the desired site after administration. This is the pre-targeting step. [95-97]

One strategy to allow the drug release is called “click and release” and require a click reaction between an azido moiety of the targeting deliver and *trans*-cyclooctene (TCO). [97, 98] Specifically, this click reaction form an unstable triazole (compound **16**, Figure 21) that releases N_2 with the formation of aldimine **17** which can be hydrolyzed giving the aldehyde **18** and the aniline **19**. This one is a self-immolative spacer that rearranges by releasing the free drug (Figure 21). [99] Even if the feasibility of this mechanism is demonstrated *in vivo* experiments are not yet reported.

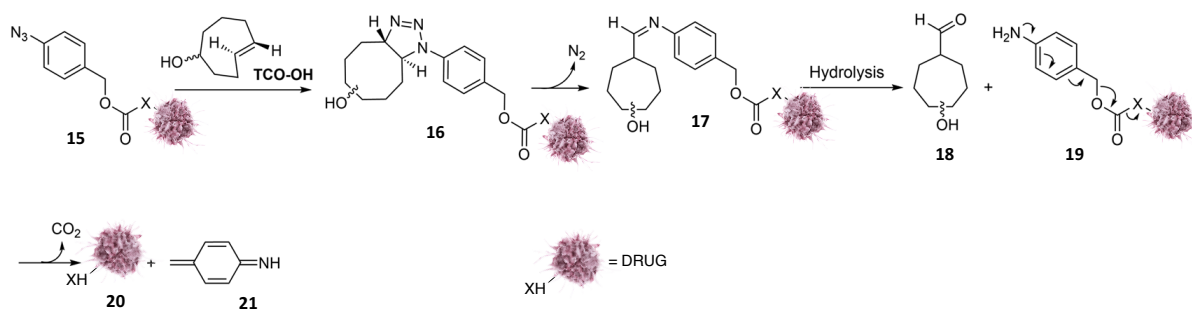


Figure 21. Mechanism of “click and release” strategy that require a click reaction between an azido moiety of the targeting deliver and *trans*-cyclooctene (TCO). X= O or NH. Drug usually used is Doxorubicin.

To accelerate the overall release process, it is possible to design a linker with TCO moiety that is very stable until when, in presence of tetrazine, it gives the formation of 1,4-dihydropyridazine intermediate **24** that tautomerized allowing the drug release by 1,4-elimination (Figure 22). [100, 101] Electro Withdrawing Groups (EWGs) accelerate the cycloaddition step contemporary decreasing the decaying reaction rate. An opposite effect is obtained by adding Electro Donating Groups in the tetrazine ring (EDGs). To take advantage from both effects, EWGs can be insert in 3-position and the donating one in the 6 (Figure 22). [102] In contrast to the “click and release” mechanism with azido e TCO, Rossin et al. demonstrated the promising release in vivo applying the strategy with tetrazine and an ADC composed of a mAb CC49 against antitumor-associated glycoprotein-72 (TAG72) and Doxorubicin *via* TCO linker. [101] The conjugate was administrated first to be accumulated in cancer cells and the extra quantity of it around the organism was removed after 24 h by the administration of albumin-based clearing agent; only after that, tetrazine with specific functional groups in 3 and 6 positions was injected without avoiding the off-target Dox release in blood. A high controlled released in the target tissues was achieved. [101]

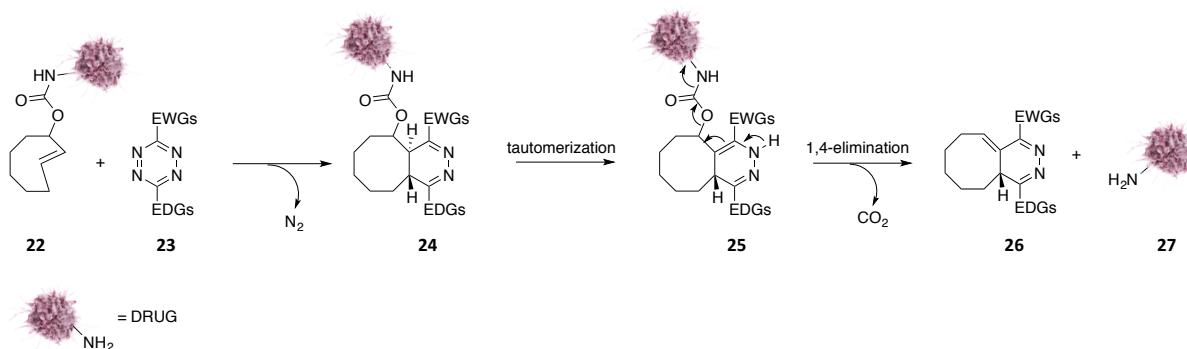


Figure 22. Mechanism of “click and release” reaction between tetrazine and *trans*-cyclooctene (TCO). the commonly used drug is Doxorubicin. EDGs = electro donating groups; EWGs = electro withdrawing groups.

The pre-targeting strategy with click reactions is a great complementation of linker chemistry design for the development of drug delivery systems, even if it presents some difficulties in drug administration that must be further investigated. This type of mechanism could be exploited for the design of non-internalizing ADCs or for SMDCs that, after the drug release tetrazine-mediated, the bystander killing effect promotes the free cytotoxic molecules diffusion in the target tumor cells. Many different non-internalizing ADCs based in biorthogonal chemistry are now in different phases of clinical trial. [103]

1.2.2.5 Self-immolative spacer

“Self-immolative spacers are covalent assemblies tailored to correlate the cleavage of two chemical bonds after the activation of a protective part in a precursor”. [104] The removal of the protecting group (PG) leads to a series of electronic rearrangements and irreversible unimolecular reactions with the release of the drugs without any linker residuals. The spacer is usually placed between the payload and the linker and it is a crucial point of an ADC, giving a more controlled release because of its ability to rearrange after linker degradation. Many different spacers are described in literature. They usually are triggered by many external *stimuli* (*i.e.* chemical reagents, enzymatic or light-driven activations) that cause a self-elimination or cyclization arrangement. [105, 106] The most famous one is the PABA-like self-immolative spacer that allows the drug release by 1,6-elimination. 1,4-, 1,6- or 1,8-eliminations in *p*-amino, hydroxyl(cinnamyl) alcohol or coumarinyl alcohol spacers involve the aromatic structure with amino, hydroxyl or thiol groups masked with a PG (linker) to reduce the nucleophilicity. After external *stimuli*, the linker is processed with the removal of the spacer capping group. In this step, the free nucleophilic group (*i.e.* amine, phenol or thiol), with its electronic pair, is able to promote the aromatic spacer arrangement releasing the drug (Figure 23). The process is irreversible and spontaneous driven by positive entropy (*i.e.* by CO₂ release). [107] An increase of electron density with electron-donating groups (*i.e.* –OMe) can promote the dearomatization by transient positive charge stabilization with an improvement of the speed of release. The release is fast when the spacer is linked to payload through carbonate or carbamate moieties because thermodynamically favored by CO₂ emission. Otherwise, drugs direct linked in benzylic position with their –NH₂ or –SH moieties are not released. [108]

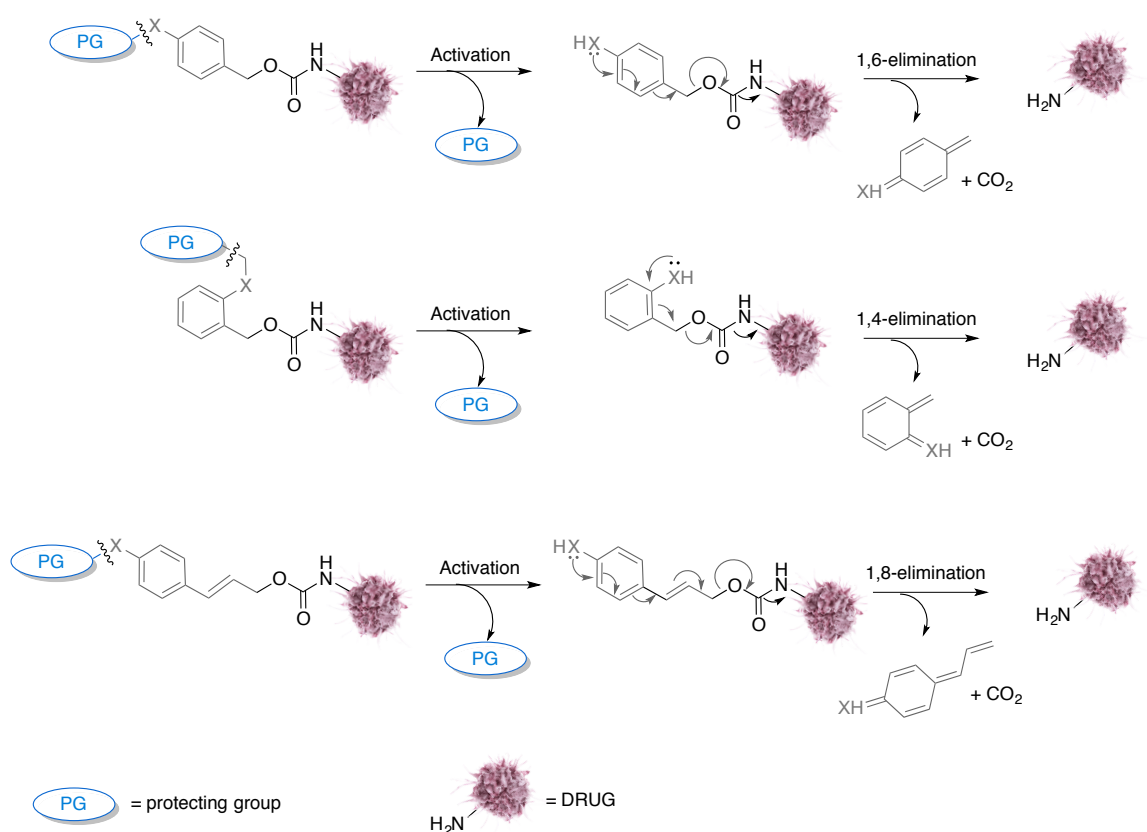
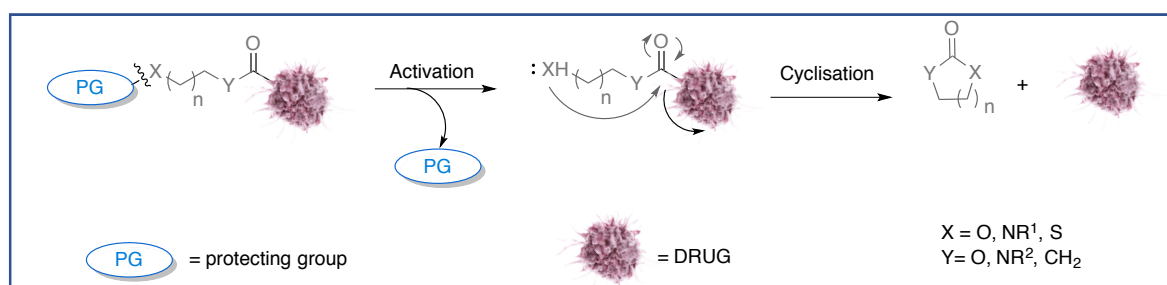


Figure 23. Self-immolative spacer relying on an electronic cascade for drug release. PG = protecting group; X = O, NH, S. **a)** 1,6-elimination (PABA like), **b)** 1,4-elimination, **c)** 1,8-elimination.

Spacers with cyclization mechanism are based on the activation of the nucleophilic group that attacks on a carbonyl moiety with a formation of thermodynamically favored 5- or 6- terms rings by-product (Figure 24). The addition of –Me in α position of the carbonyl promotes the cyclisation by Thorpe-Ingold effect. [109] The quite common cyclizing self-immolative spacers are usually composed of alkyl chains like mercaptoethanol (Figure 24 a), ethylenediamine-carbamate (EthCarb –Figure 24 c) or by *ortho*-substituted aromatic derivatives (Figure 24b). [104]



Examples:

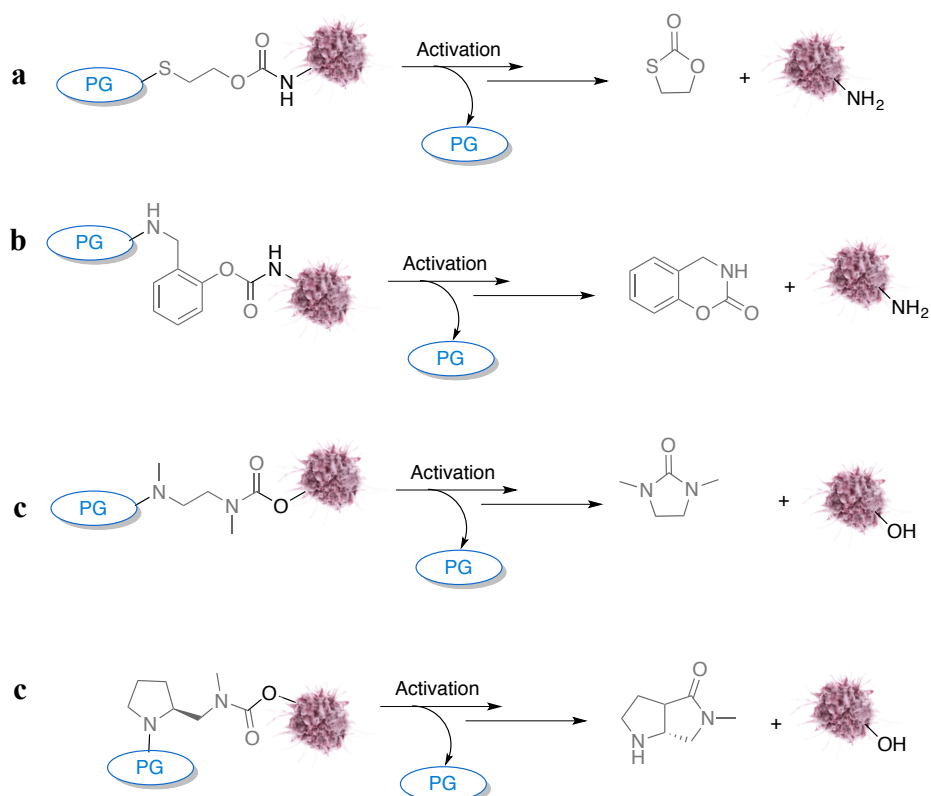


Figure 24. Self-immolative spacers relying on a cyclization for the drug release. **a)** mercaptoethanol spacer, **b)** *ortho*-substituted aromatic derivatives, **c)** ethylenediamine-carbamate (EthCarb), **d)** spacer with proline scaffold for hydroxy-bearing payload release.

Amine-containing payloads are easily connected to a self-immolative spacer by a stable carbamate moiety. Alcohol and thiol are less nucleophilic than amines (better leaving group) and consequently it is consequently difficult to bind them to the spacer. [110]

Alcohol-bearing payloads could be connected with few strategies. The most used method leads to a carbonate moiety that, however, has a poor stability at physiological pH. [111] The strategy aforementioned has been employed for the development of Trodelvy® approved by the FDA in 2020, in which PABA spacer is linked with SN-38 through a carbonate function. [25] Another solution, only for phenolic derivatives, could be the alkylation of phenol moiety with the benzyl alcohol of PABA-like spacer. The result is a more stable compound in physiological

condition and it is able to release the drug in a very efficient way. [112] A further common approach is a double self-immolative spacer with both 1,6-elimination and cyclization mechanisms that takes advantage of dicarbamate resulting moieties (*i.e.* trastuzumab duocarmazine): the limited step is the cyclisation (Figure 25). [113]

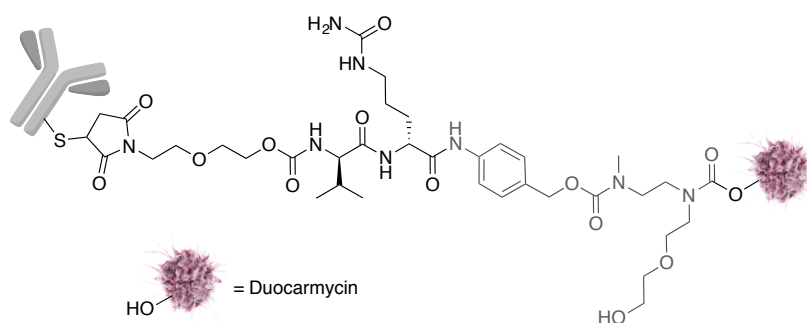


Figure 25. Trastuzumab duocarmazine: in grey, a double self-immolative spacer for hydroxy-bearing payload released by 1,6-elimination and cyclization mechanisms. The PEG chain is added to increase polarity of the ADC.

Another drug conjugation strategy involves the introduction of methylene-alkoxy carbamate (MAC) construct linked to PABA self-immolative spacer. The *N*-methylene-alkoxy spacer has been used in the ADC field since 2016. [114] The mechanism is the following: after linker cleavage, the PABA-like spacer arranges itself by 1,6-elimination to obtain a hemiaminal derivative of formaldehyde **31** giving CO₂ and the quinone **30** as byproducts. The intermediate **31**, thanks to N double pair, undergoes hydrolysis with the release of the drug (*i.e.* Auristatin E or Camptothecin derivative SN38) plus methanimine **32** as side-product (Figure 26). [115]

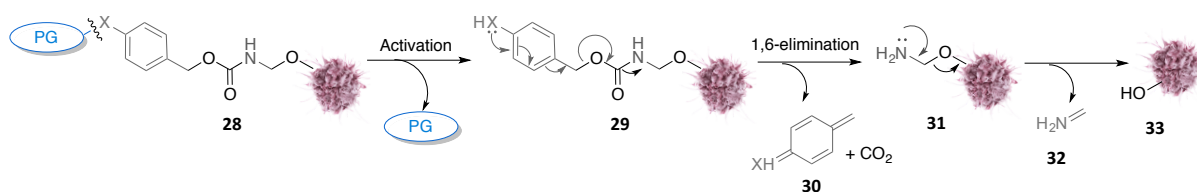


Figure 26. Mechanism of release of PABA and *N*-methylene-alkoxy spacers.

N-methylene-alkoxy spacer can be used alone without further spacers and directly connected to the alcohol group of the payload (*i.e.* topoisomerase I inhibitor DS-8201a) exploiting the same efficiency in drug release ratio. [116]

A new self-immolation by cyclization, not yet employed in the development of an ADC, is based on proline scaffold that promotes a suitable hydroxy-bearing payload release and improves anticancer efficacy *in vitro* (Figure 24d). [117]

In the field of novel anticancer prodrugs, a new spacer was developed with the aim to have a highly controlled drug release combining hypoxic status with UV illumination. Focused on the hypoxic *stimuli*, they occur during acute and chronic inflammatory diseases and tumors growth. In solid tumors, nitroreductase (NTR) is overexpressed and directly correlated to a hypoxic environment. This enzyme catalyzes the reduction of $-\text{NO}_2$ group to an $-\text{NH}_2$ moiety and, for this reason, the substitution of the aniline moiety into $-\text{NO}_2$ in a PABA-like spacer allows the release of the drug by 1,6-elimination specifically in hypoxic conditions (Figure 27). Feng et al. in 2016 designed a new anticancer prodrug using Gemcitabine as drug merging internal (hypoxia) and external (photo) sequential control in tumor cells (Figure 27). [118]

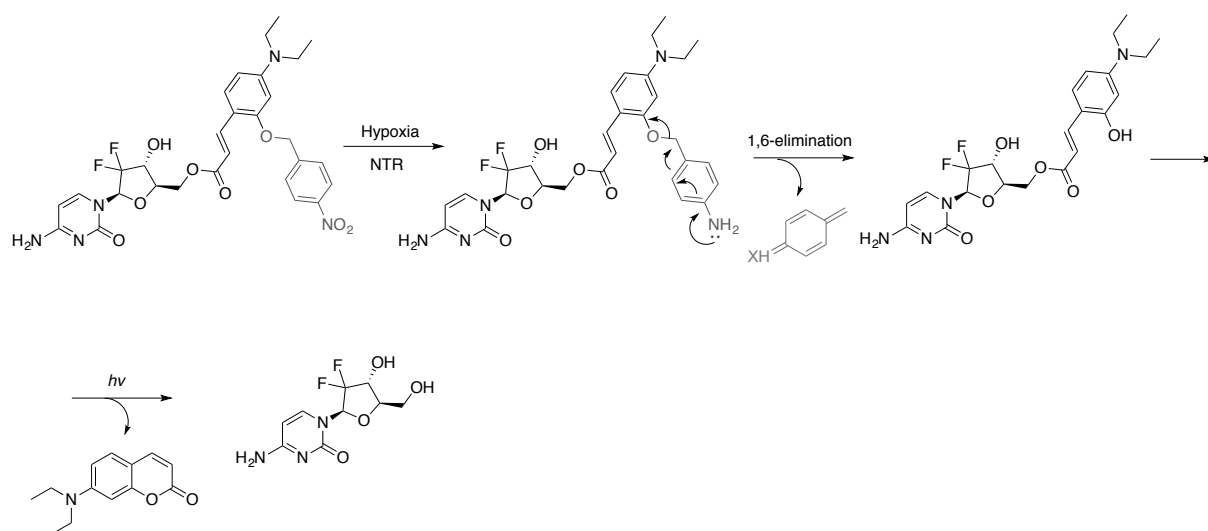


Figure 27. Prodrug based on hypoxia and photo ($h\nu$) sequential control. NTR = nitroreductase.

In a high sophisticated drug delivery system two spacers can be introduced to improve the driving force of drug release and based on a double PABA-like spacer, on a dual-cyclization spacer or matching spacers with elimination and cyclization rearrangement. When a PABA-like spacer is combined with a ethylenediamine-carbamate construct, the release is completed in only 10 minutes, contrary on what happens using a single PABA spacer with which the release is slower. An explanation could be that the extended linker with a double spacer is a better substrate to be triggered. Other linkers, with a dual-cyclization spacer, give the release in 30 minutes. The CO_2 elimination from the carbamate linker offers an additional thermodynamic driving force for the drug release, while a double cyclization is kinetically disadvantaged. [119] The structure and the kinetic release of the linker-spacer are important factors for the development of a functional ADC.

1.2.2.6 Polarity

The polarity of the linker is a key parameter for the development of ADCs. Many problems, as low water solubility, aggregation with the antibody and drug resistance by up-regulation of MDR1 gene can occur when an ADC has a low polarity. It is known that the transport of hydrophobic compounds out of the cell is more efficient than hydrophilic compounds' transport due to the presence of P glycoprotein (Pgp) as a result of MDR1 gene encoded. ADCs with a high level of aggregation have a fast clearance and poor half-life. [120] Many strategies can be used to increase the linker polarity. The most popular solution is the insertion of a small PEG chain in the linker structure (Figure 25). [121, 122] Other strategies involve the insertion of negatively charged sulfonate groups and pyrophosphate diesters. [121, 123]

1.2.3 Payloads

Although if there are a huge variety of cytotoxic drugs approved, only a limited number of those are suitable for the development of ADCs. First of all, the drug must have precise properties to be a good payload. Moreover, some ADCs can have a low penetration ability that causes a lack of anticancer activity due to a low drug concentration inside the target cells. [124] For this reason, the attention is played on high potent cytotoxic drugs that are overly toxic in the canonical chemotherapy. The activity of the drugs must be in a range from nanomolar to even picomolar IC_{50} . [125] The most important aspect is the chemistry of the active molecule that must have a "chemical handle" to bind the linker. All these restrains cause limitations in choosing the suitable cytotoxic molecule. Tubuline inhibitors as Auristatins and Maytansinoids are the most used but also other classes of cytotoxic drugs are taken in account for the design of an ADC. [10]

Maytansine is a natural benzoansamadolide that comes from the bark of the African shrub *Maytenus ovatus*. It is able to bind tubulin and inhibit microtubule assembly. [126] Various semisynthetic derivatives were developed in order to insert in the phenyl ring or in the N'-acyl group a moiety for the linker binding. The alanyl ester side chain, the epoxide moiety, the carbinol function and the double bonds are the critical elements to retain the activity. DM1 (Mertansine or Emtansine) and DM4 (Ravtansine or Soravtansine) were designed by ImmunoGen, a specialized company on the ADC field (Figure 28). The additional sulfhydryl group with different steric hindrance in these two semisynthetic compounds controls the

conjugate's intracellular clearance and offers a connection with the linker. [127] DM1 and DM4 are present in many ADCs because of their excellent stability and their great water solubility.

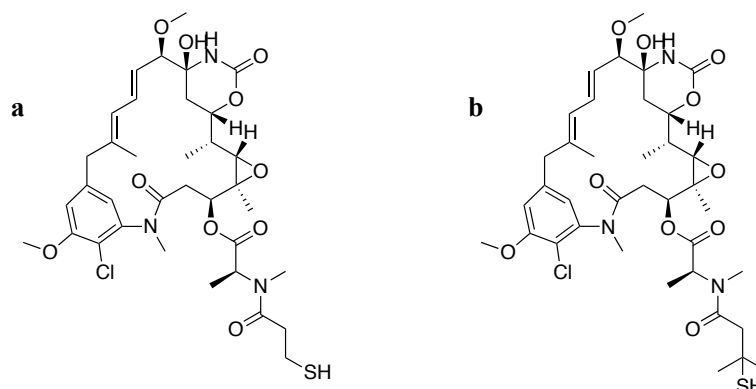


Figure 28. Structures of **a)** DM1 and **b)** DM4.

Auristatins are the main group of drugs used in ADCs field. [128] Auristatins are natural dolastatins, linear pentapeptides extracted from the sea hare *Dolabella auricularia* that have the property to inhibit tubulin. [129] Total synthetic derivatives like Monomethyl Auristatin-E (MMAE) and Monomethyl Auristatin-F (MMAF) were synthesized by Seattle Genetics, to improve the drug hydrophilicity and allow a suitable point for the linker by changing tertiary amine moiety into a secondary group (Figure 29). Both these synthetic Auristatins are currently used in many ADCs. MMAE is less toxic than MMAF. Moreover, it has a better pharmacokinetic profile due to its different polarity that allows drug release in a neutral form. [130] Today, other Auristatins, like PF-06380101, are developed as payloads in clinical trials. [131]

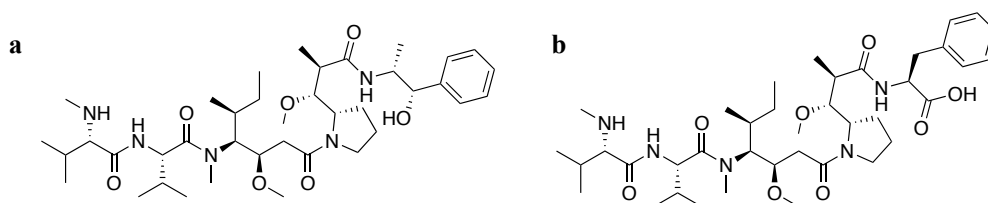


Figure 29. Structures of **a)** MMAE and **b)** MMAF.

Calicheamicins represent a class of antitumor antibiotics isolated from the actinomycete *Micromonospora echinospora*. They bind the minor groove of DNA, cleaving the double-strained DNA in a site-specific way: after the DNA binding, Calicheamicins undergo a Bergman cyclization with the generation of diradical species that tear away hydrogen atoms

from the DNA deoxyribose backbone, leading to a strand scission. [132] The 10-membered enediyne Calicheamicin γ_1^I (Figure 30) is the most studied derivative of the group and is chemically composed of:

- an aglycone containing a unique bicyclo[7.3.1]tridec-9-ene-2,6-diyne system with a labile methyl trisulfide group,
- an aryltetrasaccharide chain composed of a hydroxylamino sugar, a thio sugar (linked with a non-canonical N-O-glycosidic moiety),
- a hexasubstituted iodothio-benzoate and
- a rhamnose sugar. [133]

High potency N-acetyl Calicheamicin γ_1^I derivatives are usually used in many ADCs.

Only few molecules *per* antibody can be conjugated due to the elevated hydrophobicity of these drugs that cause aggregation problems. The complex structure of this class does not permit an accurate structure-activity study and a lack of new semisynthetic optimized derivatives is the result. [134]

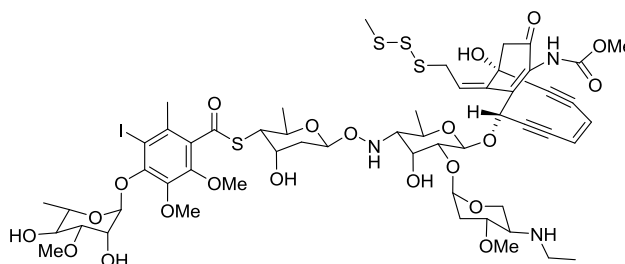


Figure 30. Structure of Calicheamicin γ_1^I .

Pyrrolobenzodiazepins (PDBs) are one of the growing class of payload. [135] Anthramycin was the first PDB isolated in 1965 from *Streptomyces refuineus*. [136] PDBs bind the DNA minor groove in a site-specific manner with a covalent bond between their C11 position and C2-NH₂ groups of DNA guanine bases. PDBs are so attractive because of their easy synthesis. For this reason, many different synthetic derivatives were developed. Especially PDB propyldioxy dimers are used as potential payloads for ADCs in clinical trials making this class the third most used after Auristatins and Maytansinoids. [137] PDB dimers have picomolar activity against specific tumor cell lines and can be divided in symmetric and non-symmetric compounds that are both able to perform a crosslink DNA binding with the opposite guanine bases. PDB dimers SGD-1882 and SG-3199 are the most commonly used for the development of ADCs exploiting as reactive point its aniline moiety or the imine group after its reduction in a secondary amine (Figure 31). [138]

Indolinobenzodiazepins (IGNs) are structural analogues of PDBs. IGNs have a higher affinity towards DNA and easier linker attachment points due to the addition of a fourth bioisosteric ring near the pyrrole ring and the insertion of an aromatic ring in the middle of PDB dimers aliphatic chain. Another important structural difference is that only one of indolinobenzodiazepins moiety contains an electrophilic imine group, while on the other side there is a non-electrophilic secondary amine. For this reason, this class mono-alkylates the DNA contrary to PBS with a decrease of toxicity (Figure 31c). [138]

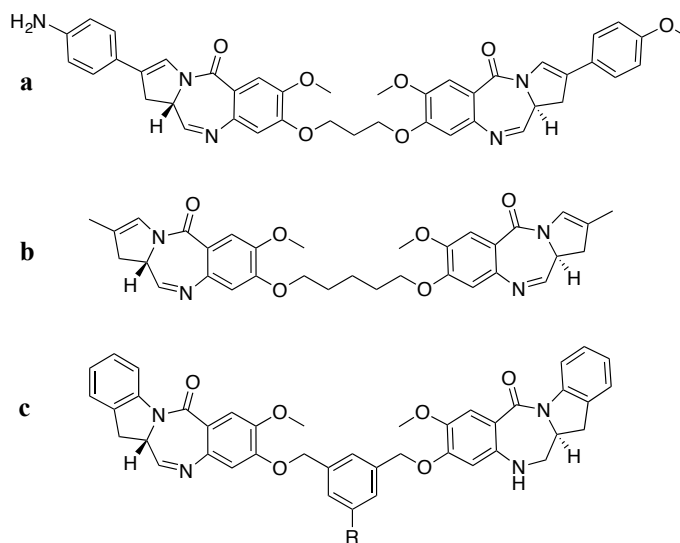


Figure 31. PBSs synthetic derivatives **a)** SGD-1882, **b)** SG-3199 and the general structure of indolinobenzodiazepins **(c)**.

Camptothecin (CPT) was isolated in 1966 from the bark and stem of *Camptotheca acuminata* and is a topoisomerase I inhibitor. It has high cytotoxic activity but low solubility and instability because of the lactone ring presence in the structure. To overcome the limits, a great number of derivatives, with different substituents in various positions of the five rings, has been developed. [139] SN-38, the active metabolite of the prodrug Irinotecan, and the water-soluble DX-8951 are used in ADCs already approved (*i.e.* Trodelvy® and Enhertu®) as well as in bioconjugates in clinical-stages (Figure 32).

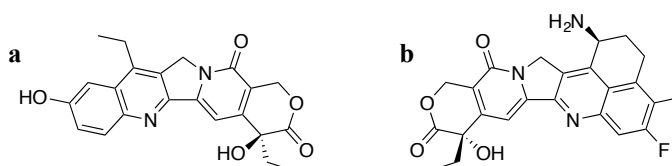


Figure 32. Structures of **a)** SN-38 and **b)** DX-8951.

Duocarmycins are isolated from various *Streptomyces* bacteria and are able to bind to the minor groove of DNA by the alkylation of the adenine at the N3 position (Figure 33). [140] Many synthetic analogues have been synthesized and, for example, the ADC trastuzumab duocarmazine results more potent than trastuzumab emtansine in cell lines with low HER2 expression. [113]

Tubulysins are linear tetrapeptides isolated from *myxobacterium Archangium gephyra* with an antimicotic activity that inhibit microtubule polymerization with the same Auristatins mechanism of action. The advantage of this class of compounds is the high affinity with MDR1. [141] These molecules (*i.e.* AZ13599185) are excellent candidates as payloads for their high hydrophilicity, their easy synthesis and their multiple moieties suitable for linker attachment (Figure 33). [142]

Amatoxins are bicyclic octapeptides isolated from *Amanita phalloide* mushroom. These molecules are RNA polymerase II inhibitors and represent a very promising class of payloads because of their high potency and their interesting pharmacokinetic properties. α -Amanitin is the active molecule that causes death by eating *Amanita phalloides* mushrooms (LD₅₀ 0.1 mg/kg) but also gives excellent results used as payload in preclinical test against colorectal cancer cells (Figure 33). [143]

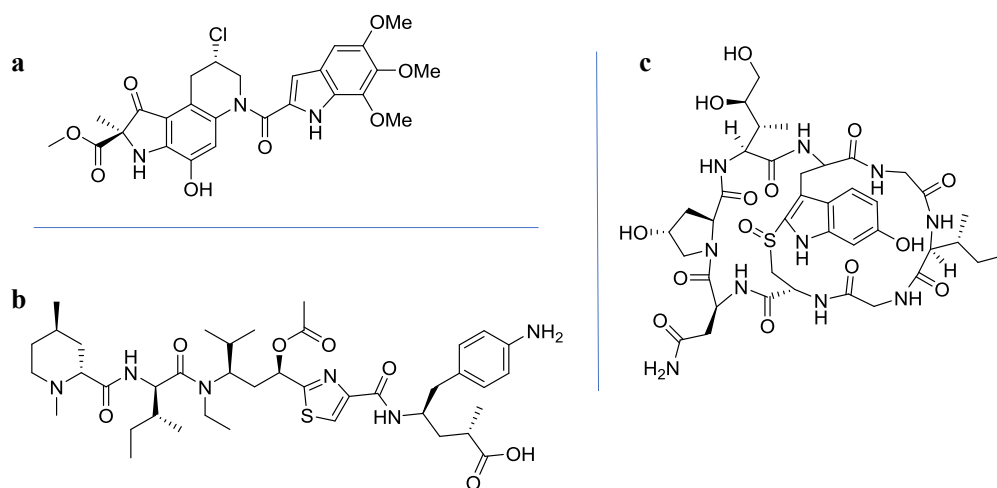


Figure 33. Structures of **a)** Duocarmycin C1, **b)** AZ13599185, **c)** α -Amanitin.

Anthracyclines (*i.e.* Doxorubicin and Epirubicin) represent a class of antimicotic cytotoxic drugs extracted from *Streptomyces* bacterium and, unluckily, they have a lower potency compared to the other payloads. Doxorubicin is still used in some clinical trials (*i.e.* Milatuzumab Doxorubicin is in clinical phase II), although it presents low efficacy and light

instability. On the other hand, Doxorubicin has a great hydrophilicity and presents in its structure different functional groups that are easy linker attachment points. Moreover, this drug is cheap and its pharmacodynamics is well-known and simple to establish (Figure 34). [144]

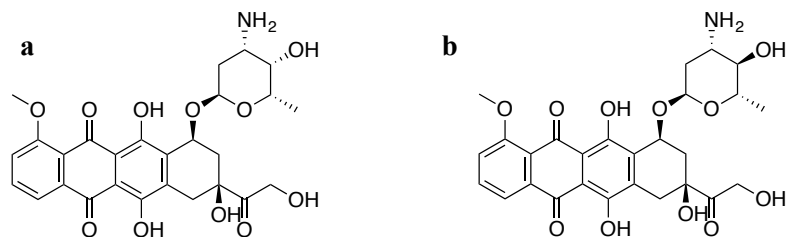


Figure 34. Structures of **a)** Doxorubicin and **b)** Epirubicin.

Combretastatins is a family of natural phenols isolated from the South Africa bush willow *Combretum caffrum*. [145] Some of these molecules have an ethene bridge between the two aromatic rings. For this chemical structure, these active molecules, such as the Combretastatin A-4, can be part of stilbenoids. Combretastatin A-4 is known as a potent cytotoxic agent due to its tubulin binding, but not yet approved by the FDA (Figure 35). Its disadvantage is the low water solubility that limits its development. The water-soluble analogue, Combretastatin A-4 phosphate (also called Fosbretabulin) could be recognized by the FDA as orphan drug for the treatment of ovarian and thyroid cancers in combination with paclitaxel and carboplatin (advanced clinical trials). [146] Nani et al. [147] and Toki et al. [148] used Combretastatin A-4 to evaluate their novel release strategy. In 2021, Huang et al. developed an ADC with the focus of enhancing the antitumor activity of Combretastatin A-4 with very good results. [149]

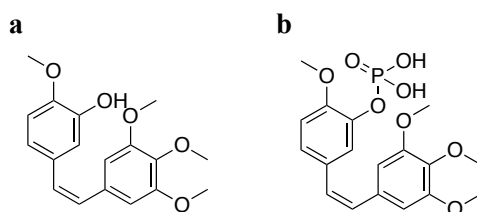


Figure 35. **a)** Combretastatin A-4, **b)** Fosbretabulin.

1.2.3.1 Other payloads

New payloads being studied to identify new potent classes of drugs able to be conjugated in the field of anticancer therapy or for other diseases. All the ADCs designed with these drugs are in preclinical or clinical study and represent a good chance for the future.

1.2.3.1.1 Epigenetic modulators

Epigenetic modulation plays the main role in maintaining the homeostasis of the cells by post-translational modifications as methylations, ubiquitinations, phosphorylations and acetylations of histone proteins that regulate the transcription of genes. A gene would be expressed depending on the degree of DNA wrapped around histones. The condensation of DNA in chromatin due to the post-translational modifications does not allowed the gene transcription. In particular, acetylation of histones, that is fully reversible, has gained much attention because of its importance on gene expression. There is a balance between the activities of histone acetyltransferases (HATs) and histone deacetylases (HDACs). The acetylation promotes gene transcription; this chemical modification of histone amines (into amides) decreases its binding to the DNA. Histones are normally positively charged for the presence of amine moieties of lysine and arginine amino acids. The acetylation neutralized the positive charges decreasing the interaction between histone and DNA with a chromatin expansion and the relative genetic transcription. HDACs play a fundamental role on the down-regulation of genes transcription. These enzymes are subdivided in 4 classes with a total of 18 isotypes. Class I, II and IV of HDACs are zinc-dependent, while class III are NAD⁺-dependent. [150]

An inhibition of HDACs influences the chromatin structure and the gene expression. In some tumors, HDAC inhibitors leads to an up-regulation of gene p21 with the induction of apoptosis and a cell cycle arrest as consequence. The inhibition of the deacetylation modulates the equilibrium between pro- and anti-apoptotic proteins (*i.e.* with the transcription of pro-apoptotic genes like Bmf and Bim) causing tumor cell death. [151]

HDAC inhibitors (*i.e.* Vorinostat also called SAHA) are currently used in anticancer therapy as well as for inflammatory and neurology diseases (*i.e.* Alzheimer). [152]

HDAC inhibitors are divided in four classes:

- 1- hydroxamates such as Vorinostat (Figure 36 a), Belinostat, Panobinostat and Dacinostat (the only one not yet approved by the FDA – Figure 36b);
- 2- cyclic peptides like Romidepsin (Figure 36c);

- 3- aliphatic acids like Valproic Acid (Figure 36d);
 4- benzamides such as Entinostat (Figure 36e). [153]

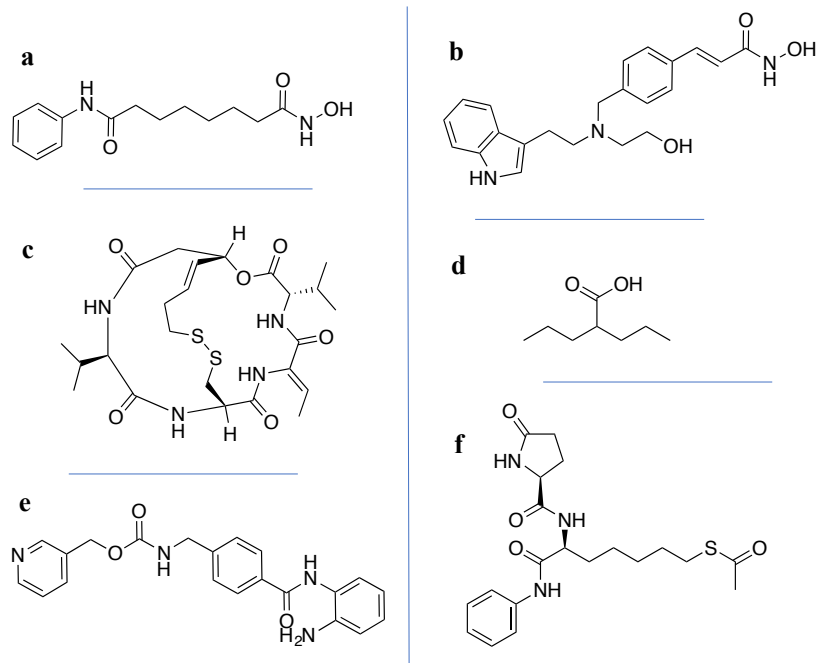


Figure 36. Structures of **a)** Vorinostat/SAHA, **b)** Dacinostat, **c)** Romidepsin, **d)** Valproic Acid, **e)** Entinostat, **f)** ST7612AA1 a novel pan-HDAC inhibitor thioacetate- ω (γ -lactam carboxamide) derivative.

In 2018, the research group in which I have worked during my PhD developed two new ADCs charged with the HDAC inhibitor ST7612AA1 for targeting epigenetic modulation (Figure 37). The novelty, described for the first time in literature, was the loading on the mAbs with not highly cytotoxic drugs. ADCs charged with ST7612AA1 showed in mice high activity and low off-target toxicity compared to ADCs conjugated with cytotoxic payloads. The difference is related to the different mechanisms of action (epigenetic mechanism of action for HDAC inhibitors). [20] ST7612AA1 (Figure 36f) is a novel pan-HDAC inhibitor ($IC_{50} = 70$ nM on NCI-H460 cell lines) developed by Alfa-Sigma in collaboration with University of Siena. It is a thioacetate- ω (γ -lactam carboxamide) derivative selected from a large class of new analogues of Vorinostat. [154] ST7612AA1 showed high activity in xenograft models of colon, lung, breast and ovarian carcinomas, leukaemia and lymphoma, and with a possible effect on HIV-1 latency reactivation. [155, 156] This inhibitor has a very low IC_{50} if compared to common cytotoxic payloads leading to low off-target toxicity with a probably retention of activity due to epigenetic mechanism of action. Using its thiol moiety, ST7612AA1 was conjugated with Cetuximab through an uncleavable linker (ADC **34**, Figure 37) and with a peptide-sensitive

linker (ADC **35**, Figure 37) that resulted to be the best one (DAR = 8). [20] In 2021, we have tried to expand the class of ADCs armed with HDAC inhibitors by using as payloads two different hydroxamic acid: Vorinostat/SAHA already approved by the FDA for the treatment of cutaneous T-cell lymphoma (CTCL) and Dacinostat. [157] Both Trastuzumab and Cetuximab mAbs as well as uncleavable and peptide-sensitive linkers were investigated. The best ADC profile in terms of anti-proliferative activity on A549 cells was achieved with Cetuximab linked with Dacinostat through a non-cleavable linker based on *p*-mercaptobenzyl alcohol structure (ADC **36**, Figure 37). ADC **36** inhibited cell proliferation in a dose-dependent manner ($IC_{50} = 90 \pm 3.4$ nM) quite similar to Dacinostat ($IC_{50} = 33 \pm 1.7$ nM). We can affirm that we have developed a new class of antibody drug conjugates which deliver non-cytotoxic hydroxamic acid for epigenetic modulation and we have designed a linker able to release hydroxamic acid-bearing payloads. [157]

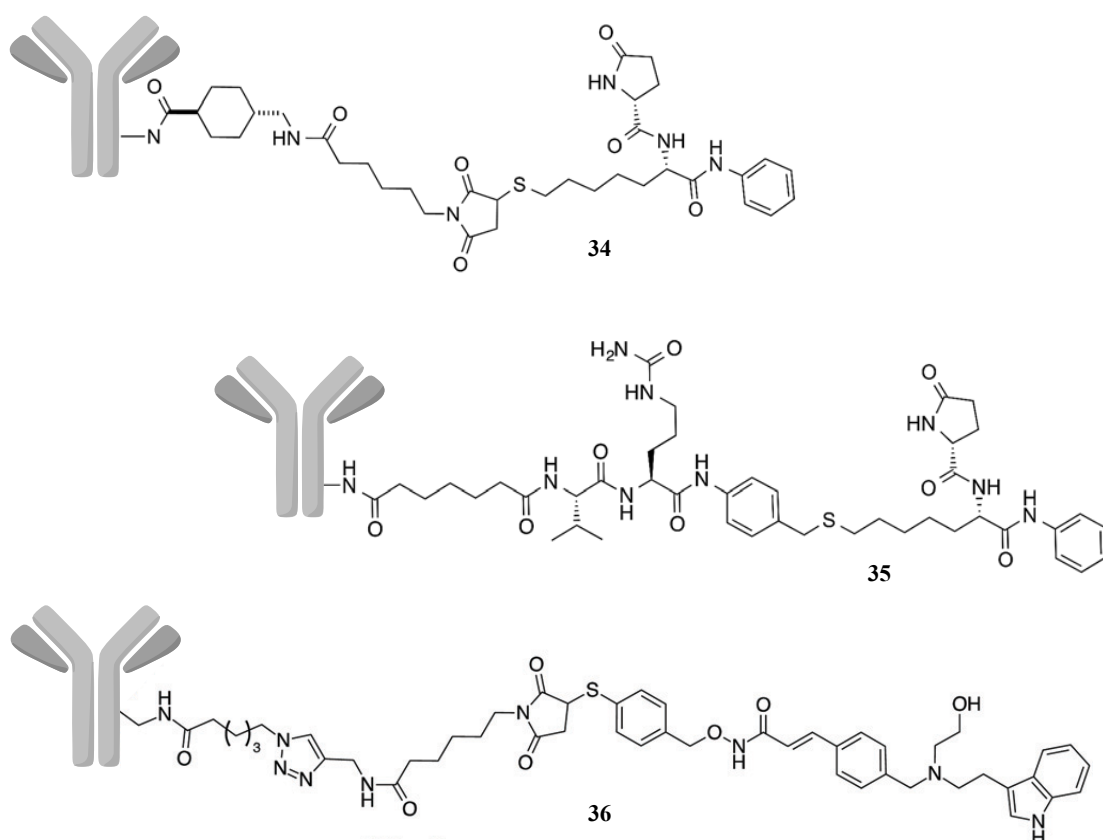


Figure 37. ADCs armed with HDAC inhibitors.

The production of an ADC based on these inhibitors may open new routes for a selective HDAC isoforms targeting not only for the treatment of tumors but also for other types of diseases that may benefit from epigenetic modulation.

The use of high cytotoxic payload could be overcome by decreasing its typical off-target toxicity. [20]

1.2.3.1.2 Payloads for non-oncology indications

A growing field is the development of ADCs for the treatment of immune and infective diseases by using well-known therapeutic drugs. [158, 159] Regarding the treatment of inflammatory diseases immunosuppressive ADCs were designed. Direct antibodies, that target the hemoglobin scavenger receptor CD163 in macrophages, were used linked with the corticosteroid drug dexamethasone. The therapeutic anti-inflammatory effect of glucocorticoids would result in anti-inflammatory response by suppressing the release of pro-inflammatory factors by macrophages as shown in studies on mice. [160] Another ADC, that modulates the inflammation cascade, is composed of an intracellular tyrosine kinase (Lck) inhibitor called Dasatinib connected to an HCLX mAb specific for human T lymphocytes through a mixed hydrazone-disulfide linker. The humanized HCLX antibody selectively binds with high affinity to CXCR4, an antigen expressed on hematopoietic cells, resulting in a suppression of T-cell-receptor-mediated T-cell activation and cytokine expression. [161] Anti-infective drug conjugates were also investigated. An ADC against intracellular *Staphylococcus aureus* was developed for the treatment of *S. aureus* resistance phenomena that causes failure of the conventional antibiotic treatments. This innovative Antibody-Antibiotic Conjugate (AAC) consists of a THIOMAB engineered *S. aureus* antibody connected by a peptide-sensitive linker to the tertiary amine of the Rifalogue (a rifamycin analogue with higher potency than vancomycin in murine models). [162]

1.2.3.1.3 SMO inhibitors: unexplored payloads

Other molecules, that during my PhD period have been taken in consideration as a new class of payloads for the development of ADCs, are the SMO inhibitors. In order to have a more comprehensive understanding of the overall project regarding the development of ADCs charged with SMO inhibitors, a brief introduction of what is SMO and which pathway is involved must be done (See Paragraph 1.3).

1.2.4 Bystander effect

The drug can be found in the extracellular space because of a linker cleavage occurred outside the target cells (*i.e.* non-internalizing ADC or prodrugs) or because of a diffusion of it through the plasmatic membrane after the drug delivery system internalization and processing in the target cell.

The drug concentrated in the extracellular target environment is taken up by the cells near to the “original targeted” ones, killing them. These cells can be tumoral or healthy and can either express or not the target antigen. For this reason, the bystander effect is not selective but can be exploited in case of heterogeneous tumors, in which the antigens are not regularly expressed. [22]

The bystander effect for the internalizing delivery systems depends on:

- the ADC internalization level after the antigen binding (Figure 5),
- the type of the linker,
- the polarity of the active molecule and the consequent permeability of the drug across the membrane. [163] For example, MMAE can usually diffuse in the immediate surroundings because it is released in its neutral form; otherwise MMAF is usually released in a charged form that does not allow the diffusion. [164]

In the case of Adcetris®, the bystander effect has a key role, because less than 10% of target tumor cells express the antigen CD30. As confirmation of the importance of bystander killing mediated by MMAE released from dying cells, tumors with different expression of CD30 were tested with Brentuximab Vedotin giving similar responses. [165, 137]

The bystander effect is the bedrock for many ADCs in clinical trials for the treatment of heterogeneous tumors and, of course, for the design of Small Molecule Drug Conjugates that fully take advantage from that. [17, 166, 167]

The bystander effect could be also enhanced for the design of internalizing target delivery system in which the drug is an inhibitor or antagonist of a transmembrane receptors (*i.e.* GPCR) and, to carry out their function, must be found in the surrounding of target cells.

1.2.4.1 Non-internalizing ADCs

At the beginning an efficient internalization of the bioconjugates was considered mandatory for a successful result. The ADC internalization is not essential for some kind of cleavable linkers that are stable in physiological condition but also able to release the drug in the extracellular

target environment. Thanks to the bystander killing effect, the drug diffuses through the membrane cells exploiting its function. According to this explanation, many ADCs direct to non-internalizing antigen have been designed. [24]

In the tumoral extracellular environment there are usually different conditions compared to healthy tissues in terms of pH, expression of enzymes and redox properties. The differences are used for the cleavage of the linker of non-internalizing ADCs and SMDCs as well resulting in potent bystander effect by drug released accumulation. The extracellular pH of tumor tissues is usually more acid than in healthy conditions and pH-sensitive linkers like hydrazones could be cleaved. [168] Tumor microenvironment has usually high reducing enzymes that carry out the degradation of disulfide linkers regardless of ADC internalization. [169] Also enzymatic-sensitive linkers, like peptides, can be cleaved by proteases outside the cell. The relative high concentration of Cathepsin B as well as extracellular proteases like the fibroblast activation protein- α (FAP- α) and the matrix metalloproteinase-2 (MMP-2) are the protagonists of this cleavage. [170] Both the Val-Cit and the Val-Ala dipeptides have been used as linkers for non-internalizing ADCs because they are able to release the drug after their cleavage by Cathepsin B in the extracellular environment. [171]

The “click to release” mechanism of drug release can be used for non-internalizing ADC using the trans-cyclooctene (TCO) and an appropriate tetrazine (Figure 22). [101]

The development of non-internalizing ADCs states that intracellular processing of ADCs it is only one of the possible mechanism of action. The selection of the right linker in addition with the bystander effect could give good opportunities for the treatment of specific tumor microenvironment features (*i.e.* hypoxia) improving the number of targetable tumors. [172]

1.2.5 Bioconjugation strategies

Lysine and cysteine are usually used as sites for conjugations because of their nucleophilicity that allowed an easy reaction with activated linkers forming stable covalent bonds. Both aminoacids allow to conjugate the sequence linker-payload without any preliminary antibody modification or the use of difficult synthetic routes, but just mixing them in aqueous buffers and DMSO. The disadvantage is the heterogeneity of the resulting products, with a wide distribution of drug-antibody ratios (DARs) that decrease the efficacy of ADCs. Moreover, aggregation problems, difficulties on purification, clearance rate increase, premature drug release, hard analytical characterization and variable pharmacokinetics properties can occur. [173] Each batch of ADC is composed of a heterogeneous mixture of free and bioconjugate

mAbs and can have a different DAR. In each ADC, the sequence linker-payload could be connected to the antibody with different aminoacids leading to different properties in the same mixture. Make an optimization is difficult also because it is still unknown which is the optimal DAR to have sufficient activity without loss of antibody physiological properties. Moreover, the attachment site influences the stability of the linker. [174] In order to overcome these problems, many different site-specific conjugation technologies have been developed by use of engineering antibodies and currently there are some ADCs in clinical trials that are conjugated in a site-specific manner. [36]

DAR is a value which indicates the number of drug conjugated to the mAb and used to identify the drug loading. UV/Vis spectroscopy is the easiest analytical method to measure it, but the most accurate method used is MALDI-TOF mass-spectroscopy. [175] DAR is can be easily calculated by MALDI spectra of purified ADCs using the formula $(\text{MALDI}_{\text{mw}} - \text{mAb}_{\text{mw}})/\text{linker-payload}_{\text{mw}}$. [176]

1.2.5.1 Classical chemical conjugation

The accessible lysines and cysteines on the antibody surface can react with the activated linker, usually represented by *N*-hydroxysuccinimide esters for lysine residues and thiol-reactive maleimides for cysteine residues (Figure 38). Regarding the lysine coupling: mAbs have over than 80 -Lys residues, and 20 of them are accessible sites for the conjugation that promote the formation of a highly stable amide bond with the activated carboxylic moiety of the linker (Figure 38 a). The typical DAR range is 3.5-4 but can swing from 0 to 8. [177] On the other side, the use of cysteine coupling can have some advantages compared to lysine coupling. Cysteine residues are less than lysines and more uniformly distributed in the monoclonal antibodies: a typical IgG has 16 cysteine pairs, 12 intra-chain and 4 inter-chain and only these last ones are accessible for disulfide binding to the linker. The S-S intra-chains are not critical for the stability of mAb and can be reduced. After this first step, the addition of maleimide-activated linker leads to thioether conjugation with a more uniform DAR distribution (DAR = 2 or 4 or 6 or 8) (Figure 38b). It is a more reproducible method that gives homogeneous ADCs compared to lysine coupling, but has some disadvantages too.

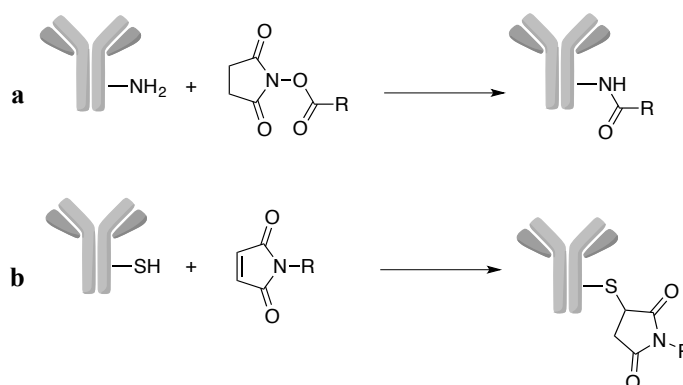


Figure 38. Classical chemical conjugation. **a)** lysine coupling; **b)** cysteine maleimide alkylation. R = linker-payload.

The reduction-oxidations conditions to open and close S-S cysteine bonds can lead to a denaturation of antibody. Moreover, thiosuccinimide moiety, obtained by the thioether conjugation, can undergo a retro-Michael elimination reaction especially in plasma where maleimide can exchange with reactive thiols in other proteins. [178] Add a basic amino group close to the thioether bond provides an intramolecular catalysis of thiosuccinimide ring hydrolysis that leads to an increase of pKa (pKa acid enolate > pKa succinimide enolate) with a better plasma stability. [179] This strategy could be an elegant way to prevent retro-Michael elimination (Figure 39) that can be achieved by ADC incubation at pH 9.2 [180], anion exchange chromatography under alkaline conditions in a solid phase system [181] or using self-hydrolysable maleimide derivative 2-(maleimidomethyl)-1,3-dioxane. [182]

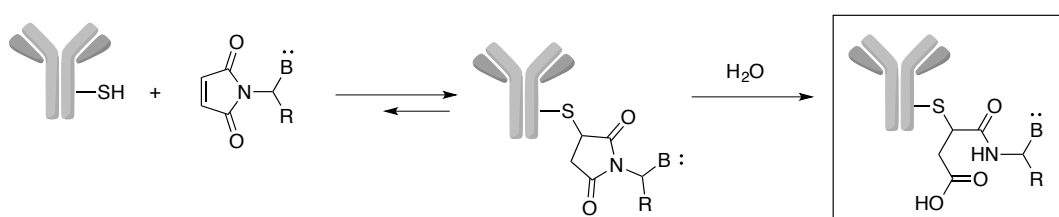


Figure 39. Michael reaction of thioether conjugation and thiol-maleimide hydrolysis that leads to the compound highlighted unable to undergo a retro-Michael elimination. R = linker-payload. B = basic group.

1.3 Hedgehog pathway

Hedgehog pathway (HH) is one of the fundamental signaling pathways responsible for embryonic development and essential for the maintenance of self-renewal processes in progenitor cells. In adult cells, it is physiologically silent but there are specific conditions in which the activation of this process occurs with the appearance of tumors. [183] This is due to

an over-expression of HH ligand or mutations of receptors and cytoplasmic proteins that lead to the development of basal cell carcinoma (BCC), medulloblastoma and melanoma. [184]

HH pathway was described for the first time by Nusslein-Volhard and Wieschaus who identified the Hedgehog gene (Hh) during a mapping on the embryos of fruit flies, the *Drosophila Melanogaster*, organisms very functional for genetic research. (Nobel Prize in 1995). [183] The two scientists realized that a lack of transcription process of Hh gene caused a blockage of the transcriptional signal which resulted in an abnormal body development along anterior-posterior body segmentation. In particular, the cuticle of insects was barbed due to an atypical development of small outgrowths (denticle hairs) that made *Drosophila* look like hedgehogs. [185]

The presence of Hh gene not only in insects but also in vertebrates, including mammals, was discovered and studied in other organisms like mice and zebrafish. The Hh gene exists in three isoforms: Desert Hedgehog (Dhh), Indian Hedgehog (Ihh) and Sonic Hedgehog (Shh) which encode for three different isoforms of protein HH (respectively DHH, IHH and SHH) that are involved in determining cell destiny, cell proliferation and embryo's body axes development. [186]

In mammals, HH pathway takes place in primary cilia, a rudimentary organelle composed of basal body and a central core of acetylated tubulin covered by plasma membrane. [187]

To simplify the overall process, HH pathway is regulated by a ON-OFF mechanism: "OFF" in absence of HH ligand (physiological condition) and "ON" in presence of ligand (Figure 40).

In physiological condition, the 12-pass transmembrane receptor Patched (PTCH), at the base of the primary cilium, inhibits the Smoothed receptor (SMO) localized in cytoplasmic vesicles (Figure 40). SMO is a transmembrane G-protein-coupled receptor (GPCR) in particular G inhibitory proteins (Gi). In this way, there is no signal transduction and the cell does not receive proliferation or differentiation inputs. [188]

On the contrary, when the HH ligand interacts with PTCH, it causes a conformational receptor swing that causes a migration of PTCH far from the base of the cilium with a loss of its inhibition on SMO. The HH-PTCH complex is internalized from the cell and degraded by lysosome activity and, as a consequence, SMO vesicles can translocate to the cilium. [189] The movement of proteins like SMO in or out of the cilia is an active process regulated by a family of kinesins (KIFs) and intraflagellar transport (IFTs) proteins [190]. The translocation of SMO into the cilium plays a crucial role for the activation of HH pathway. Once SMO receptors are concentrated in the cilium tip, they exert their action by activating the Gi that reduce the levels of cAMP which cause the inactivation of protein kinase A (PKA). This cascade leads to a lack of

phosphorylation of transcription factors, called GLIs. These factors are, now, in their active form and are able to migrate from the tip of the cilia into the nucleus inducing the transcription of specific genes. In particular, GLIs stimulate the expression of Gli, Ptch, human Hedgehog-interacting protein (Hhip) with the obtainment of the corresponding proteins that modulate the pathway with a negative feedback. At the same time, other cell-type specific genes can be transcribed such as Bcl2, Cyclin and Snail genes that play a fundamental role in tumor cells proliferation, in the angiogenesis regulation and in the metastasis increase (Figure 40). [191] Transcription is also negatively regulated by suppressor of fused (SUFU) that are directly bind to GLIs blocking their entry into the nucleus. SMO activation promotes the split of SUFU-GLI complex and the migration of GLI in its active form. [192]

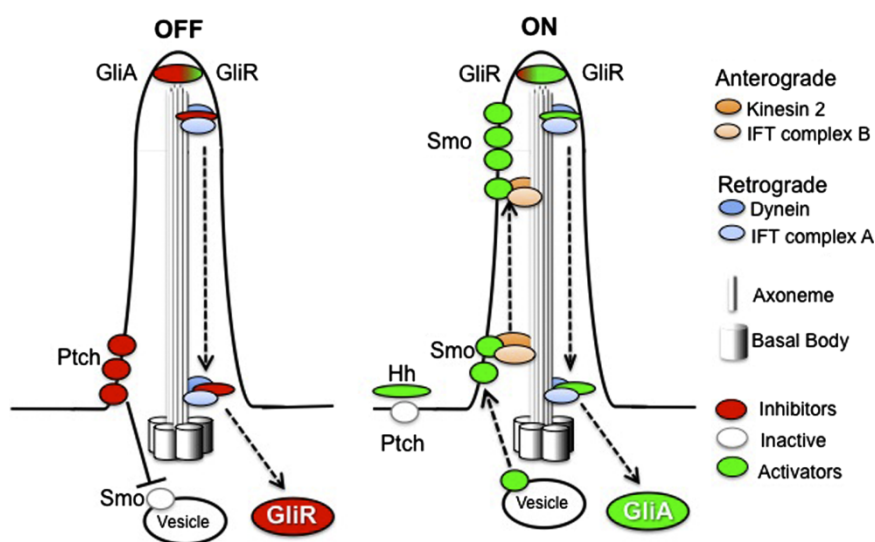


Figure 40. Simplified model of HH signalling pathway in primary cilia. [191]

As aforementioned, in adults in physiological condition, the HH signalling pathway is silent. Its activation is the cause of the development of many different types of cancers. The pathway activation is depending on mutations of receptors and of cytoplasmic proteins that are fundamental for the signal transduction.

The canonical activation of HH pathway in tumor can take place in four different ways:

1- Type I HH signalling – ligand independent, mutation driven (Figure 41a)

PTCH mutations lead to the constitutively activation of these receptors in absence of HH ligand. A high incidence of this type of mechanism is usually found in patients with basal cell carcinomas known as Gorlin syndrome.

Non-Gorlin tumors are not dependent on PTCH mutations but are the results of an up-regulation of Hh gene transcription which causes a high concentration of HH ligand.

2- Type II HH signalling – ligand dependent, autocrine (Figure 41b)

Several cancers (*i.e.* pancreatic, prostate, breast, melanoma, colorectal) are based on the overexpression of HH ligand. In this case, the cancer cells response to HH that they secrete.

3- Type III HH signalling – ligand dependent, paracrine (Figure 41c)

HH pathway in cancer cells is activated by the response of HH ligands located in the extracellular environment and produced by other neighbour tumoral cells as positive feedback for the maintenance of the tumor survival.

4- Type IV HH signalling – ligand dependent, reverse paracrine (Figure 41d)

Tumors receive HH secreted by stromal cells (*i.e.* bone marrow and lymph nodes). This is usually observed in liquid tumors like B-cells lymphoma and leukemia. [193]

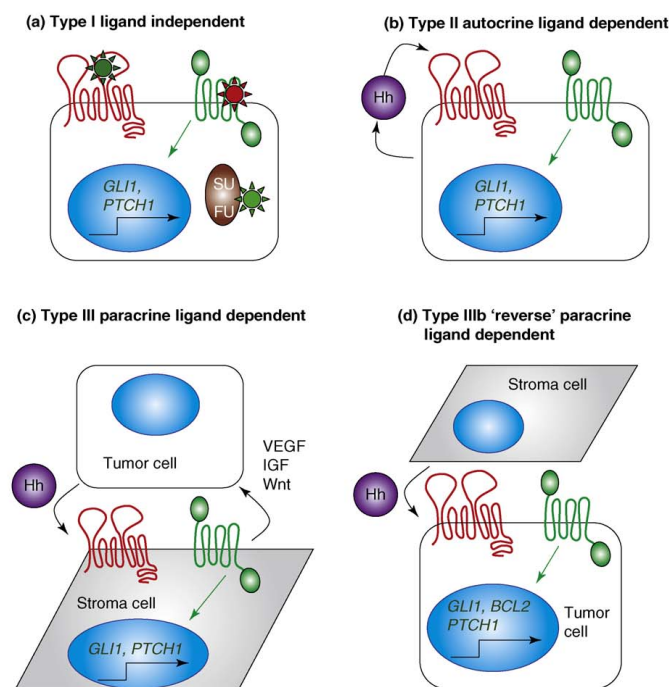


Figure 41. Different models of HH pathway activation in cancer: **a)** type I HH signalling – ligand independent, mutation driven; **b)** type II HH signalling – ligand dependent, autocrine; **c)** type III HH signalling – ligand dependent, paracrine; **d)** Type IV HH signalling – ligand dependent, reverse paracrine. [193]

Two non-canonical hedgehog signalling pathway are also discovered:

1- SHH-PTCH1-Cyclin B1 regulation of cell proliferation (Figure 42b)

During late G₂ phase, PTCH allows Cyclin B1, thanks to a physical interaction, to migrate in the nucleus of the cells to promote G₂-M transition. Cyclin B1 is a critical regulator of mitotic cell division and, associate with Cyclin Dependent Kinase-1 (CDK1), forms a regulatory

subunit of the M-phase promoting factor (MPF). MPF takes a crucial role in the proliferation of cells and is regulated by the retention of Cyclin 1 in the cytoplasm.

2- PTCH1 dependence-receptor activity (Figure 42c)

Cells that express PTCH undergo apoptosis because of its cleavage of C-terminal cytoplasmic tail at residue 1392 by caspase activity. PTCH-HH binding prevent this cleavage inducing an inhibition of apoptosis. [194, 195]

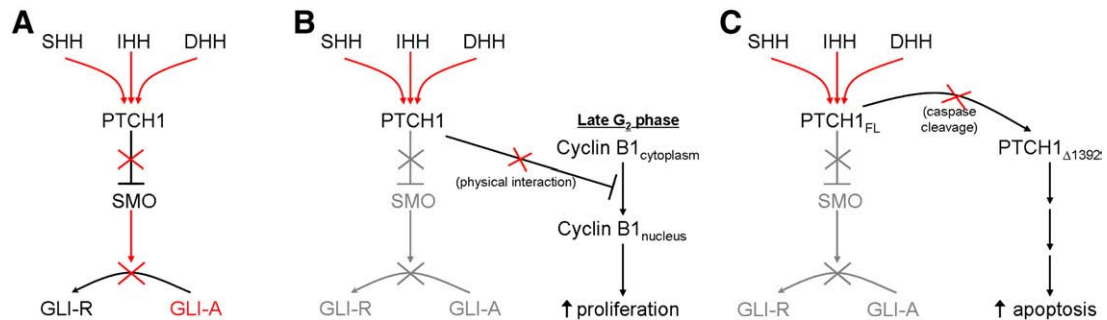


Figure 42. a) The canonical hedgehog pathway; **b)** non-canonical signaling pathway: SHH-PTCH1-Cyclin B1 regulation of cell proliferation; **c)** non-canonical signaling pathway: PTCH1 dependence-receptor activity. [194]

1.3.1 SMO receptor

The SMO receptor is one of the fundamental components of the canonical HH signaling pathway. It plays a crucial role in the expression of genes responsible for the embryonic development. Its activation in adults can cause the appearance of many different types of tumors. SMO is a G protein coupled receptor (GPCR) member of class F (frizzled/smoothed family-FDZ receptors) which binds the endogenous lipoglycoprotein ligands (WNTs). In humans, it is composed of 787 aminoacids organized in three domains: 1) a N-terminal extracellular domain (ECD) divided in cysteine-rich domain (CRD), linker domain (EDC linker domain), hinge domain and three long extracellular loops (ECL); b) an heptahelical membrane spanning (7-TM) domain (TMD); c) a C-terminal cytoplasmic domain that is less important (Figure 43). [196]

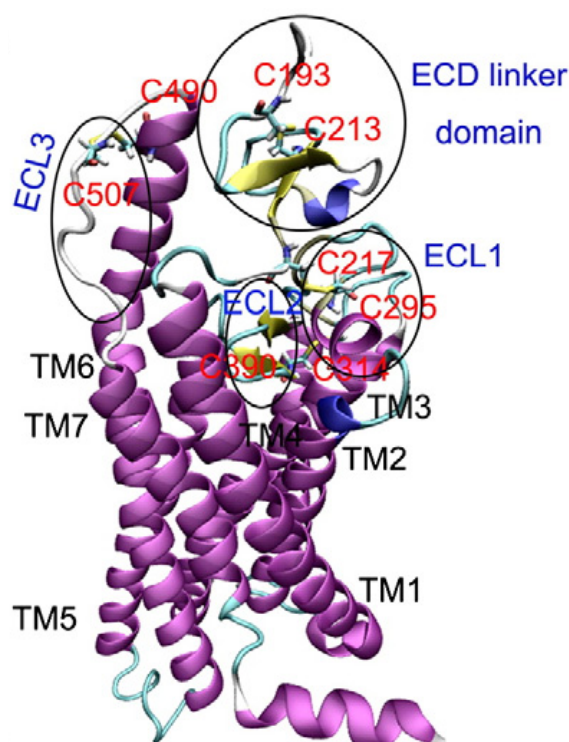


Figure 43. SMO receptor. ECD = terminal extracellular domain, ECL = extracellular loop, TM = heptahelical membrane spanning domain. [196]

In order to understand the structure of Smoothed receptor, Wang et al. in 2013 tried to express, purify and crystalize an engineered construct of SMO (human) with the antagonist LY2940680. A thermostabilized apocytochrome BRIL, fused with the receptor, was used to preserved the ligand binding property of wild type human SMO receptor. [197]

They affirmed that SMO presented the classic seven TMs, the ECD linker and the three loops (EDL) that were stabilized by four disulfide bridges between cysteines C193-C213, C217-C295, C314-C390. There was a long and narrow pocket formed of the three EDLs and the seven TMs connected to extracellular water media through a small slit between the EDC linker and the loops (ECL 2 and 3). The binding site was found localized into the core of the seven TMs, accessible only by small molecules. In particular, LY2940680 interacted with the extracellular domains of TM1, TM2, TM7 and in specific with the residue R400^{5.39} of TM5 with whom formed hydrogen bonds. In this site, two molecules of water that formed other hydrogen bonds between the residues R400^{5.39}, H470^{6.52}, D473^{6.55}, E518^{7.38} and N521^{7.41} of side chain that allow the conservation of the right pocket conformation, were detected. It was also discovered that a mutation in the residue D473^{6.55} causes a change in the functional structure and LY2940680 is not able to bind SMO receptor anymore generating drug resistance (Figure 44). [197]

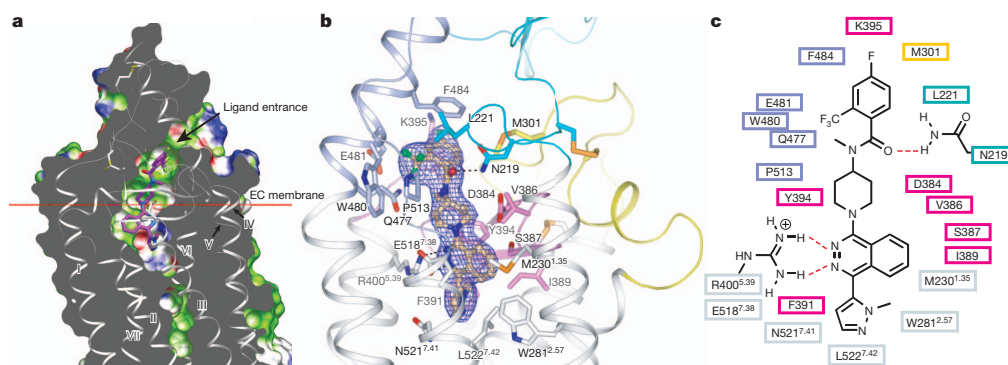


Figure 44. Crystallized structure of human SMO bind with its antagonist LY2940680. [197]

1.3.2 SMO inhibitors

In order to treat HH tumor dependent, it is possible to modulate the signal transmission reducing ligand-receptor interaction (HH-PTCH), blocking the activation of GLI and in particular inhibiting SMO. [195] In this work, the focus will be on SMO inhibitors.

The development of SMO inhibitors started from the discovery of Cyclopamine (Figure 45a), an alkaloid present in the rhizomes and in the roots of corn lily, *Veratrum californicum*. This alkaloid was responsible for cyclopia and craniofacial malformations observed in lambs born from sheeps that had eaten corn lilies. These malformations were the results of the inhibition of Cyclopamine on the HH signaling pathway, important for embryogenic development. [198] Treatment of cancer cells with this alkaloid induced a reduction of proliferation and the apoptosis induction. Cyclopamine blocks the pathway by interaction with SMO which rearranges in its inactive closed form unable to activate GLI. Despite the interesting pharmacodynamics profile, *in vivo* studies demonstrated a poor aqueous solubility and acid lability. [199]

Lewis acid or pH < 2 determinate the opening of the E ring with the destruction of the spiro connection between ring D and F with the obtainment of the analogue Veratramine (Figure 45b). Veratramine can cause hemolysis by its non-specific cytotoxic activity. [200]

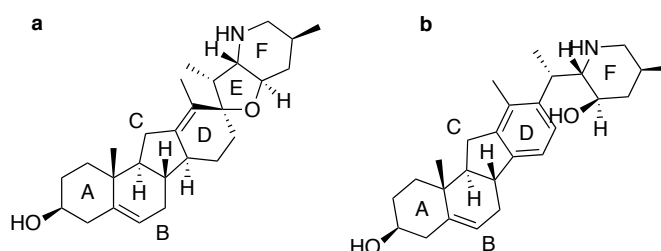


Figure 45. a) Cyclopamine, b) Veratramine.

To overcome these issues improving the stability and the solubility of Cyclopamine, structural modifications have been made with the obtainment of semisynthetic compounds. Otherwise, new small molecules with SMO antagonist activity were detected through a high-throughput screening. The derivatives developed lost the ability of Cyclopamine to pass the blood-brain barrier, an important requirement for a therapy against HH brain tumors. [201]

Among the semisynthetic derivatives, IP-926 (Saridegib) is an orally bioavailable SMO inhibitor with an improvement of metabolic stability and pharmacokinetic profile by introduction of hydrogen bond acceptor in the ring A. The study was stopped at clinical phase II because it is a substrate of P-glycoprotein with the appearance of drug resistance (Figure 46a). [201]

GDC-0049 (Vismodegib, Erivedge®) belongs to the second generation of semisynthetic SMO inhibitors and was approved by the FDA in 2012 for the treatment in adults with metastatic basal cell carcinoma and with locally advanced basal cell carcinoma that has recurred following surgery. Vismodegib is orally bioavailable without interactions with the food. It has a high affinity for albumin (HSA) once arrived in the blood and it is metabolized by CYP2C9 and CYP3A4. Its absorption depends on gastric pH, low value of pH decreases the solubility of Vismodegib and its activity. For this reason, proton pump inhibitors, anti-H₂ and other antacids can be associated. It has teratogenic effects and can be used in monotherapy or in combination. After three months of therapy, it is recommended to interrupt the treatment for the appearance of drug resistance due to H473H point mutation in SMO receptor (Figure 46b) [202-204]

NVP-LDE225 (Sonidegib, Odomzo®) is another derivative approved by the FDA in 2015 as SMO inhibitor for the treatment of locally advanced basal cell carcinoma (BCC) that has recurred following surgery or radiation therapy (Figure 46c). [205]

It is orally bioavailable and commercialized as diphosphate salt, has teratogenic effect and it is metabolized by CYP2C9 and CYP3A4. [206, 207]

Glasdegib (Daurismo®) is a SMO antagonist approved by the FDA in 2018, in combination with Cytarabine, for the treatment of newly-diagnosed acute myeloid leukemia (AML) in adult patients who are ≥ 75 years old or who have comorbidities that preclude the use of intensive induction chemotherapy. It is orally bioavailable and is able to pass the blood-brain barrier. For this reason, there are studies about its activity against HH dependent medulloblastoma (Figure 46d). [208-210]

LY-2940680 or Taladegib (Figure 46e) has a tetrahydropyrid[4,3-d]pyrimidinic structure and is active also in SMO mutant due to its ability to reduce the proliferation and increase Caspase-

3 activity leading to tumor cells apoptosis. It is not yet approved but it is in phase II trials for the treatment of oesophageal cancer and small cell lung cancer. [211]

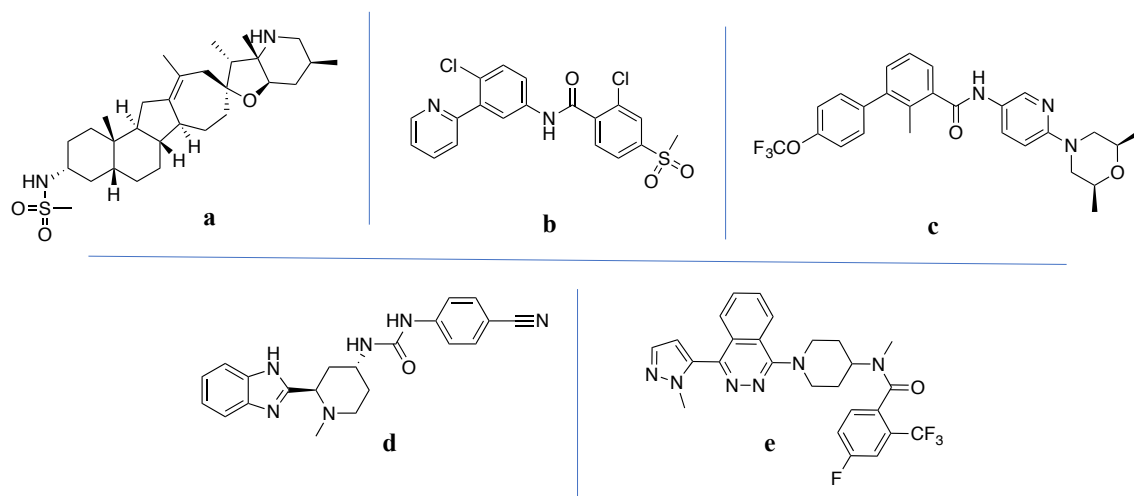


Figure 46. a) Saridegib, b) Vismodegib, c) Sonidegib, d) Glasdegib, e) Taladegib.

1.3.2.1 MRTs

SMO inhibitors rapidly develop resistance due to a D473H point mutation of the SMO receptor. This is not the only way for the appearance of resistance because also an amplification of Gli gene or an increase of P-gp can be manifested. [212, 213] As a consequence, the interruption of therapeutic treatments is required. Moreover, these SMO antagonists do not present a linear pharmacokinetic profile and have a poor solubility in water. In an attempt to identify new SMO inhibitors, the research group where I have worked conducted a virtual screening study of commercial compound libraries with the aim of developing a pharmacophore model for the interaction with the SMO receptor. The strategy led to the identification of Acylthiourea (AcTU) called MRT-10 with an Shh-light2 IC_{50} = 0.65 μ M. Through a MRT-10 structural optimization process, different AcTUs, Acyluree (AcUs) and Acylguanidine (AcGs) were obtained with an increase of activity until the nanomolar order. AcU, called MRT-14, was synthesized by an oxidative process starting from MRT-10 with an increase of Shh-light2 IC_{50} = 0.16 μ M. The corresponding AcG (MRT-78) was obtained, with the same process, with an Shh-light2 IC_{50} = 0.29 μ M (Figure 47). [214]

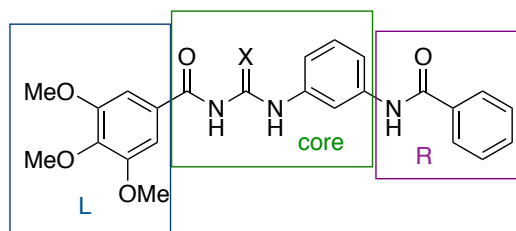


Figure 47. Scaffold of MRTs. X =S (MRT-10), X =O (MRT-14), X =NH (MRT-78).

Based on the relations structure activity (SAR), taking as scaffold the structure present in Figure 47, different and appropriate modifications in the core, in the region right (R) and left (L) were applied with the identification of AcGs MRT-86 (Shh-light2 $IC_{50} = 0.015 \pm 0.002 \mu M$, C3H10T1/2 upon stimulation by SAG $IC_{50} = 0.011 \pm 0.003 \mu M$) and MRT-84 (Shh-light2 $IC_{50} = 0.014 \pm 0.003 \mu M$, C3H10T1/2 upon stimulation by SAG $IC_{50} = 0.011 \pm 0.002 \mu M$) as the best compounds in terms of inhibition potency (Figure 48). [214, 215] An introduction of two carbon spacer into the biphenyl portion increased the activity with the obtainment of MRT-92 (Shh-light2 $IC_{50} = 0.0028 \pm 0.005 \mu M$, C3H10T1/2 upon stimulation by SAG $IC_{50} = 0.0056 \pm 0.004 \mu M$, Figure 48). [216]

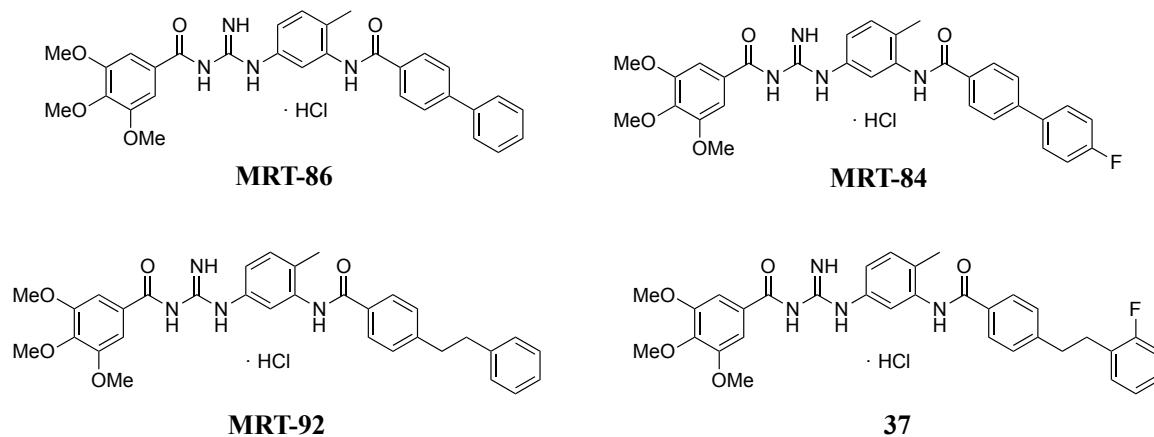


Figure 48. Structures of MRTs with the best activity profile.

AcTU, AcU and AcG are bioisosters in which an electron-rich aromatic ring in region L, a methyl group or $-Cl$ moiety and the biphenyl fragment in region R are always present and essential for establishing hydrophobic interactions with SMO receptor (Figure 49). [214]

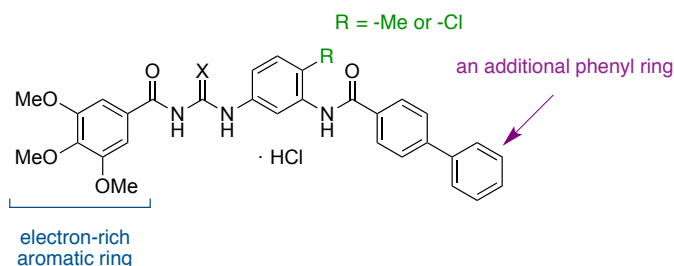


Figure 49. A general MRT ($X = O, S, NH$) with the fundamental elements to increase the potency against SMO.

MRT-86 was also compared with the corresponding AcTU for the identification of a pharmacophore model for SMO inhibitors (Figure 50). Trimethoxyphenyl group, with one of oxygen atom, acts as an acceptor of hydrogen bonds (HBA1) and the aromatic rings result important for the hydrophobic interactions (HY1-2-3). The carbonyl oxygens of the amide group and of the AcU or AcG moiety are acceptors of hydrogen bonds (HBA2-3). [214]

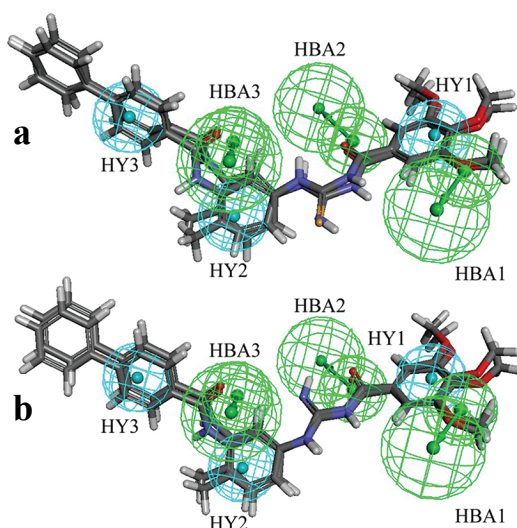


Figure 50. MRT-86 and the corresponding AcTU in two different conformations (**a**, **b**) for the identification of the pharmacophore model for SMO antagonists. Pharmacophoric features are highlighted with a sphere and colored in green for hydrogen bond acceptor groups (HBA1–3) and in light blue for hydrophobic regions (HY1–3). The atoms are color coded in gray for carbon, in white for hydrogen, in red for oxygen, in blue for nitrogen and in yellow for sulfur. [214]

The increase of inhibitory activity related to the presence of acylguanidine moiety depends on:

- the presence of an intramolecular hydrogen bond between the -H of the guanidine and the -O of carbonyl group with a decrease in the motility of the molecule (Figure 51);

- the strength of hydrogen bonds established between the receptor pocket and the N atoms of ureidic/thiouridic/guanidinic group. The binding force is inversely proportional to the electronegativity of S, O and N (Figure 50). [214]

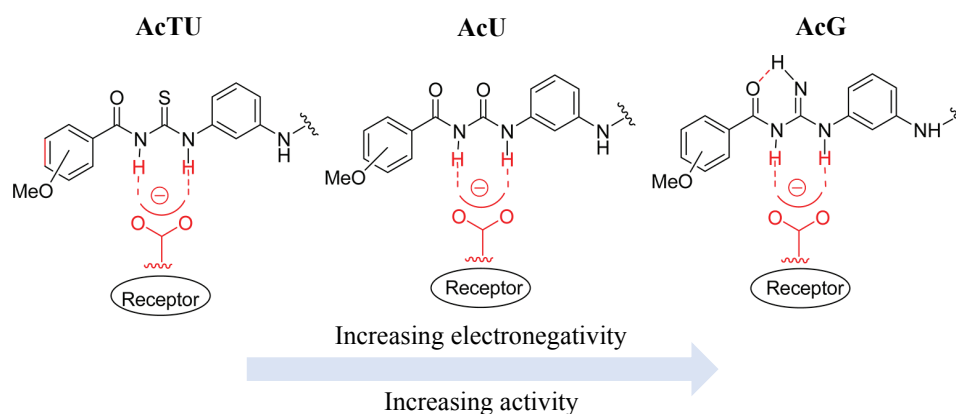


Figure 50. Proposed H bonds between the three bioisosters AcTU, AcU, AcG and SMO receptor pocket. [214]

Compared to the other antagonists (*i.e.* LY2940680), MRT derivatives interact not only with ECLs but also with the 7TM domain of the SMO receptor. The extension of biaryl portion (region R) and, in particular, the insertion of a methylene spacer in MRT-92 make these compounds great inhibitors against SMO mutants thanks to the ability to interact with both extracellular and intracellular domains of the receptor reducing drug resistance. The hit compound MRT-92 keeps its activity in different SMO mutants especially against the SMO receptor with D473H point mutation. The inhibitory constant (K_i) of a series of SMO inhibitors is reported below. As affirmed before, MRTs retain their activity (*i.e.* MRT-92 $K_i = 0.7 \text{ nM} \pm 0.1 \text{ nM}$) on both the wild type and the D473H point mutation form. On the contrary, the approved SMO inhibitors like Vismodegib ($K_i = 5.8 \text{ nM} \pm 1.3 \text{ nM}$ upon WT; $K_i = > 1000 \text{ nM}$ upon D473H mutant) loss their potency on SMO D473H mutant. [216]

In vitro and *in vivo* studies have been conducted during these years using MRT-92 as hit compound.

MRT-92 is active in chronic myeloid leukemia cells. The experiment performed using K-562 and KU-812 cell lines was the evidence of anti-proliferative and pro-apoptotic effects of this inhibitor. [217]

MRT-92 and its novel fluoride analogue 37 (Figure 48) strongly reduce growth and self-renewal of melanoma cells. The experiment was conducted in three different cell lines: A375, SSM2c and MeWo with good results. For example, in the A375 line, MRT-92 has an IC_{50} of $299 \pm 0.005 \text{ nM}$ exhibiting an anti-proliferative effect with an inhibition of the GLI level in a dose-

dependent manner. Both compounds induce apoptosis thanks to DNA damages and prevent the transition of G2 into M cell cycle by inducing mitotic aberrations. To investigate the inhibitory effect of MRT-92 and compound 37, these molecules were injected (15 mg/Kg) in melanoma xenograft mouse model and compared with vehicle. No significant loss of weight was observed with a remarkable decrease of tumor growth. [218] In 2021, we have identified SOX2-BRD4 a transcriptional complex as driver of Gli expression providing a novel mechanism of non-canonical activation of the HH pathway. SOX-2 is a transcription factor responsible of the self-renewal or pluripotency embryonic and stem cells maintenance, while BRD4 is a protein that promotes gene expression thanks to the transcription of elongation factor P-TEFb and the interaction with RNA polymerase II. There is a correlation between the increase of GLI proteins and the presence of SOX2-BRD4 in melanoma cell lines and in human melanoma samples. MZ1 is a potent BRD4 degrader and in combination with MRT-92 has given great results in A375, SSM2c and MeWo cell lines resulting in a synergistic anti-proliferative effect in melanoma with a high control on Gli expression. As proof, when these two drugs are combined, the combination index (CI) of IC_{50} is <1 . This evidence was confirmed in orthotopic melanoma tumor of A375 cells in athymic nude mice in which the combination of MRT-92 (15 mg/Kg) and BRD4 (100 mg/Kg) strongly potentiate each single antitumor activity with a high reduction of tumor volume compared to the single-treated and the vehicle-treated groups. Combo T/C% after 30 days = 16.8 compared to T/C% = 53.8 and 47.7 of MRT-92 and MZ1 respectively. [219] Those results give an opportunity to support MRTs in therapeutic approaches for melanoma and other HH dependent tumors.

1.4 Aim of this research work

ADCs have to be carefully designed particularly taking into account that the linker must be polar enough, stable at physiological conditions, and simultaneously unstable in target tissues. Due to its intrinsic precariousness, the synthesis of conjugates is complex and difficult; the intermediates are usually very unstable, and a premature release of payload could happen.

The aim of this research work is to explore the ADCs field with two specific focuses: *i.* develop innovative cleavable linkers triggered by the tumor environment (specific range of pH or hypoxic behavior) and *ii.* design new ADCs armed with SMO inhibitors for the treatment of melanoma.

1.4.1 A new pH responsive crosslinker platform for drug targeting delivery

Several cleavable acid sensitive linkers have been studied for the development of target drug delivery (paragraph 1.2.2). Moreover, the research for new linkers, as well as for new trigger moieties and different self-immolative spacers is constantly evolving with the aim to obtain a suitable tunable system with an easier introduction of different payloads, and a controlled release by using convergent synthesis approaches.

Gallic acid is a safe to handle molecule, easily to be used and functionalized because of its functional groups that can be efficiently transformed into orthoester derivatives. This transformation could provide a promising acid-sensitive linker containing an orthoester trigger moiety stable at pH 7.4 but hydrolysable at acid pH (below 5.5). The innovation of this approach is represented by the design of 5-(hydroxymethyl)pyrogallol orthoester (HMPO) as a novel drug delivery systems (Figure 51).

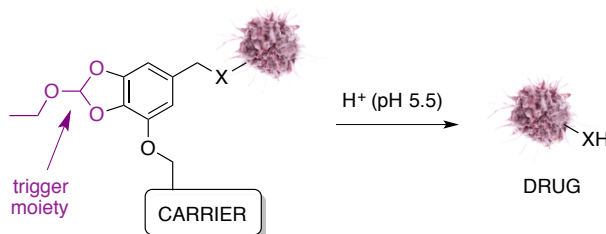


Figure 51. HMPO derivative and its hypothesized selective drug release at pH 5.5. Carrier = mAbs or ligands. X = -OH, -NH₂, -NHR, -NR₂.

1.4.2 A new reactive oxygen species (ROS) sensitive linker

The reactive oxygen species (ROS) are free radicals responsible for post-translational

modifications in proteins leading to pathological conditions such as tumors. [62, 63] As previously reported (paragraph 1.2.2.2.2), borate, thioether and thioketal moieties are used to design prodrugs or polymeric systems but not yet employed for the development of drug conjugates. A hypoxic sensitive traceless crosslinker based on a 1,6 self-immolative elimination process was investigated with the aim of easily connecting carriers (*i.e.* mAbs, ligands) with different payloads (Figure 52). Moreover, it is known that byproducts coming from boric derivatives are well-tolerated in human [69] and this is a further point to encourage the study of a suitable borate linker for the development of ADCs.

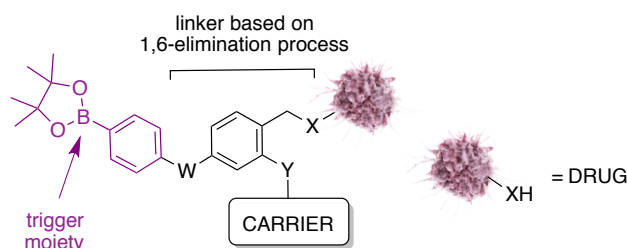


Figure 52. Schematic representation of a generic sensitive traceless crosslinker based on 1,6 self-immolative elimination process. Carrier = mAbs or ligands.

1.4.3 ADCs armed with SMO inhibitors

As reported (paragraph 1.2.3.1.3), SMO inhibitors are an unexplored class of potential payloads for the development of new ADCs for the treatment of melanoma. The cytotoxic drugs chosen for this aim are Cyclopamine, Vismodegib and MRTs inhibitors.

Cyclopamine is a metabolically unstable compound extracted from *Veratrum californicum* and dropped out of anticancer therapy due to its acid lability that leads to an off-target toxicity and a poor aqueous solubility. [119]

Vismodegib has been approved by the FDA and it has high potency against SMO WT with high cytotoxicity profile that brought to unspecific activity with many side-effects. As reported in the guidelines, after three months of therapy, it is recommended to interrupt the treatment for the appearance of drug resistance due to H473H point mutation in SMO receptor. [202]

MRTs are a new class of SMO inhibitors recently developed at the University of Siena. [214] *In vitro* and *in vivo* experiments (paragraph 1.3.2.1) showed that AcG derivatives are potentially interesting new therapeutic options for melanoma and other types of HH dependent cancers. [218, 219] On the other hand, preliminary *in vitro* studies in mice hepatocytes showed not very optimal MRTs half-life due to metabolic instability. Moreover, issues are encountered in

solubilizing these compounds in aqueous media.

Contrary to Cyclophosphamide, the new generations of SMO inhibitors have lost the ability to pass the blood-brain barrier, a fundamental feature for the treatment of HH dependent brain cancers. To solve these limitations, a valid proposal could be the development of drug delivery systems charged with SMO inhibitors.

Vismodegib, MRT-86 and MRT-92 do not present the classic “chemical handles” $-NH_2$ and $-OH$ groups available to bind a linker. The huge challenges, for the development of ADCs armed with SMO inhibitors, were represented by the design of linkers with excellent release and stability profiles, and the research of unconventional drug binding sites. For example, we hypothesized that Vismodegib (Figure 46b) could present the pyridine nitrogen, while both MRTs (Figure 48) have an interesting guanidine moiety as possible willing “chemical handles”. Innovative cleavable linkers (*i.e.* HMPO), conventional uncleavable linkers and different SMO inhibitors are investigated in a crossing way with the aim to develop the first ADCs against tumors HH dependent.

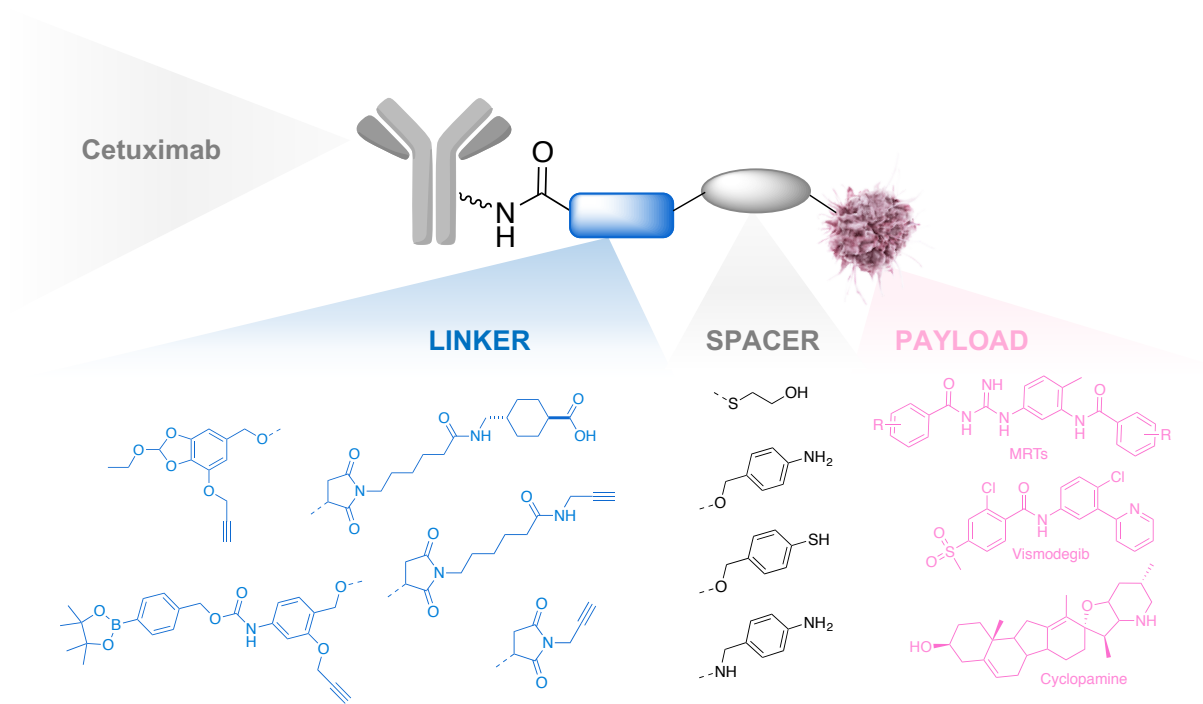


Figure 53. Summary of the wide series of linkers, spacers and drugs used in a crossing way to obtain different ADCs armed with SMO inhibitors.

Results and discussion

2.1 A new pH responsive crosslinker platform for drug targeting delivery

A well-designed acid sensitive linker is stable in plasma (pH 7.4), in the external tumor tissues at pH around 6-7, while it turns chemically unstable after processing at pH 5.5-4.5 into the lysosome. [177] The linker is the key component in the development of a drug delivery system because of its task of allowing the controlled release of the drug only by a mechanism of triggering related to its nature and weaknesses.

Most of the acid sensitive linkers developed so far [50] require complex synthetic strategies and low versatility in term of functional groups that can bind to charge drugs. For example, acylhydrazones, present in Mylotarg® and in Besponsa®, can be obtained from carbonyl or hydrazine derivatives allowing a narrow use of drugs that must have one of those functions. [220] On the other side, as could happen with phosphoramidate linkers, the drug is released in a protonated form unable to diffuse in neighboring cells losing the advantage of the bystander effect. [221] Wagner et al. [54] drew up a new potential linker based on Spiro-DiOrthoester moiety called SpiDo. To our knowledge, the SpiDo platform was applied only to *in vitro* imaging experiments with micro-organelles maybe because of the difficulty in exploiting it in a drug delivery system.

Although major improvements have been obtained for pH-sensitive linkers, new chemistry for versatile linkers with tuneable release rate is still highly desirable for the development of prodrugs including ADC and gene-delivery. The 1,6 self-immolative elimination process, typical of PABA-like spacer, is one of the most common way to exploit external *stimuli* for a sensitive release of prodrugs and bioconjugates.

With the aim to combine the high efficiency of the 1,6 self-immolative spacer with the high-racking selective hydrolysis of orthoester at pH 5.5, we propose a new acid sensitive linker (5-(hydroxymethyl)pyrogallol orthoester (HMPO) derivative – Figure 54), based on the 1,6 self-immolative *p*-hydroxybenzyl alcohol platform with an orthoester trigger moiety, designed for the drug conjugation as a targeting system.

Gallic acid is a safe to handle molecule that is easy to use and to functionalize because of its interesting chemical groups which can be turned into:

- an orthoester trigger moiety, a very promising acid-sensitive group due to its stability at pH 7.4 and its susceptibility at pH below 5.5;

- a benzyl alcohol moiety employed for binding different drugs containing a primary or secondary amine (as carbamate), a phenol (as an aryl benzyl ether) or a pyridine nitrogen (as quaternary ammonium cation);
- a “chemical handle” in the remaining phenol moiety to attach the carrier (*i.e.* antibody or ligand) by adding a triple bond through an orthogonal coupling (Figure 54).

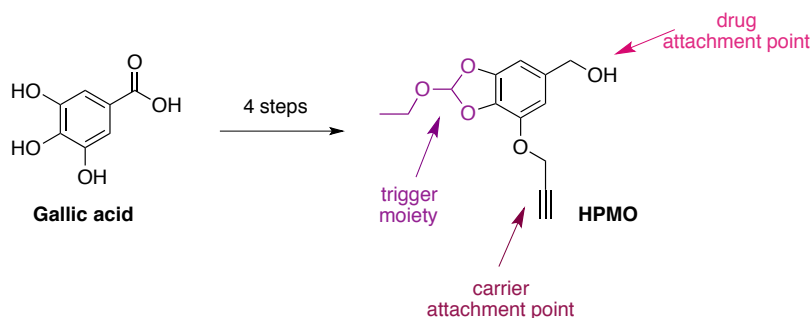


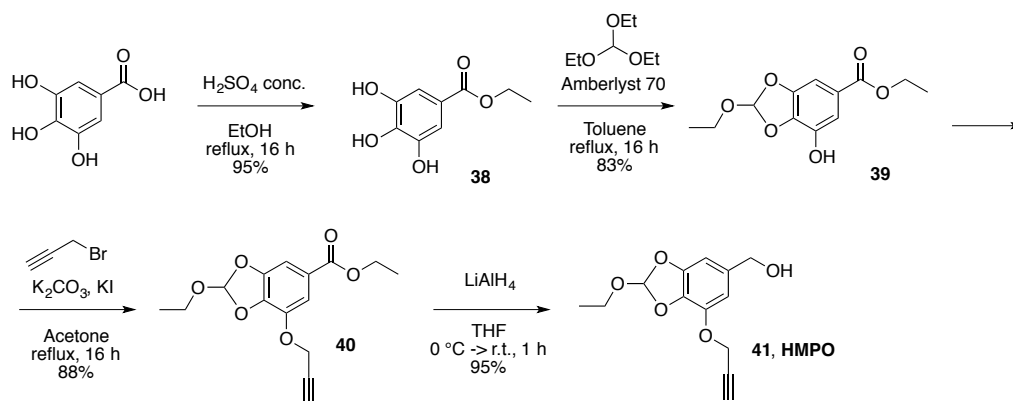
Figure 54. Gallic acid and its HMPO derivative.

Gallic acid is a natural tannic component present in several plants and available in large quantities at low price. In four simple reactions, the semisynthetic HMPO derivative can be easily obtained acquiring the characteristic of being a versatile linker for the development of drug delivery systems (*i.e.* ADCs).

Gallic acid (**1**, Scheme 1) has already all the characteristic for our design: two -OH groups to form a cyclic orthoester, another -OH for installing a triple bond for orthogonal cross coupling and the *p*-carboxylic group that could be easily reduced to benzyl alcohol giving the desired pH sensitive crosslinker platform in only four easy steps.

2.1.1 Synthesis of HMPO linker

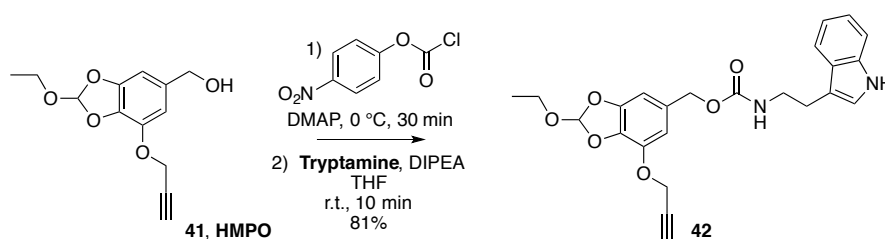
Gallic acid was esterified to the corresponding ethyl ester **38** that was submitted to a cyclisation with triethyl orthoformate furnishing the gallic acid orthoester **39** in high yield (Scheme 1). The residual free -OH moiety of **39** was alkylated by propargyl bromide using K_2CO_3 as base and KI as catalyst. The propargyl ether derivative **40** was reduced with $LiAlH_4$ in THF to give the HMPO derivative **41** in 76 % overall yield over the 4 steps synthesis starting from gallic acid (Scheme 1).



Scheme 1.

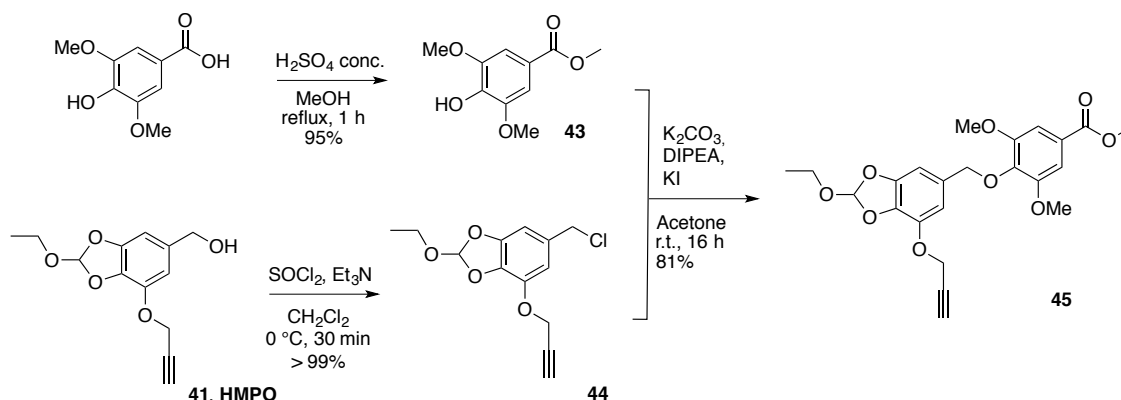
2.1.2 Experiments to evaluate the HMPO hydrolysis profile

Two model systems (**42** and **45** in Scheme 2 and 3) were prepared to evaluate the hydrolysis profile and the corresponding release of the molecules linked to the benzyloxy group.



Scheme 2.

Activation of **41** with *p*-nitrophenyl chloroformate and further reaction with the tryptamine in alkaline medium gave carbamate **42** in acceptable yields and in a short time.



Scheme 3.

Syringic acid methyl ester **43** was prepared in classic Fischer's conditions. The system model **45** was obtained from alcohol **41** by chlorination to benzylchloride **44** followed by nucleophilic displacement with the potassium salt of **43**. **44** is very instable reactive species at acid pH because of its orthoester moiety. For this reason, the addition of chlorinating agent must be done dropwise at low temperature and in an alkaline environment. The purification of this product *via* silica filtration must be very fast because the silica gel is slightly acid and can destroy the compound obtaining the starting material **41**.

Stabilities of **42** and **45** at different pH values were investigated *via* HPLC analysis using the appropriate phosphate buffer. Compound **42** gave almost complete release of the payload after 6 h at pH 5.5 (93% release, $T_{1/2} = 3$ h, Figure 55). A comparable kinetics was observed at the same pH with **45** ($T_{1/2} = 6$ h and the 94% of release reached after 12 h, Figure 56). When **42** and **45** were treated at 37 °C at pH 7.4 and 6.5 no hydrolysis occurred within 6 h. Only after 24 h in the presence of 10% of tryptamine and 25% of **43** respectively were observed by HPLC (Figure 55, 56).

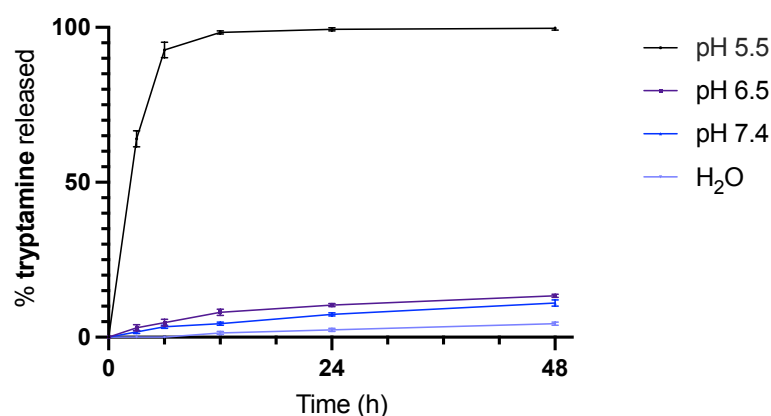


Figure 55. HPLC hydrolysis kinetics of the model system **42** at pHs 5.5, 6.5, 7.4 and in H₂O (as blank).

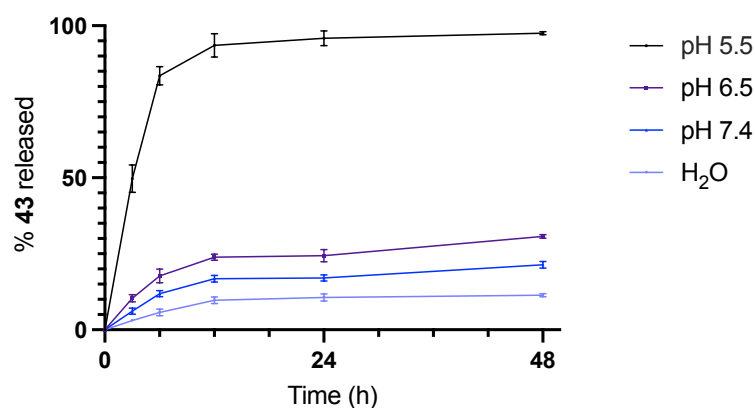


Figure 56. HPLC hydrolysis kinetics of the model system **45** at pHs 5.5, 6.5, 7.4 and in H₂O (as blank).

These results were in agreement with those reported for existing orthoester linkers, confirming that HMPO is sensitive to lysosomal pH, mimicked by the external acid *stimulus*, showing equally an excellent stability profile at physiological and extracellular solid tumor pHs.

2.1.3 The hypothetical release mechanism of HMPO linker

With the aim to elucidate the release mechanism, the model system **45** was studied at pH 5.5 through ^1H NMR analysis. After 5 minutes, traces of phenol **43** were detected by the shifts of the aromatic signals from 7.87 to 7.92 ppm and of the singlet (-OMe group) from 4.42 to 4.49 ppm (Figure 57). These data were confirmed by ^1H NMR in D_2O at 37 °C of **45** and **43** at the same concentration of **45** used for the release test (Figure 58). Moreover, we noticed a peak at 8.69 ppm assigned to the transient assembling of a formate derivative (**46f**, Scheme 4). Finally, the characteristic aromatic and aliphatic signals of a 5-(hydroxymethyl)-3-(2-propynyloxy)pyrogallol (**47**, Scheme 4) were observed, confirming of the complete release of phenol **43** (Figure 59).

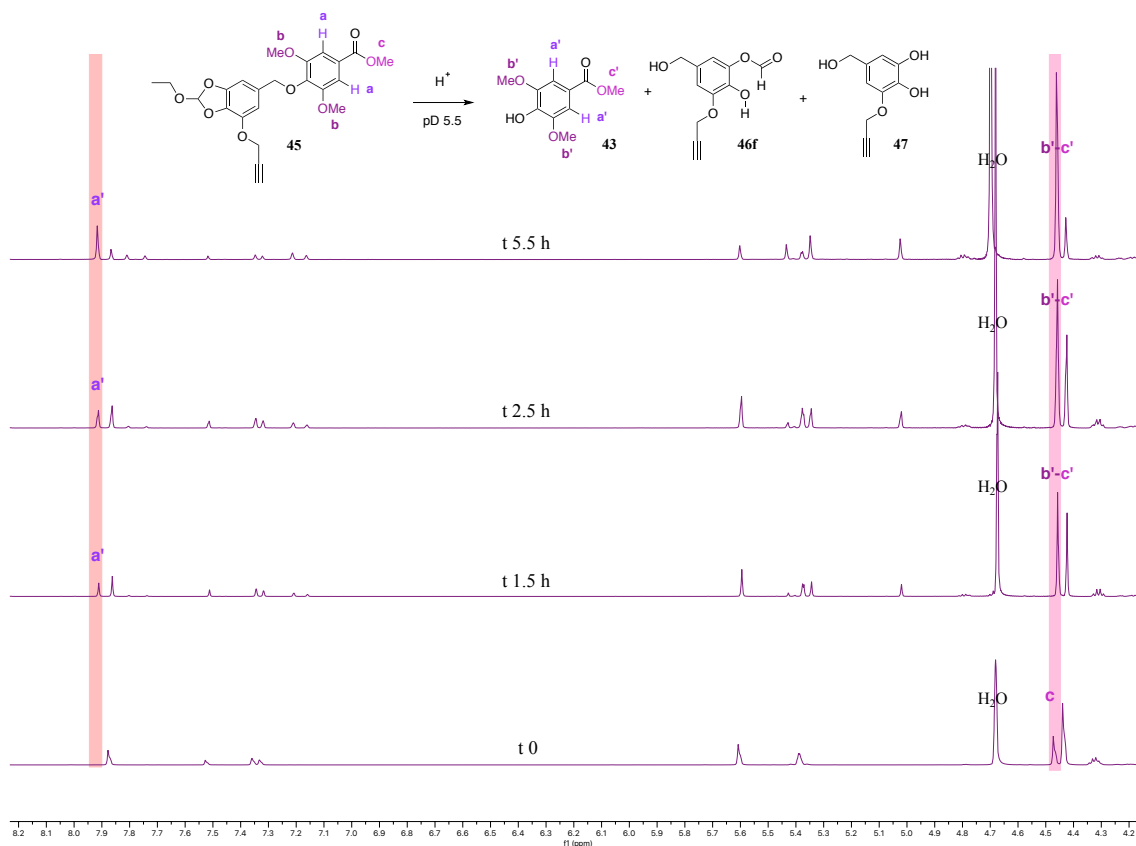


Figure 57. ^1H NMR spectra of **45** monitored during the hydrolysis process in acetic buffer D_2O (pH 5.5) at 37 °C. Highlighted in orange the aromatic –2H (a') and in pink the methoxy –9H (b'-c') of the released phenol **43**.

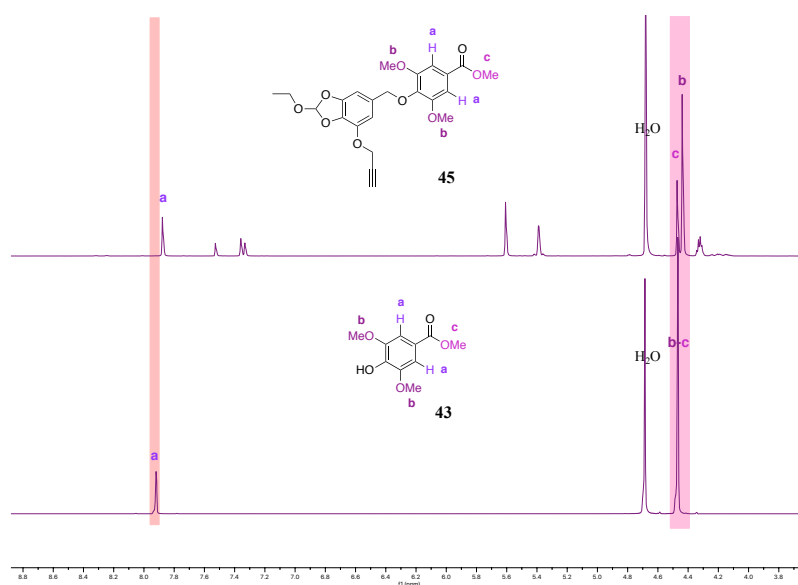


Figure 58. ^1H NMR spectra in D_2O and Acetonitrile- d_3 37 °C of the model system **45** and the phenol **43**.

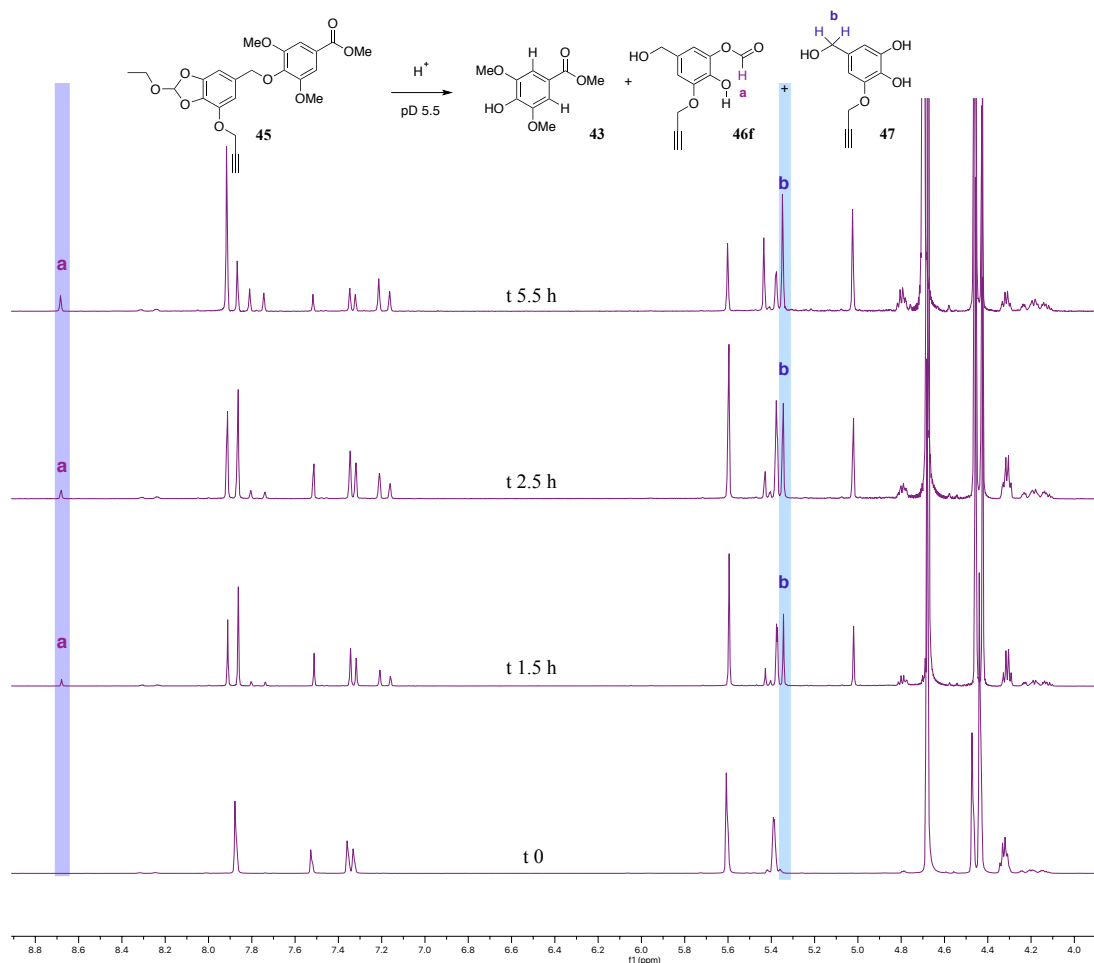
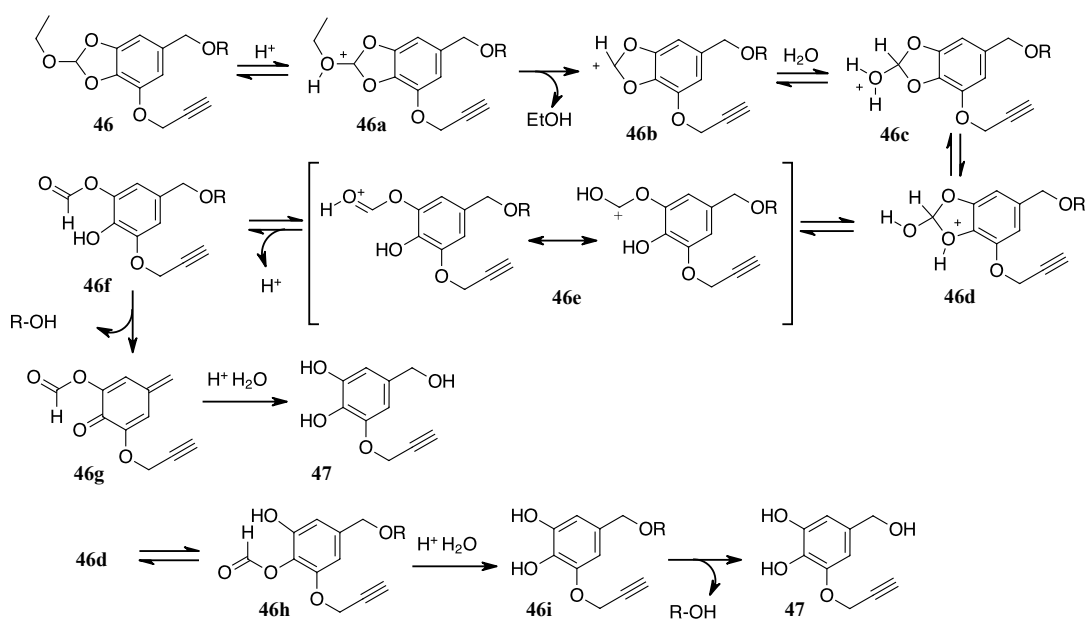


Figure 59. ^1H NMR spectra of **45** monitored during the hydrolysis process in acetic buffer D_2O (pH 5.5) at 37 °C. Highlighted in violet the transient formate (**46f**) 9f–1H (a) and in light blue the benzylic – 2H (b) of the released 5-(hydroxymethyl)-3-(2-propynyloxy)pyrogallol **47**.

Based on these results, a reasonable release mechanism of the HMPO platform was proposed (Scheme 4).



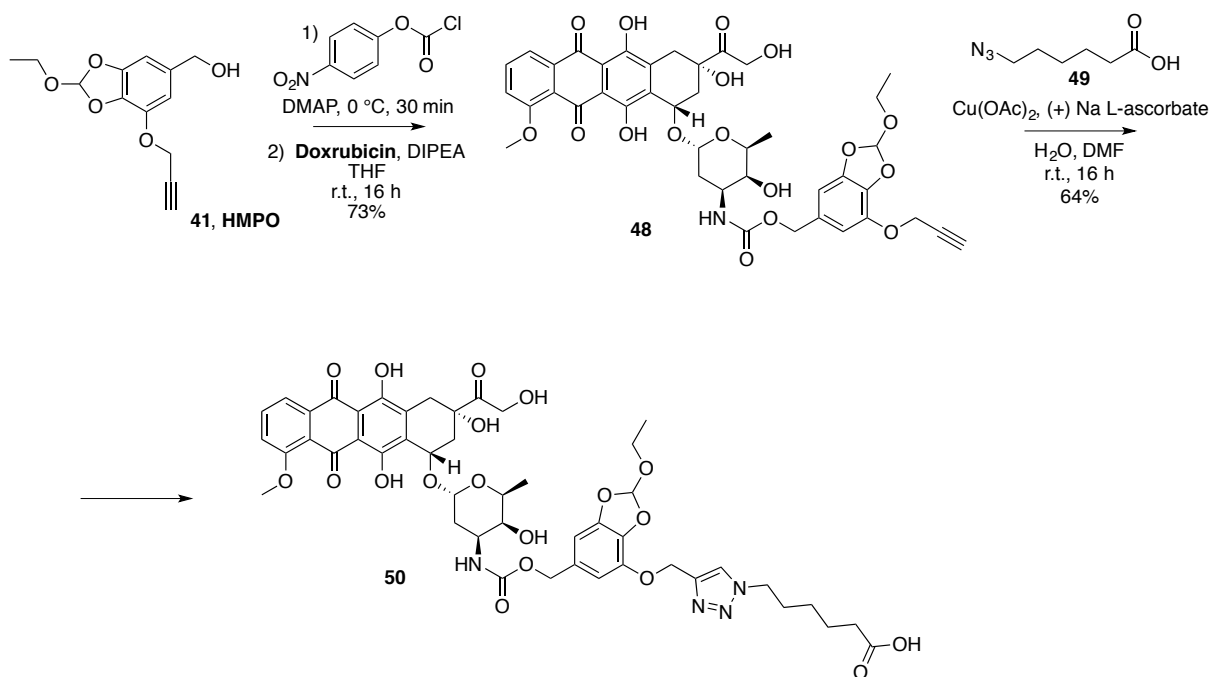
Scheme 4.

In acid conditions, the orthoester is protonated thus producing EtOH. The intermediate carbocation **46b** is immediately quenched by water. Through proton exchange, the hydroxyacetal **46b** gives the protonated **46e** which, after proton release, furnishes the pyrogallol formate **46f**. The expected 1,6-elimination occurs on this substrate thus forming the *p*-quinone methide **46g** and releasing the drug (R-OH) previously linked through the phenyl-benzyl ether moiety. Water addition to the *p*-quinone methide and phenol esters hydrolysis give the pyrogallol propargyl ether **47**. Alternatively, the protonated 2-hydroxy-benzodioxole **46d** gives **46h** that, after ester hydrolysis, releases the drug through the 1,6-elimination process.

2.1.4 ADCs based on HMPO linker

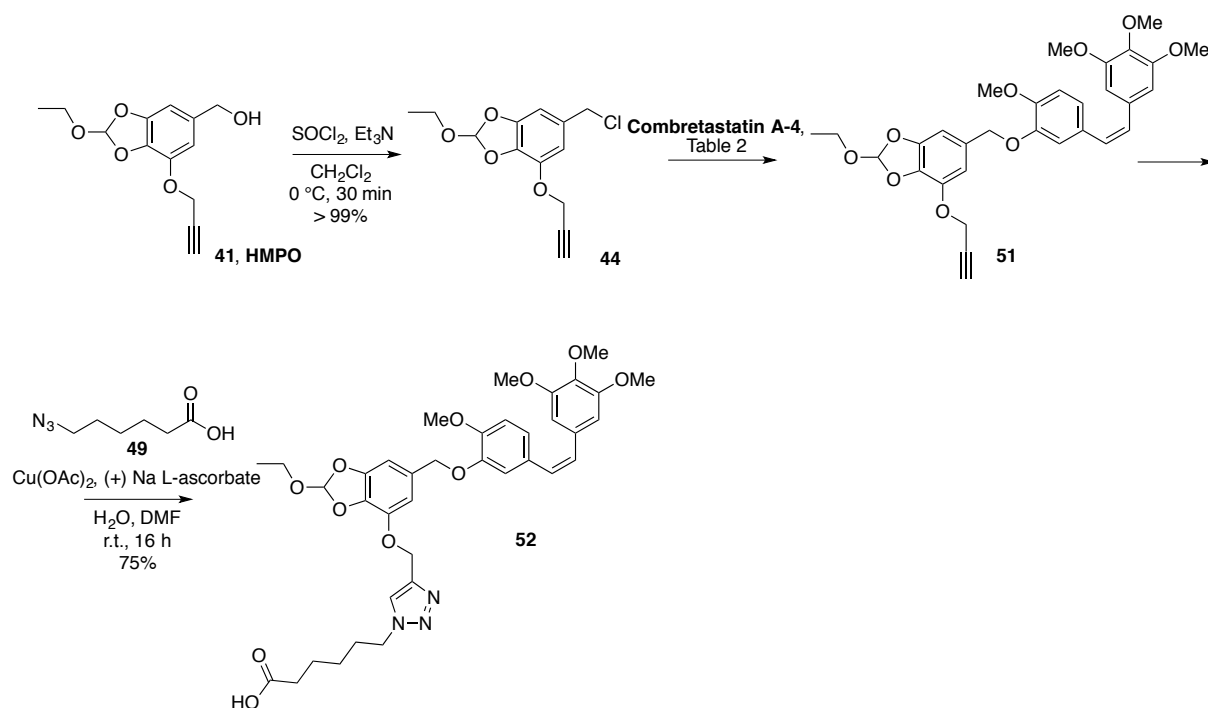
With these data on hand, we applied the HMPO based linker to the conjugation of the antitumor drugs Doxorubicin and Combretastatin A-4 with Cetuximab (Ctx), a mAb specific for the epidermal growth factor receptor (EGFR). As previously reported for the model system **42**, HMPO was activated with *p*-nitrophenyl chloroformate and treated with Doxorubicin in alkaline conditions giving the carbamate **48** in very good yields (73%) (Scheme 5). **48** was subject to Copper-Catalyzed Azide-Alkyne Cycloaddition (CCAA) with 6-azidohexanoic acid

49 in the presence of Cu(II) acetate and (+)-sodium L-ascorbate in DMF/H₂O, providing the desired compound **50** in 64% yield (Scheme 5).



Scheme 5.

Regarding the synthesis of Combretastatin A-4 derivative **52**, the chloride **44** was prepared as previously reported. The deprotonation of Combretastatin A4 was more difficult than the one of phenol **43**. As reported in Entry 1 Table 1, the use of the K₂CO₃ did not reach the product; NaOH provided the product **51** in low yield (Entry 2, Table 2). A stronger base as NaH was required to carry out the reaction with great results (Entry 3, Table 2). Combretastatin A-4 was deprotonated by 60% NaH in DMF and the chloride active compound **44**, prepared in parallel, was added to the mixture at 0 °C to obtain the compound **52** in an optimal yield (98%). CCAA click reaction with azide **49** gave the acid **52** in 75% yield (Scheme 6).



Scheme 6.

Table 2

Entry	Conditions	Yield %
1	K ₂ CO ₃ , KI, Acetone, r.t., 16 h	-
2	NaOH, MeOH/H ₂ O, r.t., 5 h	19
3	NaH 60%, DMF, 0 °C -> r.t. 16 h	98

2.1.5 Hydrolysis profile experiments of the sequences Doxorubicin-HMPO and Combretastatin A-4-HMPO

Molecules **48** and **51** were tested by HPLC analysis as previously done with **42** and **45**, resulting stable in phosphate buffers at pH 7.4 and 6.5 (Table 2, Figure 60 and 61). Only small amounts of Doxorubicin and Combretastatin A-4 were detected after 24 h at 37 °C in these conditions. Moreover, the stability in water was investigated to exclude false positive, confirming that **48** and **51** are stable after 48 h at 37 °C in water. These compounds demonstrated to be stable in human plasma as well. (Table 3).

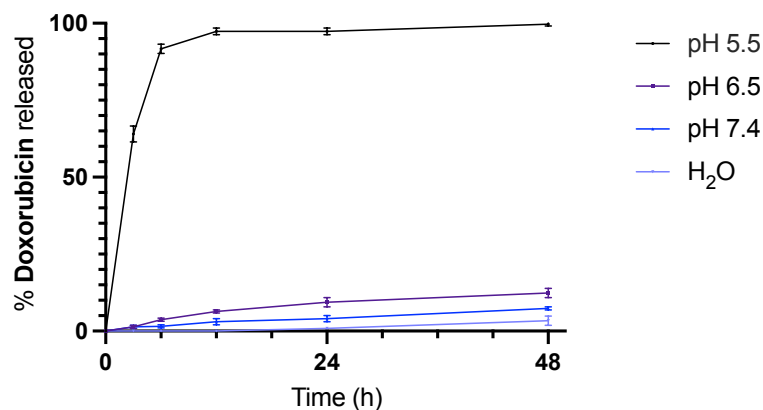


Figure 60. HPLC hydrolysis kinetics of the compound **48** at pHs 5.5, 6.5, 7.4 with phosphate buffers.

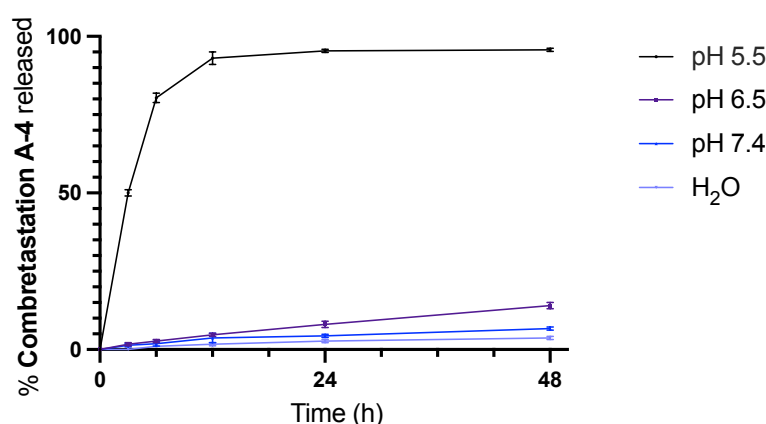


Figure 61. HPLC hydrolysis kinetics of the compound **51** at pHs 5.5, 6.5, 7.4 with phosphate buffers.

Table 3

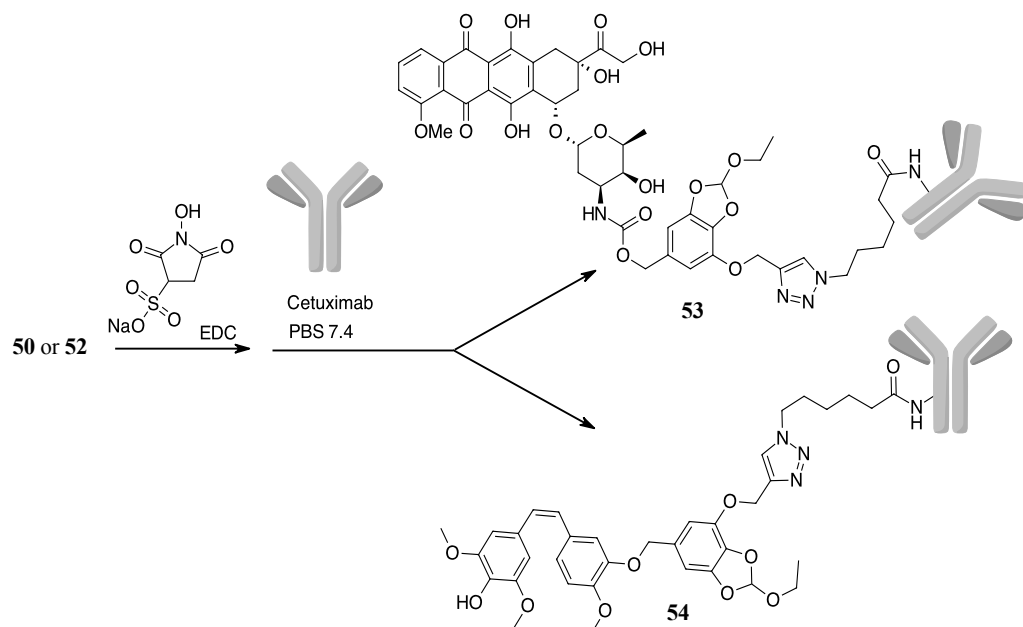
Comp.	H ₂ O ^a	pH 7.4, ^a t _{1/2} ^b	pH 6.5, ^a t _{1/2} ^b	Plasma, ^a t _{1/2} ^b
48	99%	94%, >36 h	90%, >36 h	35%, 8.3 h
51	99%	95%, >36 h	93%, >36 h	89%, 27.6 h

Value expressed as percentage of unmodified compound after 24 hours of incubation; ^b Half-life ($T_{1/2}$) expressed as the amount of time it takes before half of the drug is hydrolyzed/degraded.

The compound **48** showed a $T_{1/2}$ value in line with the general behavior in plasma of Doxorubicin alone. These results confirmed that pH-sensitive HMPO linker is stable in biological fluids such as blood. On the other hand, hydrolysis at pH 5.5 was rapid (Figure 60 and 61) showing for the sequence **48** a first order reaction occurring in the first hours with a *plateau* after 6 h, when almost the 90% of the drug was released. Although the behavior of **51** was slightly different, 93% of Combretastatin A-4 was released after 12 h.

For the bioconjugation with mAbs, carboxylic acids **50** and **52** were transformed into the corresponding NHS-esters in PBS pH 7.4 in presence of S-NHS and EDC, and dialyzed Ctx in

PBS pH 7.4 was added to obtain bioconjugates **53** and **54** (Scheme 7). Purification of **53** and **54** were carried out by dialysis, and the drug antibody ratio (DAR) was determined by MALDI analysis (DAR of ADC **53** = 1.7 and DAR of ADC **54** = 1.4).



Scheme 7.

2.1.6 MTT assay of Ctx-HMPO-Doxorubicin and Ctx-HMPO-Combretastatin A-4 ADCs

The anti-proliferative activity of the ADCs **53** and **54** was evaluated with a MTT assay on epidermoid carcinoma (A431) and human lung carcinoma (A459) cell lines. Both A431 and A459 overexpress EGFR. Treatment with **53** and **54** showed a stronger antiproliferative effect if compared with unconjugated Ctx (Figure 62). In addition, the effect was comparable to the activity of the free drugs confirming the release of Doxorubicin and Combretastatin A4 in the cell cultures.

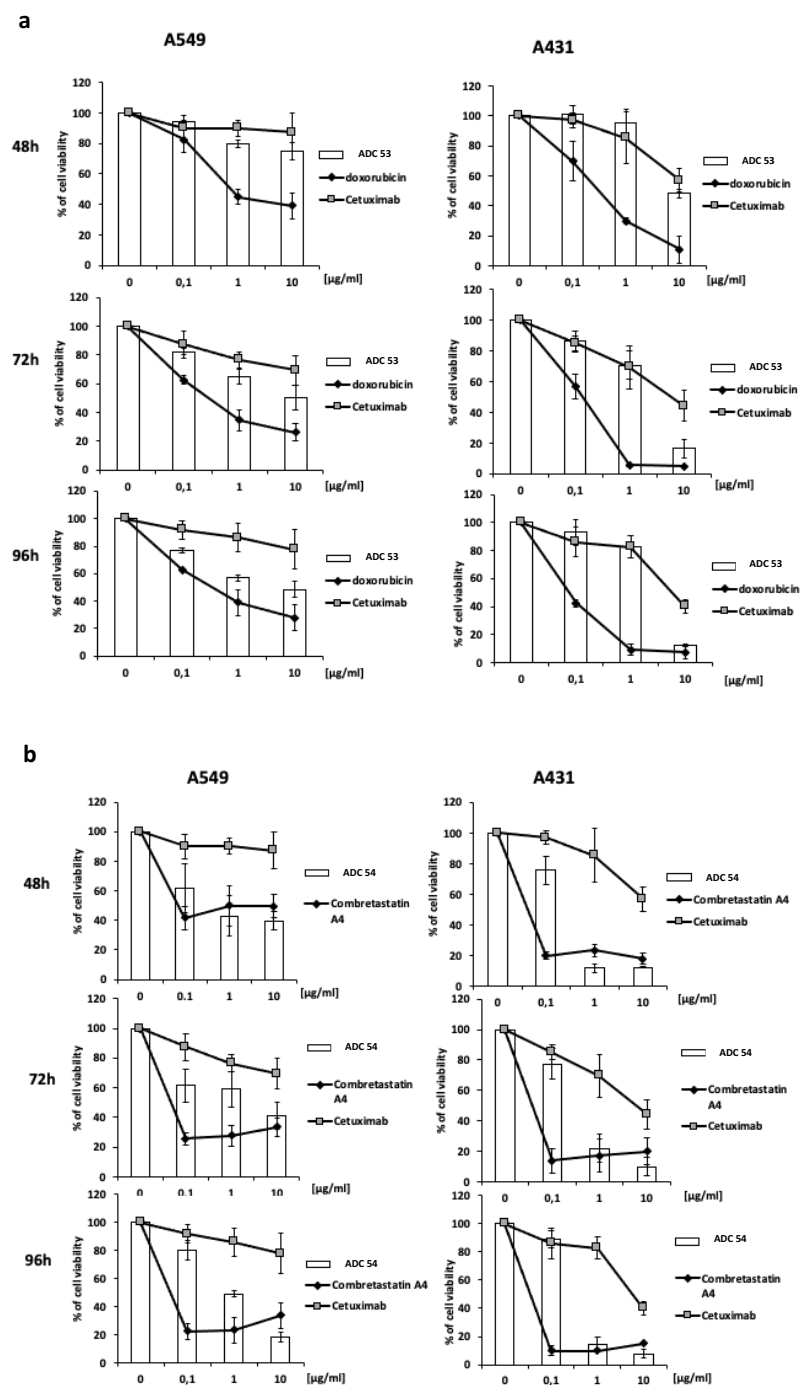


Figure 62. MTT assay of the ADC 53 and ADC 54 compared with Ctx and the corresponding free drug in A431 and A549 cell lines.

2.2 A new reactive oxygen species (ROS) sensitive linker

As reported in paragraph 1.2.2.2.2, borate, thioether and thioketals moieties were used to design prodrugs or polymeric systems but they were not yet employed for the development of drug conjugates. Our purpose was focused on the research of a hypoxic sensitive traceless crosslinker based on 1,6 self-immolative elimination process easy to apply on the design of drug conjugates

(Figure 63). As Phillips et al. reported, aryl borate esters are able to release primary/secondary alcohols or phenols giving the opportunity to link a payload not only through a classic carbamate moiety. [71] We took inspiration from this work improving the versatility of this system on the field of ADCs. Moreover, it is known that byproducts that come from boric derivatives are well-tolerated in humans. [69] This is a further point which encourages the application of our new linker for the development of drug delivery systems.

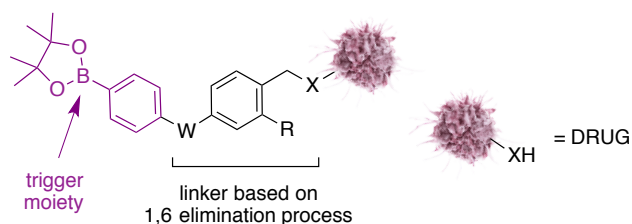


Figure 63. Schematic representation of a generic sensitive traceless crosslinker based on 1,6 self-immolative elimination process.

2.2.1 First linker proposed

At the beginning the linker in the Figure 64 was what we were supposed to synthesized.

It is composed of:

- a boronic ester trigger moiety to make the system sensible to ROS species;
- a benzyl alcohol moiety to bind different drugs carrying a primary or secondary amine (as carbamate) and a phenol (as an aryl benzyl ether);
- an alkyne group suitable for further functionalization with the carrier (*i.e.* antibody or ligand).

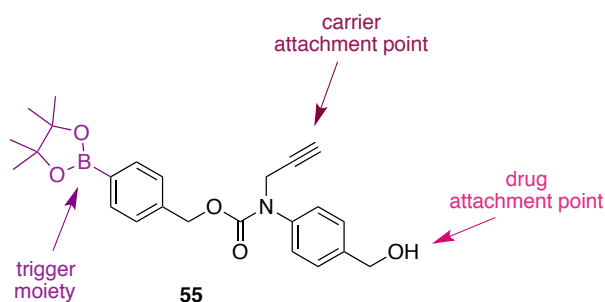
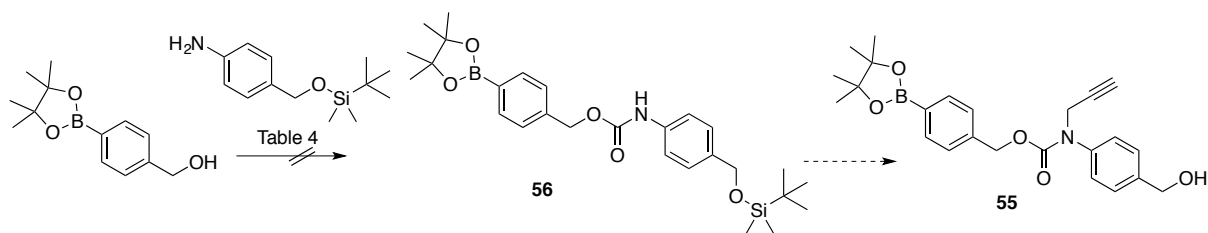


Figure 64. First linker proposed.

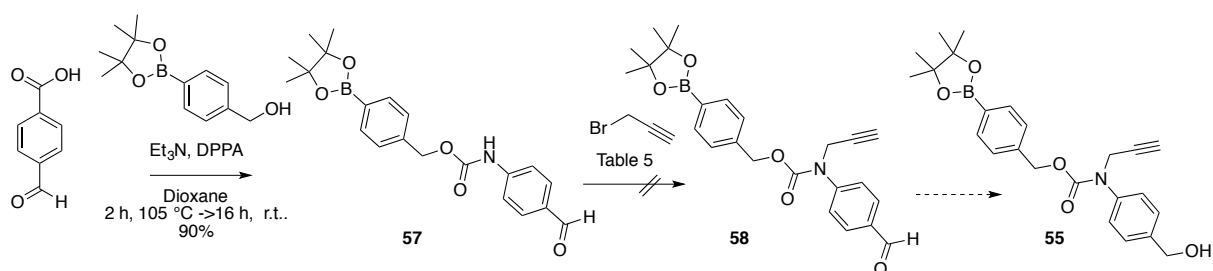


Scheme 8.

Table 4

Entry	Conditions	Yield %
1	1) <i>p</i> -nitrophenyl chlorophormate, Py, DMAP, THF, 0 °C -> r.t., 16 h 2) DIPEA, DMAP, 0 °C -> r.t., 16 h	-
2	1) CDI, CH ₂ Cl ₂ , r.t., 1 h 2) DIPEA, DMAP, r.t., 16 h	-
3	1) phosgene, Et ₃ N, Toluene, 0 °C -> r.t., 1 h 2) Et ₃ N, DMAP, 0 °C -> r.t., 16 h	-

For the synthesis of compound **56**, the alcohol moiety of 4-(hydroxymethyl)phenylboronic acid pinacol ester was activated in different conditions by using *p*-nitrophenyl chlorophormate, CDI or phosgene (Table 4). The intermediate obtained with the *p*-nitrophenyl chlorophormate was highly unstable and difficult to handle for the next step, while the imidazole derivative was too much stable hindering the formation of the carbamate. The use of phosgene led to an intermediate which is a fair middle way in terms of stability and reactivity. Anyway, with all the three different activations, the obtainment of the reactive intermediate was achieved and used in presence of the aniline in alkaline conditions (Scheme 8, Table 4). A degradation of boronic ester moiety was observed without the obtainment of compound **56**. Further experiments changing equivalents of both activator reagent and base, temperatures and type of bases were conducted (even if not reported) without providing the desired compound. This route was therefore abandoned.



Scheme 9.

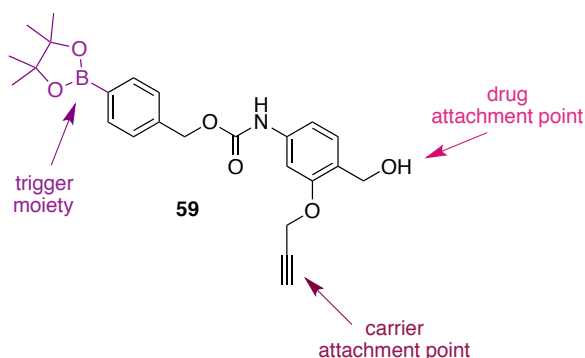
Table 5

Entry	Conditions	Yield %
1	KHMDS, THF, -78 °C -> -30 °C, 3 h 30 min	-
2	NaH, DMF, 0 °C -> r.t, 1 h 30 min	-

As reported in literature, starting from 4-formylbenzoic acid in dioxane in presence of diphenylphosphoryl azide (DPPA), Et₃N and the desired alcohol a Curtius rearrangement leads to the obtainment of a carbamate moiety [71]. Following this procedure, the compound **57** was synthesized in a very good yield (90%) (Scheme 9). In order to introduce a derivatization for an orthogonal connection to a macromolecular carrier, a deprotonation of carbamate nitrogen with a strong base such as KHMS and NaH (Table 5) was tried without providing the formation of the compound **58** (Scheme 9). A degradation of boronic ester moiety was observed as previously (Scheme 8) perhaps, due to the strong basic environment. Boronic ester moiety is very sensitive to alkaline reaction conditions which cause the hydrolysis of this function.

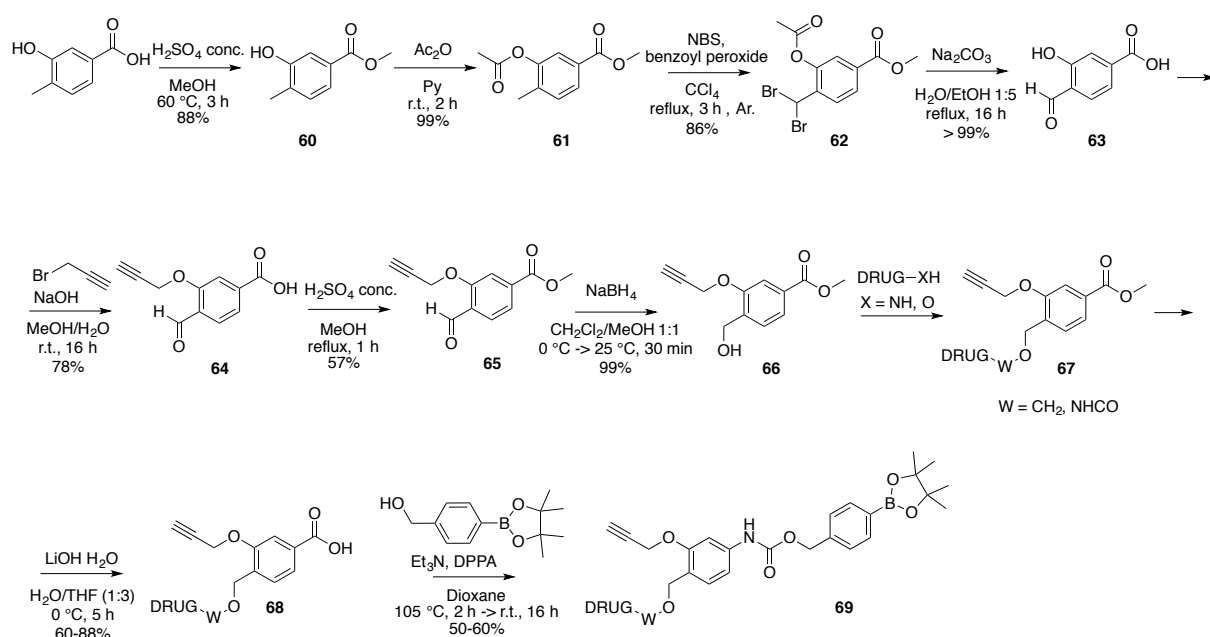
2.2.2 Second linker proposed

Because of the unsatisfactory results obtained, we decided to investigate the synthesis of a different linker (Figure 65).

**Figure 65.**

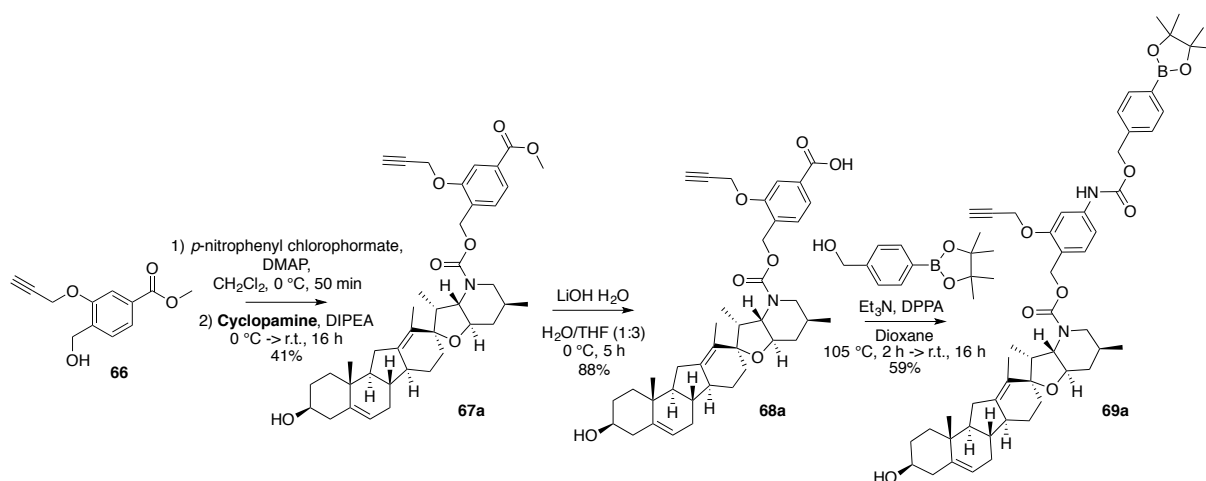
3-Hydroxy-4-methylbenzoic acid methyl ester **60** that was acetylated with Ac₂O in Pyridine as the solvent giving **61** in a very high yield (Scheme 10). [222] Compound **61** was transformed into the aldehyde **63** by treatment with NBS with a catalytic amount of benzoyl peroxide followed by debromination of the dibromo intermediate **62** in presence of Na₂CO₃. [223] **63** was deprotonated with NaOH and alkylated with propargyl bromide obtaining **64** that was esterified as already reported (Scheme 10). Based on the experiences so far, high amounts of

bases, usually required to allow the linker binding with hydroxyl- and amine-bearing payloads, in this case could cause the hydrolysis of the boronic ester (Scheme 8 and 9). For this reason, the reduction of the aldehyde and the drug binding must be done before the introduction of trigger moiety. The aldehyde **65** was treated with NaBH₄ obtaining the alcohol in excellent yield, then many drugs can be added bound to the linker by using different reaction conditions. Finally, after the hydrolysis of the methyl ester under mild conditions, the carbamate **69** was obtained by Curtius rearrangement in good yields (50-60%). This represents an unconventional route for the design of a drug delivery system where the drug cargo is before the linker synthesis ending.



Scheme 10.

The drug used to test our strategy was Cycloplamine (Scheme 11), a SMO inhibitor we were interested in for the development of ADCs for the treatment of melanoma.



Scheme 11.

The benzyl alcohol **66** was activated by a treatment with *p*-nitrophenyl chlorophormate and added to a solution of Cyclopamine in presence of DMAP and DIPEA as bases providing the desired product **67a**. The saponification of the ester was performed with LiOH giving the free carboxylic acid **68a** in good yield (88%). The acid was treated with 4-(hydroxymethyl)phenylboronic acid pinacol ester in presence of Et₃N and DPPA giving **69a**. A preliminary drug release in hypoxic environment was determined by HPLC using compound **69a** as a model. Taking inspiration from the procedure reported by Phillips et al., the compound **69a** solubilized in DMSO, diluted in a phosphate buffer at pH 7.4 and a water solution of H₂O₂-urea was added. The mixture was sonicated, incubated at 37 °C for 10 minutes and a sample was injected to the HPLC. A total release of Cyclopamine was observed encouraging further studies and a plausible extended use of this linker.

2.3 ADCs armed with SMO inhibitors

2.3.1 SMO inhibitors as potential payloads for the development of ADCs

SMO inhibitors are an unexplored class of potentially interesting payload for the development of new ADCs for, but not limited to, the treatment of melanoma. The active molecules chosen for this aim were MRTs inhibitors, Vismodegib and Cyclopamine.

The MRT selected for this work was MRT-86 because already present in large quantity in the laboratory and one of the hit compounds.

MRT-86 does not contain any alcoholic or amine group (Figure 66), thus the only suitable functional group for its introduction into an ADC could be the guanidine moiety. The challenge

was the obtainment of ADCs exploiting unconventional payload attachment points.

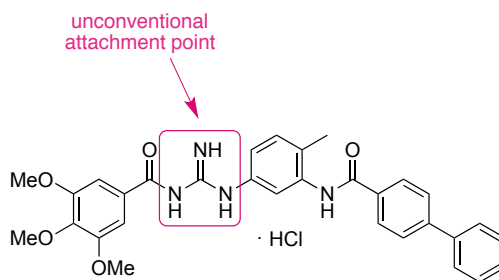


Figure 66. MRT-86

To make the use of MRTs as payloads more accessible, the only possible functional group modification can be done in the L region of the MRT scaffold (see paragraph 1.3.2.1) without losing their inhibitory activity. An analogue of MRT-92, called FRM326, was developed for this purpose (Figure 67). As already indicated by previously reported SAR analysis, [214] the replacement of a –OMe group with an –OH moiety in *para* position did not impact in the activity (preliminary *in vitro* assay: MRT-92: A375 $IC_{50} = 0.299 \pm 0.05 \mu M$, BT474 $IC_{50} = 1.0 \pm 0.1 \mu M$; FRM326: A375 $IC_{50} = 1.06 \pm 0.6 \mu M$, BT474 $IC_{50} = 0.5 \pm 0.1 \mu M$).

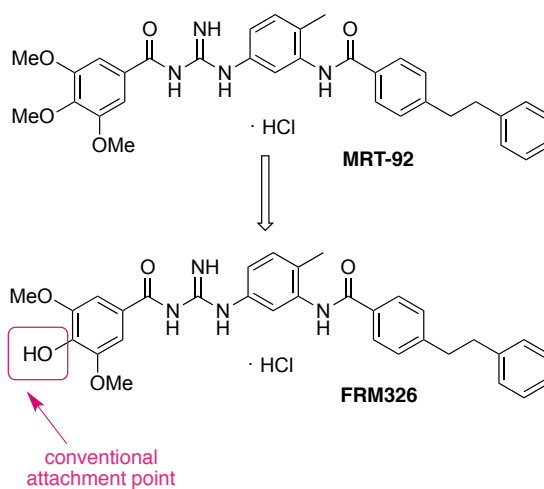


Figure 67. MRT-92 and its analogue FRM326 developed to generate a conventional attachment point for the development of a drug delivery system.

As for MRT-86, Vismodegib does not have an amine or hydroxyl group suitable for the classic linker binding and the only suitable functional group for its introduction into an ADC could be the pyridine nitrogen. (Figure 68).

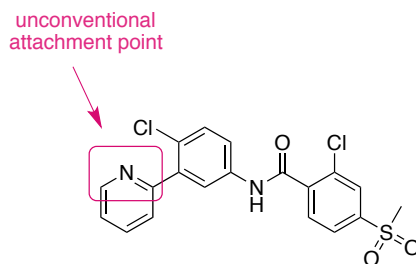


Figure 68. Vismodegib.

Finally, analyzing the molecular structure of Cyclopamine (Figure 69), it presents a conventional secondary amine that was employed for the synthesis of different ADCs.

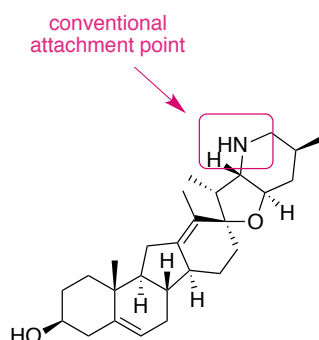


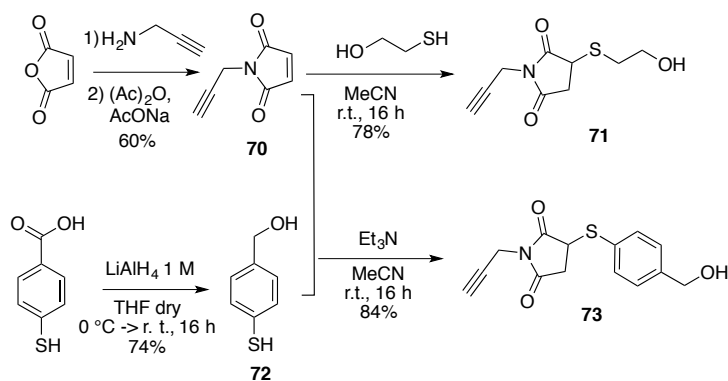
Figure 69. Cyclopamine.

2.3.2 ADCs armed with SMO inhibitors using non-cleavable linkers

2.3.2.1 Synthesis of non-cleavable linkers

Starting from maleic anhydride in presence of propargyl amine and acetic anhydride the corresponding maleimido derivative **70** was obtained [224] and two different self-immolative spacers were introduced by Michael-addition. **70** was treated with 2-mercaptoethanol [225] or freshly prepared *p*-mercaptobenzyl alcohol **72** providing compounds **71** and **73** respectively (Scheme 12). *p*-Mercaptobenzyl alcohol **72** was synthesized by reduction with LiAlH₄. [226] **72** is quite unstable and need to be quickly used.

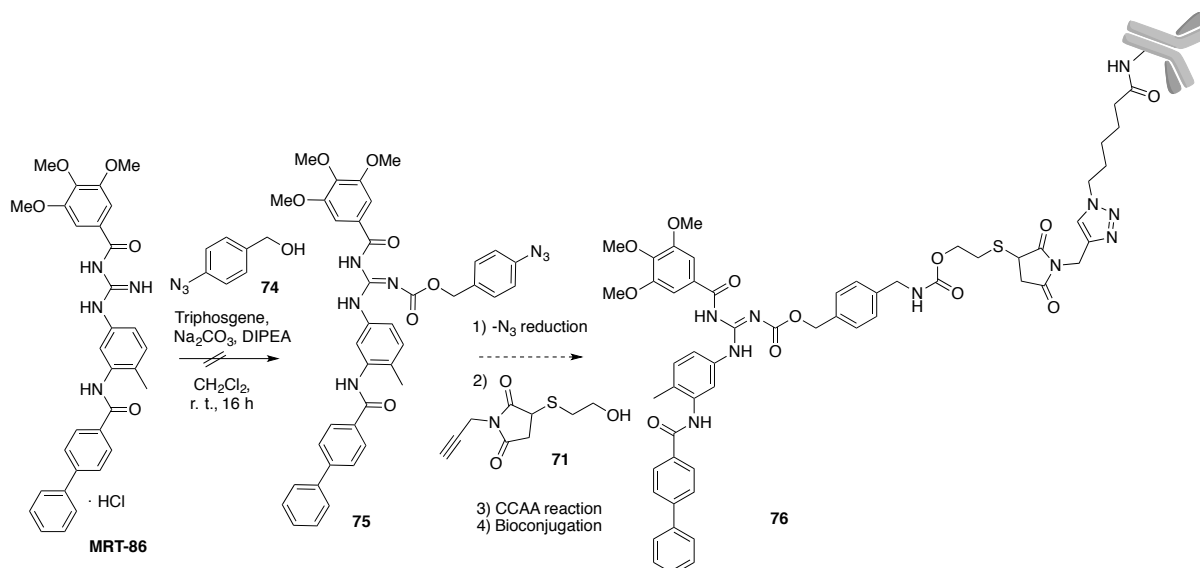
The final compound **71** was designed to release the drug with a cyclisation rearrangement while the product **73** was to allow the release thanks to a 1,6-elimination process.



Scheme 12.

2.3.2.2 Synthesis of ADCs armed with MRT-86 through a non-cleavable linker using the guanidine as drug binding moiety

First synthetic route:



Scheme 13.

In scheme 13 is reported the first approach involving the formation of a carbamate between the –NH of the guanidine and the alcohol moiety of the PABA-like derivative **74** *via* activation by triphosgene. Unfortunately, side product **77** was always obtained as the only reaction product instead of expected compound **75** (Figure 70). The structure was hypothesized taking into account that the carbonyl moiety of acylguanidine tautomerizes in its enolate form providing a nucleophilic attack to the carbonyl of carbamate just formed. This route was therefore abandoned.

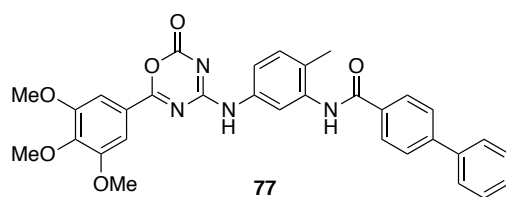
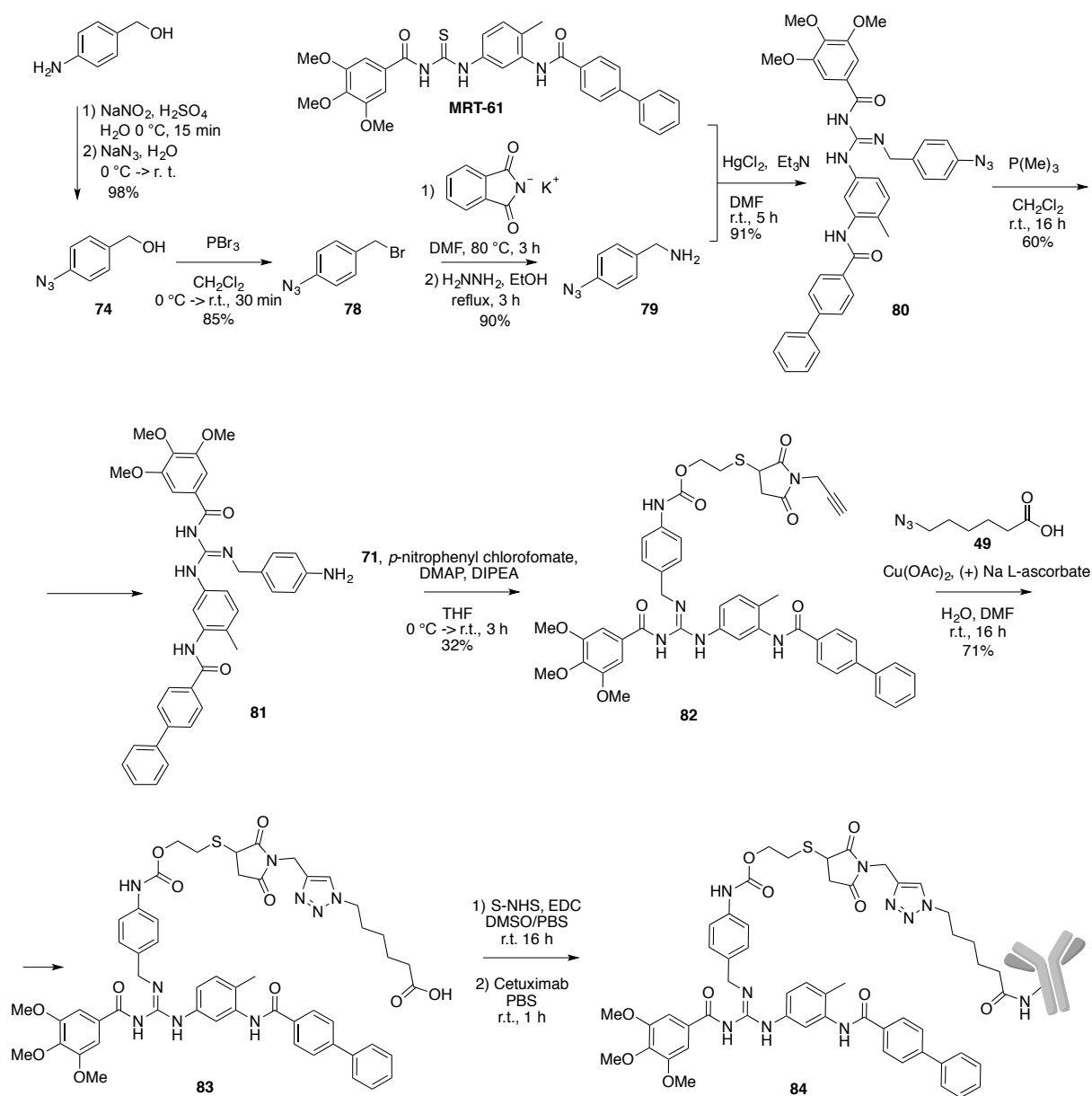


Figure 70.

Because of the unsatisfactory results obtained, we decided to investigate the synthesis of an ADC charged with MRT-86 changing the synthetic approach without the necessity to form a carbamate on the guanidine group.

Second synthetic route:



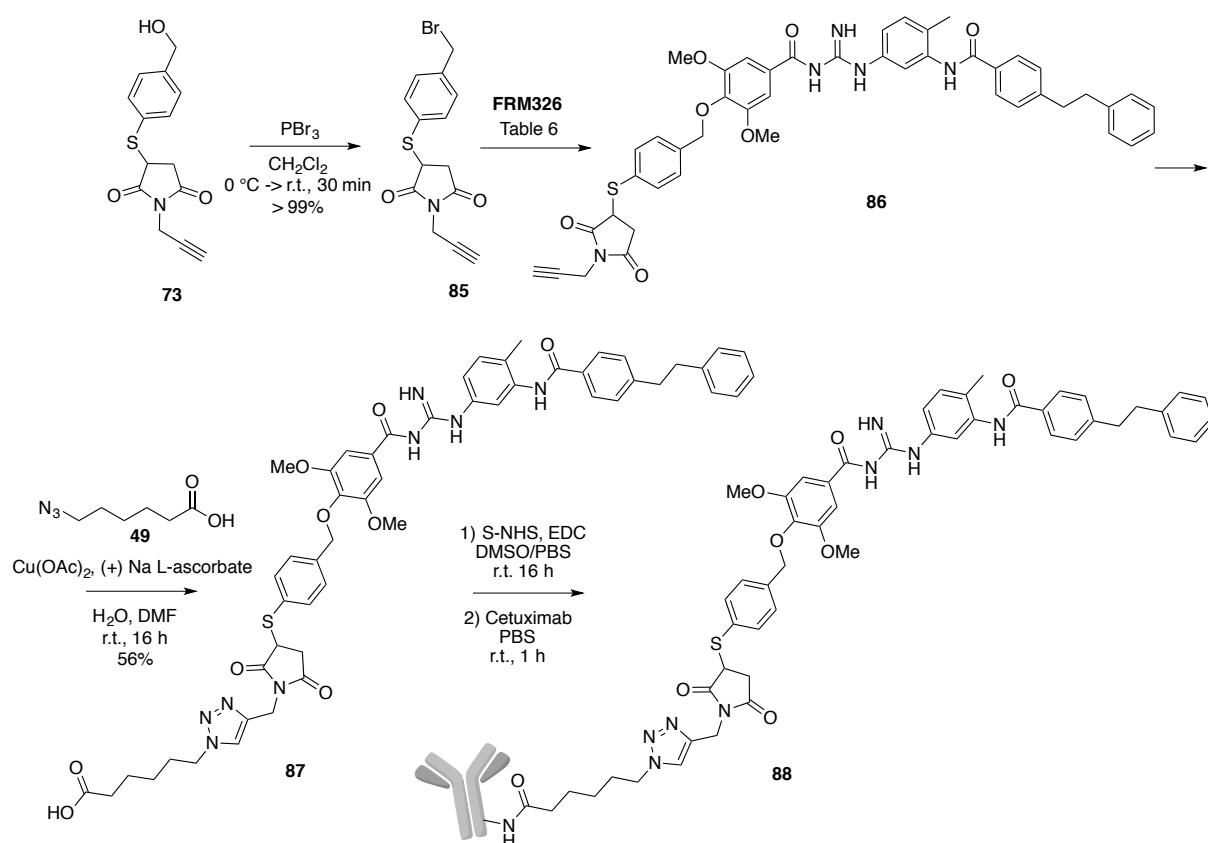
Scheme 14.

p-Amino benzyl alcohol was treated with NaNO_2 and NaN_3 giving the corresponding azide **74** [227]. The benzylic alcohol moiety was converted into the desired bromide **78** by a treatment with PBr_3 in a good yield (85%). Then, Gabriel synthesis furnished benzylic amine **79**. [228] Starting from the AcTU **MRT-61**, easier to synthesize than its AcG analogue (MRT-86), it was possible to achieve the corresponding alkylated guanidine through a guanylation reaction in the presence of HgCl_2 . [229] **MRT-61** was treated with amine **79** in the presence of HgCl_2 and Et_3N giving acylguanidine **80** in very high yield (91%). This process represents a fast way to synthesize the AcG **MRT-92** already alkylated in its guanidine moiety starting from the

corresponding AcTU. This reaction represents the crucial step that allows the PABA-like spacer binding with the drug through its unconventional attachment point (guanidine group). After the azide reduction, many different linkers or other spacers can be introduced. The azide **81** was reduced with $\text{P}(\text{Me})_3$ and in presence of the linker **71** previously activated by *p*-nitrophenyl chloroformate giving the carbamate **82**. CCAA click reaction with azide **49** provided the acid **83** in 71% yield. The carboxylic acids **83** was transformed into the corresponding NHS-esters in PBS at pH 7.4 in presence of S-NHS and EDC, and further dialyzed Ctx was added to obtain bioconjugates **84** where the payloads were linked to lysine residues of the mAb through a stable amide bond (Scheme 14). Purification of the final conjugate was carried out by dialysis, and the DAR was determined by MALDI analysis (DAR = 2.3).

2.3.2.3 Synthesis of ADCs armed with FRM326 through a non-cleavable linker using the phenol group as drug binding moiety

The linker **73** was brominated in presence of PBr_3 to obtain a better leaving group. **85** was obtained in a quantitative yield and, because of its instability and H_2O sensitivity, it could not be stored and must be immediately used to avoid the formation of the starting benzyl alcohol. **FRM 326** was deprotonated with NaOH 10 N (Table 6, Entry 2) and a solution of freshly prepared bromide **85** was added dropwise giving immediately the alkylated product **86**. K_2CO_3 was used at the beginning with no results maybe due to its minor basicity that is not enough to deprotonate the phenol which also presents a quite steric hindrance (Table 6, Entry 1). The compound **86** is the key intermediate that after the usual CCAA reaction and the bioconjugation with Ctx gave the desired ADC **88**. The carboxylic acids **87** was activated as NHS-esters and further dialyzed Ctx was added to obtain bioconjugates **88** DAR = 3.4 (Scheme 15).



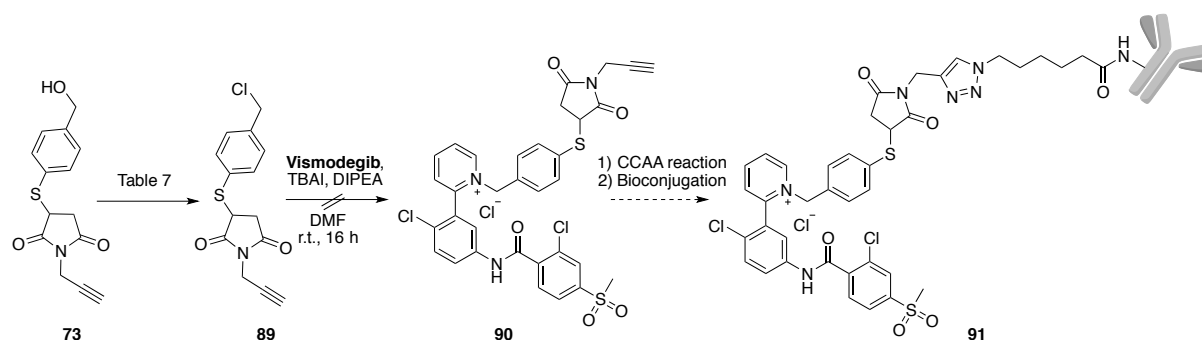
Scheme 15.

Table 6

Entry	Conditions	Yield %
1	K ₂ CO ₃ , KI, Acetone, r.t., 16 h	-
2	NaOH, MeOH/H ₂ O, r.t., 5 min	45

2.3.2.4 Synthesis of ADCs armed with Vismodegib through a non-cleavable linker using the pyridine nitrogen as drug binding moiety

The linker **73** was used in presence of SOCl₂ and 1*H*-Benzotriazole without results (Entry 1, Table 7). When Et₃N was added, the reaction worked giving the corresponding chloride **89** in a quantitative yield (Entry 2, Table 7). The compound **89** was immediately used for the alkylation of Vismodegib on pyridine nitrogen in presence of a phase-transfer catalyst without success (Scheme 16). Good results were obtained by using the cleavable HMPO linker **41** that provided the desired product with good results thus confirming its versatility (Scheme 19).



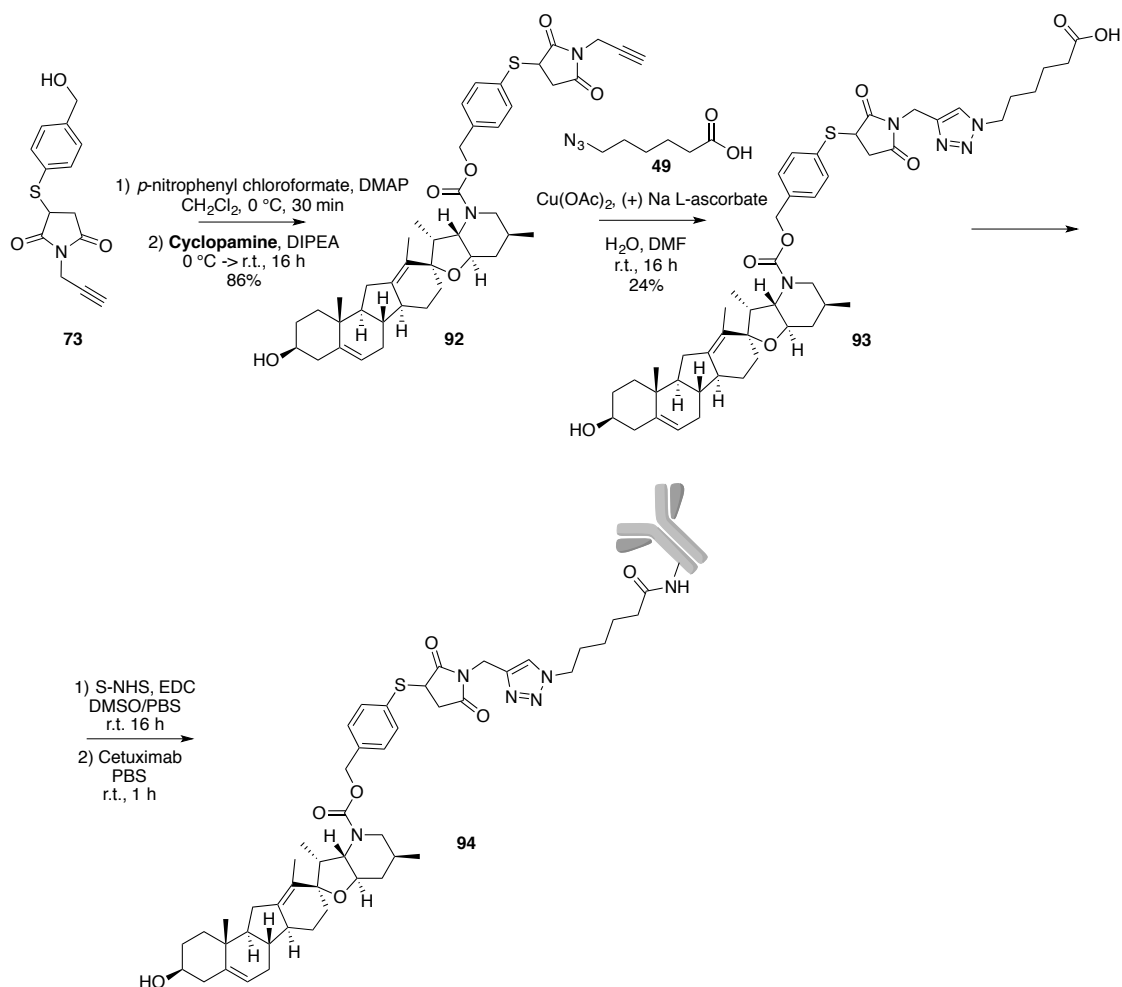
Scheme 16.

Table 7

Entry	Conditions	Yield %
1	SOCl ₂ , 1H-Benzotriazole, CH ₂ Cl ₂ , 0 °C, 10 min	-
2	SOCl ₂ , Et ₃ N, CH ₂ Cl ₂ , 0 °C, 15 min	> 99

2.3.2.5 Synthesis of ADCs armed with Cycloamine through a non-cleavable linker using the secondary amine as drug binding moiety

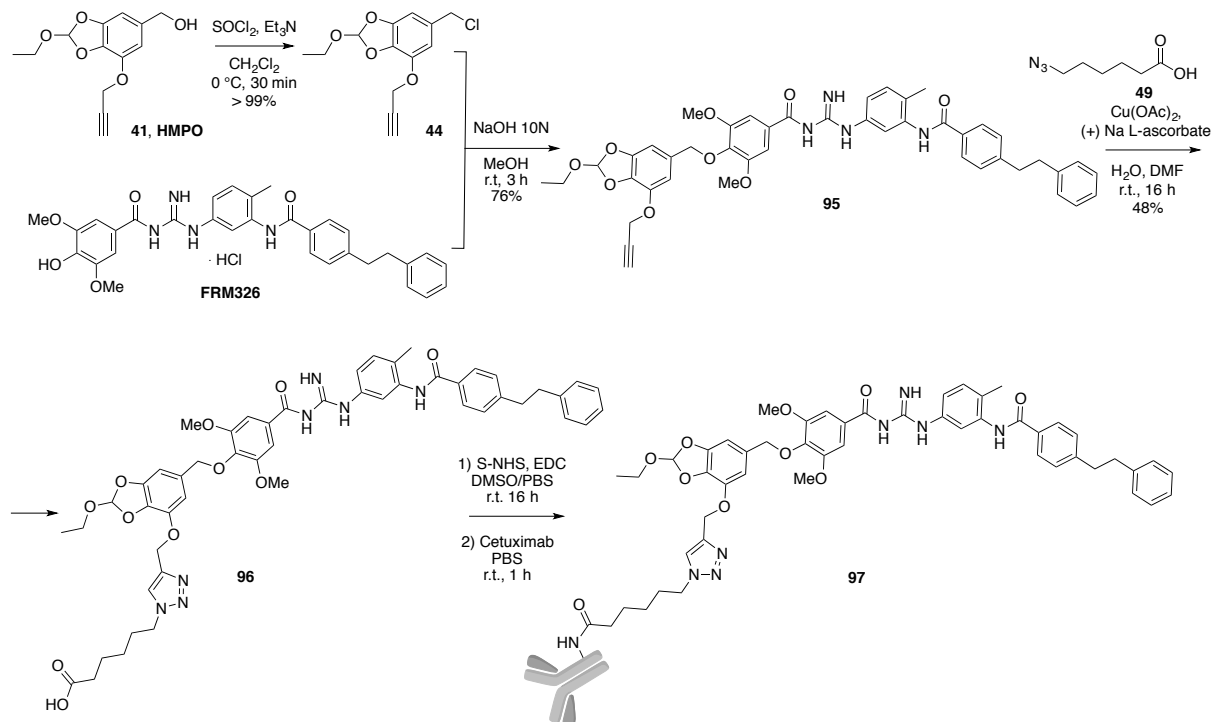
For the synthesis of the ADC **94** armed with Cycloamine, the non-cleavable linker **73** was activated in presence of *p*-nitrophenyl chloroformate and added to a solution of DIPEA and the payload providing the carbamate **92** in a very good yield (86%). The corresponding acid **93** was obtained *via* CCAA reaction. The activation of **93** as NHS-esters in presence of S-NHS and EDC and the further bioconjugation with Ctx gave the desired ADC **94**. DAR = 3.1 (Scheme 17).



Scheme 17.

2.3.3 ADCs armed with SMO inhibitors using innovative cleavable linkers

2.3.3.1 Synthesis of ADCs armed with FRM326 through HMPO linker using the phenol group as drug binding moiety



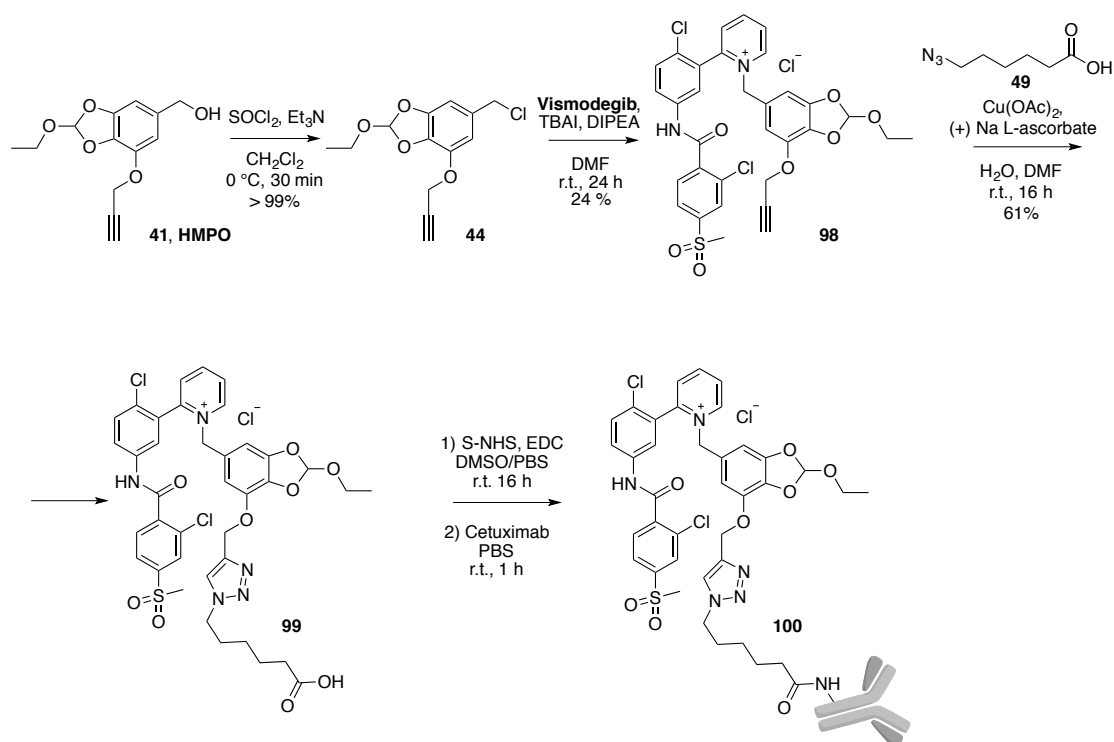
Scheme 18.

The cleavable linker **41** (HMPO) was transformed in the corresponding benzyl chloride **44** as already reported and added dropwise to a solution of **FRM 326** previously deprotonated with NaOH: alkylated key product **95** was obtained in 76% yield. **95** was treated with Cu(II) acetate and (+) sodium L-ascorbate in DMF/water, providing the desired compound **96** that was activated into the NHS-ester derivative and then bioconjugated with Ctx achieving the final ADC **97** with DAR = 1.9 (Scheme 18).

2.3.3.2 Synthesis of ADCs armed with Vismodegib through HMPO linker using the pyridine nitrogen as drug binding moiety

For the synthesis of ADC **100**, the cleavable linker **41** (HMPO) was again transformed in the corresponding benzyl chloride **44** and added dropwise to a solution of Vismodegib in presence of a phase-transfer catalyst (TBAI) and DIPEA. **98** was transformed into the carboxylic acid **99** via CCAA. Finally, the activation of **99** in presence of S-NHS and EDC and the further bioconjugation with Ctx gave the desired ADC **100**. DAR = 2.1 (Scheme 19).

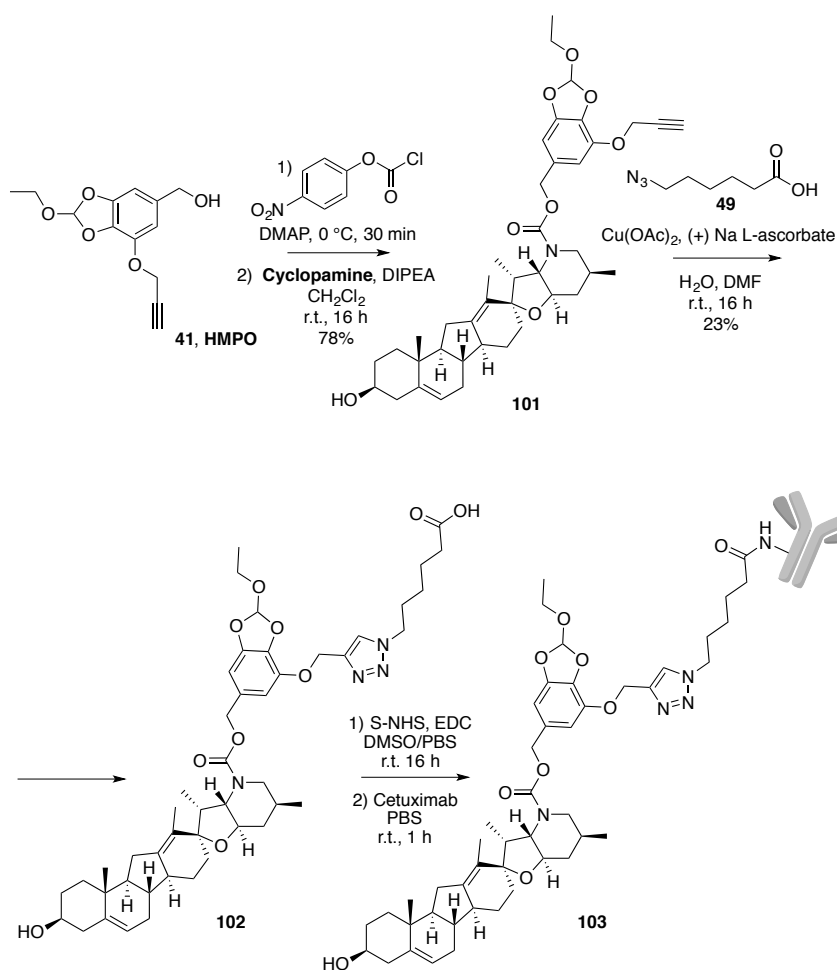
In contrast with the failed route developed with non-cleavable linker **73**, **41** HMPO allowed the alkylation of pyridine nitrogen furnishing ADC **100**. The versatility of HMPO linker with no conventional payloads has been proved and well-established.



Scheme 19.

2.3.3.3 Synthesis of ADCs armed with Cyclopamine through HMPO linker using the secondary amine as drug binding moiety

ADC **103** is armed with Cyclopamine: HMPO **41** was activated in presence of *p*-nitrophenyl chloroformate and without purification it was added dropwise to a solution of DIPEA and Cyclopamine giving the carbamate **101** in a very good yield (78%). **101** was transformed into the corresponding acid **102** via CCAA reaction in presence of Cu(II) acetate and sodium ascorbate in DMF/water. At the end, the activation of **102** as NHS-esters and the further bioconjugation with Cetuximab provided the desired ADC **103**. DAR = 2.2 (Scheme 20).

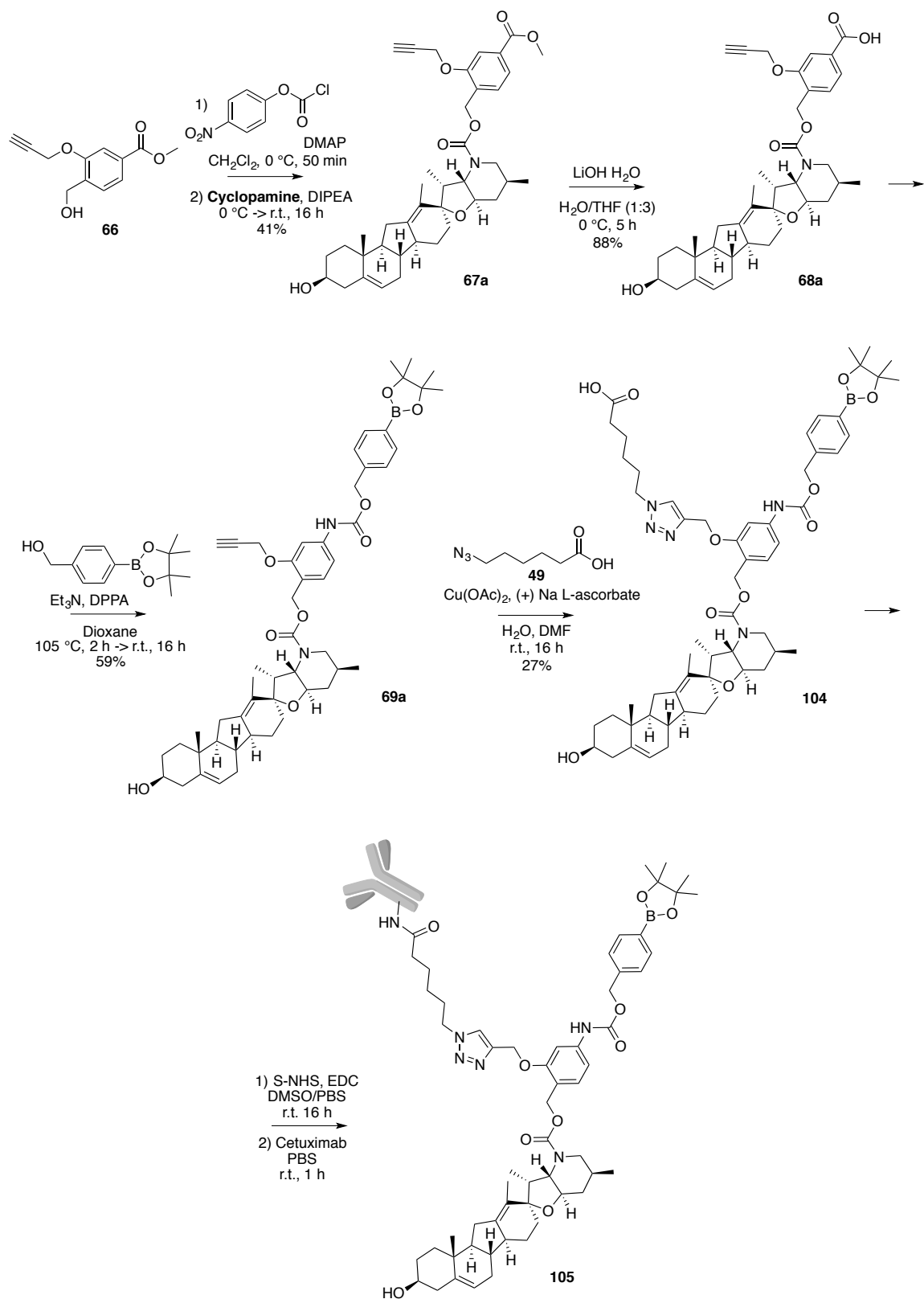


Scheme 20.

2.3.3.4 Synthesis of ADCs armed with Cyclopamine through borate cleavable linker using the secondary amine as drug binding moiety

Regarding the synthesis of the ADC **105**, the steps until the preparation of the borate ester **69a** are reported in the paragraph 2.2.2.1. As performed for all the other ADCs, CCAA reaction and the bioconjugation with Ctx were carried out providing the final compound **105** (Scheme 21). DAR = 2.4.

The hypoxic sensitive linker **59** was used only with Cyclopamine as cytotoxic drug with great results. Certainly, in the future, this strategy will be applied to other payloads.



Scheme 21.

Conclusions

This research work is devoted to the development of new ADCs for melanoma treatment. Particularly, the attention was focused both on the introduction of unconventional payloads such as SMO inhibitors, as well as on the development of versatile new cleavable linkers to be applied on different fields.

During this work, we developed the first pH sensitive traceless crosslinker based on the 1,6 self-immolative elimination process. Starting from gallic acid, 5-(hydroxymethyl)pyrogallol orthoester (HMPO) derivative was obtained in four steps. This HMPO linker was projected to easily connect the targeting agent (mAb or ligand) with payloads for an efficient drug delivery into tumor cells (Figure 54). HMPO has an orthoester trigger moiety that is stable at pH 7.4 and hydrolysable at pH below 5.5.

Doxorubicin and Combretastatin A-4 were easily bound to HMPO benzylic alcohol moiety while the linker alkyne group was employed for charging Cetuximab (Ctx) (Figure 71). The release tests, *via* HPLC, showed that HMPO released the payloads at pH 5.5 while it was stable for 24 h at pH 7.4 and 6.6. Stability in plasma was also investigated with great results. Different primary and secondary amine- and alcohol- and phenols containing molecules can be anchored through standard carbamate, carbonate or ether forming reactions while alkyne get an easy access for the conjugation with macromolecular carriers. HMPO is a very versatile linker that can be used to charge payload exploiting unconventional drug attachment points such as pyridine nitrogen of Vismodegib (ADC **100**, Figure 72).

In order to support the good operating principle of HMPO, ADCs formed by Ctx-HMPO-Doxorubicin (ADC **53**) and Ctx-HMPO-Combretastatin A-4 (ADC **54**) were tested in an anti-proliferative activity assay (MTT assay) with A431 and A459 cancer cell lines showing a stronger anti-proliferative effect of ADCs if compared with Ctx alone.

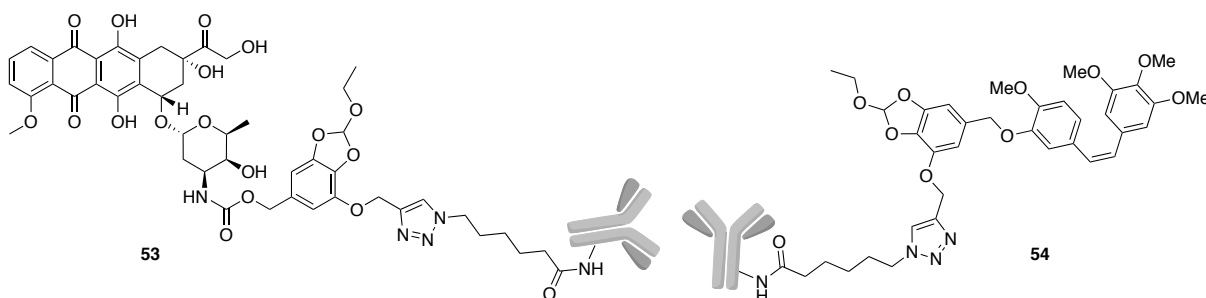


Figure 71. ADC **53**: Ctx-HMPO-Doxorubicin; ADC **54**: Ctx-HMPO-Combretastatin A-4.

In the second part of this work, we synthesized the first linker suitable for the development of drug delivery systems based on aryl borate esters as trigger moiety selective towards ROS (Figure 52). As well as for HMPO, this linker is based on 1,6 self-immolative elimination process. The drugs can be charged through the benzylic alcohol group, while the targeting agents can be bound thanks to a click chemistry reaction. Preliminary drug release studies of this platform were set up in hypoxic environment with promising results but further data with *in vitro* assays must be done to improve the knowledge of the real linker potentiality.

Up to now, only one of the ADCs, synthesized during this PhD work, is based on the linker **59** and it is armed with Cyclophosphamide (ADC **105**, Figure 72). In a future perspective, several payloads will be used because the most attractive workhorse is that byproducts coming from borate derivatives are well tolerated in humans.

The largest part of the work was based on the development of ADCs armed with SMO inhibitors. The cytotoxic drugs chosen for this aim were MRTs inhibitors (MRT-86 and FRM326), Vismodegib and Cyclophosphamide. Some of SMO inhibitors like Vismodegib and MRTs (in our case MRT-86) do not contain the traditional $-NH_2$ and $-OH$ functional groups used for their bond with the linker.

The huge challenge for the synthesis of ADCs armed with SMO inhibitors was not only the design of linkers with excellent release and stability profiles, but also the research of unconventional drugs attachment points. The ADC charged with Vismodegib (ADC **100**, Figure 72) was developed by exploiting its unconventional pyridine nitrogen, while regarding the MRT-86 bioconjugation, the ADC **84** (Figure 72) was obtained anchoring the linker through the guanidine moiety of the drug.

At the end, seven different ADCs were synthesized with:

- Ctx as mAb;
- MRT-86, FRM326, Vismodegib and Cyclophosphamide as payloads;
- classic non-cleavable linkers (compounds **71** and **73**) and new cleavable linkers as HMPO (**41**) and aryl borate ester derivative **59** (Figure 72).

All these conjugates have been sent to the “Istituto per lo Studio, la Prevenzione e la Rete Oncologica” in Florence for the *in vitro* biological evaluation in different tumor cell lines.

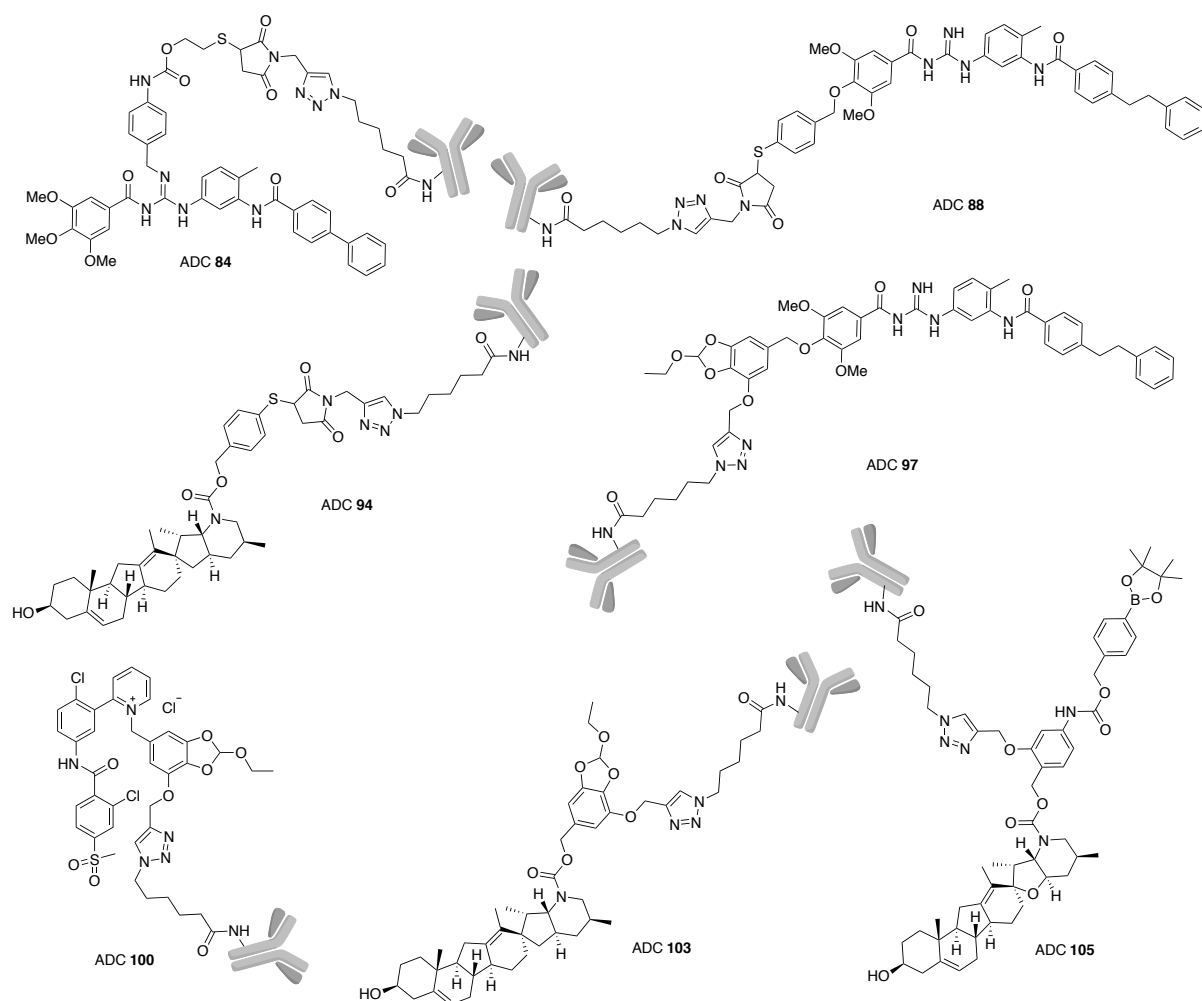


Figure 72. ADC **84**: Ctx-non-cleavable linker-MRT-86, ADC **88**: Ctx-non-cleavable linker 73-FRM326, ADC **94**: Ctx-non-cleavable linker 73-Cyclopamine, ADC **97**: Ctx-HMPO-FRM326, ADC **100**: Ctx-HMPO-Vismodegib, ADC **103**: Ctx-HMPO-Cyclopamine, ADC **105**: Ctx-borate linker 65-Cyclopamine.

Experimental part

4.1 A new pH responsive crosslinker platform for drug targeting delivery

4.1.1 General experimental procedures, materials and instruments

All reagents were used as purchased from commercial suppliers without further purification. The reactions were carried out in oven dried vessels. Solvents were dried and purified by conventional methods prior use or, if available, purchased in anhydrous form.

Flash column chromatography was performed with Merck silica gel Å 60, 0.040-0.063 mm (230-400 mesh).

MPLC Syncore® Büchi on highly resistant PP cartridges Normal Phase silica gel NP 40 – 63 µm particle size and 60 Å pore size (Si60) withstand a maximum pressure of 10 bar (145 psi) column with PE (Eluent A) and EtOAc (Eluent B) as mobile phase.

Merck aluminum backed plates pre-coated with silica gel 60 (UV254) were used for analytical thin layer chromatography and were visualized by staining with a KMnO₄ or Ninhydrin solution.

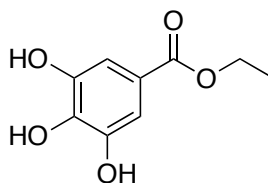
NMR spectra were recorded at 25 °C or at 37 °C with 400 or 600 MHz for ¹H and 101 or 151 MHz for ¹³C Brüker Avance NMR spectrometers. The solvent is specified for each spectrum. Splitting patterns are designated as s, singlet; d, doublet; t, triplet; q, quartet; m, multiplet; bs, broad singlet. Chemical shifts (δ) are given in ppm relative to the resonance of their respective residual solvent peaks.

High and low resolution mass spectroscopy analyses were recorded by electrospray ionization with a mass spectrometer Q-exactive Plus.

MALDI analysis were performed with the MALDI-TOF in linear mode set at 83% of laser intensity. The *m/z* range was from 30 kDa to 200 kDa.

4.1.2 Synthetic procedures

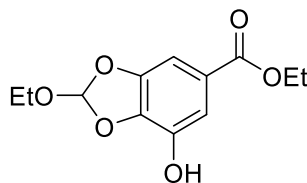
Ethyl 3,4,5-trihydroxybenzoate (**38**)



The product was prepared according to the literature. [230]

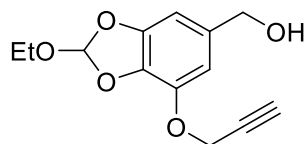
Gallic acid (1 g, 5.88 mmol) was suspended in EtOH (40 mL) in a 250 mL round-bottomed flask. A catalytic amount of H₂SO₄ conc. (600 μ L) was added at r.t. and was heated under reflux with continuous stirring for 16 h. The reaction mixture was cooled to r.t. and the solvent was evaporated under reduced pressure. The residue was dissolved in EtOAc (50 mL) and washed with a NaHCO₃ ss (2 x 100 mL) and NaCl_{ss} (30 mL). The organic phase was dried over anhydrous Na₂SO₄, filtered, and evaporated under vacuum to get the esterified compound **38** (1.10 g, 5.59 mmol, 95% yield). mp. 153-155 °C (lit. mp 148–149). Spectral data coherent with the literature. [230]

Ethyl 2-ethoxy-7-hydroxybenzo[d][1,3]dioxole-5-carboxylate (**39**) [231]



Under N₂ atmosphere, Amberlyst[®] 15 (62 mg) was suspended in dry toluene (80 mL). After 30 minutes, ethyl gallate **38** (1 g, 5.046 mmol) and triethyl orthoformate (2.5 mL, 15.098 mmol) were added at r.t. and then the mixture was heated to reflux for 16 h. The reaction was cooled to r.t., filtered on Celite pad and toluene was evaporated under reduced pressure. The compound was purified by means of chromatography on silica gel with MPLC Syncore[®] Büchi eluting 0-30 % gradient of EtAOc in petroleum ether, as a white solid (1.06 g, 4.19 mmol, 83% yield). ¹H NMR (600 MHz, CDCl₃, δ ppm, *J* Hz): δ 7.43 (s, 1H), 7.15 (s, 1H), 6.92 (s, 1H), 6.46 (bs, 1H), 4.33 (q, *J* = 7.1 Hz, 2H), 3.72 (q, *J* = 7.3 Hz, 2H), 1.35 (t, *J* = 7.1 Hz, 3H), 1.23 (t, *J* = 7.2 Hz, 3H). ¹³C NMR (151 MHz, CDCl₃, δ ppm): δ 166.84, 147.19, 139.08, 137.23, 124.21, 119.98, 114.11, 102.48, 61.47, 59.65, 14.74, 14.19. ESI: *m/z* 255 [M+H]⁺; 277 [M+Na]⁺.

(2-Ethoxy-7-(prop-2-yn-1-yloxy)benzo[d][1,3]dioxol-5-yl)methanol (41) HMPO



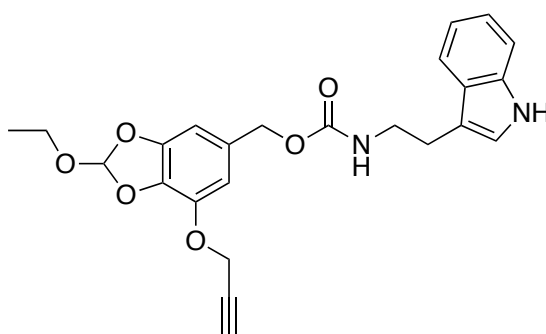
Under N₂, compound **39** (1.34 g, 5.27 mmol), K₂CO₃ (2.188 g, 15.83 mmol) and KI (875 mg, 5.27 mmol) in dry acetone (80 mL) were mixed together for 20 minutes. Then propargyl bromide (1.41 mL, 15.83 mmol) was added and the reaction was carried out to reflux for 16 h. Acetone was evaporated and the crude was solubilized in EtOAc (50 mL), washed with H₂O (2 x 25 mL) and NaCl_{ss} (25 mL) and the combined organic phases dried over anhydrous Na₂SO₄, filtered, and evaporated under reduced pressure. The alkylated product was purified by means of chromatography on silica gel with MPLC Syncore® Büchi eluting 0-20 % gradient of EtOAc in petroleum ether. (1.35 g, 4.64 mmol, 88% yield). **¹H NMR** (600 MHz, CDCl₃, δ ppm, *J* Hz): δ 7.46 (s, 1H), 7.29 (s, 1H), 6.96 (s, 1H), 4.84 (s, 2H), 4.34 (q, *J* = 7.1 Hz, 2H), 3.75 (q, *J* = 7.1 Hz, 2H), 2.54 (s, 1H), 1.37 (t, *J* = 7.1 Hz, 3H), 1.27 (t, *J* = 7.1 Hz, 3H). **¹³C NMR** (151 MHz, CDCl₃, δ ppm): δ 165.72, 147.33, 140.23, 138.48, 124.69, 120.12, 112.32, 104.19, 77.87, 76.30, 61.02, 59.59, 57.37, 14.77, 14.32. **ESI**: *m/z* 301 [M+Na]⁺. Under N₂, the alkylated compound (1.07 g, 3.85 mmol) was solubilized in dry THF (60 mL) and the mixture was cooled to 0 °C. Then a solution of LiAlH₄ 1M in THF (11.55 mL) was added slowly and the reaction was carried out at r.t. for 1 h. Then HCl 0.5 N was added until pH 5 and the mixture was extracted with EtOAc (50 mL). The organic phase was separated, washed with H₂O (25 mL) and NaCl_{ss} (25 mL) and dried over anhydrous Na₂SO₄, filtered, and evaporated under reduced pressure. Compound **41** was achieved as a white solid in a very good yield (915 mg, 3.66 mmol, 95% yield). The analytical sample was crystallized from heptane. **¹H NMR** (600 MHz, CDCl₃, δ ppm, *J* Hz): δ 6.89 (s, 1H), 6.67 (s, 1H), 6.63 (s, 1H), 4.81 (s, 2H), 4.58 (s, 2H), 3.75 (q, *J* = 7.1 Hz, 2H), 2.52 (s, 1H), 1.26 (t, *J* = 7.1 Hz, 3H). **¹³C NMR** (151 MHz, CDCl₃, δ ppm): δ 147.68, 140.58, 135.42, 133.89, 119.50, 108.82, 101.75, 78.39, 75.94, 65.23, 59.37, 57.39, 14.82. **ESI**: *m/z* 273 [M+Na]⁺. Elemental Analysis calcd. for C₁₂H₁₄O₆: C, 56.69; H, 5.55; found C, 56.82; H, 5.65.

General procedure for the synthesis of carbamates.

The **HMPO** linker (0.4 mmol) was solubilized in dry THF (5 mL) at r.t. under N₂. At 0 °C *p*-nitrophenyl chloroformate (89 mg, 0.44 mmol) and DMAP (98 mg, 0.8 mmol) were added, and

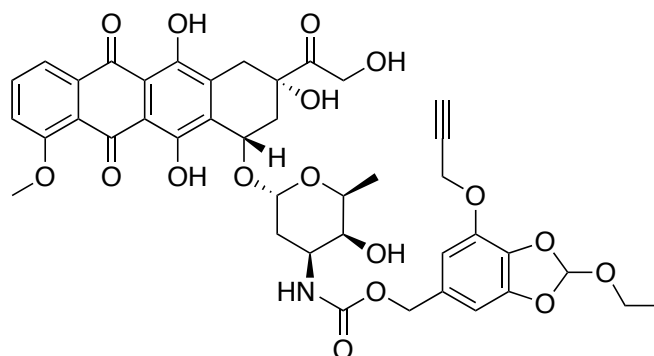
the reaction was carried out for 30 minutes at 0 °C. The activated compound was checked by TLC and was dropped into a solution of the desired amine (0.6 mmol) and DIPEA (209 μ L, 1.2 mmol) at 0 °C. The reaction was stirred at r.t. for 0.15 h-16 h. The solvent was evaporated under reduced pressure. The residue was dissolved in EtOAc (10 mL) and washed with H₂O (5 mL) and NaCl_{ss} (5 mL). The organic phase was dried over anhydrous Na₂SO₄, filtered, and evaporated under vacuum.

(2-Ethoxy-7-(prop-2-yn-1-yloxy)benzo[d][1,3]dioxol-5-yl)methyl (2-(1*H*-indol-3-yl)ethyl)carbamate (42)



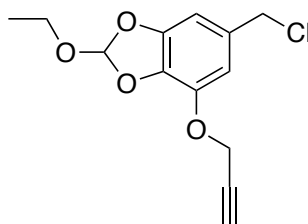
The compound **42** was purified by flash chromatography on silica gel with MPLC Syncore® Büchi eluting 0-40 % gradient of EtAOc in petroleum ether (139 mg, 0.32 mmol, 81% yield). ¹H NMR (600 MHz, CDCl₃, δ ppm, *J* Hz): δ 8.16 (bs, 1H), 8.13 (d, *J* = 8.4 Hz, 1H), 7.60 (d, *J* = 7.9 Hz, 1H), 7.37 (d, *J* = 8.1 Hz, 1H), 7.21 (t, *J* = 7.7 Hz, 1H), 7.12 (t, *J* = 7.5 Hz, 1H), 6.98 (s, 1H), 6.89 (s, 1H), 6.65 (s, 1H), 6.62 (s, 1H), 5.00 (s, 2H), 4.88 (bs, 1H), 4.80 (s, 2H), 3.76 (q, *J* = 7.2 Hz, 2H), 3.54 (t, *J* = 6.6 Hz, 2H), 2.99 (t, *J* = 6.8 Hz, 2H), 2.51 (s, 1H), 1.27 (t, *J* = 7.0 Hz, 3H). ¹³C NMR (151 MHz, CDCl₃, δ ppm): δ 162.65, 156.45, 147.60, 140.51, 136.44, 134.28, 130.92, 126.19, 122.23, 119.51, 118.71, 115.67, 112.66, 111.30, 110.26, 102.92, 76.08, 66.52, 59.58, 57.47, 41.29, 29.73, 25.65, 14.83. ESI: *m/z* 459 [M+Na]⁺. HRMS (EI) calcd. For C₂₄H₂₄N₂O₆Na [M+Na]⁺ 459.1532, found 459.1529.

(2-Ethoxy-7-(prop-2-yn-1-yloxy)benzo[d][1,3]dioxol-5-yl)methyl ((2*S*,3*S*,4*S*,6*R*)-3-hydroxy-2-methyl-6-(((1*S*,3*S*)-3,5,12-trihydroxy-3-(2-hydroxyacetyl)-10-methoxy-6,11-dioxo-1,2,3,4,6,11-hexahydrotetracen-1-yl)oxy)tetrahydro-2*H*-pyran-4-yl)carbamate (48)



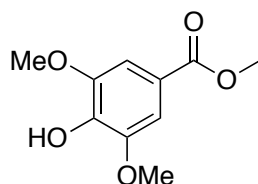
Compound **48** was purified with flash chromatography on silica gel eluting 0-10 % gradient of MeOH in CH₂Cl₂ (237 mg, 0.29 mmol, 73% yield). **¹H NMR** (600 MHz, CDCl₃, δ ppm, *J* Hz): δ 13.98 (s, 1H), 13.24 (s, 1H), 8.04 (d, *J* = 7.7 Hz, 1H), 7.79 (t, *J* = 8.0 Hz, 1H), 7.39 (d, *J* = 8.4 Hz, 1H), 6.87 (s, 1H), 6.62 (s, 1H), 6.58 (s, 1H), 5.51 (d, *J* = 4.2 Hz, 1H), 5.30 (s, 1H), 5.13 (dd, *J* = 578.3 Hz, 1H), 4.93 (s, 2H), 4.77 (s, 2H), 4.55 (s, 1H), 4.08 (s, 3H), 3.87 (bs, 1H), 3.77 – 3.60 (m, 3H), 3.15 (dd, *J* = 154.6, 18.4 Hz, 2H), 2.51 (s, 1H), 2.26 (dd, *J* = 96.8, 14.5 Hz, 2H), 1.98 – 1.74 (m, 4H), 1.62 (s, 2H), 1.35 – 1.11 (m, 6H). **¹³C NMR** (151 MHz, CDCl₃, δ ppm): δ 213.86, 187.13, 186.73, 161.09, 156.19, 155.67, 155.42, 147.59, 140.44, 135.80, 135.53, 134.35, 133.60, 133.53, 130.60, 120.90, 119.88, 119.56, 118.47, 111.64, 111.46, 110.29, 102.95, 100.70, 76.65, 76.03, 69.70, 69.59, 67.27, 66.67, 65.56, 59.34, 57.41, 56.69, 47.03, 35.66, 34.04, 30.20, 29.71, 16.84, 14.78. **ESI**: *m/z* 842 [M+Na]⁺. **HRMS** (EI) calcd. For C₄₁H₄₁NO₁₇Na [M+Na]⁺ 842.2273, found 842.2278.

6-(Chloromethyl)-2-ethoxy-4-(prop-2-yn-1-yloxy)benzo[d][1,3]dioxole (**44**)



Compound **41** (100 mg, 0.4 mmol) was solubilized in dry CH₂Cl₂ (6 mL) at 0 °C and SOCl₂ (70 μL, 0.96 mmol) and Et₃N (145 μL, 1.04 mmol), both freshly distilled, were added carefully. The reaction was carried out at 0 °C for 30 minutes. The mixture was concentrated under N₂ and quickly filtrated on a pad of silica gel using PE:EtOAc 1:1. The filtrate was concentrated under reduced pressure and was immediately used for the next step.

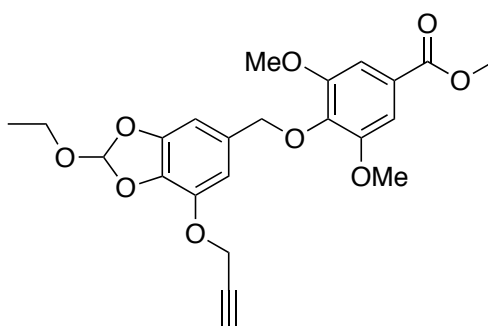
Methyl 4-hydroxy-3,5-dimethoxybenzoate (43)



The product was prepared according to the literature. [232]

Syringic acid (3 g, 15.14 mmol) was dissolved in MeOH (30 mL), and a catalytic amount of H₂SO₄ conc. (1.8 mL) was added. The reaction was stirred at reflux for 4 h. The resulting mixture was concentrated under reduced pressure and the residue dissolved in EtOAc (50 mL). The solution was transferred into a separating funnel, washed with NaHCO₃ ss (100 mL) and NaCl_{ss} (30 mL). The organic layer was dried over anhydrous Na₂SO₄, filtered, and concentrated to give the methyl ester **10** in good yield (3.03 g, 14.38 mmol, 95% yield). ¹H NMR (600 MHz, CDCl₃, δ ppm, *J* Hz): δ 7.30 (s, 2H), 3.91 (s, 6H), 3.88 (s, 3H). ¹³C NMR (151 MHz, CDCl₃, δ ppm): δ 166.87, 146.67, 139.27, 121.05, 106.67, 56.40, 52.07. ESI: *m/z* 211 [M-H]⁺.

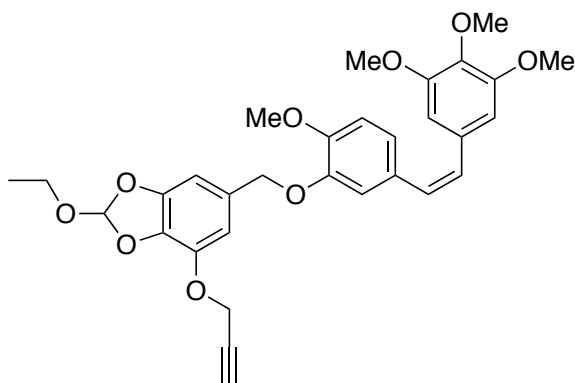
Methyl 4-((2-ethoxy-7-(prop-2-yn-1-yloxy)benzo[d][1,3]dioxol-5-yl)methoxy)-3,5-dimethoxybenzoate (45)



Compound **43** (100 mg, 0.47 mmol) was solubilized in dry acetone (10 mL) and K₂CO₃ an. (195 mg, 1.41 mmol) was added to the mixture at r.t. under Ar. After 10 min. a solution of benzoylchloride **44** (377 mg, 1.41 mmol) in dry acetone (10 mL) was added and the reaction was stirred for 16 h at r.t.. The mixture was filtered and the filtrate was concentrated under reduced pressure. EtOAc (20 mL) was added, the organic phase was washed with H₂O (10 mL) and NaCl_{ss} (5 mL). The organic layer was dried over anhydrous Na₂SO₄, filtered and evaporated *in vacuo*. The product was purified by flash chromatography on silica gel eluting 0-

40% gradient of EtAOc in petroleum ether (168 mg, 0.38 mmol, 81% yield). **¹H NMR** (600 MHz, CDCl₃, δ ppm, *J* Hz): δ 7.29 (s, 2H), 6.90 (s, 1H), 6.79 (s, 1H), 6.78 (s, 1H), 4.99 (s, 2H), 4.80 (s, 2H), 3.91 (s, 3H), 3.90 (s, 6H), 3.73 (q, *J* = 7.1 Hz, 2H), 2.51 (s, 1H), 1.25 (t, *J* = 7.0 Hz, 3H). **¹³C NMR** (151 MHz, CDCl₃, δ ppm): δ 166.74, 153.21, 147.41, 140.78, 140.25, 134.32, 131.79, 129.39, 125.38, 110.46, 110.13, 106.84, 105.44, 103.27, 75.84, 74.84, 59.13, 57.38, 56.23, 52.24, 29.71, 14.83. **ESI**: *m/z* 445 [M+H]⁺; 467 [M+Na]⁺. HRMS (EI) calcd. for C₂₃H₂₅O₉ [M+H]⁺ 445.1499, found 445.1501.

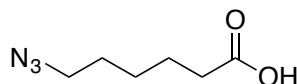
(Z)-2-Ethoxy-6-((2-methoxy-5-(3,4,5-trimethoxystyryl)phenoxy)methyl)-4-(prop-2-yn-1-yloxy)benzo[d][1,3]dioxole (51)



Combretastatin A4 (100 mg, 0.32 mmol) was solubilized in dry DMF (3 mL) and was added into a dry DMF (2 mL) solution of previously washed NaH 60% (25 mg, 0.64 mmol) under Ar. at 0 ° C. The mixture was stirred for 10 minutes and the activated linker **44** (257 mg, 0.96 mmol) solubilized in 3 mL of dry DMF was dropped slowly at 0 ° C. The reaction was carried out at r.t. for 16 h and at the end H₂O (5 mL) was added quenching NaH. The crude was extracted with EtOAc (10 mL), the organic phase was dried over anhydrous Na₂SO₄, filtered, and evaporated under reduced pressure. The product **51** was purified by means of chromatography on silica gel with MPLC Syncore® Büchi eluting 0-30 % gradient of EtAOc in petroleum ether (170 mg, 1.31 mmol, 98% yield). **¹H NMR** (600 MHz, CDCl₃, δ ppm, *J* Hz): δ 6.91 – 6.85 (m, 3H), 6.78 (d, *J* = 7.8 Hz, 1H), 6.64 (s, 1H), 6.61 (s, 1H), 6.51 (s, 2H), 6.49 – 6.39 (m, 2H), 4.81 (s, 2H), 4.79 (s, 2H), 3.86 (s, 3H), 3.83 (s, 3H), 3.77 – 3.68 (m, 8H), 2.49 (s, 1H), 1.26 (t, *J* = 6.7 Hz, 3H). **¹³C NMR** (151 MHz, CDCl₃, δ ppm): δ 153.01, 148.94, 147.68, 147.53, 140.51, 137.15, 134.13, 132.96, 131.29, 129.81, 129.62, 128.88, 122.60, 119.53, 114.68, 111.41, 109.39, 105.99, 102.16, 75.93, 70.81, 60.92, 59.29, 57.41, 55.97, 29.71, 14.82.

ESI: m/z 571 $[M+Na]^+$. HRMS (EI) calcd. for $C_{31}H_{32}O_9Na$ $[M+Na]^+$ 571.1944, found 571.1946.

6-Azidohexanoic acid (49)



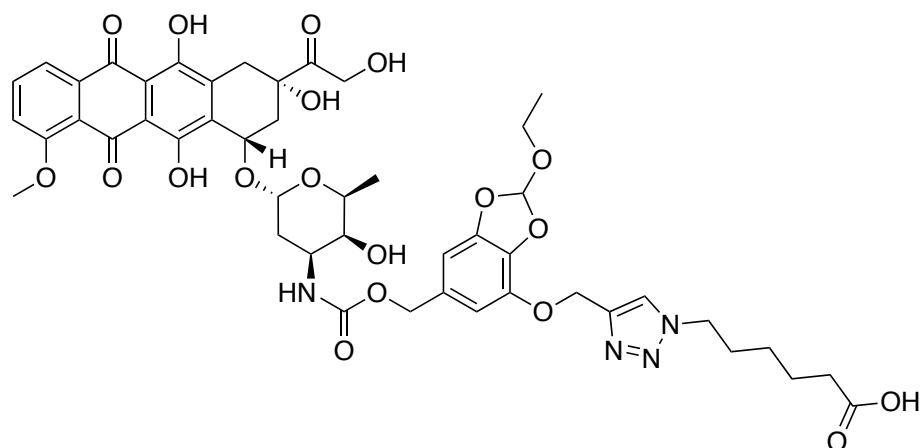
The product was prepared according to the literature. [233]

6-bromohexanoic acid (700 mg, 3.6 mmol) was solubilized in dry DMF (5 mL) and NaN_3 (1.17 g, 18 mmol) was added at the mixture at r.t.. The reaction was stirred for 16 h at 100 ° C. EtOAc (100 mL) was added at the crude filtered on Büchner and washed with $KHSO_4$ 1 M (2 x 50 mL), H_2O (2 x 30 mL) and $NaCl_{ss}$ (30 mL). The organic phase was dried over anhydrous Na_2SO_4 , filtered, and evaporated under reduced pressure. The product **49** was obtained as yellow oil (289 mg, 1.84 mmol, 51% yield). 1H NMR (400 MHz, $CDCl_3$, δ ppm, J Hz): δ 10.93 (bs, 1H), 3.19 (t, J = 6.8 Hz, 2H), 2.28 (t, J = 7.4 Hz, 2H), 1.60-1.56 (m, 4H), 1.44 – 1.26 (m, 2H). NMR data are coherent with the literature. [234]

General procedure for CuCAAC reaction.

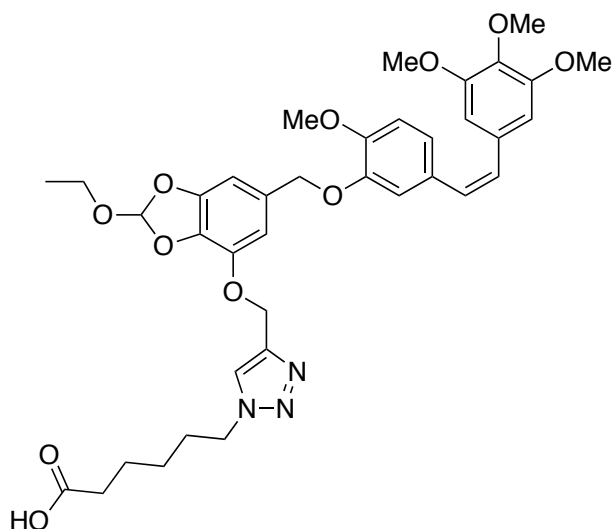
The desired alkyne (0.07 mmol) and the compound **49** (9 mg, 0.056 mmol) were dissolved in dry DMF (2 mL) under Ar. The solution was degassed with three cycles of argon/vacuum. To this solution, a freshly prepared aqueous mixture (2 mL) of $Cu(OAc)_2$ (4 mg, 0.021 mmol) and Na ascorbate (8 mg, 0.042 mmol), previously degassed by argon/vacuum cycles, was added dropwise. The reaction mixture was degassed and left to stir under Ar. at r.t. for 16 h. The solvent was evaporated and the crude was purified by silica gel flash chromatography eluting 0-10 % gradient of MeOH in CH_2Cl_2 providing the desired compound.

6-(4-(((2-ethoxy-6-((((2*S*,3*S*,4*S*,6*R*)-3-hydroxy-2-methyl-6-(((1*S*,3*S*)-3,5,12-trihydroxy-3-(2-hydroxyacetyl)-10-methoxy-6,11-dioxo-1,2,3,4,6,11-hexahydrotetracen-1-yl)oxy)tetrahydro-2*H*-pyran-4-yl)carbamoyl)oxy)methyl)benzo[*d*][1,3]dioxol-4-yl)oxy)methyl)-1*H*-1,2,3-triazol-1-yl)hexanoic acid (50)



Obtained 39 mg, 0.04 mmol, 64% yield. **¹H NMR** (600 MHz, DMSO-*d*₆, δ ppm, *J* Hz): δ 14.02 (bs, 1H), 13.26 (bs, 1H), 11.83 (bs, 1H), 8.16 (s, 1H), 7.91 (t, *J* = 8.0 Hz, 1H), 7.64 (d, *J* = 7.5 Hz, 1H), 7.04 (s, 1H), 6.82 – 6.71 (m, 2H), 6.62 (s, 1H), 5.40 (s, 1H), 5.23 (s, 1H), 5.17 (s, 2H), 4.97 (s, 1H), 4.85 (s, 2H), 4.75 (bs, 1H), 4.56 (s, 2H), 4.32 (t, *J* = 7.1 Hz, 2H), 4.14 (d, *J* = 6.6 Hz, 1H), 3.98 (s, 3H), 3.75-3.70 (m, 1H), 3.64 (q, *J* = 6.9 Hz, 2H), 3.46 (s, 1H), 2.98 (s, 2H), 2.25 – 2.10 (m, 4H), 1.87-1.77 (m, 3H), 1.50 (p, *J* = 7.4 Hz, 3H), 1.23 (q, *J* = 7.8 Hz, 3H), 1.15-1.10 (m, 6H). **¹³C NMR** (151 MHz, DMSO-*d*₆, δ ppm): δ 187.13, 187.01, 174.74, 161.37, 156.60, 155.72, 155.02, 147.17, 142.68, 141.55, 136.69, 136.10, 135.28, 134.65, 133.59, 131.94, 124.98, 120.69, 120.33, 119.54, 111.38, 111.24, 109.81, 102.32, 100.72, 90.71, 80.65, 75.54, 70.37, 68.54, 67.22, 65.60, 64.12, 62.96, 60.07, 57.12, 49.73, 47.64, 37.26, 33.92, 32.68, 30.36, 29.86, 25.88, 24.32, 17.47, 15.22. **ESI**: *m/z* 999 [M+Na]⁺. **HRMS** (EI) calcd. for C₄₇H₅₂N₄O₁₉Na [M+Na]⁺ 999.3124 (100%), 1000.3158 (51%) found 999.3127 (100%), 1000.3161 (51%).

(*Z*)-6-(4-(((2-ethoxy-6-((2-methoxy-5-(3,4,5-trimethoxystyryl)phenoxy)methyl)benzo[*d*][1,3]dioxol-4-yl)oxy)methyl)-1*H*-1,2,3-triazol-1-yl)hexanoic acid (52)



Obtained 21 mg, 0.03 mmol, 75% yield. $^1\text{H NMR}$ (600 MHz, CDCl_3 , δ ppm, J Hz): δ 7.65 (s, 1H), 6.90 – 6.86 (m, 3H), 6.79 (d, $J = 8.1$ Hz, 1H), 6.66 (s, 1H), 6.59 (s, 1H), 6.51 (s, 2H), 6.49 – 6.40 (m, 2H), 5.32 (s, 2H), 4.80 (s, 2H), 4.36 (t, $J = 7.0$ Hz, 2H), 3.86 (s, 3H), 3.83 (s, 3H), 3.76 – 3.70 (m, 8H), 2.35 (t, $J = 7.2$ Hz, 3H), 1.96-1.92 (m, $J = 7.7$ Hz, 2H), 1.69-1.65 (m, 2H), 1.40-1.35 (m, 2H), 1.26 (t, $J = 6.7$ Hz, 3H). $^{13}\text{C NMR}$ (151 MHz, CDCl_3 , δ ppm): δ 177.29, 152.99, 148.90, 147.56, 147.51, 141.34, 137.11, 133.87, 132.99, 131.46, 129.82, 129.62, 128.91, 122.59, 119.48, 114.65, 111.41, 109.08, 106.00, 101.88, 70.81, 63.52, 60.93, 59.55, 55.98, 50.08, 33.33, 29.86, 29.72, 25.80, 23.91, 14.84. **ESI:** m/z 707 $[\text{M}+\text{H}]^+$; 729 $[\text{M}+\text{Na}]^+$. **HRMS** (EI) calcd. for $\text{C}_{37}\text{H}_{44}\text{N}_3\text{O}_{11}$ $[\text{M}+\text{H}]^+$ 706.2976, found 706.2979.

4.1.3 General procedure for preparation of ADCs. **53** (Ctx-NH-50), **54** (Ctx-NH-52)

The proper carboxylic acid (28 μL , 10 mM in DMSO) was activated by adding S-NHS (5 μL , 100 mM in mQ) and EDC (5 μL , 100 mM in mQ). The reaction was left for 16 h at r.t.. PBS at pH 7.4 (35 μL) and Cetuximab freshly dialyzed using a 10 kDa cutoff dialysis membrane (100 μL , 5 mg/mL in PBS pH 7.4) were added to the activated carboxylic acid solution. The reaction was mixed in a shaker at r.t. and after 1 h quenched with a 20 mM glycine aqueous solution (27 μL). The final products (**53**, **54**) were purified using PD SpinTrapTM G-25 column removing the unreacted excess of small molecules. DAR was detected by MALDI analysis.

4.1.4 MALDI analysis of bioconjugates

Samples preparation: the matrix solutions were prepared at two different concentrations, and both were used in parallel. 20.0 mg or 25 mg of Super DHB were dissolved in a solution of MeCN (150 μL), H_2O (350 μL) and TFA (0.05 μL) and deposited in a stainless-steel target

placed in a thermoblock set at 39 °C. When the sample was dried, 1.65 µL of matrix solution was added and once completely dried and crystalized, the target plate was removed from the thermoblock.

The target plate was analyzed with MALDI-TOF set in linear mode at 83% of laser intensity. The *m/z* range was from 30 kDa to 200 kDa.

For each sample spot, 10 shots were acquired to improve the spectra quality and mass accuracy.

Table 8. Drug antibody ratio

Antibody	Payload MW	MALDI monocharged peak M^+	MALDI bicharged peak M^{2+}	DAR (M^+)	DAR (M^{2+})	DAR
Ctx	-	154326	77818	-	-	-
ADC-53	974	155825	78734	1.54	1.88	1.7
Ctx	-	152240	76361	-	-	-
ADC-54	704	153208	76862	1.37	1.42	1.4

4.1.5 HPLC method for hydrolysis

Samples were prepared according to the literature. [54]

A 10 mM solution of the desired compound (**42**, **45**, **48**, **51**) was prepared in DMSO and diluted in H₂O or in the corresponding buffer to obtain a final 1 mM solution of the compound. For pH 7.4, 6.5, 5.5, phosphate buffers 0.1 M was used (KH₂PO₄/K₂HPO₄). Each solution was analyzed by analytical HPLC. Reaction was performed at 25 °C, incubated at 37 °C and the crude was injected every 1 h up to 48 hours. All data were recorded in triplicate.

HPLC analysis were performed on a LC/MSD system InfinityLab LC/MSD iQ, Column: InfinityLab PoroShell 120 EC-C18 2.1x50mmx2.7µm. Flow: 0.4 mL/min. Eluent A/B: H₂O/MeCN. Gradient: 5% B to 95% B in 10 min., 4 min. at 95 % B and 3 min. of re-equilibration. Detection: 254 nm and 260 nm.

4.1.6 ¹HNMR method to study the disassembling mechanism for HMPO conjugates

The products **45** and **43** ($4.8 \cdot 10^{-6}$ mol) were solubilized in acetonitrile-d₃ (160 µL) and added to a previously prepared deuterated buffer at pH 5.5 (50 mM, 640 µL) or D₂O (640 µL). The NMR tubes were incubated at 37 °C, and the FID was recorded every 30 minutes at 37 °C using 600 MHz Brüker Avance NMR spectrometer.

4.1.7 Stability in human plasma of HMPO derivatives

Pooled human plasma (0.9 mL, 55.7 µg protein/mL), [235] hepes buffer (1.0 mL, 25 mM, NaCl 140 mM, pH 7.4) and tested compound dissolved in DMSO (100 µL, 2.0 mM) were mixed in a test tube that was incubated at 37 °C under continuous mechanical agitation. At set time points (0.0, 0.25, 0.50, 1.0, 3.0, 5.0, 8.0, and 24.0 h), samples of 100 µL were taken, mixed with 400 µL of cold MeCN and centrifuged at 5000 rpm for 15 min.. [236] The supernatant was collected and analysed by UV/LC-MS to monitor the amount of unmodified compound. For each product, the determination was performed in three independent experiments.

UV/LC-MS methods

LC analyses of plasma stability tests were performed by using Agilent 1100 LC/MSD VL system (G1946C) (Agilent Technologies, Palo Alto, CA) constituted by a vacuum solvent degassing unit, a binary high-pressure gradient pump, an 1100 series UV detector, and an 1100 MSD model VL benchtop mass spectrometer. MSD single-quadrupole instrument was equipped with the orthogonal spray API-ES (Agilent Technologies, Palo Alto, CA). The pressure of the nebulizing gas and the flow of the drying gas (nitrogen used for both) were set at 40 psi, 9 L/min, respectively. The capillary voltage, the fragmentor voltage, and the vaporization temperature were 3000 V, 10 V, and 350 °C, respectively. MSD was used in the positive and negative ion mode. Spectra were acquired over the scan range m/z 100-2000 using a step size of 0.1. Chromatographic analyses were performed using a Phenomenex Kinetex EVO C18-100Å (150 x 4.6 mm, 5 µm particle size) at r.t., at flow rate of 0.6 mL/min, and injection volume of 10 µL, operating with a gradient elution of A: water (H₂O) and B: MeCN. Both solvents were acidified with 0.1% v/v of HCOOH. UV detection was monitored at 254 nm. The analysis started with 0% of B, then B was increased to 80% (from t = 0 to t = 20 min.), then kept at 80% (from t = 20 to t = 25 min.) and finally return to 0% of eluent B in 5.0 min..

4.1.8 MTT assay of ADCs (ADC 53 and 54)

Cell culture. A431 epidermoid carcinoma cells and A549 lung carcinoma cells (ATCC, Rockville, MD, USA) were cultured in DMEM (Euroclone) supplemented with 10% fetal bovine serum (FBS, Euroclone), 100 U/ml penicillin/streptomycin (Euroclone), and 4 mM L-glutamine (Euroclone). All cell lines were grown at 37°C and 5% CO₂.

MTT. 2.5×10^3 cells/well were seeded in 96-multiwell plates in medium 10% FBS. After adherence, cells were incubated in fresh medium with increasing concentrations of Doxorubicin (0.05-50 µM), Combretastatin A4 (0.1-100 µM), Cetuximab (0.1-10 µg/ml), **53** (0.1-10 µg/ml related to the DAR value) and **54** (0.1-10 µg/ml related to the DAR value). At the indicated

time (48, 72 and 96 h) the medium was removed, and cells were incubated for 4h with fresh medium in the presence of 1.2 mM MTT (3-(4,5-dimethylthiazol-2-yl)-2,5-diphenyltetrazolium bromide) (Sigma-Aldrich). The MTT solution was then removed and 50 μ L of DMSO were added to the each well to dissolve the blue formazan crystals. The absorbance of the formazan dye was measured at 570 nm with a microplate reader (EnVision, PerkinElmer, Waltham, MA, USA). Data were expressed as a percentage of the basal control.

4.2 A new reactive oxygen species (ROS) sensitive linker

4.2.1 General experimental procedures, materials and instruments

All reagents were used as purchased from commercial suppliers without further purification. The reactions were carried out in oven dried vessels. Solvents were dried and purified by conventional methods prior use or, if available, purchased in anhydrous form.

Flash column chromatography was performed with Merck silica gel Å 60, 0.040-0.063 mm (230-400 mesh).

MPLC Syncore® Büchi on highly resistant PP cartridges Normal Phase silica gel NP 40 – 63 µm particle size and 60 Å pore size (Si60) withstand a maximum pressure of 10 bar (145 psi) column with petroleum ether (Eluent A) and EtOAc (Eluent B) as mobile phase.

Merck aluminum backed plates pre-coated with silica gel 60 (UV254) were used for analytical thin layer chromatography and were visualized by staining with a KMnO₄ or Ninhydrin solution.

NMR spectra were recorded at 25 °C with 400 MHz and 101 MHz for ¹H and ¹³C Brüker Avance NMR spectrometers. The solvent is specified for each spectrum. Splitting patterns are designated as s, singlet; d, doublet; t, triplet; q, quartet; m, multiplet; bs, broad singlet. Chemical shifts (δ) are given in ppm relative to the resonance of their respective residual solvent peaks.

High and low resolution mass spectroscopy analyses were recorded by electrospray ionization with a mass spectrometer Q-exactive Plus.

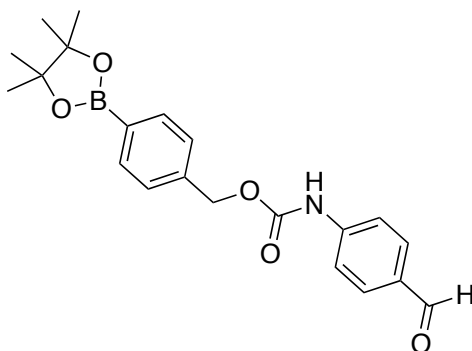
4.2.2 Synthetic procedures

General procedure of Curtius rearrangement

The products were prepared according to the literature. [71]

To a round-bottom flask were added sequentially the desired aldehyde (0.13 mmol), 1,4-dioxane (0.3 mL), Et₃N (21 µL, 0.147 mmol), DPPA (31 µL, 0.147 mmol), and of 4-(hydroxymethyl)phenylboronic acid pinacol ester (34 mg, 0.147 mmol). The flask was equipped with a cold-finger reflux condenser, and the reaction mixture was heated to 105 °C. After the solution was stirred for 2 h at 105 °C, the product mixture was cooled to 25 °C. The reaction was evaporated under reduced pressure, and the resulting residue was purified by silica gel flash column chromatography eluting 0-70% EtOAc in petroleum ether providing the desired compound.

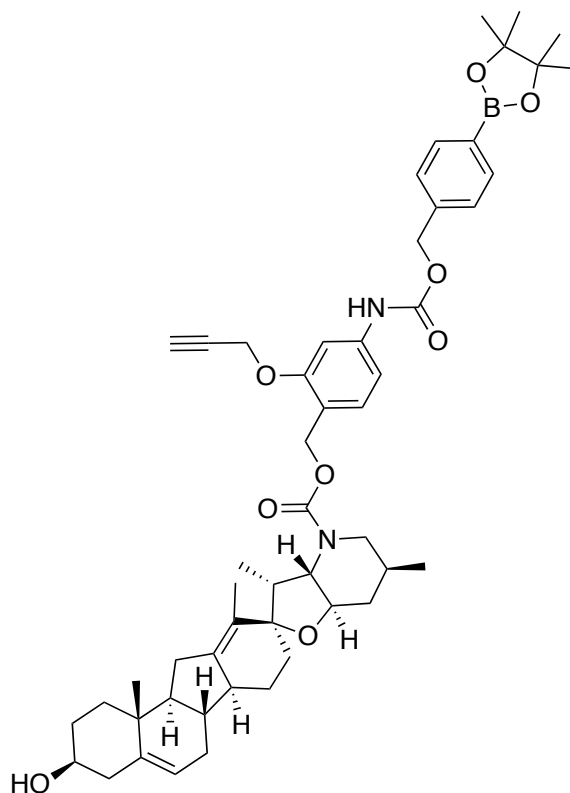
4-(4,4,5,5-tetramethyl-1,3,2-dioxaborolan-2-yl)benzyl (4-formylphenyl)carbamate (57)



Obtained 44 mg, 0.12 mmol, 90% yield.

NMR data and ESI analysis are coherent with the literature. [71]

2-(prop-2-yn-1-yloxy)-4-((((4-(4,4,5,5-tetramethyl-1,3,2-dioxaborolan-2-yl)benzyl)oxy)carbonyl)amino)benzyl (4*S*,6*aR*,8*aR*,8*bS*,11*S*,12*aR*,13*aR*,15*bS*)-4-hydroxy-6*a*,11-dimethyl-3,4,5,6,6*a*,6*b*,7,8,8*a*,8*b*,10,11,12,12*a*,14,15,15*a*,15*b*-octadecahydrobenzo[7'',8'']fluoreno[2'',1':2',3']cyclobuta[1',2':4,5]furo[3,2-*b*]pyridine-9(1*H*)-carboxylate (69a)

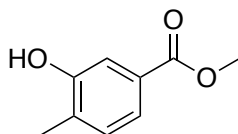


Obtained 9 mg, 0.010mmol, 59% yield.

¹H NMR (400 MHz, CDCl₃, δ ppm, J Hz): δ 7.79 (d, J = 8.0 Hz, 2H), 7.73 (d, J = 7.4 Hz, 1H), 7.67 (s, 1H), 7.42 (d, J = 7.9 Hz, 1H), 7.36 (d, J = 7.7 Hz, 2H), 5.35 (t, J = 4.3 Hz, 1H), 5.26 (s, 2H), 5.18 (s, 2H), 4.76 (s, 2H), 3.69 – 3.36 (m, 4H), 3.19 (dd, J = 10.2, 7.3 Hz, 1H), 2.86 (ddd, J = 47.8, 13.8, 7.4 Hz, 2H), 2.35 (dd, J = 13.2, 4.9 Hz, 2H), 2.29 – 2.05 (m, 5H), 1.93 – 1.70 (m, 4H), 1.64 (d, J = 15.9 Hz, 3H), 1.48 (td, J = 14.0, 12.7, 7.2 Hz, 2H), 1.43 – 1.29 (m, 4H), 1.31 (s, 12H), 0.99 (d, J = 6.8 Hz, 3H), 0.89 (s, 3H), 0.85 (d, J = 7.2 Hz, 3H).

ESI: m/z 875 [M+H]⁺, 897 [M+Na]⁺.

methyl 3-hydroxy-4-methylbenzoate (60)

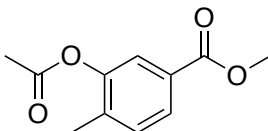


The product was prepared according to the literature. [222]

To a solution of 3-hydroxy-4-methylbenzoic acid (500 mg, 3.28 mmol) in MeOH (5 mL), H₂SO₄ conc. (0.375 mL) was added dropwise. The solution was stirred at reflux for 3 h. The product mixture was cooled to 25 °C and the solvent was removed under reduced pressure. The residue was dissolved in EtOAc (50 mL), washed with NaHCO₃ ss (2 x 25 mL) and H₂O (25 mL), dried over anhydrous Na₂SO₄, filtered, and evaporated under vacuum to get the esterified compound **60** as an oil (480 mg, 2.89 mmol, 88% yield).

NMR data are coherent with the literature. [222]

methyl 3-acetoxy-4-methylbenzoate (61)



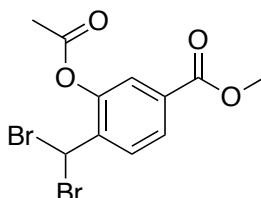
The product was prepared according to the literature. [222]

A solution of compound **60** (500 mg, 3.01 mmol) in pyridine (2 mL) was treated with acetic anhydride (1.3 mL, 13.65 mmol). The resulting solution was stirred for 2 h at r.t.. The mixture was concentrated under reduced pressure. The residue was dissolved in EtOAc (50 mL) and washed with H₂O (25 mL) and NaCl_{ss} (25 mL); the organic layer was dried over anhydrous

Na₂SO₄, filtered, and evaporated *in vacuo*. The compound **61** was obtained as an orange-brown oil (620g, 2.98 mmol, 99% yield).

NMR data and ESI analysis are coherent with the literature. [222]

methyl 3-acetoxy-4-(dibromomethyl)benzoate (62)

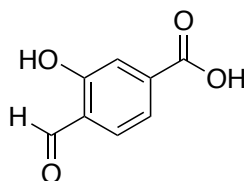


The product was prepared according to the literature. [223]

A mixture of **61** (100 mg, 0.48 mmol), NBS (171 mg, 0.96 mmol) and a catalytic amount of benzoyl peroxide (5 mg) in CCl₄ (5 mL) was refluxed for 3 h under Ar. The reaction mixture was cooled to r.t. and filtrated with a Büchner. The filtrate was evaporated under reduced pressure and the residue was purified by flash chromatography chromatography eluting 0-6% gradient of CH₂Cl₂ in petroleum ether providing the desired compound **62** (150 mg, 0.41 mmol, 86% yield).

NMR data and ESI analysis are coherent with the literature. [223]

4-formyl-3-hydroxybenzoic acid (63)



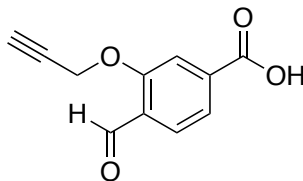
The product was prepared according to the literature. [223]

The compound **62** (150 mg, 0.40 mmol) was dissolved in EtOH (3 mL) and a solution of Na₂CO₃ (911 mg) in 2 mL of H₂O was added. The reaction was carried out at reflux for 16 h, then EtOH was evaporated. The resulting aqueous solution was acidified by addition of HCl 4 N until pH =2 and the product was extracted with EtOAc (40 mL). The organic layer was dried over anhydrous Na₂SO₄, filtered, and evaporated *in vacuo* to provide the desired compound **63** (66 mg, 0.40 mmol, > 99% yield).

¹H NMR (400 MHz, DMSO-*d*₆, δ ppm, *J* Hz): δ 13.20 (bs, 1H) 10.91 (bs, 1H), 10.31 (s, 1H),

7.68 (d, $J = 8.1$ Hz, 1H), 7.52 (s, 1H), 7.41 (d, $J = 8.1$ Hz, 1H).

4-formyl-3-(prop-2-yn-1-yloxy)benzoic acid (64)

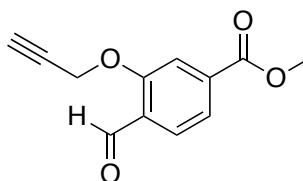


The phenol **63** (500 mg, 3.012 mmol) was dissolved in MeOH (25 mL) and NaOH 10 N (904 μ L, 9.04 mmol) was added. The resulting mixture was stirred for 10 min. and then added to the propargyl bromide (2.46 g, 16.57 mmol). The reaction was carried out at r.t. for 16 h. The base was neutralized with HCl 1 N, diluted with CH_2Cl_2 , dried over anhydrous Na_2SO_4 , filtered and evaporated *in vacuo*. The crude was purified by silica gel flash chromatography eluting 0-10% gradient of MeOH in CH_2Cl_2 to provide compound **64** (480 mg, 2.35 mmol, 78% yield) as a yellow solid.

^1H NMR (400 MHz, $\text{DMSO}-d_6$, δ ppm, J Hz): δ 10.90 (bs, 1H), 10.34 (s, 1H), 7.76 (s, 1H), 7.68 (d, $J = 8.0$ Hz, 1H), 7.62 (d, $J = 8.1$ Hz, 1H), 5.04 (s, 2H), 3.65 (s, 1H).

ESI: m/z 203 $[\text{M}-\text{H}]^+$.

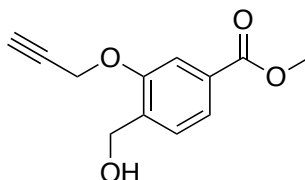
methyl 4-formyl-3-(prop-2-yn-1-yloxy)benzoate (65)



To a **64** (132 mg, 0.65 mmol) in MeOH (1.3 mL), H_2SO_4 conc. (63 μ L) was added dropwise. The solution was stirred at reflux for 1 h. The product mixture was cooled to 25 $^\circ\text{C}$ and the solvent was removed under reduced pressure. The residue was dissolved in EtOAc (50 mL), washed with NaHCO_3 ss (2 x 25 mL) and H_2O (25 mL), dried over anhydrous Na_2SO_4 , filtered, and evaporated under vacuum to get the esterified compound **65** as an oil (80 mg, 0.37 mmol, 57% yield).

¹H NMR (400 MHz, CDCl₃, δ ppm, *J* Hz): δ 10.49 (s, 1H), 7.87 (d, *J* = 7.5 Hz, 1H), 7.75 (s, 1H), 7.70 (d, *J* = 8.0 Hz, 1H), 4.86 (s, 2H), 3.92 (s, 3H), 2.56 (s, 1H).

methyl 4-(hydroxymethyl)-3-(prop-2-yn-1-yloxy)benzoate (66)

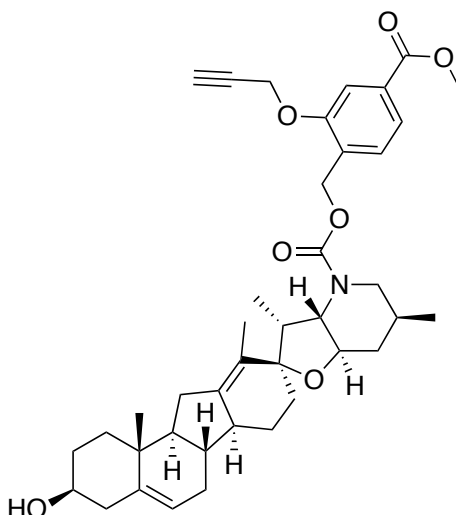


In a round-bottom flask the aldehyde **65** (40 mg, 0.18 mmol) was solubilized in MeOH (1 mL). The mixture was cooled to 0 °C, and NaBH₄ (8 mg, 0.20 mmol) was added. The resulting mixture was stirred at 0 °C for 30 min.. The MeOH was evaporated under reduced pressure and the residue was solubilized in CH₂Cl₂ (10 mL), washed with NH₄Cl (5 mL) and with NaCl_{ss} (5 mL). The organic layer was dried over anhydrous Na₂SO₄, filtered, and evaporated under vacuum to provide the reduced compound **66** (39 mg, 0.18 mmol, > 99% yield).

¹H NMR (400 MHz, CDCl₃, δ ppm, *J* Hz): δ 7.65 (d, *J* = 7.8 Hz, 1H), 7.58 (s, 1H), 7.39 (d, *J* = 7.9 Hz, 1H), 4.76 (s, 2H), 4.71 (s, 2H), 3.88 (s, 3H), 2.51 (s, 1H).

ESI: *m/z* 221 [M+H]⁺, 441 [2M+H]⁺, 463 [2M +Na]⁺.

**4-(methoxycarbonyl)-2-(prop-2-yn-1-yloxy)benzyl
(4*S*,6*aR*,8*aR*,8*bS*,11*S*,12*aR*,13*aR*,15*bS*)-4-hydroxy-6*a*,11-dimethyl-
3,4,5,6,6*a*,6*b*,7,8,8*a*,8*b*,10,11,12,12*a*,14,15,15*a*,15*b*-
octadecahydrobenzo[7'',8'']fluoreno[2'',1'':2',3']cyclobuta[1',2':4,5]furo[3,2-*b*]pyridine-
9(1*H*)-carboxylate (67a)**



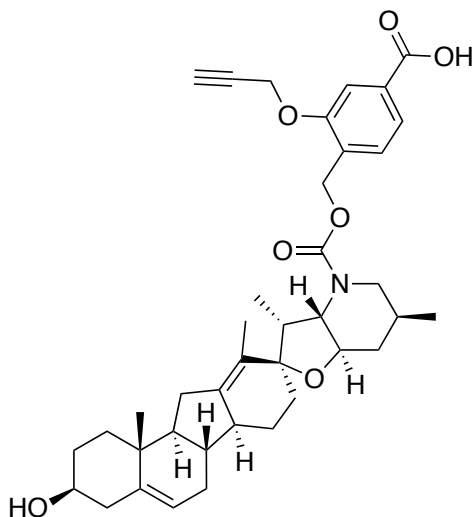
The benzyl alcohol **66** (42 mg, 0.19 mmol) was solubilized in CH_2Cl_2 (1 mL) at r.t. under N_2 . At 0 °C *p*-nitrophenyl chloroformate (42 mg, 0.21 mmol) and DMAP (46 mg, 0.38 mmol) were added, and the reaction was carried out for 50 min. at 0 °C. The activated compound was checked by TLC and was dropped into a solution of **Cyclopamine** (128 mg, 0.29 mmol) and DIPEA (99 μL , 0.57 mmol) at 0 °C and the reaction was stirred at r.t. for 16 h. The solvent was evaporated under reduced pressure. The residue was dissolved in EtOAc (10 mL) and washed with H_2O (5 mL) and NaCl_{ss} (5 mL). The organic phase was dried over anhydrous Na_2SO_4 , filtered, and evaporated under vacuum. The carbamate was purified by means of chromatography on silica gel with MPLC Syncore® Büchi eluting 0-70 % gradient of EtAOc in petroleum ether. (53 g, 0.08 mmol, 41% yield).

^1H NMR (400 MHz, CDCl_3 , δ ppm, J Hz): δ 7.65 (d, J = 7.4 Hz, 1H), 7.61 (s, 1H), 7.38 (d, J = 7.9 Hz, 1H), 5.33 (t, J = 4.3 Hz, 1H), 5.22 (s, 2H), 4.74 (s, 2H), 3.89 (s, 3H), 3.71 – 3.37 (m, 4H), 3.19 (dd, J = 10.2, 7.3 Hz, 1H), 2.89 (ddd, J = 47.8, 13.8, 7.4 Hz, 2H), 2.34 (dd, J = 13.2, 4.9 Hz, 2H), 2.28 – 2.07 (m, 5H), 1.94 – 1.72 (m, 4H), 1.64 (d, J = 15.9 Hz, 3H), 1.48 (td, J = 14.0, 12.7, 7.2 Hz, 2H), 1.43 – 1.02 (m, 4H), 0.99 (d, J = 6.8 Hz, 3H), 0.89 (s, 3H), 0.86 (d, J = 7.2 Hz, 3H).

^{13}C NMR (101 MHz, CDCl_3 , δ ppm): δ 166.69, 157.79, 155.01, 143.20, 141.64, 130.95, 128.72, 126.58, 126.14, 122.80, 121.88, 115.65, 112.49, 110.81, 85.07, 72.50, 71.83, 63.31, 62.28, 56.14, 52.31, 52.03, 50.93, 49.25, 41.80, 41.57, 38.15, 36.55, 35.17, 32.59, 31.38, 31.08, 29.03, 28.37, 24.59, 20.51, 18.67, 13.49, 10.44.

ESI: m/z 658 $[\text{M}+\text{H}]^+$.

4-((((4*S*,6*aR*,8*aR*,8*bS*,11*S*,12*aR*,13*aR*,15*bS*)-4-hydroxy-6*a*,11-dimethyl-1,3,4,5,6,6*a*,6*b*,7,8,8*a*,8*b*,9,10,11,12,12*a*,14,15,15*a*,15*b*-icosahydrobenzo[7'',8'']fluoreno[2'',1'':2',3']cyclobuta[1',2':4,5]furo[3,2-*b*]pyridine-9-carbonyl)oxy)methyl)-3-(prop-2-yn-1-yloxy)benzoic acid (68a)



LiOH·H₂O (3 mg, 0.078 mmol) in 250 μ L of H₂O was added to a solution of **67a** (16 mg, 0.024 mmol) in THF (750 μ L) at 0 °C. The resulting mixture was stirred at r.t. for 5 h. THF and MeOH were evaporated under reduced pressure. The resulting aqueous mixture was acidified by adding HCl 1 N dropwise and extracted with EtOAc (3 mL). The organic layer was dried over Na₂SO₄, filtered, and evaporated under vacuum to obtain the reduced compound **68a** (13 mg, 0.020 mmol, 88% yield).

¹H NMR (400 MHz, CDCl₃, δ ppm, *J* Hz): δ 7.73 (d, *J* = 7.4 Hz, 1H), 7.67 (s, 1H), 7.42 (d, *J* = 7.9 Hz, 1H), 5.35 (t, *J* = 4.3 Hz, 1H), 5.26 (s, 2H), 4.76 (s, 2H), 3.69 – 3.36 (m, 4H), 3.19 (dd, *J* = 10.2, 7.3 Hz, 1H), 2.86 (ddd, *J* = 47.8, 13.8, 7.4 Hz, 2H), 2.35 (dd, *J* = 13.2, 4.9 Hz, 2H), 2.29 – 2.05 (m, 5H), 1.93 – 1.70 (m, 4H), 1.64 (d, *J* = 15.9 Hz, 3H), 1.48 (td, *J* = 14.0, 12.7, 7.2 Hz, 2H), 1.43 – 1.02 (m, 4H), 0.99 (d, *J* = 6.8 Hz, 3H), 0.89 (s, 3H), 0.85 (d, *J* = 7.2 Hz, 3H).

¹³C NMR (101 MHz, CDCl₃, δ ppm): δ 170.54, 165.46, 159.73, 157.76, 154.99, 143.21, 141.61, 131.70, 129.75, 128.70, 126.58, 123.47, 121.90, 112.88, 85.09, 72.50, 71.87, 63.30, 62.29, 56.17, 52.03, 50.92, 49.25, 41.74, 38.15, 36.55, 35.15, 32.59, 31.34, 29.70, 29.03, 28.38, 24.59, 20.54, 18.68, 13.49, 10.46, 1.02.

ESI: *m/z* 642 [M-H]⁺, 666 [2M + Na]⁺.

4.2.3 HPLC method for hydrolysis

A 28 mM solution of the **69a** was prepared in MeCN/MeOH 1:1 (500 μ L) and diluted up to 14 mM in a phosphate buffers (500 μ L) at pH 7.4 ($\text{KH}_2\text{PO}_4/\text{K}_2\text{HPO}_4$, 0.1M). A water solution of H_2O_2 -urea (0.11 mmol in 400 μ L) was added. The final mixture (**69a** 10 mM) was sonicated, incubated at 37 °C for 10 min. and a sample was injected to the HPLC.

HPLC analysis were performed on a LC/MSD system InfinityLab LC/MSD iQ, Column: InfinityLab PoroShell 120 EC-C18 2.1x50mmx2.7 μ m. Flow: 0.4 mL/min. Eluent A/B: H_2O /MeCN. Gradient: 5% B to 95% B in 10 min., 4 min. at 95 % B and 3 min. of re-equilibration. Detection: 254 nm and 260 nm.

4.3 ADCs armed with SMO inhibitors

4.3.1 General experimental procedures, materials and instruments

All reagents were used as purchased from commercial suppliers without further purification. The reactions were carried out in oven dried vessels. Solvents were dried and purified by conventional methods prior use or, if available, purchased in anhydrous form.

Flash column chromatography was performed with Merck silica gel Å 60, 0.040-0.063 mm (230-400 mesh).

MPLC Syncore® Büchi on highly resistant PP cartridges Normal Phase silica gel NP 40 – 63 µm particle size and 60 Å pore size (Si60) withstand a maximum pressure of 10 bar (145 psi) column with PE (Eluent A) and EtOAc(Eluent B) as mobile phase.

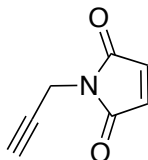
Merck aluminum backed plates pre-coated with silica gel 60 (UV254) were used for analytical thin layer chromatography and were visualized by staining with a KMnO₄ or Ninhydrin solution.

NMR spectra were recorded at 25 °C with 400 1H and 101 MHz for 13C Brüker Avance NMR spectrometers. The solvent is specified for each spectrum. Splitting patterns are designated as s, singlet; d, doublet; t, triplet; q, quartet; m, multiplet; bs, broad singlet. Chemical shifts (δ) are given in ppm relative to the resonance of their respective residual solvent peaks.

High and low resolution mass spectroscopy analyses were recorded by electrospray ionization with a mass spectrometer Q-exactive Plus.

4.3.2 Synthetic procedures

1-(prop-2-yn-1-yl)-1*H*-pyrrole-2,5-dione (70)

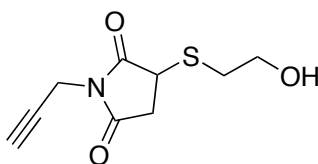


The product was prepared according to the literature. [224]

Maleic anhydride (700 mg, 7.14 mmol) and propargylamine (0.5 mL, 7.85 mmol) were dissolved in glacial acetic acid (14 mL) and stirred at r.t. for 16 h. The reaction mixture was concentrated under reduced pressure, the residue suspended in acetic anhydride (5 mL) and NaOAc (311 mg, 3.57 mmol) was added. The reaction vessel was heated at 65 °C for 2 h. After cooling to r.t., the reaction mixture was diluted in H₂O (70 mL) and extracted with Et₂O (3 × 100 mL). The combined organic phases were dried over Na₂SO₄, filtered, and evaporated under vacuum. The compound was purified by means of chromatography on silica gel with MPLC Syncore® Büchi eluting 0-50 % gradient of EtAOc in petroleum ether, as a transparent oil (582 g, 4.28 mmol, 60% yield).

¹H NMR (400 MHz, CDCl₃, δ ppm, *J* Hz) δ 6.66 (s, 2H), 4.12 (s, 2H), 2.13 (s, 1H).

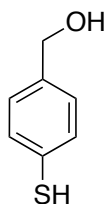
3-((2-hydroxyethyl)thio)-1-(prop-2-yn-1-yl)pyrrolidine-2,5-dione (71)



The compound **70** (1.39 g, 10.3 mmol) was solubilized in MeCN (40 mL) and 2-mercaptoethanol (1.44 mL, 20.6 mmol) was added dropwise. The reaction mixture was stirred at r.t. for 16 h. The product was purified by means of chromatography on silica gel with MPLC Syncore® Büchi eluting 0-100 % gradient of EtAOc in petroleum ether, as a transparent oil (1.91 g, 8.03 mmol, 78% yield).

¹H NMR (400 MHz, CDCl₃, δ ppm, *J* Hz): δ 4.15 (s, 2H), 3.75 (t, *J* = 7.0 Hz, 2H), 3.24 – 3.12 (m, 2H), 2.88 (ddd, *J* = 83.2, 14.3, 7.2 Hz, 2H), 2.50 (dd, *J* = 19.0, 3.6 Hz, 1H), 2.19 (s, 1H).

(4-mercaptophenyl)methanol (72)

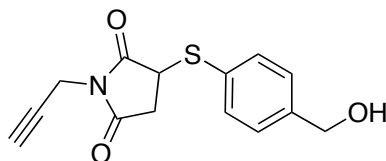


The product was prepared according to the literature [157]

Obtained 1.204 g, 8.60 mmol, 74% yield.

¹H NMR (400 MHz, CDCl₃, δ ppm, *J* Hz): δ 7.23 (d, *J* = 8.1 Hz, 2H), 7.19 (d, *J* = 8.2 Hz, 2H), 4.60 (s, 2H).

3-((4-(hydroxymethyl)phenyl)thio)-1-(prop-2-yn-1-yl)pyrrolidine-2,5-dione (73)

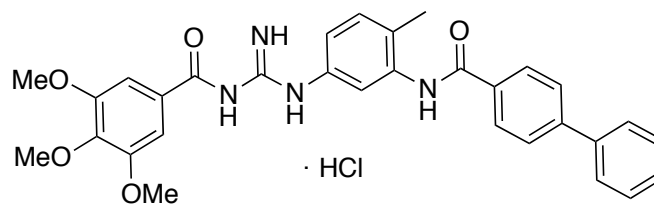


The compound **70** (600 mg, 4.36 mmol) and the thiol **72** (350 mg, 2.57 mmol) were solubilized in MeCN (15 mL) and a catalytic amount of Et₃N (18 μL, 0.1 mmol) was added dropwise. The reaction mixture was stirred at r.t. for 16 h and after the crude was concentrated *in vacuo*. The product was purified by means of chromatography on silica gel with MPLC Syncore® Büchi eluting 0-100 % gradient of EtAOc in petroleum ether, as a transparent oil (594 mg, 2.16 mmol, 84% yield).

¹H NMR (400 MHz, CDCl₃, δ ppm, *J* Hz): δ 7.47 (d, *J* = 7.9 Hz, 2H), 7.30 (d, *J* = 7.7 Hz, 2H), 4.66 (s, 2H), 4.15 (s, 2H), 3.99 (dd, *J* = 9.2, 4.1 Hz, 1H), 3.14 (dd, *J* = 18.8, 9.2 Hz, 1H), 2.67 (dd, *J* = 18.8, 4.2 Hz, 1H), 2.13 (s, 1H).

ESI: *m/z* 276 [M+H]⁺, 298 [M+Na]⁺.

***N*-(2-methyl-5-(3-(3,4,5-trimethoxybenzoyl)guanidino)phenyl)-[1,1'-biphenyl]-4-carboxamide hydrochloride (MRT-86)**



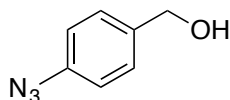
The product was prepared according to the literature. [214]

¹H NMR (400 MHz, DMSO-*d*₆, δ ppm, *J* Hz): δ 9.18 (bs, 1 H), 9.00 (bs, 1H), 8.06 (bs, 2H), 7.80-7.10 (m, 14H), 3.70 (s, 6H), 3.68 (s, 3H), 2.77 (s, 3 H).

¹³C NMR (101 MHz, DMSO-*d*₆, δ ppm): δ 176.0, 168.2, 165.0, 160.0, 156.5, 150.0, 146.3, 139.0, 137.4, 133.1, 131.8, 131.4, 131.0, 128.9, 128.6, 127.1, 127.0, 126.4, 123.5, 121.0, 119.3, 118.5, 116.0, 61.3, 56.0, 34.9.

ESI: *m/z* 539 [M + H]⁺.

(4-azidophenyl)methanol (74)



The product was prepared according to the literature. [227]

4-Aminobenzyl alcohol (3 g, 24.35 mmol) was dissolved in a solution of H₂SO₄ 2 M (20 mL) at 0 °C and to the resulting mixture, a solution of sodium nitrite (2.52 g, 36.52 mmol) in H₂O (10 mL) was added. The reaction was stirred at 0 °C for 15 min. and a H₂O solution (10 mL) of sodium azide (2.36 g, 36.52 mmol) was added dropwise. The mixture was stirred at r.t. into the dark for 1 h. The crude was extracted with Et₂O (2 x 30 mL). The combined organic layers were washed with HCl 1 N (20 mL), H₂O (20 mL) and NaCl_{ss} (30 mL), dried over anhydrous Na₂SO₄, filtered and concentrated under reduced pressure to provide compound **74** (3.55 g, 23.86 mmol) as a yellow oil without further purification in a 98% yield.

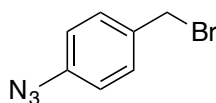
¹H NMR (400 MHz, CDCl₃, δ ppm, *J* Hz): δ 7.42 (d, *J* = 8.0, 2H), 6.97 (d, *J* = 8.0, 2H), 4.57 (s, 2H), 1.87 (bs, 1H).

¹³C NMR (101 MHz, CDCl₃, δ ppm): δ 139.01, 137.45, 128.36, 118.88, 64.05.

General procedure for the bromination of benzyl alcohols

The desired benzyl alcohol (0.4 mmol) was dissolved in CH₂Cl₂ (10 mL) at 0 °C and PBr₃ (56 μL, 0.60 mmol) was added dropwise. The resulting solution was stirred at r.t. for 30 min..

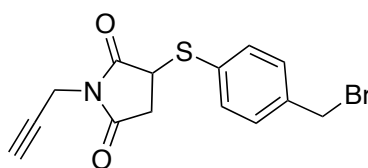
1-azido-4-(bromomethyl)benzene (78)



The crude was quenched with Na₂CO₃ ss (10 mL). The phases were separated and the aqueous phase was extracted with CH₂Cl₂ (2 x 10 mL). The combined organic layers were dried over anhydrous Na₂SO₄, filtered and concentrated under reduced pressure to provide compound **78** (72 mg, 0.34 mmol, 85% yield) as a bright orange oil without further purification.

¹H NMR (400 MHz, CDCl₃, δ ppm, *J* Hz): δ 7.33 (d, *J* = 8.0, 2H), 6.95 (d, *J* = 8.0, 2H), 4.42 (s, 2H).

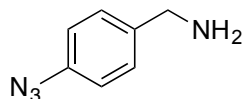
3-((4-(bromomethyl)phenyl)thio)-1-(prop-2-yn-1-yl)pyrrolidine-2,5-dione (85)



The mixture was concentrated under N₂ and quickly filtrated on a pad of silica gel using PE:EtOAc 1:1. The resulting filtrate was concentrated under reduced pressure and the bromide **85** was immediately used for the next step (135 mg, 0.4 mmol, 99%).

R_f: 0.85 (PE:EtOAc 1:1).

(4-azidophenyl)methanamine (79)



The product was prepared according to the literature. [228]

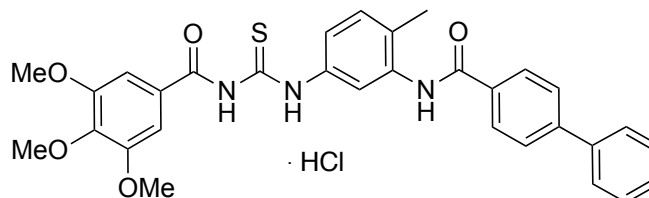
The bromide **78** (536 mg, 2.53 mmol) was solubilized in dry DMF (25 mL) and phthalimide potassium (468 mg, 2.53 mmol) was added at r.t.. The reaction was heated at 80 °C for 3 h. The

mixture was cooled to r.t. and the solvent was evaporated under reduced pressure. The residue was dissolved in EtOAc (40 mL) and washed with H₂O (2 x 80 mL) and NaCl_{ss} (30 mL). The organic phase was dried over anhydrous Na₂SO₄, filtered and concentrated *in vacuo*. The phthalimide derivative was purified by means of flash chromatography on silica gel with MPLC Syncore® Büchi eluting 0-60 % gradient of EtOAc in petroleum ether (570 mg, 2.05 mmol, 81% yield). ¹H NMR (400 MHz, CDCl₃, δ ppm, *J* Hz): δ 7.82 (dd, *J* = 5.6, 3.1 Hz, 2H), 7.68 (dd, *J* = 5.6, 3.1 Hz, 2H), 7.41 (d, *J* = 8.2 Hz, 2H), 6.94 (d, *J* = 8.4 Hz, 2H), 4.79 (s, 2H).

The phthalimide derivative (295 mg, 1.06 mmol) and hydrazine monohydrate (155 μL, 3.18 mmol) were solubilized in EtOH (20 mL). The reaction mixture was carried out at reflux for 3 h and was concentrated *in vacuo* after cooled at r.t.. The residue was diluted in EtOAc (15 mL) and washed with NaOH 1 N (2 x 10 mL) and NaCl_{ss} (10 mL). The organic layer was dried over anhydrous Na₂SO₄, filtered and concentrated under reduced pressure to provide the desired compound **79** as brown solid (155 mg, 1.05 mmol, 99%).

¹H NMR (400 MHz, CDCl₃, δ ppm, *J* Hz): δ 7.26 (d, *J* = 8.0, 2H), 6.95 (d, *J* = 8.0, 2H), 3.80 (s, 2H), 1.91 (bs, 2H).

***N*-(2-methyl-5-(3-(3,4,5-trimethoxybenzoyl)thioureido)phenyl)-[1,1'-biphenyl]-4-carboxamide hydrochloride (MRT-61)**



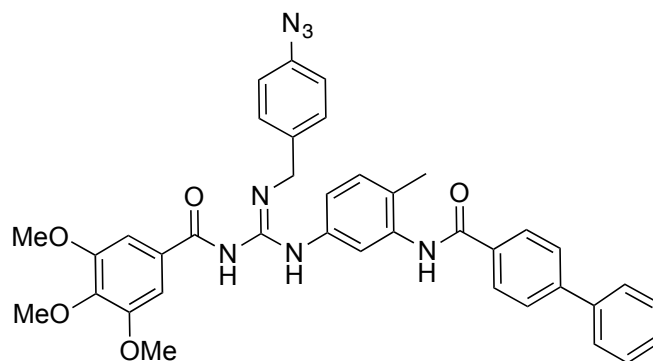
The product was prepared according to the literature. [214]

¹H NMR (400 MHz, DMSO-*d*₆, δ ppm, *J* Hz): δ 11.00 (s, 1H), 9.12 (s, 1H), 8.80 (s, 1H), 7.70-7.00 (m, 12H), 6.87 (s, 2H), 3.96 (s, 9H), 2.10 (s, 3H).

¹³C NMR (101 MHz, DMSO-*d*₆, δ ppm): δ 180.4, 166.5, 164.3, 156.9, 142.6, 142.1, 142.0, 140.4, 136.7, 135.4, 128.8, 128.7, 126.8, 125.6, 121.1, 118.7, 110.1, 61.2, 57.6, 20.1.

ESI: *m/z* 556 [M+H]⁺.

***(E)*-N-(5-(2-(4-azidobenzyl)-3-(3,4,5-trimethoxybenzoyl)guanidino)-2-methylphenyl)-[1,1'-biphenyl]-4-carboxamide (80)**

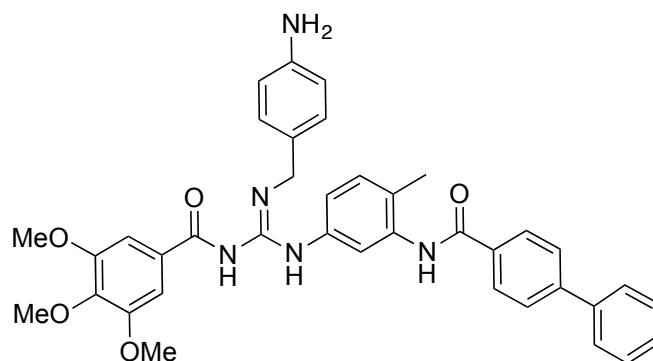


The AcTU **MRT-61** (574 mg, 1.03 mmol) and the benzyl amine **79** (153 mg, 1.03 mmol) were solubilized in DMF dry (10 mL), and Et₃N (287 μ L, 2.06 mmol) and HgCl₂ (280 mg, 1.03 mmol) were added at 0 °C. The mixture was stirred at r.t. for 16 h and was concentrated *in vacuo*. The residue was diluted in EtOAc (30 mL) and washed with H₂O (2 x 40 mL) and NaCl_{ss} (30 mL). The organic layer was dried over anhydrous Na₂SO₄, filtered and concentrated under reduced pressure. The product was purified by flash chromatography on silica gel eluting 0-5% gradient of MeOH in CH₂Cl₂ (629 mg, 0.94 mmol, 91% yield).

¹H NMR (400 MHz, CDCl₃, δ ppm, *J* Hz): 12.01 (bs, 1H), 9.26 (bs, 1H), 7.98-7.91 (m, 6H), 7.68 (d, *J* = 8.4, 2H), 7.60 (d, *J* = 8.0, 1H), 7.49 (s, 2H), 7.45 (d, *J* = 8.0, 2H), 7.40 (t, *J* = 7.6, 1H), 7.24 (t, *J* = 4.0, 2H), 6.97 (s, 2H), 4.66 (s, 2H), 3.84 (s, 3H), 3.79 (s, 6H), 2.28 (s, 3H).

ESI: *m/z* 670 [M + H]⁺.

(*E*)-N-(5-(2-(4-aminobenzyl)-3-(3,4,5-trimethoxybenzoyl)guanidino)-2-methylphenyl)-[1,1'-biphenyl]-4-carboxamide (81**)**



The azide **80** (90 mg, 0.13 mmol) was solubilized in CH₂Cl₂ (5 mL), and P(Me)₃ (400 μ L, 3.2 mmol) and H₂O (7 μ L, 3.2 mmol) were added. The mixture was stirred at r.t. for 16 h. The crude was concentrated *in vacuo* and the product **81** was achieved by precipitation with PE:Et₂O 3:1 (20 mL). Yield: 60% (51 mg, 0.08 mmol).

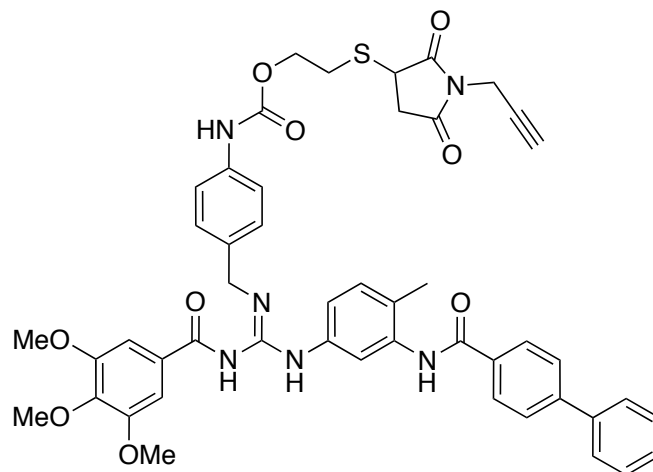
¹H NMR (400 MHz, CDCl₃, δ ppm, *J* Hz): 12.07 (bs, 1H), 7.94 (d, *J* = 8.0, 2H), 7.71 (d, *J* = 4.0, 4H), 7.63-7.49 (m, 6H), 7.41 (d, *J* = 5.2, 2H), 7.23 (d, *J* = 5.6, 1H), 7.20 (d, *J* = 6.0, 1H), 6.62 (d, *J* = 7.2, 2H), 4.63 (s, 2H), 3.88 (s, 9 H), 2.33 (s, 3H).

ESI: *m/z* 644 [M + H]⁺, 666 [M + Na]⁺.

General procedure for the synthesis of carbamates.

The desired linker (0.4 mmol) was solubilized in dry THF or dry CH₂Cl₂ (5 mL) at r.t under N₂. At 0 °C *p*-nitrophenyl chloroformate (89 mg, 0.44 mmol) and DMAP (98 mg, 0.8 mmol) were added, and the reaction was carried out for 30-50 minutes at 0 °C. The activated compound was checked by TLC and was dropped into a solution of the desired amine or aniline (0.6 mmol) and DIPEA (209 μL, 1.2 mmol) at 0 °C. The reaction was stirred at r.t. for 0.15 h-16 h. The solvent was evaporated under reduced pressure and the residue was dissolved in EtOAc (10 mL) and washed with H₂O (5 mL) and NaCl_{ss} (5 mL). The organic phase was dried over anhydrous Na₂SO₄, filtered, and evaporated under vacuum.

2-((2,5-dioxo-1-(prop-2-yn-1-yl)pyrrolidin-3-yl)thio)ethyl (*Z*)-(4-((((3-([1,1'-biphenyl]-4-carboxamido)-4-methylphenyl)amino)(3,4,5-trimethoxybenzamido)methylene)amino)methyl)phenyl)carbamate (**82**)

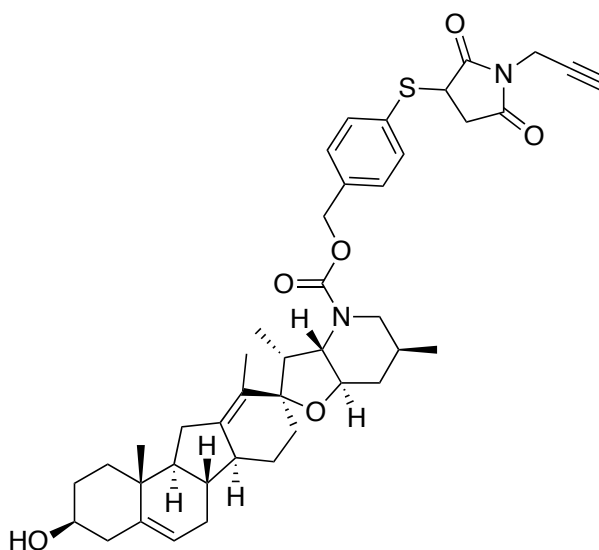


Linker used: compound **71**. Solvent used: dry THF. Reaction time after aniline **81** adding: 3 h. The carbamate **82** was purified by flash chromatography on silica gel with MPLC Syncore® Büchi eluting 0-100 % gradient of EtAOc in petroleum ether (114 mg, 0.13 mmol, 32% yield). **¹H NMR** (400 MHz, CDCl₃, δ ppm, *J* Hz): δ 12.05 (bs, 1H), 7.93 (d, *J* = 8.0, 2H), 7.70 (d, *J* = 8.01, 2H), 7.63-7.49 (m, 8H), 7.54 (d, *J* = 5.2, 2H), 7.46 (d, *J* = 7.5, 1H), 7.32 (d, *J* = 6.0, 1H),

6.61 (d, $J = 8.0$, 2H), 4.68 (s, 2H), 4.32 (t, $J = 7.0$ Hz, 2H), 4.24 (s, 2H), 3.88 (s, 9 H), 3.06 (m, 2H), 3.00 – 2.79 (m, 3H), 2.32 (s, 3H), 2.14 (s, 1H).

ESI: m/z 906 $[M + Na]^+$.

**4-((2,5-dioxo-1-(prop-2-yn-1-yl)pyrrolidin-3-yl)thio)benzyl
(4*S*,6*aR*,8*aR*,8*bS*,11*S*,12*aR*,13*aR*,15*bS*)-4-hydroxy-6*a*,11-dimethyl-
3,4,5,6,6*a*,6*b*,7,8,8*a*,8*b*,10,11,12,12*a*,14,15,15*a*,15*b*-
octadecahydrobenzo[7'',8'']fluoreno[2'',1'':2',3']cyclobuta[1',2':4,5]furo[3,2-*b*]pyridine-
9(1*H*)-carboxylate (92)**



Linker used: compound **73**. Solvent used: dry CH_2Cl_2 . Reaction time after **Cyclopamine** adding: 16 h.

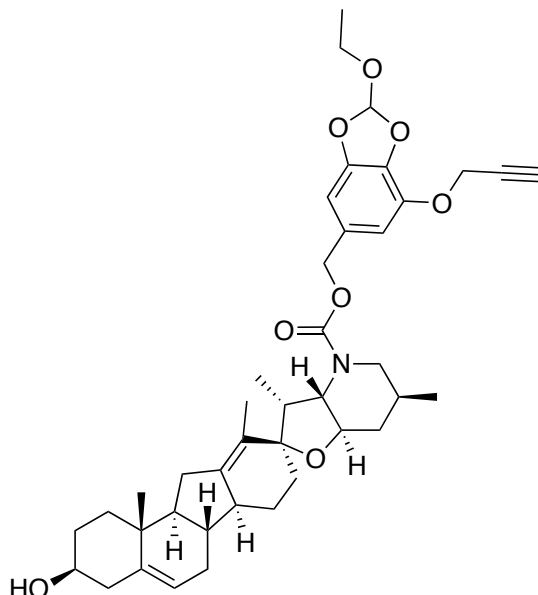
The carbamate **92** was purified by flash chromatography on silica gel eluting 0-2 % gradient of MeOH in CH_2Cl_2 (242 mg, 0.34 mmol, 86% yield).

1H NMR (400 MHz, $CDCl_3$, δ ppm, J Hz): δ 7.35 – 7.16 (m, 4H), 5.33 (t, $J = 4.3$ Hz, 1H), 5.13 (s, 2H), 4.04 (s, 2H), 3.69 – 3.36 (m, 4H), 3.19 (dd, $J = 10.2$, 7.3 Hz, 1H), 2.86 (ddd, $J = 47.8$, 13.8, 7.4 Hz, 2H), 2.35 (dd, $J = 13.2$, 4.9 Hz, 2H), 2.29 – 2.05 (m, 6H), 1.93 – 1.70 (m, 4H), 1.64 (d, $J = 15.9$ Hz, 3H), 1.48 (td, $J = 14.0$, 12.7, 7.2 Hz, 2H), 1.43 – 1.02 (m, 5H), 0.99 (d, $J = 6.8$ Hz, 3H), 0.89 (s, 3H), 0.85 (d, $J = 7.2$ Hz, 3H).

ESI: m/z 735 $[M + Na]^+$.

**(2-ethoxy-7-(prop-2-yn-1-yloxy)benzo[*d*][1,3]dioxol-5-yl)methyl
(4*S*,6*aR*,8*aR*,8*bS*,11*S*,12*aR*,13*aR*,15*bS*)-4-hydroxy-6*a*,11-dimethyl-**

3,4,5,6,6a,6b,7,8,8a,8b,10,11,12,12a,14,15,15a,15b-octadecahydrobenzo[7'',8'']fluoreno[2'',1'':2',3']cyclobuta[1',2':4,5]furo[3,2-*b*]pyridine-9(1*H*)-carboxylate (101**)**



Linker used: compound **41**. Solvent used: dry CH₂Cl₂. Reaction time after **Cyclopamine** adding: 16 h.

The carbamate **101** was purified by flash chromatography on silica gel eluting 0-60 % gradient of EtOAc in petroleum ether (213 mg, 0.31 mmol, 78% yield).

¹H NMR (400 MHz, CDCl₃, δ ppm, *J* Hz): 6.85 (s, 1H), 6.63 (s, 1H), 6.59 (s, 1H), 5.33 (t, *J* = 4.3 Hz, 1H), 5.00 (s, 2H), 4.76 (s, 2H), 3.69 – 3.38 (m, 4H), 3.19 (dd, *J* = 10.2, 7.3 Hz, 1H), 2.89 (ddd, *J* = 47.8, 13.8, 7.4 Hz, 2H), 2.34 (dd, *J* = 13.2, 4.9 Hz, 2H), 2.29 – 2.08 (m, 7H), 1.92 – 1.75 (m, 4H), 1.64 (d, *J* = 15.9 Hz, 3H), 1.48 (td, *J* = 14.0, 12.7, 7.2 Hz, 2H), 1.43 – 1.02 (m, 7H), 0.99 (d, *J* = 6.8 Hz, 3H), 0.88 (s, 3H), 0.86 (d, *J* = 7.2 Hz, 3H).

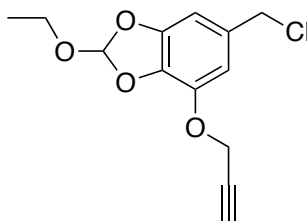
¹³C NMR (101 MHz, CDCl₃, δ ppm): 162.84, 157.83, 147.62, 143.35, 141.59, 140.51, 130.71, 126.52, 126.16, 121.90, 119.61, 115.66, 110.29, 102.87, 85.10, 72.54, 71.87, 67.21, 63.28, 59.53, 57.46, 52.01, 50.96, 49.22, 41.75, 41.58, 38.14, 36.53, 35.16, 32.60, 31.34, 31.07, 29.03, 28.36, 24.58, 20.44, 18.65, 14.83, 13.52, 10.46.

ESI: *m/z* 688 [M + H]⁺.

General procedure for benzyl alcohols chlorination

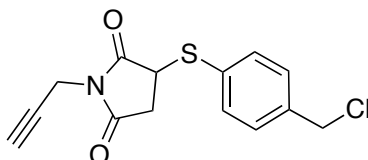
The desired benzyl alcohol (0.4 mmol) was solubilized in dry CH_2Cl_2 (6 mL) at 0°C and SOCl_2 (70 μL , 0.96 mmol) and Et_3N (145 μL , 1.04 mmol), both freshly distilled, were added carefully. The reaction was carried out at 0°C for 15-30 minutes. The mixture was concentrated under N_2 and quickly filtrated on a pad of silica gel using PE:EtOAc 1:1. The filtrate was concentrated under reduced pressure and the product was immediately used for the next step.

6-(Chloromethyl)-2-ethoxy-4-(prop-2-yn-1-yloxy)benzo[d][1,3]dioxole (44, HMPO)



Reaction time: 30 minutes. R_f : 0.92 (PE:EtOAc 1:1).

3-((4-(chloromethyl)phenyl)thio)-1-(prop-2-yn-1-yl)pyrrolidine-2,5-dione (89)



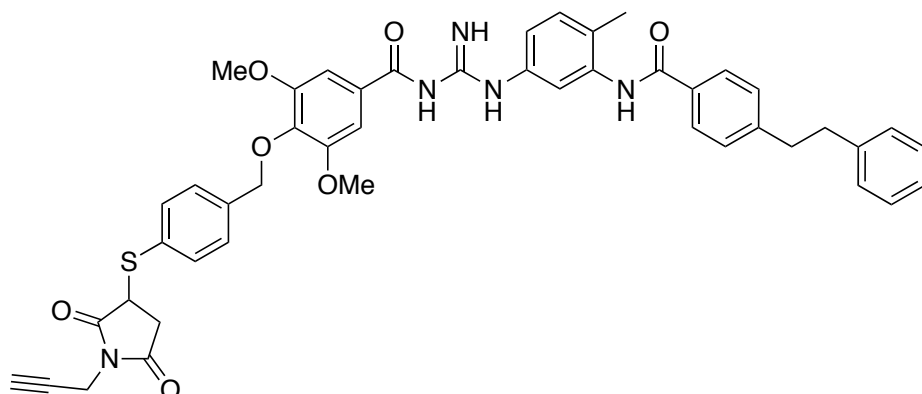
Reaction time: 15 minutes R_f : 0.85 (PE:EtOAc 1:1).

General procedure for phenols alkylation

The products were prepared according to the literature. [157]

The desired phenol (0.038 mmol) was dissolved in MeOH (1 mL) and NaOH 10 N (8 μL , 0.076 mmol) was added. The resulting mixture was stirred for 10 min. and then added to the bromide or chloride compound (0.115 mmol). The reaction was carried out at r.t. for 0.08-3 h. The base was neutralized with HCl 1 N, diluted with CH_2Cl_2 , dried over anhydrous Na_2SO_4 , filtered and evaporated *in vacuo*. The crude was purified by silica gel flash chromatography eluting 0-10% gradient of MeOH in CH_2Cl_2 to provide corresponding product.

4-((4-((2,5-dioxo-1-(prop-2-yn-1-yl)pyrrolidin-3-yl)thio)benzyl)oxy)-3,5-dimethoxy-*N*-(*N*-(4-methyl-3-(4-phenethylbenzamido)phenyl)carbamimidoyl)benzamide (86)



Activated linker used: compound **85**. Reaction time: 5 minutes.

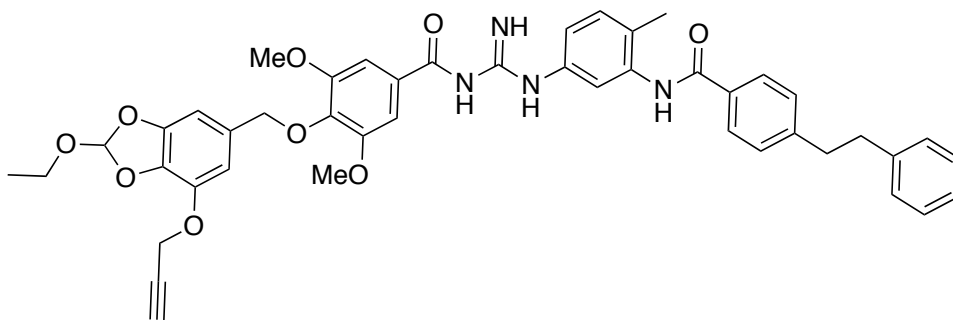
Obtained 16 mg, 0.02 mmol, 45% yield.

¹H NMR (400 MHz, CDCl₃, δ ppm, *J* Hz): δ 7.77 (d, *J* = 8.0 Hz, 2H), 7.55 (s, 2H), 7.42 (dt, *J* = 13.5, 6.8 Hz, 2H), 7.32 – 7.22 (m, 6H), 7.21 – 7.07 (m, 6H), 5.06 (s, 2H), 3.92 (s, 6H), 3.07 – 2.80 (m, 4H), 2.28 (s, 3H).

¹³C NMR (101 MHz, CDCl₃, δ ppm): δ 174.20, 173.01, 165.90, 165.46, 156.20, 153.41, 146.78, 141.00, 139.06, 137.25, 134.30, 132.66, 132.34, 131.64, 129.75, 129.14, 128.47, 127.31, 126.20, 121.60, 119.58, 106.46, 82.51, 74.17, 74.04, 71.84, 63.03, 56.81, 52.06, 47.89, 44.08, 37.68, 37.40, 36.42, 36.12, 36.04, 29.70, 28.12, 17.52, 1.02.

ESI: *m/z* 810 [M + H]⁺, 842 [M + Na]⁺.

4-((2-ethoxy-7-(prop-2-yn-1-yloxy)benzo[d][1,3]dioxol-5-yl)methoxy)-3,5-dimethoxy-*N*-(*N*-(4-methyl-3-(4-phenethylbenzamido)phenyl)carbamimidoyl)benzamide (95)



Activated linker used: compound **44**. Reaction time: 3 h.

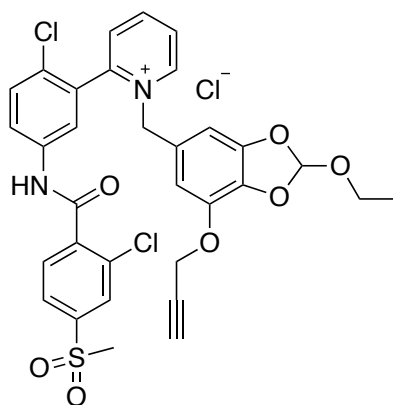
Obtained 23 mg, 0.03 mmol, 76% yield.

¹H NMR (400 MHz, CDCl₃, δ ppm, *J* Hz): 7.76 (d, *J* = 8.2 Hz, 1H), 7.48 (s, 2H), 7.31 – 7.07 (m, 5H), 6.86 (s, 1H), 6.77 – 6.59 (m, 7H), 6.53 (s, 1H), 4.95 (s, 2H), 4.29 (s, 2H), 3.88 (s, 6H), 3.69 (q, *J* = 7.3 Hz, 2H), 3.06 – 2.78 (m, 4H), 2.27 (s, 3H), 2.50 (s, 1H), 1.21 (t, *J* = 7.1 Hz, 3H).

¹³C NMR (101 MHz, CDCl₃, δ ppm): 165.90, 153.16, 147.40, 146.66, 145.14, 144.37, 141.02, 140.39, 140.27, 137.01, 134.29, 131.99, 129.75, 129.11, 128.47, 127.26, 126.18, 121.36, 119.44, 110.39, 109.48, 106.21, 104.67, 103.28, 76.08, 75.93, 74.85, 74.58, 59.08, 57.85, 57.37, 57.22, 56.34, 37.68, 37.43, 29.72, 24.05, 17.41, 14.83, 1.02.

ESI: *m/z* 785 [M + H]⁺.

2-(2-chloro-5-(2-chloro-4-(methylsulfonyl)benzamido)phenyl)-1-((2-ethoxy-7-(prop-2-yn-1-yloxy)benzo[d][1,3]dioxol-5-yl)methyl)pyridin-1-ium chloride (98)



Vismodegib (50 mg, 0.12 mmol) and the chloride **44** (50 mg, 0.19 mmol) were solubilized in DMF (1 mL), and TBAI (22 mg, 0.06 mmol) and DIPEA (52 μL, 0.30 mmol) were added. The reaction mixture was stirred at r.t. for 24 h. The crude was concentrated under reduced pressure and directly purify by silica gel flash chromatography eluting 0-20% gradient of MeOH in CH₂Cl₂ to provide corresponding alkylated product **98** (21 mg, 0.03 mmol, 24% yield)

¹H NMR (600 MHz, CDCl₃, δ ppm, *J* Hz): 11.37 (bs, 1H), 9.15 (d, *J* = 5.9 Hz, 1H), 8.65 (dd, *J* = 9.3, 2.5 Hz, 1H), 8.46 (t, *J* = 7.7 Hz, 1H), 8.06 – 7.78 (m, 7H), 7.52 (d, *J* = 8.8 Hz, 1H), 6.88 (s, 1H), 6.55 (s, 1H), 6.49 (s, 2H), 4.76 (s, 2H), 3.73 (q, *J* = 7.0 Hz, 2H), 3.09 (s, 3H), 2.53 (s, 1H), 1.26 (t, *J* = 7.2 Hz, 3H).

¹³C NMR (151 MHz, CDCl₃, δ ppm) δ 164.73, 153.04, 148.28, 145.78, 145.09, 142.74, 141.14, 140.23, 139.00, 135.70, 133.24, 131.30, 130.75, 129.38, 129.08, 127.54, 126.36, 125.77, 125.47, 124.94, 123.21, 120.06, 114.21, 112.29, 104.01, 103.86, 62.87, 60.09, 57.66, 57.64, 44.44, 14.78.

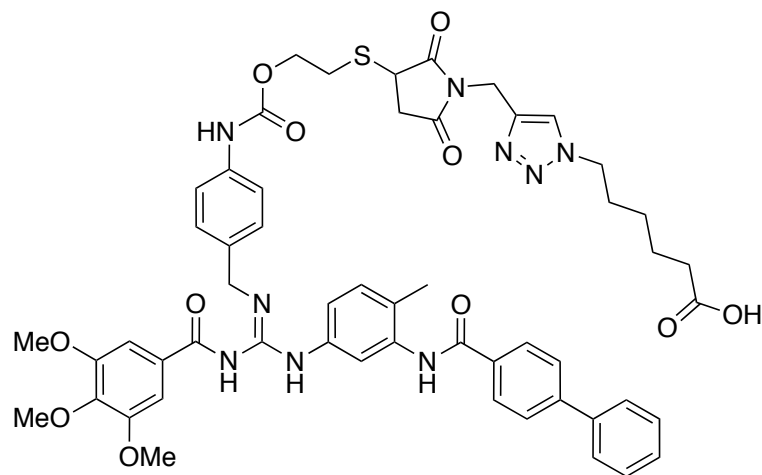
ESI: m/z 653 $[M]^+$.

General procedure for CCAA reaction

The desired alkyne (0.07 mmol) and the azide **49** (9 mg, 0.056 mmol) were dissolved in dry DMF (2 mL) under Ar. The solution was degassed with three cycles of argon/vacuum. To this solution, a freshly prepared aqueous mixture (2 mL) of $\text{Cu}(\text{OAc})_2$ (4 mg, 0.021 mmol) and Na ascorbate (8 mg, 0.042 mmol), previously degassed by argon/vacuum cycles, was added dropwise. The reaction mixture was degassed and left to stir under Ar. at r.t. for 16 h. The solvent was evaporated and the crude was purified by silica gel flash chromatography eluting 0-10 % gradient of MeOH in CH_2Cl_2 provide the desired compound.

Synthetic procedure of azide **49** already reported in paragraph 4.1.2.

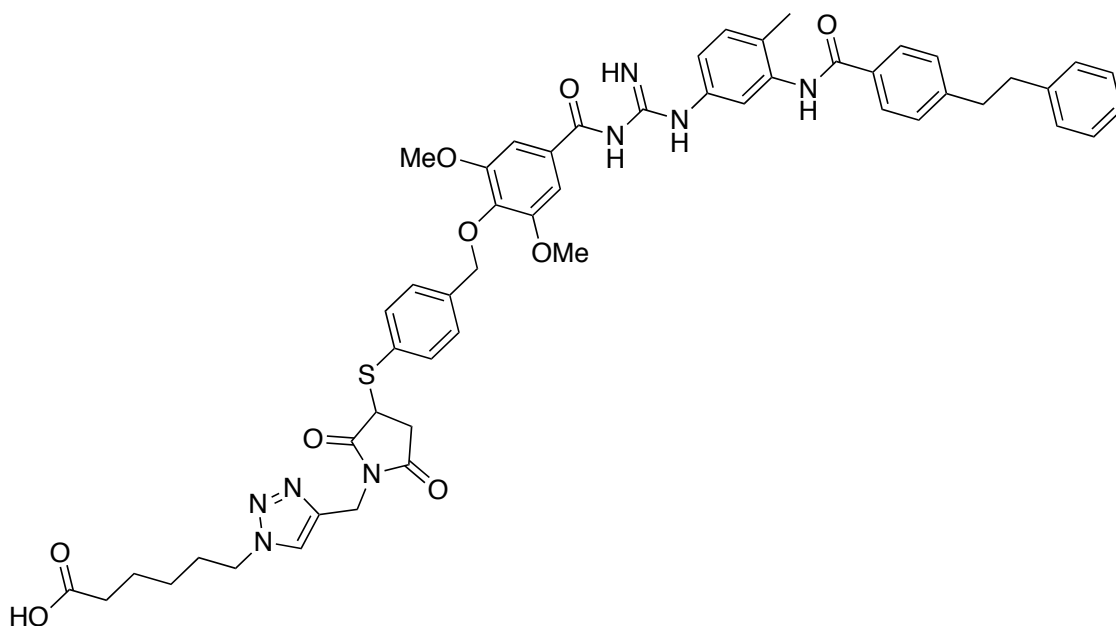
(Z)-6-(4-((3-((2-(((4-(((3-([1,1'-biphenyl]-4-carboxamido)-4-methylphenyl)amino)(3,4,5-trimethoxybenzamido)methylene)amino)methyl)phenyl)carbamoyl)oxy)ethyl)thio)-2,5-dioxopyrrolidin-1-yl)methyl)-1H-1,2,3-triazol-1-yl)hexanoic acid (83**)**



Obtained: 41 mg, 0.4 mmol, 71% yield.

ESI: m/z 1041 $[M + H]^+$.

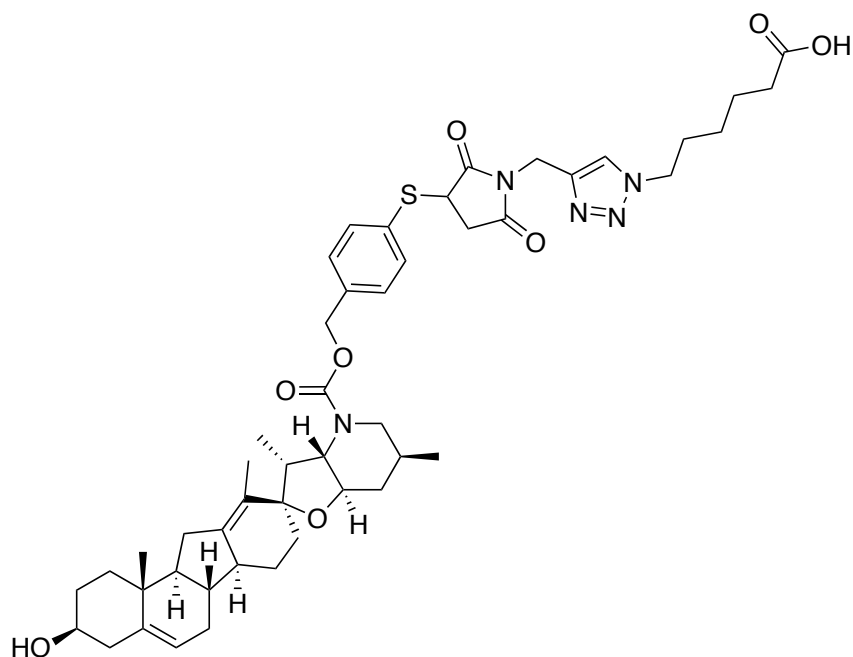
6-(4-((3-((4-((2,6-dimethoxy-4-((N-(4-methyl-3-(4-phenethylbenzamido)phenyl)carbamimidoyl)carbamoyl)phenoxy)methyl)phenyl)thio)-2,5-dioxopyrrolidin-1-yl)methyl)-1H-1,2,3-triazol-1-yl)hexanoic acid (87**)**



Obtained: 29 mg, 0.03 mmol, 56% yield.

ESI: m/z 967 $[M + H]^+$.

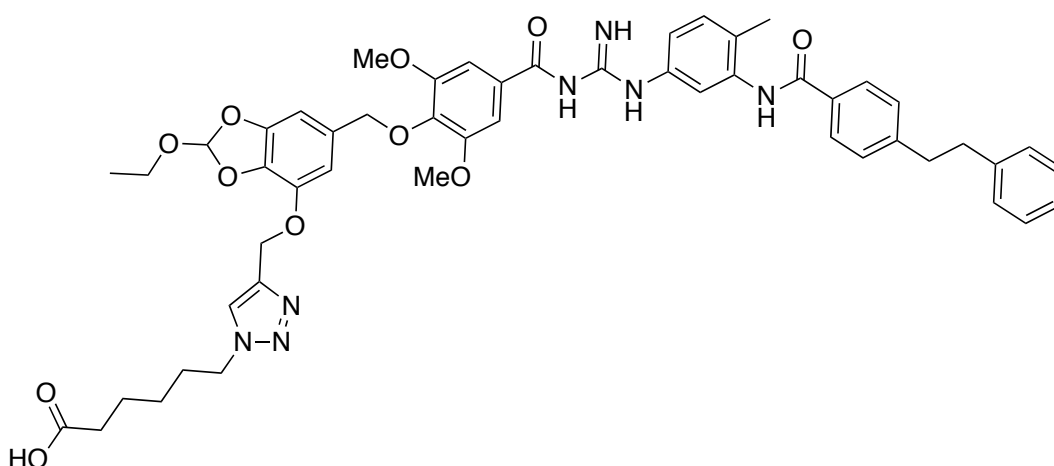
6-(4-((3-((4-(((4*S*,6*aR*,8*aR*,8*bS*,11*S*,12*aR*,13*aR*,15*bS*)-4-hydroxy-6*a*,11-dimethyl-1,3,4,5,6,6*a*,6*b*,7,8,8*a*,8*b*,9,10,11,12,12*a*,14,15,15*a*,15*b*-icosahydrobenzo[7'',8'']fluoreno[2'',1':2',3']cyclobuta[1',2':4,5]furo[3,2-*b*]pyridine-9-carbonyl)oxy)methyl)phenyl)thio)-2,5-dioxopyrrolidin-1-yl)methyl)-1*H*-1,2,3-triazol-1-yl)hexanoic acid (93)



Obtained: 8.5 mg, 0.01 mmol, 24% yield.

ESI: m/z 892 $[M + Na]^+$.

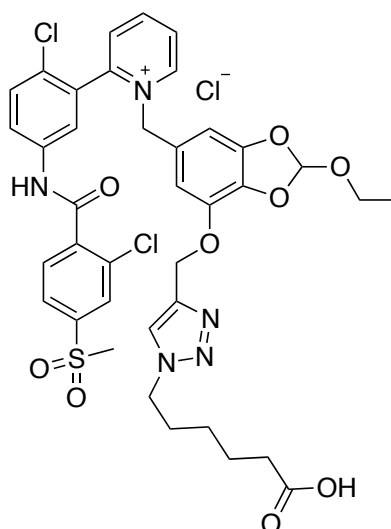
6-(4-(((6-((2,6-dimethoxy-4-((*N*-(4-methyl-3-(4-phenethylbenzamido)phenyl)carbamimidoyl)carbamoyl)phenoxy)methyl)-2-ethoxybenzo[*d*][1,3]dioxol-4-yl)oxy)methyl)-1*H*-1,2,3-triazol-1-yl)hexanoic acid (96)



Obtained: 28 mg, 0.03 mmol, 48% yield.

ESI: m/z 942 $[M + H]^+$, 964 $[M + Na]^+$.

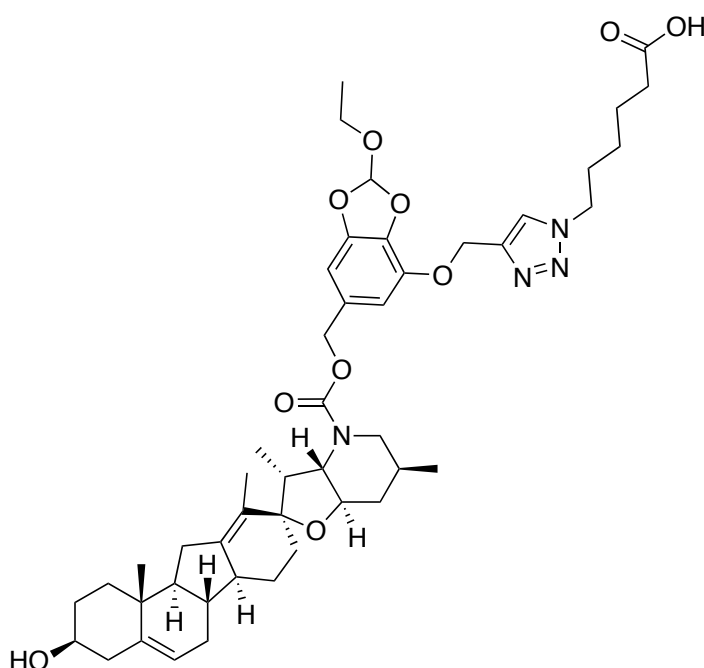
1-(((7-((1-(5-carboxypentyl)-1*H*-1,2,3-triazol-4-yl)methoxy)-2-ethoxybenzo[*d*][1,3]dioxol-5-yl)methyl)-2-(2-chloro-5-(2-chloro-4-(methylsulfonyl)benzamido)phenyl)pyridin-1-ium chloride (99)



Obtained: 24 mg, 0.03 mmol, 61% yield.

ESI: m/z 811 $[M + H]^+$, 824 $[M + Na]^+$.

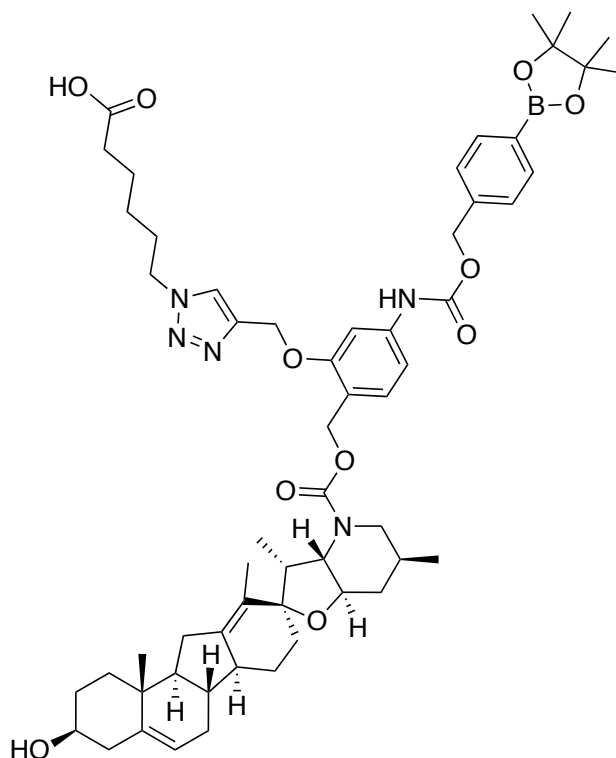
6-(4-(((2-ethoxy-6-(((4*S*,6*aR*,8*aR*,8*bS*,11*S*,12*aR*,13*aR*,15*bS*)-4-hydroxy-6*a*,11-dimethyl-1,3,4,5,6,6*a*,6*b*,7,8,8*a*,8*b*,9,10,11,12,12*a*,14,15,15*a*,15*b*-icosahydrobenzo[7'',8'']fluoreno[2'',1'':2',3']cyclobuta[1',2':4,5]furo[3,2-*b*]pyridine-9-carbonyl)oxy)methyl)benzo[*d*][1,3]dioxol-4-yl)oxy)methyl)-1*H*-1,2,3-triazol-1-yl)hexanoic acid (102)



Obtained: 9 mg, 0.01 mmol, 23% yield.

ESI: m/z 868 $[M + H]^+$, 884 $[M + Na]^+$.

6-(4-(((2-(((4*S*,6*aR*,8*aR*,8*bS*,11*S*,12*aR*,13*aR*,15*bS*)-4-hydroxy-6*a*,11-dimethyl-1,3,4,5,6,6*a*,6*b*,7,8,8*a*,8*b*,9,10,11,12,12*a*,14,15,15*a*,15*b*-icosahydrobenzo[7'',8'']fluoreno[2'',1'':2',3']cyclobuta[1',2':4,5]furo[3,2-*b*]pyridine-9-carbonyl)oxy)methyl)-5-(((4-(4,4,5,5-tetramethyl-1,3,2-dioxaborolan-2-yl)benzyl)oxy)carbonyl)amino)phenoxy)methyl)-1*H*-1,2,3-triazol-1-yl)hexanoic acid (104)



The synthetic route to provide the starting alkyne **69a** is reported in paragraph 4.2.2.

Obtained: 20 mg, 0.02 mmol, 27% yield.

ESI: m/z 1033 $[M + H]^+$.

4.3.3 General procedure for preparation of ADCs. ADCs **84**, **88**, **94**, **97**, **100**, **103**, **105**.

The proper carboxylic acid (28 μ L, 10 mM in DMSO) was activated by adding S-NHS (5 μ L, 100 mM in mQ) and EDC (5 μ L, 100 mM in mQ). The reaction was left for 16 h at r.t.. PBS at pH 7.4 (35 μ L) and Cetuximab freshly dialyzed using a 10 kDa cutoff dialysis membrane (100 μ L, 5 mg/mL in PBS pH 7.4) were added to the activated carboxylic acid solution. The reaction was mixed in a shaker at r.t. and after 1 h quenched with a 20 mM glycine aqueous solution (27 μ L). The final products (**84**, **88**, **94**, **97**, **100**, **103**, **105**) were purified using PD SpinTrapTM G-25 column removing the unreacted excess of small molecules. DAR was detected by MALDI analysis.

4.3.4 MALDI analysis of bioconjugates

Samples preparation: the matrix solutions were prepared at two different concentrations, and both were used in parallel. 20.0 mg or 25 mg of Super DHB were dissolved in a solution of MeCN (150 μ L), H₂O (350 μ L) and TFA (0.05 μ L) and deposited in a stainless-steel target placed in a termoblock set at 39 °C. When the sample was dried, 1.65 μ L of matrix solution

was added and once completely dried and crystalized, the target plate was removed from the termoblock.

The target plate was analyzed with MALDI-TOF set in linear mode at 83% of laser intensity.

The m/z range was from 30 kDa to 200 kDa.

For each sample spot, 10 shots were acquired to improve the spectra quality and mass accuracy.

SECTION B

Micellar catalysis for sustainable hydroformylation

Introduction

1.1 Green chemistry

Green chemistry is the part of chemistry interested in the development of suitable processes in the chemical industry with the aim to improve the efficiency of reactions in terms of yield, waste reduction and avoiding the use of toxic and hazardous substances. Paul Anastas and John Warner introduced the concept of Twelve Principles of Green Chemistry (Table 9). [237-240]

Table 9. Twelve Principles of Green Chemistry

1. Waste prevention	7. Use of Renewable Feedstocks
2. Atom economy	8. Shorter synthesis
3. Less hazardous/toxic materials	9. Catalysis
4. Safer products by design	10. Design for Degradation
5. Safer solvents and auxiliaries	11. Real-Time Analysis
6. Energy efficient by design	12. Inherently Safe Chemistry

Following these principles, reactions and their purifications can be improved in terms of biodegradability and safety. [241] The focus is to reduce waste by carrying out one-pot reactions with the obtainment of a final compound without intermediates purification. Another strategy is represented by performing reactions with catalytic species to decrease the reaction time and to raise the selectivity of the process. [242]

1.1.1 Atom economy and E-Factor

Atom Economy and E-Factor are used to measure the greenness of the process. [243] The Atom Economy is the result of the ratio between the molecular weight of the product and the molecular weight of all the reagents used. This is only a theoretical value that does not take note of solvents employed to carry out reactions and work-ups. The E-factor is a number that comes up from the ratio of the total mass of the waste with the mass of the product giving a total vision of the amount of overall process waste (including all the auxiliary components used also during the purification). [244] The optimal value is zero and, consequently, a high E-Factor

means that the process has a bad impact on the environment. Both industry and academia have the goal to develop new synthetic convergence routes increasing yield and reducing waste and cost of materials. [245]

1.1.2 Solvents

Solvents used in the manufacture of API are basically organic (80-90%) and represent 56% of materials employed in the total process. [246]

Solvents as benzene, petroleum ether, diethyl ether, chloroform and dichloromethane are not green and their used is restricted. Regardless of their declared toxicity and danger, they are still used because less expensive than the green solvents. There are many solvent selection guides (SSGs) encouraged by pharmaceutical companies. [247] For example, Pfizer guideline divides solvents in preferred, usable and undesirable, respectively labeled in green, orange and red. [248] ACS Green Chemistry Institute's Pharmaceutical Round Table consortium and the European collaborative research project developed an assessment known as CHEM21 that split solvents into four categories: highly hazardous, hazardous, problematic and recommended. [249]

Hazardous or highly hazardous are solvents very toxic or flammable like many hydrocarbons, chlorinated hydrocarbons, ethers and dipolar aprotic solvents such as dimethylformamide (DMF), dimethylacetamide (DMAC) and N-methyl pyrrolidone (NPM). Dimethyl sulfoxide (DMSO) is included in the problematic category in terms of stability and safety issues at high temperature. The greenest solvents are alcohols, ethyl acetate, water and other less known ones like ethyl-*tert*-butyl ether (ETBE), cyclopentyl methyl ether (CPME), *tert*-amyl-methyl ether (TAME) and dimethyl isosorbide and 2-methyl tetrahydrofuran (2-MeTHF). Solvents coming from biomasses like ethyl lactate, isobutyl acetate, diethyl succinate and γ -valerolactone (GVL) and diethyl carbonates are considered safe solvents that could be added in the recommended category. [250]

1.1.3 Catalysis

Metal hydride reagents (LiAlH_4 , NaBH_4), oxidants (KMnO_4 , MnO_2 , chromium (VI) reagents), mineral acids (H_2SO_4 , HF , H_3PO_4) and Lewis Acid (AlCl_3 , ZnCl_2 , BF_3) are the major cause of waste. Recyclable solid acids and bases in catalytic amounts are a valid alternative to inorganic salts. Atom economic catalytic reaction can be performed as alternative synthetic routes to

improve the environmental sustainability of the process. Catalytic hydrogenation, olefin metathesis, oxidation, carbonylation and hydroformylation are some examples of atom economic reactions largely used in organic synthesis especially in the pharmaceutical industry for the development of APIs. [251, 252] The best way for a green process is the use of catalysts in organic synthesis. Catalytic reactions can be divided in: homogeneous or heterogeneous catalysis and biocatalysis. In a homogeneous catalysis, the catalyst performs its function in the same phase of the reactants instead of in a heterogeneous one where the catalytic specie exists in a different phase in relation to reagents. In other words, heterogeneous catalysis takes place on the surface of the catalyst solid phase promoting the reaction between reagents in gas or liquid phases. In this way, recycle catalyst results easier. [253]

With the use of organic catalysts, a complex multistep transformation can be realized in a single step, in a shorter time and the by-products are minimized. [245]

In biocatalysis, the enzymes catalyze reactions in a very specific and efficient way thanks to their specific active sites. For this reason, biocatalysis is widely used for enantioselective synthesis especially for API. Thanks to recombinant DNA technology many different enzymes can be obtained at accessible price. [254, 255] The enzymes present economic and environmental advantages because of their biodegradability, not-toxicity, biocompatibility and their characteristics that allow to carry out reactions under mild condition at physiological pH, at room temperature using water as solvent. They are, at the same time, highly selective and the pure compound can be obtained without the necessity of using protection and deprotection steps with a reduction in waste and with the increase of the atom economy of the process. [256]

1.1.4 Use of alternative reaction medium and micellar catalysis

Organic solvents negatively influence the costs, the environmental impact and the safety of chemical processes. The quantity of solvents used to achieve the final product is bigger than other components such as raw materials and reagents. The limitations in their use depends on toxic and ignitable properties and low possibility to recycle them. [257] Water is the best candidate to overcome these issues because it is not toxic, non-inflammable, abundantly available and cheap. The handicap, in using water as solvent, concerns the lack of solubility of organic compounds in it. Many reactions have been performed in biphasic systems to achieve the solubility of reactants. [258, 259] Moreover, through an easy separation, the product can be isolated from the aqueous layer and the latter could be used for other cycles. Another alternative approach is based on the use of surfactants, compounds which decrease the surface tension

between two phases (*i.e.* liquid-liquid, gas-solid or liquid-solid phases). A generic surfactant is composed of a hydrophobic group (called tail) and by a hydrophilic group (called head) which give it an amphiphilic behavior. A surfactant can be used in small amount in water where the hydrophobic effect leads to the formation of spontaneous aggregates called micelles once the surfactant critical micellar concentration is exceeded. The lipophilic tails orient themselves inside the aggregates (core), while the heads are exposed to the aqueous media resulting in a hydrophilic surface disposed towards the aqueous environment. As a consequence, the insoluble organic compounds tend to stay in the core of micelles that act as nanoreactors in which the reaction takes place in high concentrations. These nanoreactors allow an increase of the organic compounds' solubility in water and represents the physical place where reactions are carried out. The nano-micelles are usually formed by an aggregation of 50-100 monomers that are in thermodynamic equilibrium to their monomer free form. The nature of the aggregate depends on the balance between hydrophilic and hydrophobic portions, the molecule's geometry and the reaction conditions used (temperature, pH and inorganic salts). [260–264]

There are different kinds of surfactants: anionic, cationic, non-ionic, gemini and zwitterionic types. For a positive outcome, the choice of surfactant results a crucial aspect. In the last decade, new surfactants were designed to improve their properties as dispersing agents giving a wider list of surfactants suitable for different reactions. Based on Triton X-100 and Brij-35 a new generation of surfactants called “designer” are developed in order to extend the nanoreactor properties of micelles. The suitable development of a catalytic system with low environmental impact, in presence of surfactants, permits to perform green reactions in a simple and economic way. [265]

The commercial anionic and cationic amphiphiles like sodium dodecyl sulfate (SDS) or cetrimonium bromide (CITAB) are charged and could react as ligands or nucleophiles leading to side reactions. Non-ionic surfactants are exploited to overcome this issue and to improve their universal versatility. [261]

The fundamental property to take into consideration is the hydrophilic-lipophilic balance (HBL), the ratio of the hydrophilic to the lipophilic parts of surfactant that define its affinity with aqueous phase or organic layer. This parameter influences the size of micelles and their ability to solubilize the organic molecules. Regarding non-ionic surfactants, the HBL is in the range between 0 and 20. $HBL > 10$ means that amphiphiles have more affinity to water, while values of $HBL > 10$ are typical of lipophilic surfactants. [266]

Lipshutz and co-workers [266–268] developed novel generations of non-ionic surfactants starting from polyoxyethanyl- α -tocopherol sebacate (PTS) composed of racemic vitamin E as

the apolar portion, sebacic acid as linker, and PEG-600 (Figure 73) or PEG-1000 as hydrophilic portion. Generally, organometallic compounds are quite soluble in water and this represents a valid chance to exploit cross-coupling reactions *via* micellar catalysis. PTS-600 was used to carried out Heck coupling and ring closing metathesis with non-water-soluble substrates at room temperature without using cosolvents. [269-270]

In order to find a cheaper alternative to the PTS, and to expand the variety of surfactants with different HBLs and sizes of the micelles forming, polyoxyethanyl- α -tocopherol succinate (TPGS-750-M) was designed as green surfactant (Figure 72). It is formed of α -tocopherol as lipophilic moiety, a cheaper succinic linker and a hydrophilic poly(ethyleneglycol)methyl ether chain (PEG-750-M). PTS-600 and PTS-1000 form particles spheres-shaped measuring in diameter 7 μ m or 25 μ m respectively, while micelles composed of TPGS-750 M measure 53 nm in diameter (measures determined by dynamic light scattering - DLS). Long PEG chains, that for example feature PTS-1000, have shown a size reduction of nanoparticles giving final different shapes. Moreover, TPGS has more lipophilic affinity than PTS surfactants, in fact, $HBL_{TPGS}=13$ and $HBL_{PTS}=10$. [266]

Recently, SPGS-550-M called “Nok”⁷⁹ was developed based on β -sitosterol methoxypolyethylene glycol succinate structure (Figure 73). [266-268]

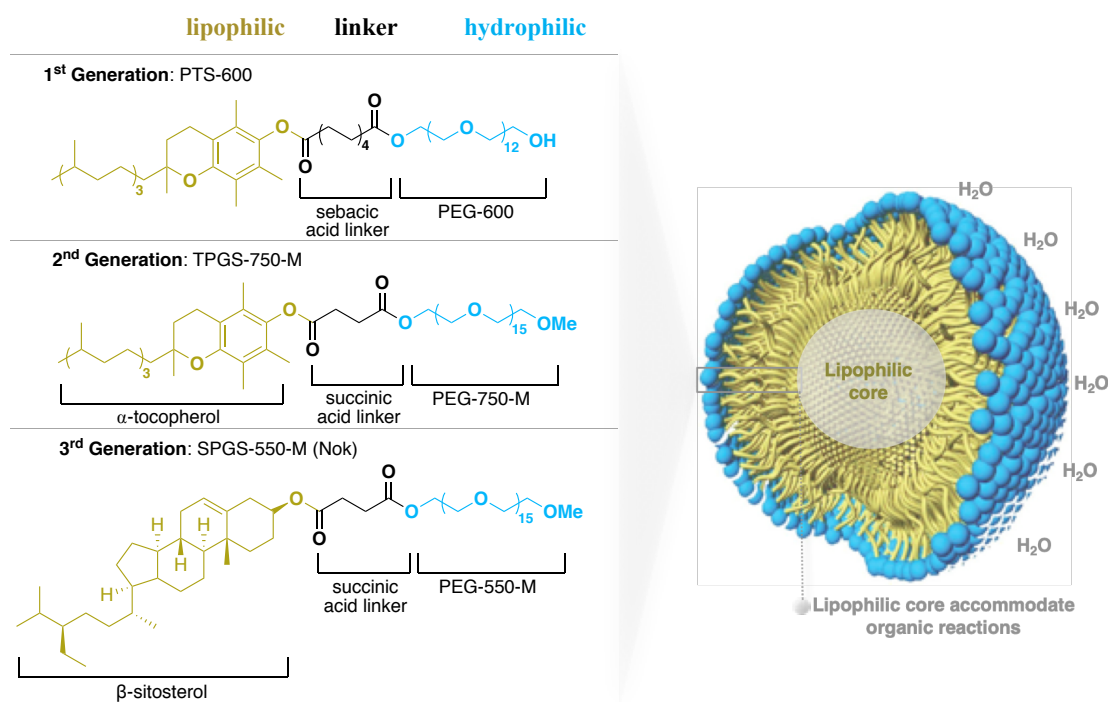


Figure 73. Non-ionic surfactants.

These new surfactants are used mainly for a variety of transformations performed under mild conditions in water, in particular cross coupling reactions. The product could be obtained from micellar catalysis by an extraction with a small quantity of organic solvent (*i.e.* ethyl acetate) or by precipitation because of their insolubility in water. [271]

Among the cross-couplings possible there are some reactions as Heck, [269] Suzuki-Miyaura, [263, 272-274] Sonogashira and Buchwald-Hartwig amination. [275-277] Other reactions [278-286] such as metathesis, click, and amidation process are also reported.

Considering the promising results obtained in cross-couplings reported in literature, surfactants like TPGS-750M could be used for the development of a green hydroformylation process.

1.2 Hydroformylation

Hydroformylation reaction is one of the most useful catalytic processes for the preparation of aldehydes by addition of hydrogen (H_2) and carbon monoxide (CO) to double bonds. [287-289] The corresponding higher homologous aldehydes achieved with this process are very versatile and reactive functional groups used as intermediates for further transformations. Alcohols, amines or condensation final products can be synthesized by using domino and tandem protocols. [288] The oxo process, as called by Otto Roelen [287], is the most applied catalytic atom-economic process used in industries for the synthesis of API [290], fragrances (*i.e.* linalool, β -citronellene) and detergents. [291]

This homogeneous catalytic transformation can be mediated by different transition metals (*i.e.* Co [287, 292, 293], Ru [294], Pt [295], Fe [296], and Rh [297] in presence of specific ligands that define the regio-and the chemoselectivity of the process. [288, 298, 299]

If the alkene is symmetrical, only one aldehyde is the product, otherwise, more isomers can be obtained. Double bond hydrogenation and isomerization usually are the main side reactions at HF conditions. [300] To overcome the fast double bond isomerization and a lack of regioselectivity in the addition of -CHO, strong conditions are required: high pressures (10-100 bar) of H_2 and CO mixtures (syngas) in different ratios (*i.e.* 1:1, 2:1, 4:1) in stainless steel autoclaves, long reaction times (1-4 days), high temperatures (80-200 °C), and not eco-friendly solvents like toluene or THF. [287-289, 301-303] In other words, the addition of CO/ H_2 to the double bond must be faster than the isomerization or hydrogenation *phenomena* (Figure 74).

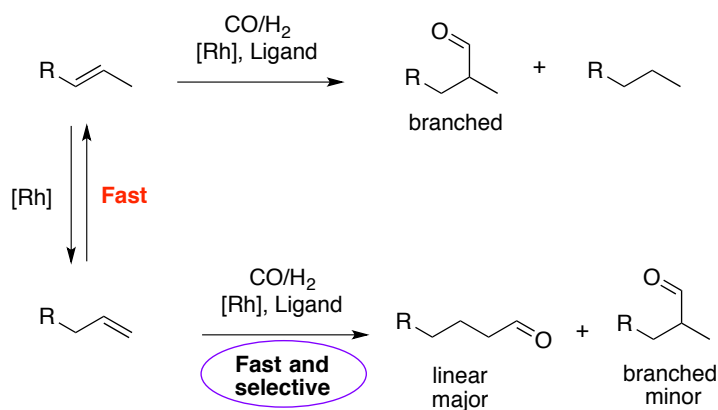


Figure 74. Hydroformylation and side reactions.

The hydroformylation mechanism was proposed by Heck using $Co(CO)_4H$ as catalyst. He identified the first reaction step: high pressure and temperatures gave the coordination of olefin with the active catalyst that led to alkyl-complex **II**. The following addition of CO to the activated complex and its insertion on the metal provided the intermediate **IV** that after an oxidative insertion of H_2 (**VI**) achieved the transfer of two hydrides from metal to the acyl carbon. Aldehyde was then obtained by reductive elimination, while the catalyst was regenerated (Figure 75). [304]

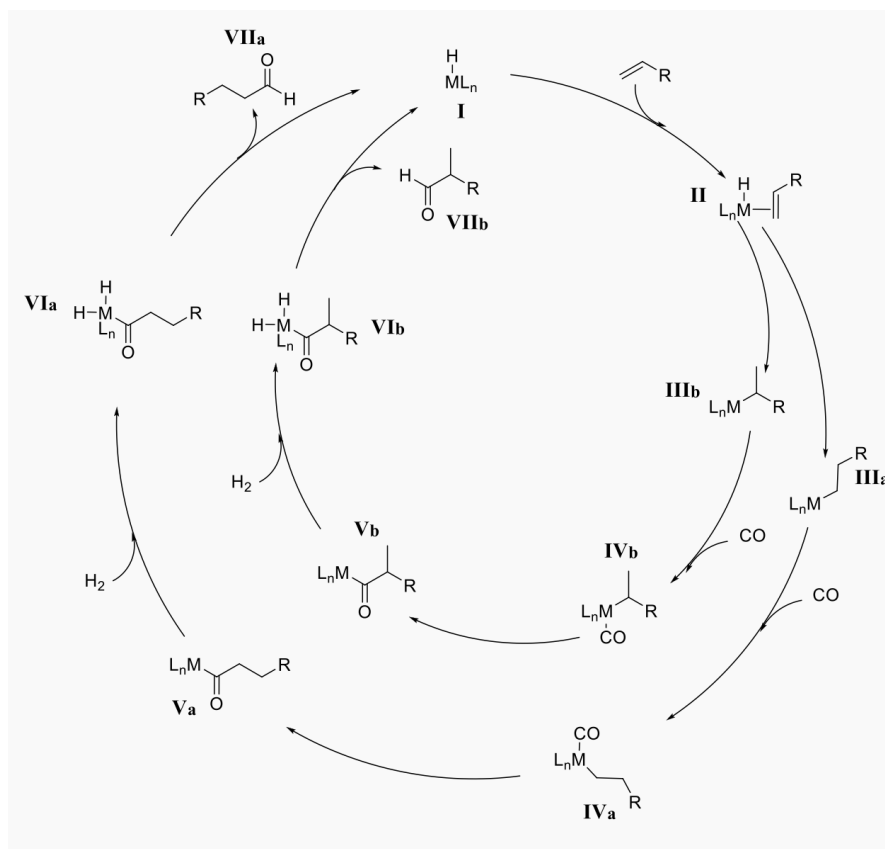


Figure 75. Hydroformylation mechanism.

The process aforementioned produced both linear and branched aldehydes. Pacenti et al. performed a study with marked alkenes affirming that the formation of linear or branched products is due to the rearrangement of the complex **II** and not to the isomerization of starting material double bond. With the purpose to increase the regioselectivity toward the linear aldehyde, ligands (*i.e.* Xantphos, Biphephos) were introduced and studied. The basicity and the steric hindrance of these compounds influence and promote the formation of the linear isomer instead of the branched one. [305]

Our attention is focused on Rh catalysts that are well-known to improve the reaction outcomes. An important turning point was given by Wilkinson who discovered chloridotris(triphenylphosphine)rhodium(I) catalyst $[\text{RhCl}(\text{PPh}_3)_3]$ also called Wilkinson's catalyst. Thanks to this species, hydroformylation was conducted at temperatures between 55 °C and 100 °C with pressure ranges of 20-100 bar and reaction times of hours order. [301]

$[\text{RhCl}(\text{PPh}_3)_3]$ is a precursor of the active species $[\text{RhH}(\text{CO})(\text{PPh}_3)_3]$ which is formed in situ. Wilkinson's catalyst is an air sensitive compound difficult to handle. $[\text{Rh}(\text{CO})(\text{PPh}_3)_3]$ has a better stability profile and provide a faster active ligand-complex formation. [301] The $[\text{Rh}(\text{CO})(\text{PPh}_3)_3]$ is the most successful catalyst adopted in the oxo process.

An important breakthrough to Rh-catalyzed hydroformylation was the introduction of bidentate phosphine ligands based on Xantene structure (Figure 76). Ligands give more stability to the catalyst and in particular to the complex **II** (Figure 75) thanks to electronic interactions with its metal center. [306] Landis et al. explored, with a modeling study, the influence of Xantphos on the regioselectivity in favor of linear aldehydes. The calculations developed provided data that are fully in agreement with the experimental results. In presence of Xantphos both short-chain alkenes and other many complex were hydroformylated by providing predominantly the higher homologous aldehyde linear type. [306]

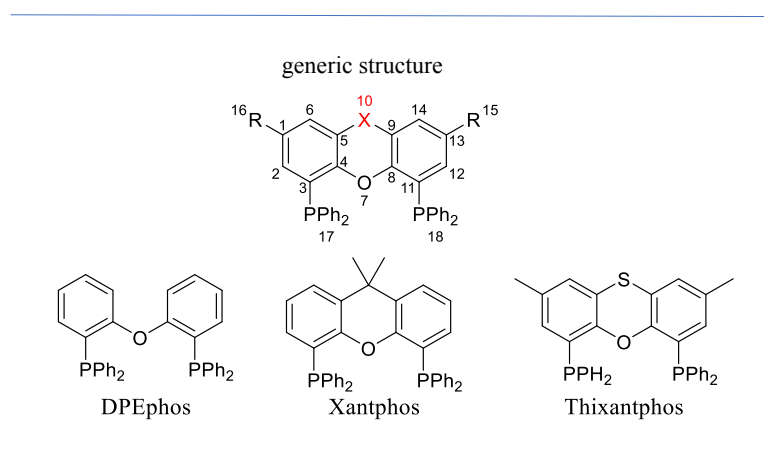


Figure 76. Generic structure and bidentate phosphine ligands.

Other ligands like Biphephos and 6-DPPon and DPEPhos are largely used in hydroformylation and thanks to their applications, problems related to catalyst degradation or reorganization into Rh monomeric cluster, are solved. [307]

As stated previously, classic hydroformylation requires long reaction times (1-4 days), high temperatures (80-200 °C), not properly eco -friendly solvents, and high pressures of syngas (10-100 bar) that need specific and hazardous equipment like stainless steel autoclaves stored in specific rooms. [287-289, 301-303]

Since several years, the interest of the research group, in which I worked, is focused on the development of processes for terminal alkenes hydroformylation in mild and more ecofriendly conditions, at low pressure of syngas, including taking advantages of microwave (MW) irradiation. [308-309] Discover microwave oven, equipped with the 80 mL vial, was adapted for reaction under pressure. The 80 mL glass vial, tested for resisting up to 250 psi (17 bar), has a connection to an external pressure controlling system equipped with a valve and an exit tube for venting the vial at the end of the reaction. If the valve is closed, the vial is under pressure (registered by the system), whereas when the valve is open, the vial is in open vessel. The exit tube is connected to a cylinder containing the mixture CO/H₂ 1:1 (syngas) through a three-way connector equipped with two taps (Figure 77). Syngas was introduced in the tube until the internal pressure reached 40 psi (the pressure was registered in real time by the computer connected to the Discover device). Tap A (Figure 77) was closed, and the vial irradiated at 150 W of power. [308]

In this way, hydroformylation of alkenes can be carried out in few minutes (4 minutes) under microwave heating at low pressure (40 psi) using the commercially available catalyst

[Rh(CO)(PPh₃)₃] and ligand Xantphos with high conversion into the corresponding aldehyde without isomerized alkene as byproduct. At the end, the vial was cooled to room temperature, and the taps A and C were opened to release outside the gas contained in the vial. [308]

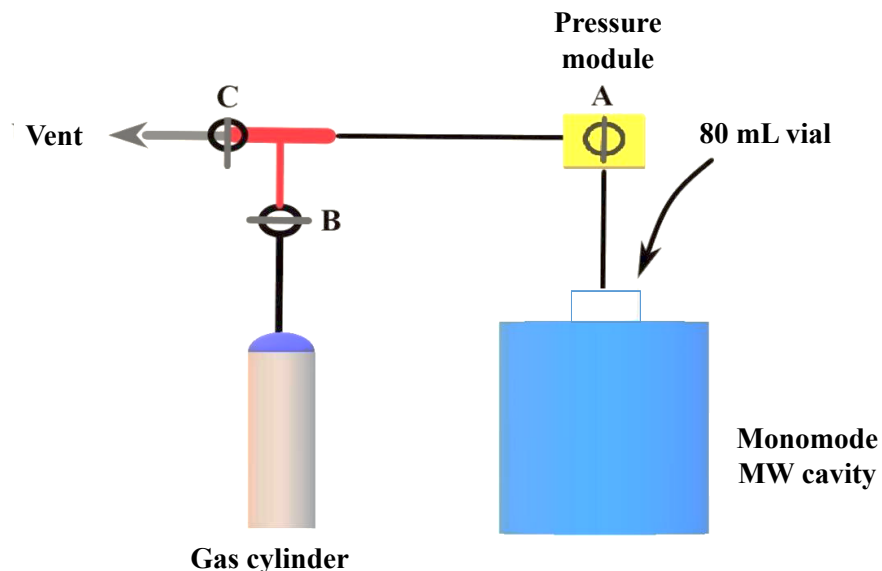


Figure 77. Schematic representation of a Discover Microwave Oven to carry out MW-Assisted Hydroformylation.

Another approach to make this reaction eco-friendlier, reducing the use of hazardous or problematic solvents, is the use of water as safe and non-toxic solvent in presence of surfactants in biphasic system or in micellar catalysis.

The first example of hydroformylation in biphasic olefin/water system was reported in 1975 in the patented OXEA process taking advantage of the water soluble trisulfonated triphenylphosphine ligand (TPPTS). [310-311]

Johnson Matthey patented the use of cationic surfactants based on sulfonated phosphine ligands suitable for hydroformylation processes. [312]

A recent study reports an efficient protocol applied also in industry mediated by surfactants in three phases microemulsions systems that still involved the use of non-sustainable solvents (*i.e.* toluene, 1,4-dioxane). [313-315]

The micellar catalytic hydroformylation conditions still suffer from low yields (30-73%), [316-317] use of expensive ligands (*i.e.* SulfoXantphos 260 €/g vs. Xantphos 45 €/g), [316-318] tailor-made surfactants not suite for standardizing a process, and high pressures of syngas (15-100 bar).

In some cases, the process is not green because the extraction and the column chromatography, used to purify the aldehydes, require high quantities of toxic solvents (*i.e.* Et₂O), without catalyst recover leading to a negative impact in the E-Factor. [319]

Since the 80's, the attention has been paid to catalysts and conditions for aqueous (or aqueous/organic biphasic) hydroformylation but there is still a need for new approaches that bind high aldehyde selectivity to cheap and eco-sustainable process characterized by simple purification, high catalyst stability, cheap ligands and green solvents. [320]

1.3 Microwave assisted reactions

The research on technologies to facilitate a synthetic transformation promoting an impact on both efficiency and sustainability of the process is still ongoing. Flow reactors with their fast heating and mass transferring properties represent an efficient alternative to batch reactors. [321] The microwave (MW) dielectric heating is one of the most efficient methods for heating up a reaction reducing energy consumption.

In the last thirty years microwave assisted organic synthesis (MAOS) has been receiving interest from chemists in order to accelerate organic chemical transformations. At the beginning, between 1980s and 1990s the utilization was less common and a lack of knowledge led to issues in terms of reproducibility and controllability of different parameters (temperature and pressure). Other problems encountered were related to the flammability of organic solvents. For the early experiments in MAOS, no suitably equipped domestic kitchen microwave ovens were used in chemical laboratories. Explosions and lack of reproducibility occurred because of the absence of a proper technology. Year after year, innovative instruments were built. The use of microwave frequency resulted advantageous due to the possibility to reduce reaction times and the by-products with an increase of the yields. MW heating has been applied for the heterocycle's synthesis, in homogeneous transition-metal catalysis and in medicinal chemistry. [309]

Microwave heating is based on the use of electromagnetic waves in a range from 1 cm to 1 m and of frequencies between 0.3 and 300 GHz. All microwaves operate at a frequency of 2.45 GHz (12.24 cm corresponding value of wavelength) which permits not to have interference with other frequencies. The energy corresponding to the microwave photon is not high enough to break chemical bond. On the other hand, solvents and reagents are able to convert the absorbed microwave energy into heat, that is fundamental for breaking bonds. [322, 323]

Each material has dielectric properties. The factor $\tan \delta$, called loss tangent, measures the capacity of each substances to convert electromagnetic energy into heat at a certain temperature and frequency. Solvents have been subdivided as high, medium and low microwave absorbing with the $\tan \delta$ respectively of > 0.5 , $0.1-0.5$ and <0.1 . Only compounds that have a low $\tan \delta$ could be used (Table 10). There are different processes such as absorption, transmission and reflection which characterize the interaction between the microwave irradiation and the material. Polar organic solvents, like ethylene glycol, cause a high absorption of microwaves with consequently rapid heating of the medium, while non-polar microwave transparent materials, like hexane, create small interactions with the microwaves with poor performance (Table 10). In many cases, small amounts of ions (as ionic liquids) can be used as polar additives to increase the capacity of heating the mixture. [324-326]

Solvent	$\tan \delta$	Solvent	$\tan \delta$
ethylene glycol	1.350	DMF	0.161
ethanol	0.941	1,2-dichloroethane	0.127
DMSO	0.825	water	0.123
2-propanol	0.799	chlorobenzene	0.101
formic acid	0.722	chloroform	0.091
methanol	0.659	acetonitrile	0.062
nitrobenzene	0.589	ethyl acetate	0.059
1-butanol	0.571	acetone	0.054
2-butanol	0.447	tetrahydrofuran	0.047
1,2-dichlorobenzene	0.280	dichloromethane	0.042
NMP	0.275	toluene	0.040
acetic acid	0.174	hexane	0.020

Table 10. Loss factors ($\tan \delta$) of different solvents at 2.45 GHz, 20 °C. [327]

The conventional heating usually requires an external heat source by using oil-bath to perform reactions. The energy transfers to the mixture depends on convection currents and thermal conductivity of the used solvents and reagents. During the traditional heating, the temperature of the reaction vessel results higher than the temperature inside the reaction mixture. On the other hand, an efficient homogeneous internal heating is produced using the microwave where the microwave energy is directly transferred to the molecules that take part to the reaction

(Figure 78). As a consequence, in MW assisted reactions the temperature increases in the whole volume at the same time. [324-326]

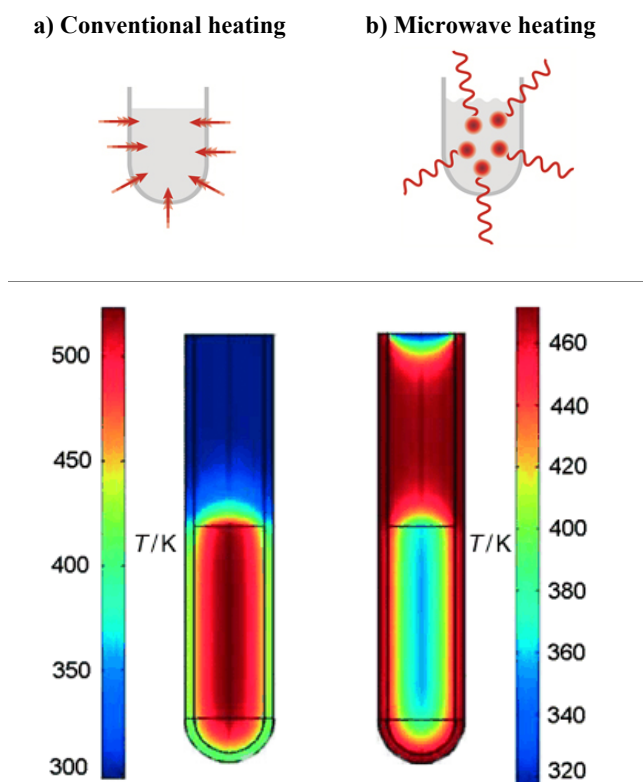


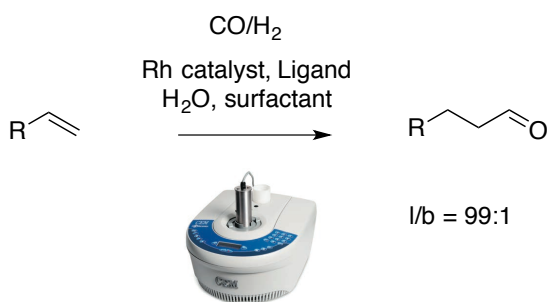
Figure 78. **a)** Conventional heating: in the oil-heated tube, the reaction mixture in contact with vessel wall is heated first. **b)** with microwave irradiation, the temperature raises up in all the volume at the same time. [325]

1.4 Aim of this research work

Hydroformylation reaction is one of the most useful atom-economic catalytic process. Double bond hydrogenation and isomerization are the main side reactions. [300] To overcome these issues and a lack of regioselectivity in the addition of -CHO, strong non-ecofriendly conditions are required: high pressures (10-100 bar) of syngas in stainless steel autoclaves, long reaction times (1-4 days) and high temperatures (80-200 °C). In almost of HF protocols, the catalyst recycle is not evaluated and the poor regioselectivity of some conditions requires column chromatography purification impacting in the sustainability of the process. Moreover, the presence of non-sustainable solvents (*i.e.* toluene) do not still give the possibility to define the process as green at all.

As said in the paragraph 1.2, since several years, the interest of the research group, where I worked, has been focused on the development of processes for terminal alkenes hydroformylation in mild and more ecofriendly conditions, at low pressure of syngas, including taking advantages of microwave (MW) irradiation. [308-309] However, the main limitation of this protocol is still represented by the use of toluene as solvent, in diluted conditions (*i.e.* 0.1M), unsuitable for industrial applications. To overcome these limitations, we figured that micellar catalysis could represent a valid option for our purposes. [261, 264, 267, 328-330]

The aim of this work is the examination and optimization of a sustainable and generally applicable protocol for the regioselective hydroformylation of terminal alkenes, using cheap commercially available catalysts (*i.e.* $[\text{Rh}(\text{CO})(\text{PPh}_3)_3]$) and ligands (*i.e.* Xantphos), in mild reaction conditions (Scheme 22). The process can take advantages from both micellar catalysis and microwave irradiation to obtain the linear aldehydes as the major product (Scheme 22). Intramolecular hemiacetalization, large scale conditions and catalyst recycle have also been investigated to demonstrate the compatibility with a variety of functional groups, the applicability on industry and the sustainability of the process further corroborated by compounds purification thanks to a particular derivatization of -CHO group.



Scheme 22.

Results and discussion

2.1 Optimization of reaction conditions

Allylbenzene (**106**) was selected as the model substrate for the optimization of HF process. The reaction conditions under MW irradiation already developed in toluene were tested changing the solvent. [308] **106** was suspended in TPGS-750-M (5 wt%) plus H₂O and irradiated in presence of a 1:1 CO/H₂ mixture (9 bar), [Rh(CO)H(PPh₃)₃] (2 mol%), Xantphos (Rh/L 1:4) at 110 °C for 10 min obtaining the corresponding aldehyde with a 53% conversion with a good regioselectivity (Figure 79). Starting from Pogrzeba and co-workers' studies, [39] NaCl (1 mol%) was added to obtain better performances in term of catalyst stability and reaction yields. Not great changes were observed, and the expected products **107a-b** were obtained in a 50% conversion with a good 9:1 regioselectivity towards liner aldehyde **107a** (Figure 79). Even the use of different salts such as MgBr or CsF had a low impact on both conversions and regioselectivities probably caused by the use of a non-ionic surfactant in the reaction medium. [320]

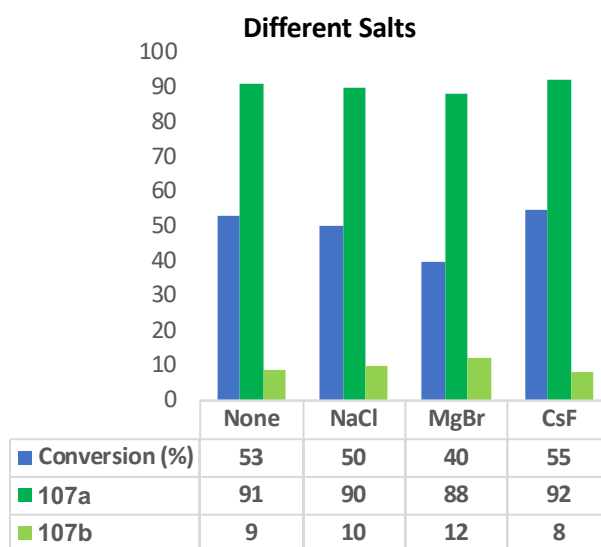
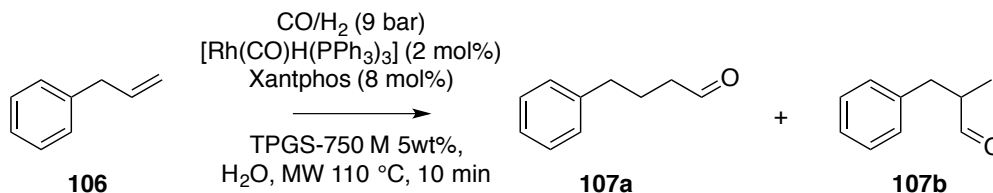


Figure 79. **106** (0.75 mmol), 1-dodecanal (internal standard, 0.075mmol), [Rh(CO)H(PPh₃)₃] (0.015 mmol), Xantphos (0.06 mmol), salt (0.0075 mmol), TPGS-750-M 5wt% in H₂O (3 mL), MW 110 °C, 10 min. Conversions are determined by GC/MS (%) as reported in experimental part.

Irradiation using $[\text{Rh}(\text{CO})\text{H}(\text{PPh}_3)_3]$ as catalyst at different temperatures in presence of different ligands (Figure 80a) were tested and higher temperatures increased the reduction and the isomerization of the starting material **106**, together with the reduction of aldehyde **107** into the corresponding alcohol.

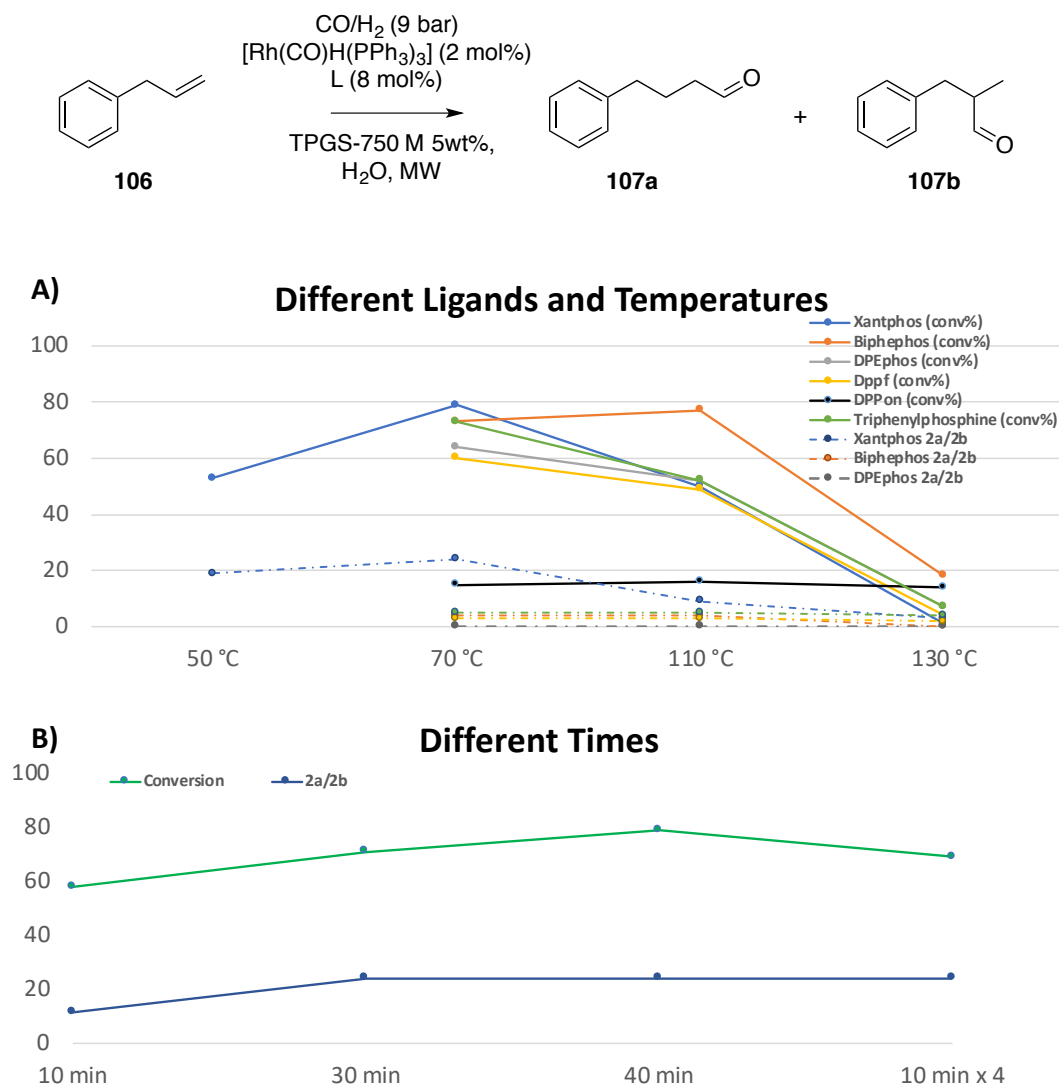


Figure 80. a) **106** (0.75 mmol), 1-dodecanal (internal standard, 0.075mmol), $[\text{Rh}(\text{CO})\text{H}(\text{PPh}_3)_3]$ (0.015 mmol), L (0.06 mmol), TPGS-750M 5wt% in H_2O (3 mL), MW (max power 300 Watt), 10 min. Conversion determined by GC/MS (%) as report in experimental part. **b)** **106** (0.75 mmol), 1-dodecanal (internal standard, 0.075mmol), $[\text{Rh}(\text{CO})\text{H}(\text{PPh}_3)_3]$ (0.015 mmol), Xantphos (0.06 mmol), TPGS-750M (5wt%) in H_2O (3 mL), MW (max power 300 Watt), 70 °C. Conversion determined by GC/MS (%) as reported in experimental part.

Different ligands (*i.e.* Biphephos, DPEphos, Dppf, 6- DPPon) were tested and surprisingly, dropping the temperature at 70 °C, the best results were achieved with Xantphos. Therefore, the optimized reaction conditions were applied with longer reaction times. An improvement of

both conversion and regioselectivity was obtained after 40 minutes of MW irradiation (Figure 80b).

It is interesting to note that the conversions are directly proportional to the logP of the different ligands used, 6-DPPon (logP = 3.51) being the worst and Xantphos (logP = 10.39) the best one. Irradiating at 70 °C, shortening reaction times (40 minutes) or repeating 4 cycles of irradiation for 10 min. each, negatively impacted the conversion (Figure 80b). A reduction of heating has been possible thanks to the particular combination of the MW effect on the triphasic micellar catalysis system: a gas- liquid-solid dispersion. We can probably associate the lower conversions observed at high temperatures (> 70 °C) to the minor interface area related to a lower down in droplet size responsible for a difficult mass transfer into the micelles. [39] At the end, the best conditions observed for these transformations were: irradiation for 40 minutes at 70 °C in presence of [Rh(CO)H(PPh₃)₃], and Xantphos at 9 bar of a mixture CO/H₂ 1:1.

The impact of MW irradiation on the reaction outcome was investigated by using a fixed power irradiation at 300 Watt (maximum temperature settled 70 °C) and further optimizations were tried in presence of the most powerful ligand (Xantphos), thus obtaining a full conversion (>99%) and high regioselectivity (**107a/107b** 96:4). The lowering down of the amount of catalyst from 2 to 1 mol% (Entries 1-2, Figure 81) and of TPGS-750M to 2.5 wt% (Entry 3, Figure 81) had no impact on conversion. The addition of sustainable co-solvents such as 2Me-THF worsened the reaction rate (Entry 4, Figure 81) as well as a change in the catalyst to ligand ratio from 1:4 to 1:8 (Entry 6, Table 81). Different catalysts like RhCl(cod)₂ and Rh(CO)₂acac (Entries 7-8, Figure 81) and ionic surfactants as SDS and CITAB (Entries 9-10, Figure 81) were tested, with not improvements observed. It is interesting to note that the structure of the surfactant directly impacts both on yield and regioselectivity, therefore demonstrating its active role in the reaction. This is further confirmed by the absence of any aldehyde while performing the transformation just in water without any surfactant (Entry 11, Figure 81). Blank tests were also carried out to demonstrate the catalyst, the surfactant and the syngas roles in this reaction conditions (Entries 10-12, Figure 81).

The best conditions (> 99% conv.; **107a/107b** 96:4) were obtained irradiated allybenzene **106** for 40 min at 70 °C, with Rh(CO)H(PPh₃)₃ 1mol% as catalyst in a ratio Cat/L 1:4 in presence of TPGS-750M wt 2.5% as surfactant (Entry 3 highlighted in violet, Figure 81).

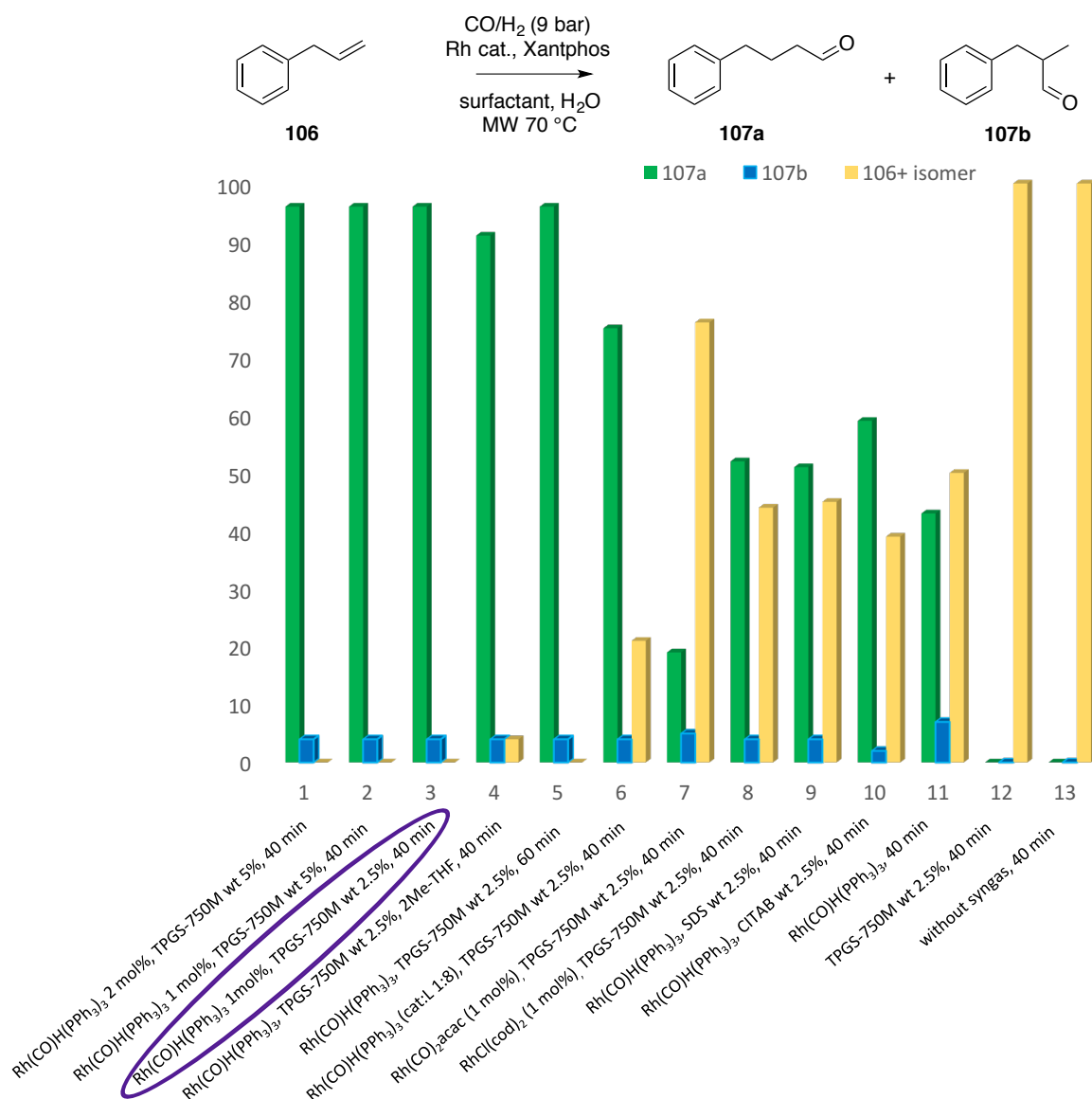


Figure 81. **106** (0.75 mmol), 1-dodecanal (internal standard, 0.075 mmol), Rh cat and Xantphos at different mol% and ratio, different surfactants with different amount in H₂O (3 mL), MW dielectric heating at 70 °C with fixed power irradiation at 300 Watt, cooling while heating (max T 70 °C). Conversion determined by GC/MS.

2.2 Evaluation of reaction conditions for a future application in industrial scale

In order to evaluate the sustainability of the overall process, by using the best reaction conditions (Entry 3, Figure 81) in presence of allylbenzene 0.25 M, reactions involving in larger scale at different concentrations of **106** (0.50, 0.75 and 1 M) were performed (Figure 82). Up to 0.50 M, a decrease of both conversion and regioselectivity were observed highlighting the influence of starting material concentration on the reaction outcome. Higher concentrations (0.75 mmol/mL or 1.00 mmol/mL) of **106** had an impact on both yield and selectivity because, probably, a part of the starting olefin is not able to enter into the already saturated micelles, thus

being subjected to both reduction and double bond isomerization. However, even by working at 1 mmol/mL, the results obtained were better if compared to other protocols already reported in the literature for the same products. [331] Despite the increase of by-products, **107a**/**107b** ratio is still very high without extreme pressure of CO/H₂ (9 bar) that positively influence the formation of linear aldehyde instead of the branched one.

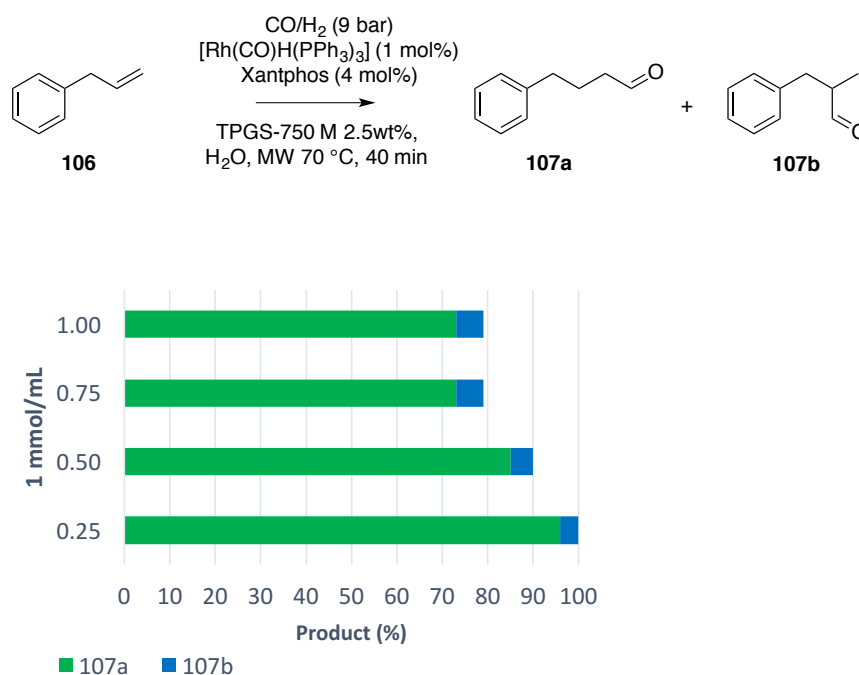


Figure 82. How concentration influences reaction yield.

2.3 Expedient of bisulfite adduct and catalyst and micelles recycle

The linear aldehyde **107a** was recovered after extraction with AcOEt and column chromatography, in 90% isolated yields (**107b** was isolated in 1% yield).

With the aim to reduce the use of organic solvents and recycle the catalyst and the ligand making greener the overall process, the reaction (Entry 3, Figure 81) was repeated by adding 1.5 eq. of NaHSO₃ in the reaction mixture (Figure 83).

EXPEDIENT OF ALDEHYDE BISULFITE ADDUCTS

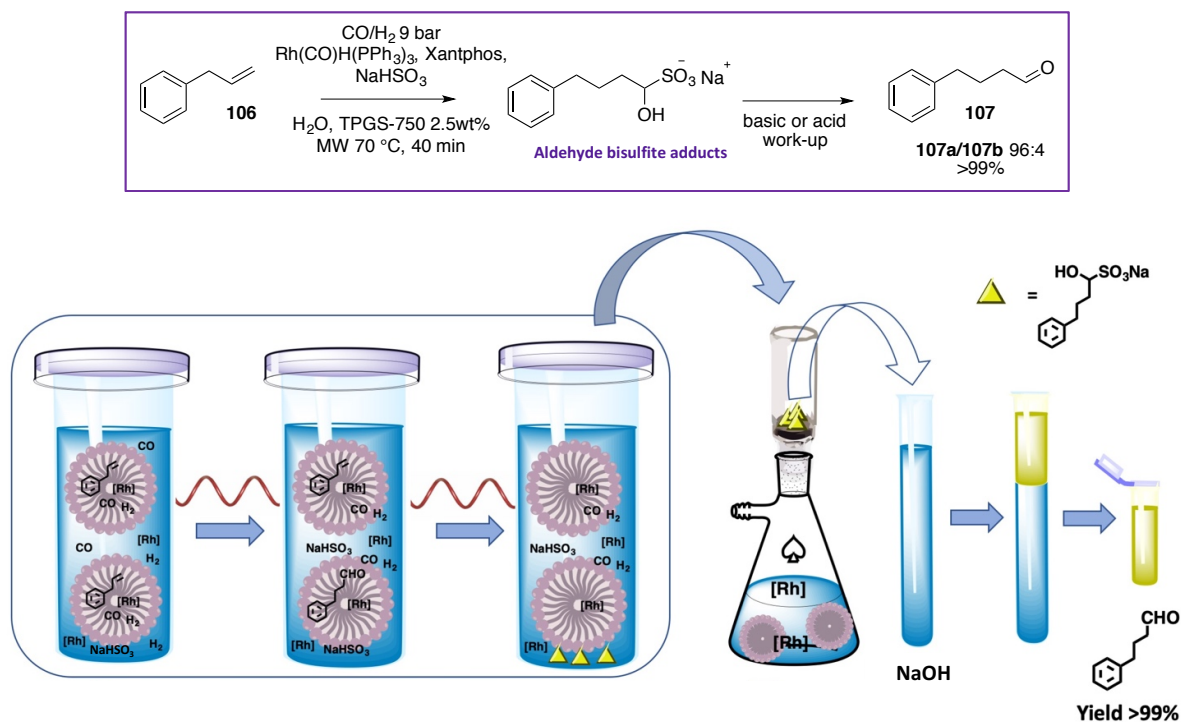


Figure 83. Expedient of aldehyde derivatization into Bertagnini's salt to purify the products in an easy and eco-friendly way.

In these conditions, aldehydes **107a/b** was directly obtained after microwave irradiation as the corresponding Bertagnini's salt (aldehyde bisulfite adducts) [332] that precipitates in micellar suspension (Figure 83). The reaction mixture was filtered and the Bertagnini's salt treated with 1 equivalent of NaOH 10 M, with a full recovery of **107** as an oil in >99% isolated yields by centrifugation and decantation (Figures 83 and 84). The possible catalyst recycle was evaluated by adding NaHSO_3 and allylbenzene **106** to the micellar phase recovered after filtration and exposing that suspension to MW irradiation at 70 °C, for 40 minutes in the presence of syngas (9 bar). The conversion into **107** was complete (>99%) and the process has been repeated for further 3 times without almost any impact in reaction yields, demonstrating a full recyclability of the catalyst (Figure 84). Expedient of aldehyde derivatization into Bertagnini's salt, in order to purify products, is an easy and eco-friendly way to avoid the use of chromatography with a fine recycle of catalyst, ligand, water and surfactant.

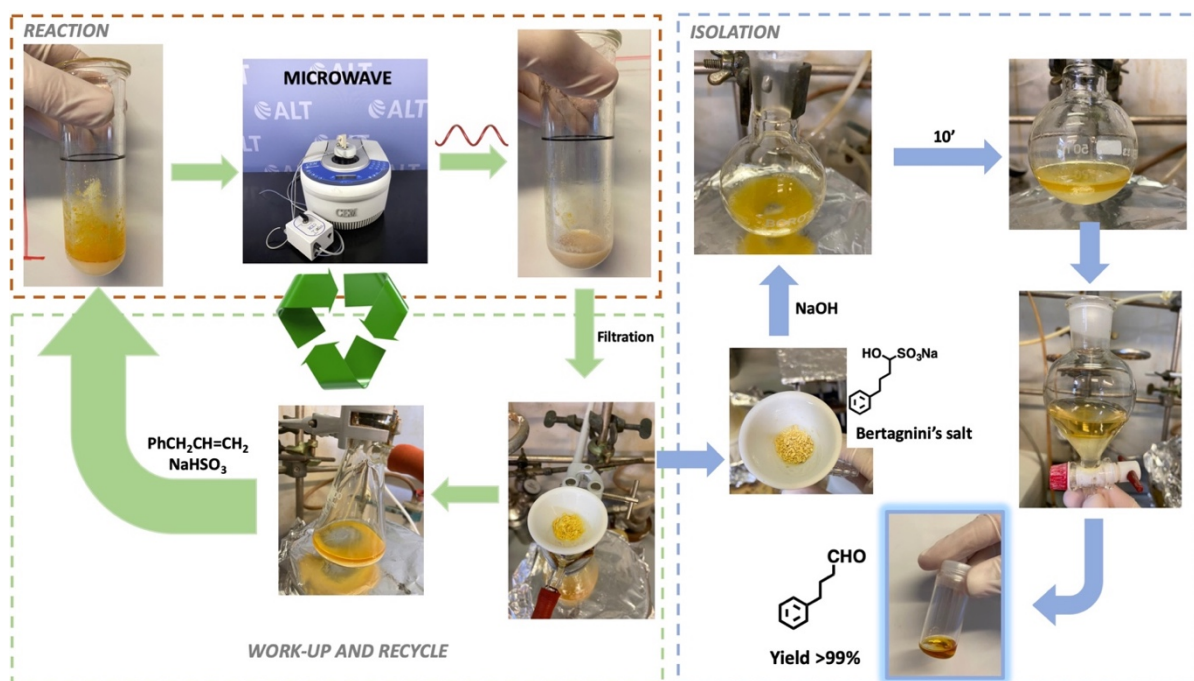


Figure 84. Catalyst and micelles recycle, work-up and purification.

2.4 TON, TOF and DLS, Z-potential and TEM analysis

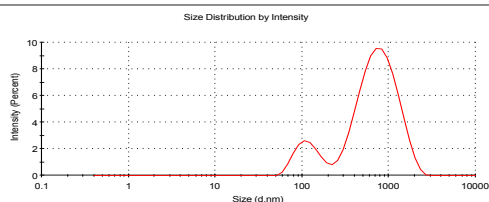
The TON for a single reaction cycle is 99.1 while the TOF at 70% of conversion is 280 h^{-1} . The E-Factor for a single cycle performed with 1-octene is only 1.08, a comparable value with ones suitable for the scale-up of industrial HF transformation reported in literature. [316-318]

Further investigation concerning micellar structure by DLS and Z-potential analysis were performed in order to have a clear characterization of micelles after MW irradiation and the catalyst recycling process. The data about the micellar suspension at the first and fourth cycle were recorded before and after the MW irradiation. A high homogeneity in micellar size and a high Z- potential value were found indicating an overall micellar stabilization (Figure 85a-e).

A. H₂O – TPGS-750M 2.5% wt

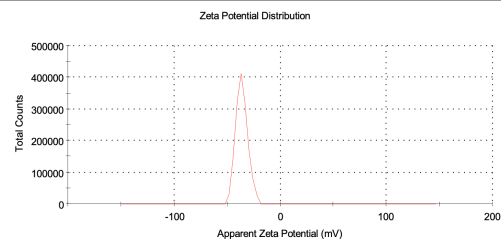
	Size (d.n...)	% Intensity:	St Dev (d.n...
Z-Average (d.nm): 436,8	Peak 1: 827,7	84,7	402,6
Pdl: 0,385	Peak 2: 121,8	15,3	40,33
Intercept: 0,812	Peak 3: 0,000	0,0	0,000

Result quality **Refer to quality report**



	Mean (mV)	Area (%)	St Dev (mV)
Zeta Potential (mV): -36,2	Peak 1: -36,2	100,0	5,51
Zeta Deviation (mV): 5,51	Peak 2: 0,00	0,0	0,00
Conductivity (mS/cm): 0,0454	Peak 3: 0,00	0,0	0,00

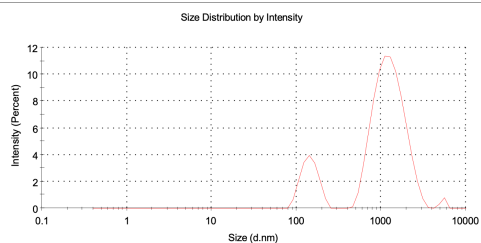
Result quality **Good**



B. H₂O – TPGS-750M 2.5% wt after MW irradiation (70 °C)

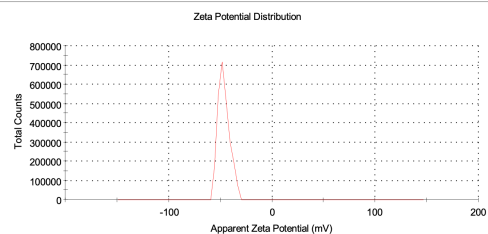
	Size (d.n...)	% Intensity:	St Dev (d.n...
Z-Average (d.nm): 666,9	Peak 1: 1316	82,7	525,1
Pdl: 0,530	Peak 2: 145,4	16,2	31,78
Intercept: 0,846	Peak 3: 5350	1,1	339,6

Result quality **Refer to quality report**



	Mean (mV)	Area (%)	St Dev (mV)
Zeta Potential (mV): -46,5	Peak 1: -46,5	100,0	5,49
Zeta Deviation (mV): 5,49	Peak 2: 0,00	0,0	0,00
Conductivity (mS/cm): 0,0111	Peak 3: 0,00	0,0	0,00

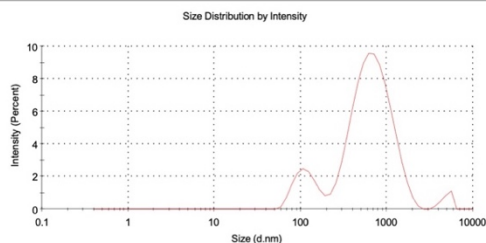
Result quality **Good**



C. Reaction mixture before irradiation

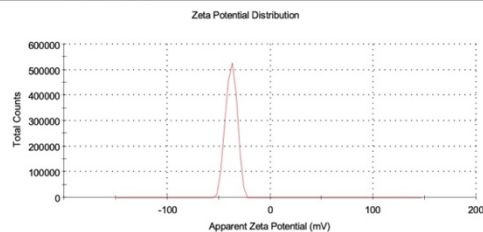
	Size (d.n...)	% Intensity:	St Dev (d.n...
Z-Average (d.nm): 423,3	Peak 1: 736,7	84,5	365,6
Pdl: 0,507	Peak 2: 116,2	13,0	33,00
Intercept: 0,767	Peak 3: 4933	2,5	638,6

Result quality **Good**



	Mean (mV)	Area (%)	St Dev (mV)
Zeta Potential (mV): -37,6	Peak 1: -37,6	100,0	5,33
Zeta Deviation (mV): 5,33	Peak 2: 0,00	0,0	0,00
Conductivity (mS/cm): 0,00804	Peak 3: 0,00	0,0	0,00

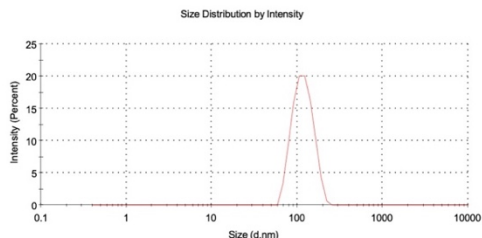
Result quality **Good**



D. Reaction mixture after irradiation at 70 °C

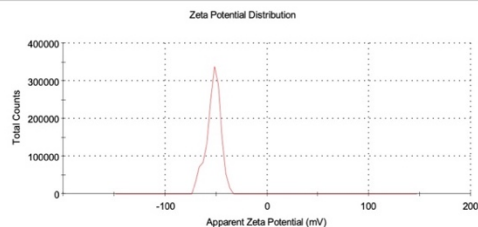
	Size (d.n...)	% Intensity:	St Dev (d.n...
Z-Average (d.nm): 111,4	Peak 1: 119,0	100,0	31,11
Pdl: 0,035	Peak 2: 0,000	0,0	0,000
Intercept: 0,668	Peak 3: 0,000	0,0	0,000

Result quality **Good**



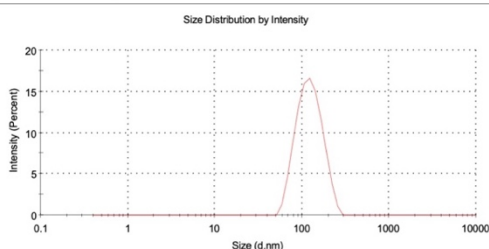
	Mean (mV)	Area (%)	St Dev (mV)
Zeta Potential (mV): -52,4	Peak 1: -52,4	100,0	6,98
Zeta Deviation (mV): 6,98	Peak 2: 0,00	0,0	0,00
Conductivity (mS/cm): 0,0173	Peak 3: 0,00	0,0	0,00

Result quality **Good**

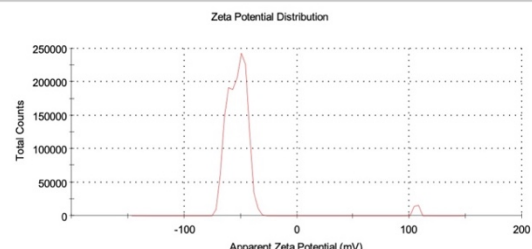


E. Reaction mixture after recycling 3 times

	Size (d.n.m)	% Intensity	St Dev (d.n.m)
Z-Average (d.nm): 113,4	Peak 1: 126,4	100,0	41,01
Pdi: 0,099	Peak 2: 0,000	0,0	0,000
Intercept: 0,663	Peak 3: 0,000	0,0	0,000
Result quality Good			

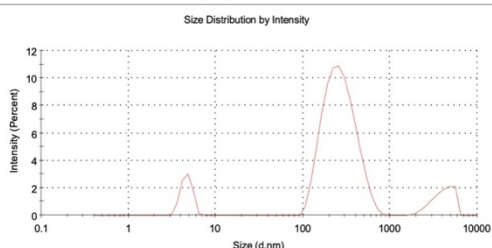


	Mean (mV)	Area (%)	St Dev (mV)
Zeta Potential (mV): -49,7	Peak 1: -49,0	62,2	5,45
Zeta Deviation (mV): 23,9	Peak 2: -61,0	36,0	3,89
Conductivity (mS/cm): 0,0134	Peak 3: 106	1,8	1,87
Result quality Good			



F. Reaction mixture after irradiation at 120 °C

	Size (d.n.m)	% Intensity	St Dev (d.n.m)
Z-Average (d.nm): 134,2	Peak 1: 278,9	81,3	117,5
Pdi: 1,000	Peak 2: 4107	10,4	1044
Intercept: 0,543	Peak 3: 4,699	8,3	0,6568
Result quality Refer to quality report			



	Mean (mV)	Area (%)	St Dev (mV)
Zeta Potential (mV): -24,5	Peak 1: -29,6	59,1	4,63
Zeta Deviation (mV): 7,89	Peak 2: -16,8	40,9	3,63
Conductivity (mS/cm): 0,0400	Peak 3: 0,00	0,0	0,00
Result quality Good			

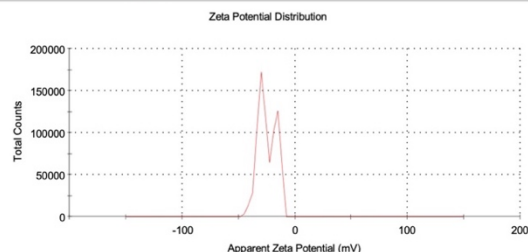


Figure 85. Dynamic light scattering (DLS) data (left) and Zeta-Potenzial (right) of: **A)** H₂O, TPGS-750M 2.5%wt; **B)** H₂O, TPGS-750M 2.5%wt after MW irradiation at 70 °C for 40 min; **C)** reaction mixture before irradiation: **106** (0.75 mmol), Rh(CO)H(PPh₃)₃ (0.015 mmol), Xantphos (0.06 mmol), TPGS-750M (2.5wt%) in H₂O (3 mL); **D)** reaction mixture after MW dielectric heating at 70 °C with fixed power irradiation at 300 Watt, cooling while heating (max T = 70 °C) for 40 min; **E)** reaction mixture after recycling micellar phase for 3 times. **F)** reaction mixture after MW dielectric heating at 120 °C for 40 min.

TEM analysis of the reaction mixture after irradiation at 70 °C shows a multi-micelle structure according to the data in the literature for traditional heating. [333] This structure is maintained for all of the 4 cycles of catalyst recycle (Figure 86 B and C).

As reported before (Figure 80a), irradiating at higher temperatures (> 90 °C) the reaction yields decreased. As we can see in Figures 85e and 86d, at high heating (*i.e.* 120 °C) there is a destabilization of micelles with nanoparticles formation. Rh nanoparticles are detrimental for the outcome of HF reaction carried out in water and surfactants, and for this reason there is a loss system efficiency at temperature > 100 °C.

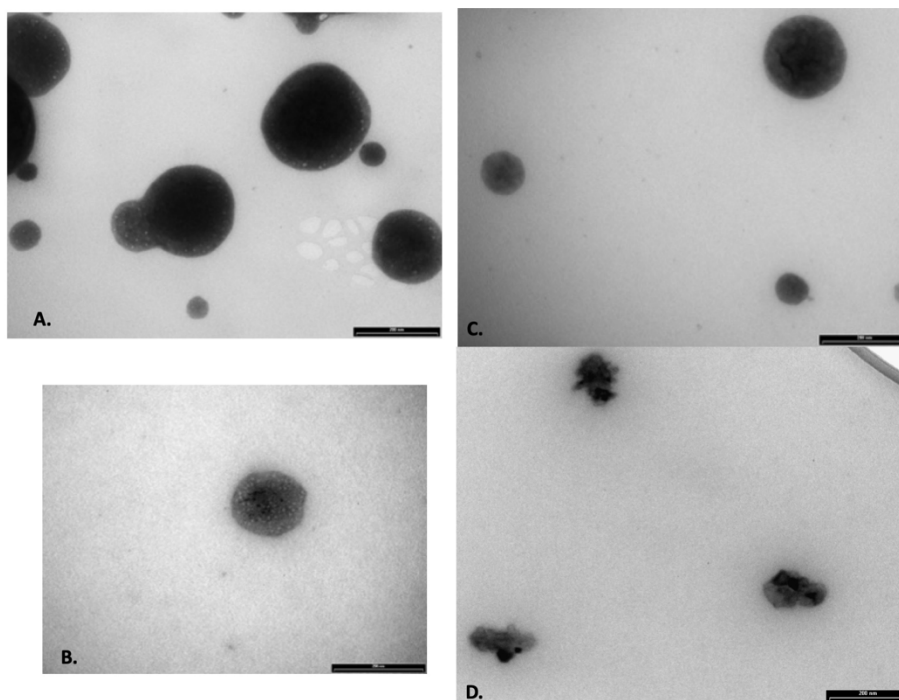


Figure 86. TEM analysis of: **A)** reaction mixture before irradiation: **106** (0.75 mmol), Rh(CO)H(PPh₃)₃ (0.015 mmol), Xantphos (0.06 mmol), TPGS-750-M 2.5 wt% in H₂O (3 mL); **B)** reaction mixture after MW dielectric heating at 70 °C with fixed power irradiation at 300 Watt, cooling while heating (max T 70 °C) for 40 min; **C)** reaction mixture after recycling micellar phase for 3 times; **D)** reaction mixture after MW dielectric heating at 120 °C for 40 min. The TEM images are 200 x 200 nm.

2.5 Scope of reaction

Therefore, the reaction versatility, by using different terminal alkenes as substrates, was explored (Figure 87) in order to demonstrate that these MW assisted hydroformylation conditions can be applied in presence of different functional groups like ester, amide, acetal, ether.

Starting from 1-octene, nonanal **109** was isolated in 95% yield confirming the versatility of this process for producing long chain olefins very used and synthesized in industry. (Figure 87) The reaction was performed with different terminal alkenes even in the presence of reduction-sensitive functional groups such as nitrile (**110**), benzyl ether (**120**), and internal double bond (**128**, Scheme 23) as a confirm of its high chemoselective property. Amides **120-124** were synthesized with different yields and regioselectivities depending on the substituents on the aromatic ring. Electron withdrawing groups brought a negative impact on reaction yields as reported for the not obtained product **123** (Figure 87).

The outcome of a reaction sets in presence of water and micelles depends on the hydrophobicity of the starting material as demonstrated with the two silyloxy derivatives **113** and **114** (Figure 87).

As expected, styrene furnished the branched aldehyde **119** as the major reaction product in good yields (Figure 87).

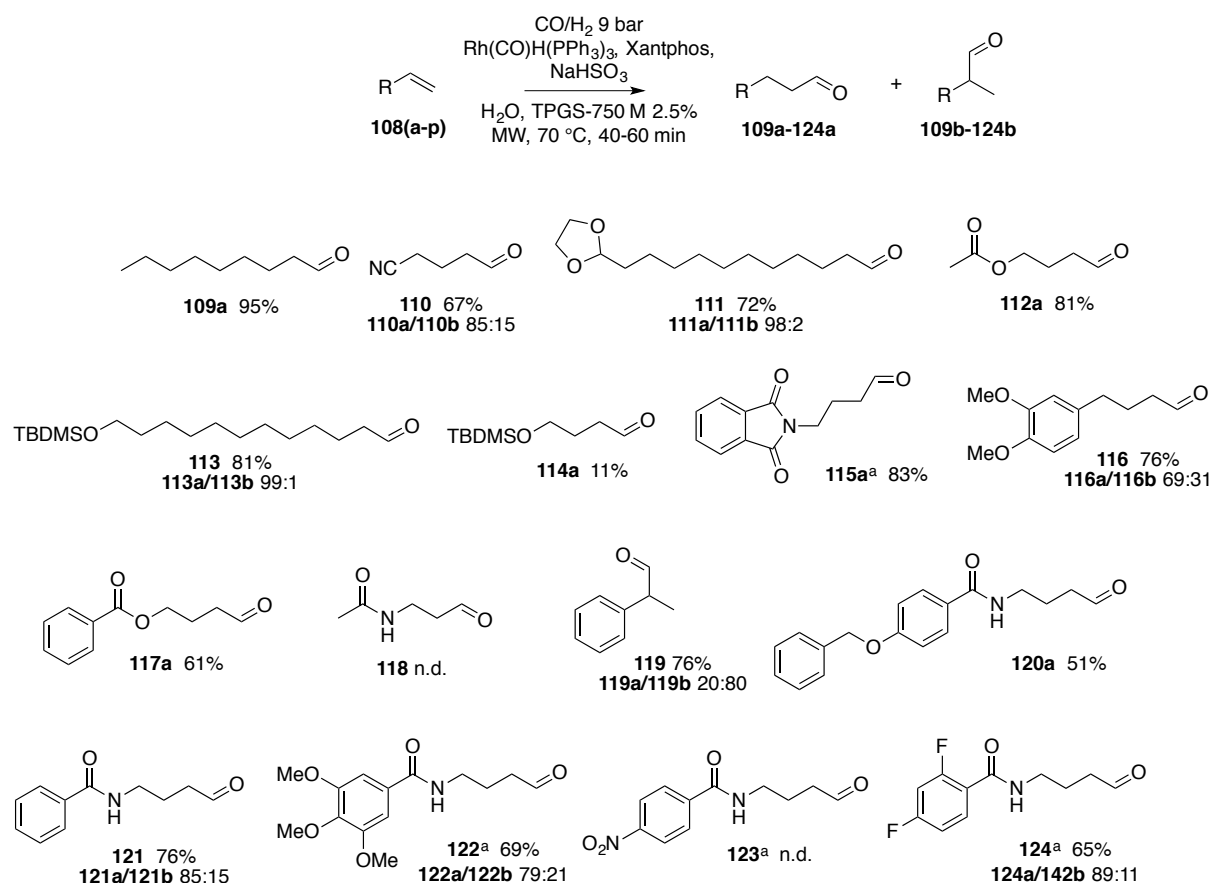
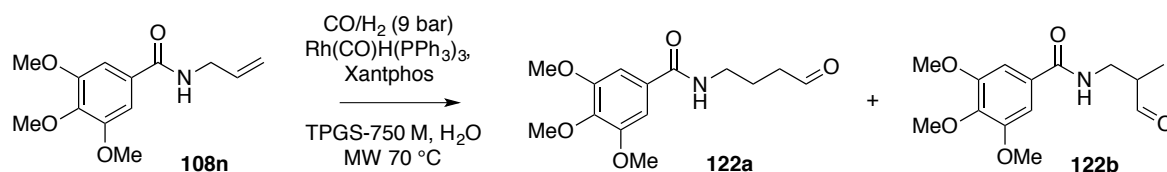


Figure 87. Alkene (1.5 mmol), $\text{Rh(CO)H(PPh}_3)_3$ (1 mol%, 0.015 mmol), Xantphos (4 mol%, 0.03 mmol), NaHSO_3 (1.72 mmol), TPGS-750-M 2.5 wt% in H_2O (3 mL), CO/H_2 (9 bar), MW dielectric heating at 70 °C with fixed power irradiation at 300 Watt, cooling while heating (max T 70 °C) for 40 min. [a] Alkene (1.5 mmol), $\text{Rh(CO)H(PPh}_3)_3$ (2 mol%, 0.03 mmol), Xantphos (8 mol%, 0.12 mmol), NaHSO_3 (1.72 mmol), TPGS-750-M 2.5 wt% in H_2O (3 mL), CO/H_2 (9 bar), MW dielectric heating at 70 °C with fixed power irradiation at 300 Watt, cooling while heating (max T 70 °C) for 60 min.

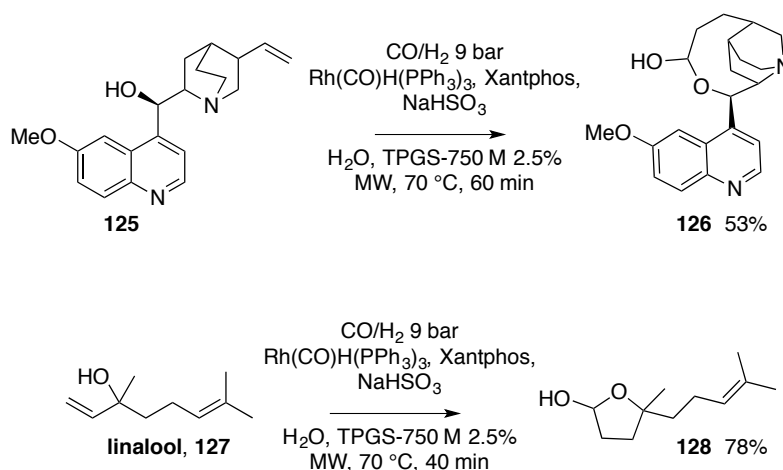
The micellar catalyzed processes reported in the literature are usually performed with liquid starting materials or solid water-soluble substrates. [261, 264, 267, 328-330, 333, 336] The most difficult compounds to be hydroformylated in water were the solid alkenes. The amide **108n** was detected as system model and some experiments were performed with it changing the amount of catalyst and the surfactant (Table 11). It is possible to obtain linear aldehydes in good yields even starting from solid alkenes by using 2 mol% of the catalyst instead of 1 % with only 2.5 wt% of TPGS-750M as surfactant (Entry 4, Table 11). These reaction conditions were applied with all the solid terminal alkenes and the products **115**, **122**, **124** in Figure 87 and compound **126** in Scheme 23 were achieved with good results.



Entry	Conditions	Conv. %	121a/121b
1	TPGS-750M 5wt%, Rh cat. 1 mol%, 40 min	-	-
2	TPGS-750M 5wt%, Rh cat. 2 mol%, 40 min	50	75:25
3	TPGS-750M 2.5wt%, Rh cat. 2 mol%, 40 min	80	75:25
4	TPGS-750M 2.5wt%, Rh cat. 2 mol%, 60 min	> 99	89:21

Table 11.

Starting from quinoline **125** containing a hydroxyl-group, instead of obtain the usual corresponding aldehyde, a 9 terms cyclic hemiacetal was directly isolated in 53% yield with a full regioselectivity (Scheme 23). The same result was achieved starting from linalool **127**, the 5 terms ring was directly formed in 78% isolated yield from the cyclization of linear aldehyde as unique product (Scheme 23).

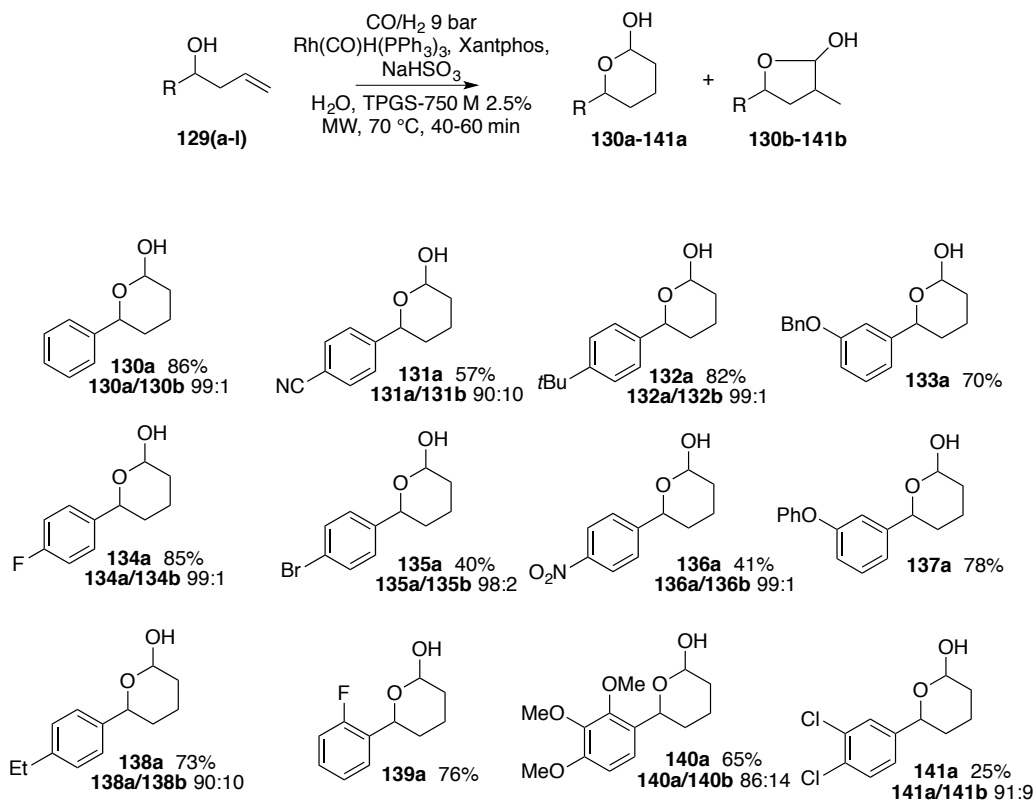


Scheme 23.

2.6 Tandem reaction with intramolecular hemiacetalization

Starting from these interesting transformations, the possibility to obtain cyclic hemiacetals by hydroformylating alkenes containing alcohol moieties in β position was investigated (Scheme 24). With the same high chemoselectivity, as already established for the aldehydes derivatives, hemiacetals were obtained in acceptable yields. Especially in these compounds always

characterized by an aromatic ring, it was possible to appreciate how the presence of electron-donating moieties positively influenced the reaction yields instead of the presence of electron-withdrawing groups (Scheme 24).



Scheme 24.

Conclusions

A fully sustainable and generally applicable protocol for the regioselective hydroformylation of terminal alkenes, using cheap commercially available catalysts and ligands, in mild reaction conditions has been optimized. Low pressure of syngas (9 bar), low temperature (70 °C), for an hydroformylation transformation, in 40 minutes are sufficient to obtain a chemo- and regioselective process which take advantages from both micellar catalysis and microwave irradiation. The linear aldehydes have been obtained as the major or only regioisomers in good to high yields. The optimized protocol is compatible with different functional groups (*i.e.* amides, nitrile, nitro, ester, etc.) and can be used in tandem with intramolecular hemiacetalization for the synthesis of 5 or 6 member cyclic hemiacetals starting from β hydroxy group containing starting alkenes. The reaction is efficient even in large scale and the catalyst and micellar water phase can be reused at least 3 times without any impact in regioselectivity and in reaction yields. The efficiency and sustainability of this protocol is strictly related to the *in situ* transformation of the aldehyde into the corresponding Bertagnini's salt that precipitates in the reaction mixture avoiding organic solvent mediated purification steps to obtain the final aldehydes as pure compounds. [337]

This work demonstrates how efficient can be the coupling of micellar catalysis with microwave irradiation for the development of sustainable hydroformylation protocols with general applicability. Micelles appear to be stable and more homogenous in term of size distribution after irradiation. [337] The process can be easily applied in laboratory scale by using commercial microwaves hoping to find future applications in industrial scale.

Experimental part

4.1 General experimental procedures, materials and instruments

All reagents were used as purchased from commercial suppliers (*i.e.* Merck for surfactant and ligand, TCI for Rh catalysts) without further purification.

Flash column chromatography was performed with Merck silica gel Å 60, 0.040-0.063 mm (230-400 mesh).

Merck aluminum backed plates pre-coated with silica gel 60 (UV254) were used for analytical thin layer chromatography and were visualized by staining with a solution *p*-Anisaldehyde in EtOH or a KMnO₄ solution.

NMR spectra were recorded at 25 °C with 400 or 600 MHz for ¹H and 101 or 151 MHz for ¹³C Brüker Avance NMR spectrometers. Splitting patterns are designated as s, singlet; d, doublet; t, triplet; q, quartet; m, multiplet; bs, broad singlet. Chemical shifts (δ) are given in ppm relative to the resonance of their respective residual solvent peaks.

GC/MS analysis were collected with GC/MS spectrometer Varian Saturn 2000 with ion trap detector and equipped with 30 m OV-101 capillary column, splitting injector at 240 °C. Methods for GC analysis: A) 40 °C - 3 min, 40-200 °C 10 °C/min – 17 min, 200-240 °C 20 °C/min–5min; B) 40 °C-3min, 40-200 °C 10 °C/min–1 min, 200-240 °C 20 °C/min – 8 min, 240-280 °C 20 °C/min, 8 min.

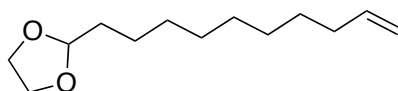
Reactions carried out under MW dielectric heating were performed with a modified Discover microwave oven equipped with the 80 mL vial for reaction under pressure. [21]

Scanning transmission electron microscopy (STEM) and Energy- dispersive X-ray spectroscopy (EDS) analysis was done using a FIB/SEM TESCAN GAIA 3 installed at the Microscopy Center (Ce.me.) at ICCOM- CNR (Florence). DLS, Z-potential measurements were done using a Zetasizer NanoZS90 instrument (Malvern, Worcestershire, UK).

4.2 Synthetic procedures

4.2.1 Preparation of not commercially available starting alkenes

2-(Dec-9-en-1-yl)-1,3-dioxolane (108c)

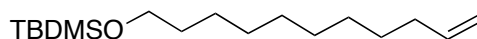


10-undecenal (2.38 mL, 12.0 mmol) was dissolved in anhydrous ethylene glycol (136 mL, 2436.0 mmol) and a catalytic amount of *p*TSA (193 mg, 1.02 mmol) in 40 mL of anhydrous toluene was added. The resulting mixture was heated to reflux for 1 h. The mixture was extracted with CH₂Cl₂ (3 x 50 mL), and the organic layer was evaporated after drying with anhydrous Na₂SO₄ furnishing the protected aldehyde (2.06 g, 9.72 mmol, 81% yield). **GC-MS** (*m/z*): 212; *R*_t = 16.563 (Method A). **¹H NMR** (600 MHz, CDCl₃) δ 5.83 – 5.68 (m, 1H), 4.95 (d, *J* = 17.1 Hz, 1H), 4.89 (d, *J* = 10.0 Hz, 1H), 4.80 (t, *J* = 4.5 Hz, 1H), 3.98 – 3.87 (m, 2H), 3.85 – 3.77 (m, 2H), 2.00 (q, *J* = 6.5 Hz, 2H), 1.66 – 1.59 (m, 2H), 1.41 – 1.22 (m, 12H). **¹³C NMR** (151 MHz, CDCl₃) δ 139.1, 114.1, 104.7, 64.8, 33.9, 33.7, 29.5, 29.5, 29.3, 29.1, 28.9, 24.0.

General procedure of alcohols silylation

Imidazole (1.16 g, 16.97 mmol) and TBDMSCl (2.56 g, 16.97 mmol) were added to a solution of the desired alcohol (11.31 mmol) in dry CH₂Cl₂ (35 mL) at 0 °C. Stirring was continued at r.t. for 4 h. H₂O (20 mL) was added and the organic layer was washed with NaClss (20 mL) and concentrated after drying with anhydrous Na₂SO₂. The crude was purified by column chromatography on silica gel (20% EtOAc in petroleum ether) to provide the title compound as a colorless liquid.

tert-Butyldimethyl(undec-10-en-1-yloxy)silane (108e)



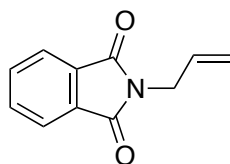
Obtained 2.09 g, 7.35 mmol, 65% yield. **GC-MS** (*m/z*): 284; *R*_t = 17.876 min (Method A). **¹H NMR** (600 MHz, CDCl₃): δ 5.81 (ddt, *J* = 17.1, 10.2, 6.8 Hz, 1H), 5.03-4.98 (m, 1H), 4.95-4.91 (m, 1H), 3.59 (t, *J* = 6.7 Hz, 2H), 2.10-2.02 (m, 2H), 1.57-1.48 (m, 2H), 1.41-1.36 (m, 2H), 1.33-1.23 (m, 10H), 0.09 (s, 9H), 0.05 (s, 6H). **¹³C NMR** (151 MHz, CDCl₃): δ 139.2, 114.2, 63.3, 33.8, 32.8, 29.5, 29.4, 29.2, 28.9, 26.0, 25.8, 18.4, 5.3.

(Allyloxy)(*tert*-butyl)dimethylsilane (108f)



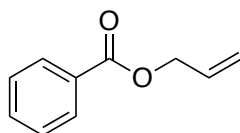
Obtained 1.60 g, 9.27 mmol, 82% yield. **GC-MS** (m/z): 172; R_t = 10.465 min (Method A). **^1H NMR** (400 MHz, CDCl_3) δ 6.08-5.74 (m, 1H), 5.25 (d, J = 17.0 Hz, 1H), 5.05 (d, J = 9.0 Hz, 1H), 4.32-4.01 (m, 2H), 0.92 (s, 9H), 0.20 (s, 6H). **^{13}C NMR** (101 MHz, CDCl_3) δ 137.5, 113.9, 64.1, 25.9, 18.4, 5.3.

2-Allylisoindoline-1,3-dione (108g)



To a solution of phthalimide (1.5 g, 10.2 mmol) in DMF (10 mL) were added K_2CO_3 (1.41 g, 10.2 mmol) and allyl bromide (882 μL , 10.2 mmol). After the solution was stirred for 16 h at r.t., Et_2O (30 mL) was added to the reaction mixture, and this latter was then washed with NaClss (3 x 15 mL). The organic layer was evaporated under reduced pressure after drying with anhydrous Na_2SO_4 to provide the desired compound (1.66 g, 8.87 mmol, 87% yield). **GC-MS** (m/z): 187; R_t = 16.697 (Method A). **^1H NMR** (600 MHz, CDCl_3) δ 7.86 (dd, J = 5.3, 3.1 Hz, 2H), 7.72 (dd, J = 5.3, 3.1 Hz, 2H), 5.95 – 5.81 (m, 1H), 5.25 (dd, J = 17.0, 0.9 Hz, 1H), 5.20 (d, J = 10.2 Hz, 1H), 4.30 (d, J = 5.7 Hz, 2H). **^{13}C NMR** (151 MHz, CDCl_3) δ 167.9, 134.0, 132.1, 131.5, 123.3, 117.8, 40.1.

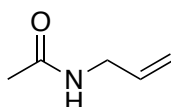
Allyl benzoate (108i)



In a dry round bottom flask charged with benzoic acid (1.50 g, 12.30 mmol) and dry CH_2Cl_2 (40 mL) allyl alcohol (557 μL , 8.2 mmol) and DMAP (100 mg, 0.82 mmol) were added. The solution was cooled to 0 $^\circ\text{C}$ and stirred for 15 min. before the addition of DCC (3.4 g, 16.4 mmol). The reaction was stirred at r.t. for 16 h under N_2 . The mixture was filtered, concentrated *in vacuo*, and the crude was purified by flash chromatography on silica gel (20% EtOAc in

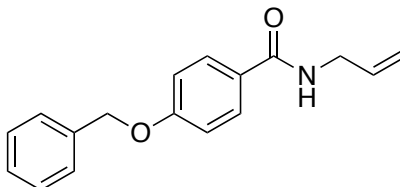
petroleum ether) giving a clear product as a colorless oil (708 mg, 4.35 mmol, 53% yield). **GC-MS** (m/z): 163; R_t = 12.670 min (Method A). **^1H NMR** (400 MHz, CDCl_3): δ 8.04 (d, J = 8.0 Hz, 2H), 7.52 (t, J = 7.3 Hz, 1H), 7.41 (t, J = 7.2 Hz, 2H), 6.02 (ddt, J = 16.3, 10.7, 5.4 Hz, 1H), 5.32 (dd, J = 50.5, 14.1 Hz, 2H), 4.80 (d, J = 5.4 Hz, 2H). **^{13}C NMR** (151 MHz, CDCl_3): δ 166.3, 133.1, 132.2, 130.1, 129.7, 128.5, 118.3, 65.6.

***N*-Allylacetamide (108j)**



Allylamine (2.63 mL, 35.0 mmol) was dissolved in dry CH_2Cl_2 (50 mL) followed by the addition of Et_3N (7.30 mL, 52.5 mmol) and dropwise addition of acetyl chloride (2.75 mL, 38.5 mmol) at 0°C . After stirring for 16 hours at r.t. 30 mL of H_2O were added to the reaction. The organic phase was separated and the aqueous layer was extracted with CH_2Cl_2 (3 x 50 mL). The resulting organic layer was dried over anhydrous Na_2SO_4 and concentrated. The product was purified by silica gel flash chromatography using a mixture of EtOAc/PE (5:95) as the eluent (1.90 g, 19.25 mmol, 55% yield). **GC-MS** (m/z): 99; R_t = 7.812 min (Method A). **^1H NMR** (400 MHz, CDCl_3): δ = 5.81 (ddt, J = 17.0, 10.2, 5.8 Hz, 1H), 5.16 (q, J = 17.0 Hz, 1H), 5.10 (q, J = 10.1 Hz, 1H), 3.84 (tt, J = 5.7, 1.5 Hz, 2H), 1.99 (s, 3H). **^{13}C NMR** (101 MHz, CDCl_3): δ = 170.1, 134.3, 116.3, 42.2, 23.6.

***N*-allyl-4-(benzyloxy)benzamide (108l)**



Dry K_2CO_3 (15 g, 110.0 mmol) was added to a solution of 4-hydroxybenzoic acid (1.5 g, 11.0 mmol) in dry acetone (81 mL) at r.t.. After stirred for 30 minutes, benzyl bromide (5.2 mL, 44.0 mmol) was added dropwise and the reaction was stirred for another 30 minutes at r.t.. The mixture was heated to reflux for 16 h. K_2CO_3 was filtered on Büchner washing with acetone and the filtrate was evaporated under reduced pressure. The desired benzyl 4-

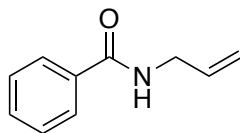
(benzyloxy)benzoate was precipitated with petroleum ether (30 mL) and filtrated on Büchner washing the white powder with cold petroleum ether (3.22 g, 10.12 mmol, 92% yield). ¹H NMR (600 MHz, CDCl₃) δ 8.07 (d, *J* = 8.7 Hz, 2H), 7.51 – 7.32 (m, 8H), 7.02 (d, *J* = 8.7 Hz, 2H), 5.37 (s, 2H), 5.13 (s, 2H). ¹³C NMR (151 MHz, CDCl₃) δ 166.2, 131.8, 128.7, 128.6, 128.3, 128.2, 128.1, 127.5, 114.5, 70.1, 66.5. 10 N NaOH (6 mL, 59.43 mmol) was added to a suspension of intermediate benzyl 4-(benzyloxy)benzoate (2.7 g, 8.49 mmol) in MeOH (85 mL). The mixture was heated to reflux for 1 h then concentrated under reduced pressure. The residue was poured into H₂O (50 mL) and washed with petroleum ether (25 mL). The aqueous phase was acidified until pH = 2 with HCl 4 N until the formation of a white solid was observed. The desired 4-(benzyloxy)benzoic acid was filtered on Büchner, washed with cold H₂O and dried *in vacuo* (1.50 g, 6.8 mmol, 80% yield). ¹H NMR (600 MHz, CD₃OD) δ 7.93 (d, *J* = 8.5 Hz, 2H), 7.45 – 7.27 (m, 5H), 6.98 (d, *J* = 8.5 Hz, 2H), 5.12 (s, 2H). ¹³C NMR (151 MHz, CD₃OD) δ 161.6, 131.2, 128.2, 127.7 (2C), 127.2, 113.9, 69.7. A mixture of allylamine (539 μL, 7.18 mmol), 4-(benzyloxy)benzoic acid (1.8 g, 7.90 mmol), EDCI (1.4 mL, 7.90 mmol) and HOBt (1.07 g, 7.90 mmol) in anhydrous DMF (20 mL) was stirred at r.t. for 16 h. H₂O (30 mL) was added and the mixture was extracted with Et₂O (3 x 30 mL). The organic layer was washed with NaCl_{ss} (30 mL), dried over dry Na₂SO₄, filtered and concentrated under reduced pressure. The resulting residue was purified by flash chromatography (20% EtOAc in petroleum ether) to give the desired product **108I** (1.04 g, 3.88 mmol, 54% yield). ¹H NMR (600 MHz, CD₃OD): δ 7.76 (d, *J* = 8.4 Hz, 2H), 7.43 (d, *J* = 7.5 Hz, 2H), 7.39 (t, *J* = 7.5 Hz, 1H), 7.35 (d, *J* = 7.2 Hz, 2H), 6.99 (d, *J* = 8.5 Hz, 2H), 6.29 (bs, 1H), 5.93 (ddt, *J* = 16.2, 10.7, 5.6 Hz, 1H), 5.21 (dd, *J* = 48.5, 13.6 Hz, 2H), 5.10 (s, 2H), 4.06 (d, *J* = 5.8 Hz, 2H). ¹³C NMR (151 MHz, CD₃OD): δ 166.9, 161.4, 136.4, 134.2, 129.0, 128.8, 128.7, 128.2, 127.5, 127.0, 125.3, 120.3, 116.5, 114.7, 109.4 70.1, 42.4.

General method for the formation of benzoyl allylamides

A mixture of the appropriate carboxylic acid (16 mmol) in freshly distilled SOCl₂ (12 mL) was heated to reflux for 2 h, then cooled to r.t. and evaporated under vacuum to dryness to obtain quantitatively the corresponding acid chloride. In a dried flask under N₂ atmosphere, a solution of allylamine (1.8 mL, 24 mmol) and Et₃N (3.3 mL, 24 mmol) in dry CH₂Cl₂ (25 mL) was cooled in an ice bath to 0 °C. Then, the appropriate benzoyl chloride (16 mmol) was added dropwise. The solution was stirred at r.t. for 16 h. H₂O (15 mL) was added and the organic layer was separated. The aqueous layer was extracted with CH₂Cl₂ (2 x 30 mL). The combined organic phases were washed with NaCl_{ss} (15 mL), dried over Na₂SO₄ and the solvent

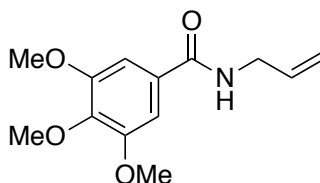
evaporated *in vacuo*. The crude product was purified by precipitation or column chromatography on silica gel.

***N*-Allylbenzamide (108m)**



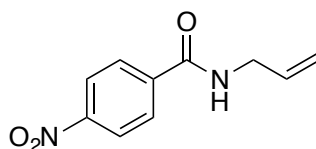
The crude was purified by means of flash chromatography on silica gel using a PE/CH₂Cl₂ mixture (8:2) as the eluent (2.01 g, 12.48 mmol, 78% yield). **¹H NMR** (400 MHz, CDCl₃) δ 7.75 (d, *J* = 7.6 Hz, 2H), 7.50 – 7.35 (m, 3H), 6.21 (bs, 1H), 5.91 (qd, *J* = 10.8, 5.7 Hz, 1H), 5.23 (dd, *J* = 17.3, 1.4 Hz, 1H), 5.15 (dd, *J* = 10.2, 1.2 Hz, 1H), 4.11 – 4.02 (m, 2H). **¹³C NMR** (101 MHz, CDCl₃): δ 167.5, 134.6, 134.3, 131.6, 128.7, 127.1, 116.7, 42.5.

***N*-Allyl-3,4,5-trimethoxybenzamide (108n)**



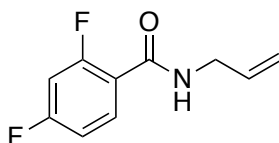
The crude was solubilized in the minimum amount of CH₂Cl₂ (10 mL) and petroleum ether (50 mL) was added slowly in order to obtain a white precipitate that was filtered on Büchner washing with cold petroleum ether (2.81 g, 11.2 mmol, 70% yield). **¹H NMR** (600 MHz, CDCl₃): δ 7.02 (s, 2H), 6.42 (bs, 1H), 5.96 – 5.55 (m, 1H), 5.20 (dd, *J* = 45.4, 13.7 Hz, 2H), 4.04 (d, *J* = 5.7 Hz, 2H), 3.87 (s, 9H). **¹³C NMR** (151 MHz, CDCl₃): δ 167.1, 153.2, 140.9, 134.2, 129.9, 116.7, 104.4, 60.9, 56.4, 42.7. Elemental Analysis Calcd. for C₁₃H₁₇NO₄: C, 62.14; H, 6.82; N, 5.57; O, 25.47. Found: C, 62.14; H, 6.82; N, 5.57; O, 25.47.

***N*-Allyl-4-nitrobenzamide (108o)**



The product was purified by means of flash chromatography using EtOAc in petroleum ether mixture as the eluent (2.57 g, 12.48 mmol, 78% yield). **¹H NMR** (600 MHz, CDCl₃) δ 8.28 (d, *J* = 8.4 Hz, 2H), 7.96 (d, *J* = 8.4 Hz, 2H), 6.45 (s, 1H), 6.01 – 5.88 (m, 1H), 5.28 (d, *J* = 17.1 Hz, 1H), 5.22 (d, *J* = 10.2 Hz, 1H), 4.11 (t, *J* = 5.3 Hz, 2H). **¹³C NMR** (151 MHz, CDCl₃) δ 165.4, 149.6, 140.0, 133.4, 128.2, 123.9, 117.4, 42.8.

***N*-Allyl-2,4-difluorobenzamide (108p)**



The product was purified by means of flash chromatography using EtOAc in petroleum ether mixture as the eluent (2.27 g, 11.54 mmol, 72% yield). **¹H NMR** (600 MHz, CDCl₃): δ 8.23 – 7.99 (m, 1H), 6.98 – 6.95 (m, 1H), 6.86 – 6.82 (m, 1H), 6.76 (bs, 1H), 5.91 (ddq, *J* = 15.2, 10.0, 5.0, 4.5 Hz, 1H), 5.21 (dd, *J* = 47.2, 13.6 Hz, 2H), 4.08 (d, *J* = 5.7 Hz, 2H). **¹³C NMR** (151 MHz, CDCl₃): δ 165.6, 162.3, 160.1, 133.9, 117.6, 116.5, 112.3, 104.4, 104.0, 42.4.

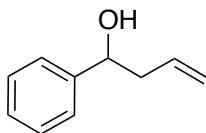
General methods for the Barbier reaction yielding allylalcohols 129(a-l)

Method I – Indium-catalysis. A suspension of indium powder (3 eq) and allyl bromide (4.5 eq) in THF (6 mL) was stirred at r.t. under N₂ atmosphere for 1 h. Then, the appropriately substituted aldehyde (1 eq) dissolved in THF (2 mL) was added. After 1 h, the suspension was treated with HCl 1 N (4 mL) and the mixture was extracted with CH₂Cl₂ (3 x 20 mL). The organic layers were combined, washed with a saturated solution of NaCl (5 mL), dried over Na₂SO₄, filtered and concentrated under reduced pressure. The resulting residue was purified by flash chromatography on silica gel to give the desired product as an oil (if not otherwise specified).

Method II – Zinc-catalysis. To a stirred solution of the appropriate aldehyde (1 eq) in THF (4 mL), allylbromide (4 eq) was added, followed by the addition of NH₄Cl (4 mL). Zinc dust (4 eq) was added portion wise at 0 °C and the reaction was then allowed to warm to r.t. and stirred for 12 h. The white precipitate was filtered off, the crude was diluted with H₂O and the aqueous phase was extracted with EtAOc (3 x 20 mL). The combined organic layers were dried over Na₂SO₄, filtered and evaporated *in vacuo*. The crude was purified by means of flash

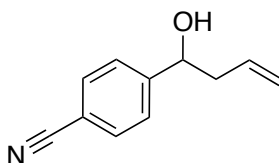
chromatography on silica gel to obtain the pure compound as a yellow oil (if not otherwise specified).

1-Phenylbut-3-en-1-ol (129a)



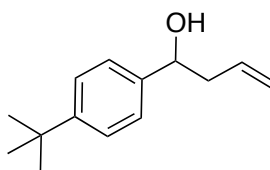
Prepared starting from benzaldehyde following Method I. Purification: 20% EtAOc in petroleum ether (461 mg, 3.11 mmol, 89% yield). **GC-MS** (m/z): 148.2, R_t = 15.010 min (Method A). **^1H NMR** (400 MHz, CDCl_3 , ppm) δ 7.59-7.51 (m, 5H), 5.72-5.26 (m, 1H), 5.21-5.19 (d, J = 8.0 Hz, 1H), 5.07 (s, 1H), 2.74-2.68 (m, 1H), 2.02-1.98 (m, 2H); **^{13}C NMR** (101 MHz, CDCl_3 , ppm) δ 128.4, 126.2, 125.3, 124.3, 116.3, 112.9, 72.1, 56.1.

4-(1-Hydroxybut-3-en-1-yl)benzonitrile (129b)



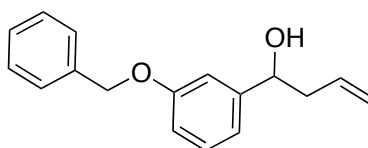
Prepared starting from 4-formylbenzonitrile following Method I. Purification: 20% EtAOc in petroleum ether (415 mmol, 2.4 mmol, 48% yield). **GC-MS** (m/z): 173.4, R_t = 16.999 min (Method A). **^1H NMR** (400 MHz, CDCl_3) δ 7.57 (d, J = 8.1 Hz, 2H), 7.42 (d, J = 8.1 Hz, 2H), 5.84 – 5.60 (m, 1H), 5.21 – 5.02 (m, 2H), 4.74 (dd, J = 7.5, 5.0 Hz, 1H), 2.52 – 2.33 (m, 2H). **^{13}C NMR** (101 MHz, CDCl_3): δ 149.2, 133.3, 132.1, 126.4, 119.2, 118.7, 110.9, 72.3, 43.6.

1-(4-(*tert*-Butyl)phenyl)but-3-en-1-ol (129c)



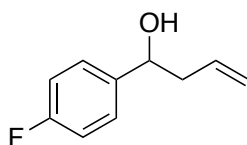
Prepared starting from 4-(*tert*-butyl)benzaldehyde following Method II. Purification: 5-50% gradient of EtAOc in petroleum ether (918 mg, 4.5 mmol, 90% yield). **GC-MS** (*m/z*): 204.3, *R*_t = 16.491 min (Method B). **¹H NMR** (400 MHz, CDCl₃) δ 7.35 (d, *J* = 8.2 Hz, 2H), 7.27 (d, *J* = 8.4 Hz, 2H), 5.81 (ddt, *J* = 17.1, 10.1, 7.1 Hz, 1H), 5.13 (t, *J* = 13.3 Hz, 2H), 4.69 (dd, *J* = 7.3, 5.7 Hz, 1H), 2.59 – 2.43 (m, 2H), 1.29 (s, 9H). **¹³C NMR** (151 MHz, CDCl₃) δ 150.5, 140.9, 134.8, 125.6, 125.4, 118.2, 73.2, 43.7, 31.4.

1-(3-(Benzyloxy)phenyl)but-3-en-1-ol (129d)



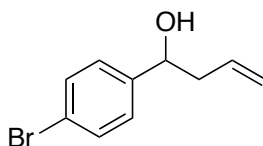
Prepared starting from 3-(benzyloxy)benzaldehyde following Method II. Purification: 5-25% gradient of EtAOc in petroleum ether (635 mg, 2.5 mmol, 50% yield). **GC-MS** (*m/z*): 254.7, *R*_t = 22.571 min (Method B). **¹H NMR** (400 MHz, CDCl₃) δ 7.46 – 7.27 (m, 5H), 7.27 – 7.21 (m, 1H), 7.00 (s, 1H), 6.93 (d, *J* = 7.6 Hz, 1H), 6.87 (dd, *J* = 8.1, 2.4 Hz, 1H), 5.78 (ddt, *J* = 17.1, 10.2, 7.1 Hz, 1H), 5.17 (d, *J* = 1.4 Hz, 1H), 5.15 – 5.09 (m, 2H), 5.06 (s, 2H), 4.70 (dd, *J* = 7.6, 5.2 Hz, 1H), 2.64 – 2.34 (m, 2H). **¹³C NMR** (151 MHz, CDCl₃) δ 147.5, 138.9, 136.3, 131.4, 130., 129.9, 129.4, 120.4, 120.3, 115.8, 114.3, 75.1, 71.9, 45.6. Elemental analysis calcd. for C₁₇H₁₈O₂: C, 80.28; H, 7.13; O, 12.58. Found: C, 80.31; H, 7.11.

1-(4-Fluorophenyl)but-3-en-1-ol (129e)



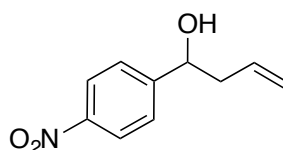
Prepared starting from 4-fluorobenzaldehyde following Method I. Purification: 15-65% gradient of EtAOc in petroleum ether (390 mg, 2.35 mmol, 47% yield). **GC-MS** (*m/z*): 166.4, *R*_t = 12.936 min. (Method A). **¹H NMR** (400 MHz, CDCl₃) δ 7.29 (dd, *J* = 8.4, 5.5 Hz, 2H), 7.00 (t, *J* = 8.7 Hz, 2H), 5.86 – 5.66 (m, 1H), 5.14 (d, *J* = 6.1 Hz, 1H), 5.11 (s, 1H), 4.76 – 4.63 (m, 1H), 2.54 – 2.36 (m, 2H). **¹³C NMR** (101 MHz, CDCl₃): δ 162.3 (d, *J*_{C-F} = 243.2 Hz), 139.7 (d, *J*_{C-F} = 3.1 Hz), 134.3, 127.6 (d, *J*_{C-F} = 8.4 Hz), 118.7, 115.3 (d, *J*_{C-F} = 21.3 Hz), 72.8, 44.0.

1-(4-Bromophenyl)but-3-en-1-ol (129f)



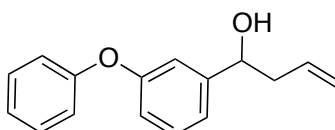
Prepared starting from 4-bromobenzaldehyde following Method I. Purification: 20% EtAOc in petroleum ether (795 mg, 3.5 mmol, 70% yield). **GC-MS** (m/z): 226.8-228.4 (Br isotopes), R_t = 15.000 min (Method A). **^1H NMR** (400 MHz, CDCl_3) δ 7.41 (d, J = 8.4 Hz, 2H), 7.15 (d, J = 8.3 Hz, 2H), 5.78 – 5.62 (m, 1H), 5.08 (d, J = 12.1 Hz, 2H), 4.60 (t, J = 6.2 Hz, 1H), 2.60 – 2.33 (m, 2H). **^{13}C NMR** (101 MHz, CDCl_3) δ 142.9, 134.0, 131.5, 127.6, 121.2, 118.7, 72.7, 43.7.

1-(4-Nitrophenyl)but-3-en-1-ol (129g)



Prepared starting from 4-nitrobenzaldehyde following Method I. Purification: 20% EtAOc in petroleum ether (666 mg, 3.45 mmol, 69% yield). **GC-MS** (m/z): 193.3, R_t = 18.389 min (Method A). **^1H NMR** (400 MHz, CDCl_3): δ 8.22 (d, J = 8.8 Hz, 2H), 7.55 (d, J = 8.8 Hz, 2H), 5.84–5.74 (m, 1H), 5.21–5.16 (m, 2H), 4.89 (q, J = 4.8 Hz, 1H), 2.60–2.55 (m, 1H), 2.50–2.42 (m, 1H), 2.29 (bs, 1H); **^{13}C NMR** (101 MHz, CDCl_3): δ 151.3, 147.2, 133.3, 126.7, 123.6, 119.5, 72.4, 43.9.

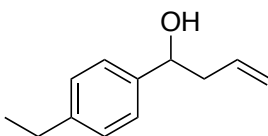
1-(3-Phenoxyphenyl)but-3-en-1-ol (129h)



Prepared starting from 3-phenoxybenzaldehyde following Method II. Purification: 5-25% gradient of EtAOc in petroleum ether (492 mg, 2.05 mmol, 41% yield). **GC-MS** (m/z): 240.4,

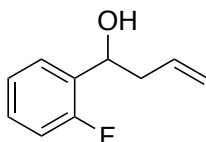
$R_t = 21.315$ min (Method B). **^1H NMR** (400 MHz, CDCl_3) δ 7.37 – 7.25 (m, 3H), 7.14 – 7.05 (m, 2H), 7.05 – 6.96 (m, 3H), 6.92 – 6.85 (m, 1H), 5.87 – 5.71 (m, 1H), 5.23 – 5.02 (m, 2H), 4.70 (dd, $J = 7.8, 5.0$ Hz, 1H), 2.64 – 2.33 (m, 3H). **^{13}C NMR** (151 MHz, CDCl_3) δ 157.4, 146.01, 134.2, 129.8, 129.7, 123.3, 120.7, 118.9, 118.6, 117.9, 116.4, 72.9, 43.8. Elemental analysis calcd. for $\text{C}_{16}\text{H}_{16}\text{O}_2$: C, 79.97; H, 6.71; O, 13.32. Found: C, 79.93; H, 6.68.

1-(4-Ethylphenyl)but-3-en-1-ol (129i)



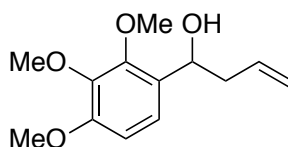
Prepared starting from 4-(ethyl)benzaldehyde following Method II. Purification: 5-50% gradient of EtAOc in petroleum ether (567 mg, 3.22 mmol, 92% yield). **GC-MS** (m/z): 176.6; $R_t = 14.941$ min (Method B). **^1H NMR** (400 MHz, CDCl_3) δ 7.26 (d, $J = 8.0$ Hz, 2H), 7.17 (d, $J = 8.1$ Hz, 1H), 5.80 (ddt, $J = 17.1, 10.2, 7.1$ Hz, 1H), 5.13 (t, $J = 12.0$ Hz, 2H), 4.69 (d, $J = 7.0$ Hz, 1H), 2.63 (q, $J = 7.6$ Hz, 2H), 2.56 – 2.43 (m, 2H), 1.22 (t, $J = 7.6$ Hz, 3H). **^{13}C NMR** (151 MHz, CDCl_3) δ 143.6, 141.3, 134.8, 127.9, 125.9, 118.1, 73.3, 43.7, 28.6, 15.6.

1-(2-Fluorophenyl)but-3-en-1-ol (129j)



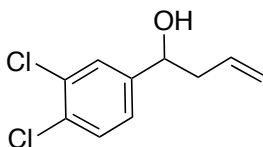
Prepared starting from 2-fluorobenzaldehyde following Method I. Purification: 5-50% gradient of EtAOc in petroleum ether (552 mg, 3.33 mmol, 95% yield). **GC-MS** (m/z): 166.2, $R_t = 12.173$ min (Method A). **^1H NMR** (400 MHz, CDCl_3) δ 7.43 (t, $J = 7.5$ Hz, 1H), 7.25 – 7.17 (m, 1H), 7.11 (t, $J = 7.5$ Hz, 1H), 7.02 – 6.94 (m, 1H), 5.84 – 5.72 (m, 1H), 5.13 (d, $J = 9.2$ Hz, 1H), 5.10 (s, 1H), 5.02 (dt, $J = 7.8, 4.0$ Hz, 1H), 2.59 – 2.41 (m, 2H). **^{13}C NMR** (101 MHz, CDCl_3) δ 162.6 (d, $J_{\text{C-F}} = 164.0$ Hz), 139.4, 134.5, 131.0, 128.8, 119.8, 116.5, 76.0, 42.4.

1-(2,3,4-Trimethoxyphenyl)but-3-en-1-ol (129k)



Prepared starting from 2,3,4-trimethoxybenzaldehyde following Method II. Purification: 15-65% gradient of EtAOc in petroleum ether (1.12 g, 4.7 mmol, 94% yield). **GC-MS** (m/z): 238.2, R_t = 18.483 min (Method B). **^1H NMR** (400 MHz, CDCl_3) δ 7.01 (d, J = 8.6 Hz, 1H), 6.64 (d, J = 8.6 Hz, 1H), 5.83 (ddt, J = 17.1, 10.2, 7.1 Hz, 1H), 5.11 (t, J = 12.2 Hz, 2H), 4.88 (dt, J = 7.6, 5.1 Hz, 1H), 3.92 (s, 3H), 3.84 (d, J = 2.2 Hz, 6H), 2.55 – 2.43 (m, 2H), 2.33 (d, J = 5.0 Hz, 1H). **^{13}C NMR** (151 MHz, CDCl_3) δ 135.1, 129.5, 128.7, 121.1, 117.7, 116.6, 116.3, 107.2, 69.0, 61.1, 60.7, 56.0, 42.8.

1-(3,4-Dichlorophenyl)but-3-en-1-ol (129l)



Prepared starting from 3,4-dichlorobenzaldehyde following Method II. Purification: 5-50% gradient of EtAOc in petroleum ether (922 mg, 4.25 mmol, 85% yield). **GC-MS** (m/z): 216.8 (217.8) - 218.7 (219.5) (Cl isotopes); R_t = 17.340 min (Method B). **^1H NMR** (400 MHz, CDCl_3) δ 7.45 (d, J = 1.9 Hz, 1H), 7.39 (d, J = 8.3 Hz, 1H), 7.17 (dd, J = 8.3, 2.0 Hz, 1H), 5.82 – 5.69 (m, 1H), 5.18 (s, 1H), 5.14 (d, J = 5.6 Hz, 1H), 4.69 (dd, J = 7.9, 4.8 Hz, 1H), 2.59 – 2.34 (m, 2H). **^{13}C NMR** (151 MHz, CDCl_3) δ 144.1, 133.5, 132.5, 131.3, 130.3, 127.9, 125.2, 119.3, 72.0, 43.8.

4.2.2 General methods for the hydroformylation reaction

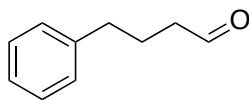
Method A (for liquid alkenes). A 80 mL MW tube was charged with a solution of TPGS-750 M (2.5 wt. % in H_2O , 3 mL) and alkene (2.25 mmol, 0.75 M solution). Then NaHSO_3 (269 mg, 2.59 mmol), $\text{Rh}(\text{CO})\text{H}(\text{PPh}_3)_3$ (21 mg, 0.0225 mmol) and Xantphos (52 mg, 0.09 mmol) were added. The yellow suspension was stirred for 5 min. under N_2 . The mixture was subjected to 3 cycles of vacuum/syngas inside the microwave cavity. Syngas was added since 130 psi (8.8 bar are detected), and irradiated at 70 °C for 40 minutes cooling while heating with a fixed power

of 300 Watt. After irradiation, the mixture was cooled-down to r.t. and the internal gas released by opening the external pressure valve. The mixture was filtered on Büchner washing with EtOAc (5 mL) to provide the bisulfite adduct as a crystalline powder that was solubilized in H₂O. If no precipitation was observed, the mixture was extracted with EtOAc (9 mL). Depending on the substrate, NaOH 10 N or HCl 4 N was added to the aqueous phase since pH = 8 or pH = 2, respectively. EtOAc (9 mL) was added and the mixture stirred at r.t. for 15 minutes. The two phases were separated and the organic phase was washed with NaCl_{ss} (2 x 5mL) and H₂O (5 mL), dried with dry Na₂SO₄, filtered, evaporated under reduced pressure and analyzed by GC/MS or ¹H-NMR, furnishing the desired aldehyde (or the hemiacetal in a 1:1 diastereoisomeric mixture).

Method B (for solid alkenes). A 80 mL MW tube was charged with a solution of TPGS-750 M (2.5 wt. % in H₂O, 3 mL) and alkene (2.25 mmol, 0.75 M). Then NaHSO₃ (269 mg, 2.59 mmol), Rh(CO)H(PPh₃)₃ (42 mg, 0.045 mmol) and Xantphos (104 mg, 0.18 mmol) were added. The suspension was vigorously stirred for 15 minutes under N₂. The mixture was subjected to 3 cycles of vacuum/syngas inside the microwave cavity. Syngas was added since 130 psi (8.8 bar) are detected, and irradiated at 70 °C for 60 minutes cooling while heating with a fixed power of 300 Watt. After irradiation, the mixture was cooled-down to room temperature and the internal gas released by opening the external pressure valve. The mixture was worked up as for Method A.

When necessary, the crude was purified by chromatography on silica gel using EtOAc in petroleum ether as the eluent (see single methods for ratios). The yields are referred to the isolated linear products. If not described, the branched products were not isolated from the crude materials.

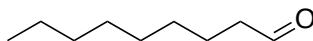
4-Phenylbutanal (107a)



The title compound was obtained following general Method A, starting from allylbenzene and using 10 N NaOH during the work-up (288 mg, 1.94 mmol, 86% yield). **GC/MS** (*m/z*): 149; *R*_t = 12.744 min (Method A). **¹H NMR** (400 MHz, CDCl₃): δ 9.73 (s, 1H), 7.28 (t, *J* = 7.3 Hz, 2H), 7.18 (q, *J* = 7.5 Hz, 3H), 2.65 (t, *J* = 7.2 Hz, 2H), 2.43 (t, *J* = 7.4 Hz, 2H), 1.95 (q, *J* = 8 Hz,

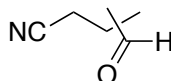
2H). ^{13}C NMR (101 MHz, CDCl_3): δ 202.5, 141.3, 129.1, 128.9, 128.5, 128.3, 126.2, 43.2, 35.0, 23.7.

Nonanal (109a)



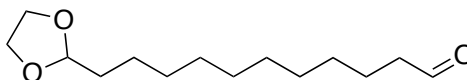
The title compound was obtained following general Method A starting from 1-octene and using 10 N NaOH during the work-up (303 mg, 2.14 mmol, 95% yield). **GC/MS** (m/z): 142; R_t = 10.818 min (Method A). ^1H NMR (400 MHz, CDCl_3) δ 9.73 (t, J = 1.8 Hz, 1H), 2.38 (td, J = 7.3, 1.7 Hz, 2H), 1.61–1.57 (m, 2H), 1.26–1.23 (m, 10H), 0.84 (t, J = 6.3 Hz, 3H). ^{13}C NMR (101 MHz, CDCl_3) δ 203.1, 70.6 44.0, 31.9, 29.4, 29.2, 22.8, 22.2, 14.2.

5-Oxopentanenitrile (110a), 3-methyl-4-oxobutanenitrile(110b) (110a/110b 85:15)



The compounds mixture was obtained following general Method A, starting from allyl cyanide and using 10 N NaOH during the work-up. Purification: by means of chromatography on silica gel, using an increasing gradient of EtAOc in petroleum ether, it was not possible to isolate the linear aldehyde to the branched one. Obtained 90 mg, 0.92 mmol, 41% yield (of the mixture). **GC/MS** (m/z): 98; R_t linear aldehyde= 8.039 min; R_t branched aldehyde = 8.139 min. ^1H NMR analysis allowed to establish the ratio between linear and branched compound (85:15).

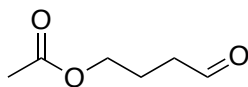
11-(1,3-Dioxolan-2-yl)undecanal (111a)



The title compound was obtained following general Method A, starting from **108c** and using 10 N NaOH during the work-up. Purification: 10% EtAOc in petroleum ether (392 mg, 1.62 mmol, 72% yield). **GC/MS** (m/z): 242; R_t = 20.425 min (Method A). ^1H NMR (600 MHz, CDCl_3): δ 9.76 (s, 1H), 4.84 (t, J = 4.8 Hz, 1H), 3.96 (t, J = 6.8 Hz, 2H), 3.84 (t, J = 6.8 Hz, 2H), 2.41 (t, J = 7.2 Hz, 2H), 1.63 (dp, J = 17.5, 7.0, 6.3 Hz, 2H), 1.41 (p, J = 7.1 Hz, 2H), 1.35

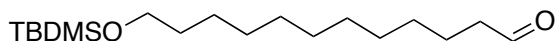
– 1.23 (m, 14H). ^{13}C NMR (151 MHz, CDCl_3): δ 203.0, 104.7, 64.8, 43.9, 33.9, 29.5, 29.4 (2C), 29.3 (2C), 29.12, 24.1, 22.1. Elemental analysis calcd. for $\text{C}_{14}\text{H}_{26}\text{O}_3$: C, 69.38; H, 10.81; O, 19.80. Found: C, 69.44; H, 10.84.

4-Oxobutyl acetate (112a)



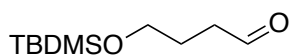
The title compound was obtained following general Method A, starting from allyl benzoate and using 4 N HCl during the work-up (237 mg, 1.82 mmol, 81% yield). **GC/MS** (m/z): 130; R_t = 8.655 min (Method A). ^1H NMR (600 MHz, CDCl_3): δ 9.80 (s, 1H), 4.11 (t, J = 6.2 Hz, 2H), 2.55 (t, J = 6.9 Hz, 2H), 2.05 (s, 3H), 1.98 (q, J = 6.4 Hz, 2H). ^{13}C NMR (151 MHz, CDCl_3): δ 201.2, 171.0, 63.4, 40.5, 21.3, 20.9.

12-((*tert*-Butyldimethylsilyl)oxy)dodecanal (113a)



The title compound was obtained following general Method A, starting from **108e** and using 10 N NaOH during the work-up (571 mg, 1.82 mmol, 81% yield). **GC/MS** (m/z): 314; R_t = 21.415 min (Method A). ^1H NMR (400 MHz, CDCl_3) δ = 9.76 (t, J = 1.9 Hz, 1H), 3.59 (t, J = 6.6 Hz, 2H), 2.41 (td, J = 7.4, 1.9 Hz, 2H), 1.67-1.58 (m, 2H), 1.52-1.47 (m, 2H), 1.35-1.24 (m, 14H), 0.89 (s, 9H), 0.05 (s, 6H). ^{13}C NMR (101 MHz, CDCl_3) δ = 203.0, 63.4, 44.0, 33.0, 29.7, 29.6, 29.5 (3C), 29.3, 26.1 (3C), 25.9, 22.2, 18.5, -5.1 (2C).

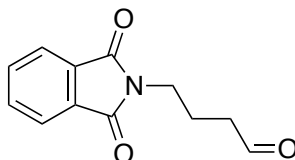
4-((*tert*-Butyldimethylsilyl)oxy)butanal (114a)



The title compound was obtained following general Method A, starting from **108f** and using 10 N NaOH during the work-up (50 mg, 0.25 mmol, 11% yield). **GC/MS** (m/z): 202; R_t = 10.995 min (Method A). ^1H NMR (400 MHz, CDCl_3) δ : 5.82 (ddt, J = 6.8, 10.5, 12.6 Hz, 1H), 5.05–

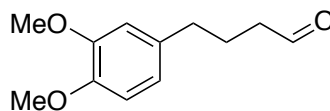
4.92 (m, 2H), 3.61 (t, $J = 6.8$ Hz, 2H), 2.12 (m, 2H), 1.63-1.58 (m, 2H), 0.90 (s, 9H), 0.05 (s, 6H); ^{13}C NMR (101 MHz, CDCl_3) δ : 138.8, 114.6, 62.7, 32.1, 30.2, 26.1, 18.5, 5.1.

4-(1,3-Dioxoisindolin-2-yl)butanal (115a)



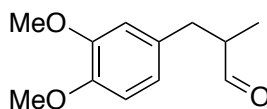
The title compound was obtained following general Method B, starting from **108g** and using 10 N NaOH during the work-up (405 mg, 1.87 mmol, 83% yield). **GC/MS** (m/z): 217; $R_t = 21.046$ min (Method A). ^1H NMR (400 MHz, CDCl_3) δ 9.77 (s, 1H), 7.87–7.83 (m, 2H), 7.74–7.71 (m, 2H), 3.74 (t, $J = 6.6$ Hz, 2H), 2.54 (t, $J = 6.8$ Hz, 2H), 2.05–1.98 (m, 2H). ^{13}C NMR (101 MHz, CDCl_3) δ 201.2, 168.7, 134.4, 132.3, 123.6, 41.4, 37.4, 21.5.

4-(3,4-Dimethoxyphenyl)butanal (116a)



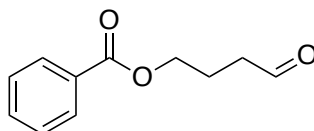
The title compound was obtained following general Method A, starting from 4-allyl-1,2-dimethoxybenzene and using 10 N NaOH during the work-up. Purification: 10% EtAOc in petroleum ether (304 mg, 1.46 mmol, 65% yield). **GC/MS** (m/z): 208; $R_t = 18.345$ min (Method A). ^1H NMR (600 MHz, CDCl_3): δ 9.76 (s, 1H), 6.80 (d, $J = 7.9$ Hz, 1H), 6.71 (d, $J = 9.1$ Hz, 1H), 6.70 (s, 1H), 3.88 (s, 3H), 3.86 (s, 3H), 2.61 (t, $J = 7.5$ Hz, 2H), 2.61 (t, $J = 7.5$ Hz, 2H), 1.95 (p, $J = 7.3$ Hz, 2H). ^{13}C NMR (151 MHz, CDCl_3): δ 202.4, 148.9, 147.4, 133.9, 120.3, 111.7, 111.3, 56.0, 43.1, 34.6, 23.8. Elemental analysis calcd. for $\text{C}_{12}\text{H}_{16}\text{O}_3$: C, 69.21; H, 7.74; O, 23.05. Found: C, 69.17; H, 7.72.

3-(3,4-Dimethoxyphenyl)-2-methylpropanal (116b)



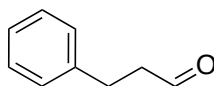
The title compound was obtained following general Method A, starting from 4-allyl-1,2-dimethoxybenzene and using 10 N NaOH during the work-up. Purification: 10% EtAOc in petroleum ether (52 mg, 0.25 mmol, 11% yield). **GC/MS** (m/z): 208; R_t = 17.359 min (Method A). **^1H NMR** (600 MHz, CDCl_3): δ 9.64 (s, 1H), 6.87 (d, J = 6.5 Hz, 1H), 6.75 (d, J = 9.9 Hz, 1H), 6.66 (s, 1H), 3.90 (s, 3H), 3.88 (s, 3H), 2.13 – 2.04 (m, 1H), 1.77-1.70 (m, 1H), 1.67 (q, J = 8 Hz, 1 H), 0.91 (s, 3H). **^{13}C NMR** (151 MHz, CDCl_3): δ 201.0 121.1, 119.7, 111.6, 111.1, 109.7, 60.4, 55.9, 22.8, 11.7, 10.3. Elemental analysis calcd. for $\text{C}_{12}\text{H}_{16}\text{O}_3$: C, 69.21; H, 7.74; O, 23.05. Found: C, 69.19; H, 7.72.

4-Oxobutyl benzoate (117a)



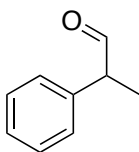
The title compound was obtained following general Method A, starting from **108i** and using 4 N HCl during the work-up (263 mg, 1.37 mmol, 61% yield). The reaction was analyzed through ^1H NMR (600 MHz). **^1H NMR** (400 MHz, CDCl_3): δ 9.81 (s, 1H), 8.08 (d, J = 7.5 Hz, 2H), 7.58 (t, J = 7.5 Hz, 1H), 7.44 (t, J = 7.7 Hz, 2H), 4.34 (t, J = 6.3 Hz, 2H), 2.61 (t, J = 7.1 Hz, 2H), 2.09 (q, J = 6.8 Hz, 2H). **^{13}C NMR** (151 MHz, CDCl_3): δ 194.5, 157.6, 133.7, 133.1, 130.2, 129.6, 128.5, 128.4, 63.9, 40.6, 29.7.

3-Phenylpropanal (119a)



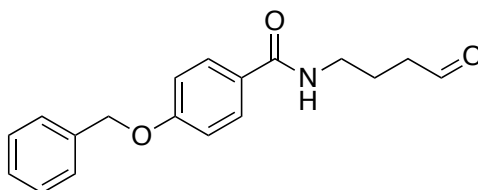
The title compound was obtained following general Method A, starting from styrene and using 10 N NaOH during the work-up. Purification: 10% EtAOc in petroleum ether (57 mg, 0.43 mmol, 19% yield). **GC-MS** (m/z): 134.4, R_t = 11.527 min (Method A). **^1H NMR** (400 MHz, CDCl_3) δ 9.80 (s, 1H), 7.28-7.23 (m, 2H), 7.21-7.17 (t, J = 8.1 Hz, 3H), 2.88 (t, J = 7.54 Hz, 2H), 2.75 (t, J = 7.3 Hz, 2H). **^{13}C NMR** (101 MHz, CDCl_3) δ 201.6, 140.6, 128.7, 128.5, 126.3, 45.7, 28.2.

2-Phenylpropanal (119b)



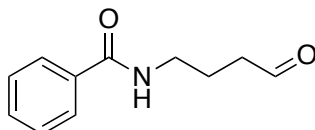
The title compound was obtained following general Method A, starting from styrene and using 10 N NaOH during the work-up. Purification: 10% EtAOc in petroleum ether (171 mg, 1.28 mmol, 57% yield). **GC-MS** (m/z): 134.5, R_t = 10.405 min (Method A). **^1H NMR** (400 MHz, CDCl_3) δ 9.72 (d, J = 1.4 Hz, 1H), 7.44-7.37 (m, 2H), 7.30 (tt, J = 7.4, 2.1 Hz, 1H), 7.24-7.18 (m, 2H), 3.65 (qd, J = 7.2, 0.8 Hz, 1H), 1.41 (d, J = 7.1 Hz, 3H). **^{13}C NMR** (101 MHz, CDCl_3) δ 201.2, 137.9, 129.2, 128.4, 127.7, 53.1, 14.7.

4-(Benzyloxy)-*N*-(4-oxobutyl)benzamide (120a)



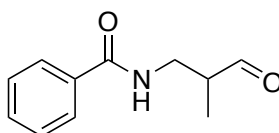
The title compound was obtained following general Method B, starting from **108l** and using 10 N NaOH during the work-up (341 mg, 1.15 mmol, 51% yield). **^1H NMR** (600 MHz, CDCl_3): δ 9.83 (s, 1H), 7.74 (d, J = 8.0 Hz, 2H), 7.58 (bs, 1H), 7.46 – 7.38 (m, 5H), 7.00 (d, J = 7.9 Hz, 2H), 5.12 (s, 2H), 3.49 (t, J = 5.9 Hz, 2H), 2.63 (t, J = 6.8 Hz, 2H), 1.98 (q, J = 6.8 Hz, 2H). **^{13}C NMR** (151 MHz, CDCl_3): δ 202.3, 136.4, 129.6, 129.5, 129.4, 128.7, 128.2, 127.5, 126.9, 123.9, 114.7, 114.6, 114.5, 114.3, 70.1, 39.6, 29.7, 22.7. Elemental analysis calcd. for $\text{C}_{18}\text{H}_{19}\text{NO}_3$: C, 72.71; H, 6.44; N, 4.71; O, 16.14. Found: C, 72.66; H, 6.48; N, 4.78.

N-(4-Oxobutyl)benzamide (121a)



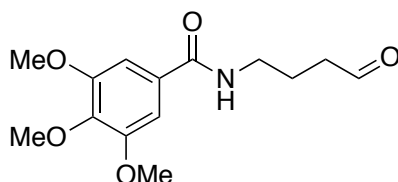
The title compound was obtained following general Method A, starting from **108m** and using 10 N NaOH during the work-up. Purification: 10% EtAOc in petroleum ether (266 mg, 1.40 mmol, 62% yield). **GC-MS** (m/z): 191.2, R_t = 15.050 min (Method A). **^1H NMR** (400 MHz, CDCl_3) δ 9.42 (s, 1H), 7.81 (d, J = 8.3 Hz, 2H), 7.72 (d, J = 8.4 Hz, 2H), 7.47 (dd, J = 7.4, 7.4 Hz, 1H), 7.44 (dd, J = 7.4, 7.4 Hz, 1H), 7.42 (dd, J = 7.5, 7.4 Hz, 2H), 7.34 (dd, J = 7.8, 7.7 Hz, 2H), 6.70 (bs, 1H), 6.64 (dd, J = 7.5, 7.4 Hz, 1H), 6.44 (bs, 1H), 3.54 (dd, J = 6.5, 6.5 Hz, 2H), 3.53 (dd, J = 6.4, 6.4 Hz, 2H), 2.65 (dd, J = 6.0, 6.0 Hz, 2H), 2.59 (dd, J = 7.5, 7.5 Hz, 1H), 2.58 (dd, J = 7.0, 7.0 Hz, 1H), 1.92 (ddd, J = 7.0, 7.0, 6.9 Hz, 2H), 1.44 (bs, 2H). **^{13}C NMR** (101 MHz, CDCl_3) δ 202.1, 170.9, 167.6, 135.7, 134.3, 131.2, 130.3, 128.4, 128.3, 127.1, 126.7, 82.3, 49.1, 41.4, 39.3, 32.1, 23.6, 21.7.

***N*-(2-Methyl-3-oxopropyl)benzamide (121b)**



The title compound was obtained following general Method A, starting from **108m** and using 10 N NaOH during the work-up. Purification: 10% EtAOc in petroleum ether (60 mg, 0.315 mmol, 14% yield). **GC-MS** (m/z): 191.3, R_t = 16.716 min (Method A). **^1H NMR** (400 MHz, CDCl_3): δ 9.69 (s, 1H), 7.70 (d, J = 7.0 Hz, 2H), 7.45 (d, J = 7.3 Hz, 1H), 7.41 – 7.36 (m, 2H), 3.78 – 3.43 (m, 2H), 2.77 (td, J = 7.6, 4.3 Hz, 1H), 1.19 (d, J = 7.5 Hz, 3H). **^{13}C NMR** (101 MHz, CDCl_3): δ 204.4, 167.6, 134.2, 131.6, 128.6, 126.9, 46.8, 39.8, 11.5.

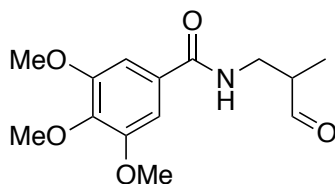
3,4,5-Trimethoxy-*N*-(4-oxobutyl)benzamide (122a)



The title compound was obtained following general Method B, starting from **108n** and using 10 N NaOH during the work-up. Purification: 2% MeOH in CH_2Cl_2 (379 mg, 1.35 mmol, 60% yield). **^1H NMR** (400 MHz, CDCl_3): δ 9.79 (s, 1H), 6.98 (s, 2H), 3.87 (s, 3H), 3.83 (s, 6H),

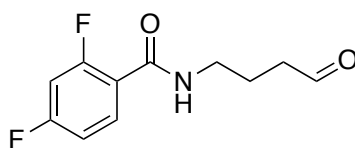
3.44 (t, $J = 6.3$ Hz, 2H), 2.61 (t, $J = 6.6$ Hz, 2H), 1.94 (q, $J = 6.7$ Hz, 2H). ^{13}C NMR (151 MHz, CDCl_3): δ 200.0, 167.1, 153.3, 141.4, 129.1, 104.6, 60.9, 60.3, 56.3, 39.9, 23.2, 22.2. Elemental analysis calcd. for $\text{C}_{14}\text{H}_{19}\text{NO}_5$: C, 59.78; H, 6.81; N, 4.98; O, 28.44. Found: C, 59.80; H, 6.87; N, 4.93.

3,4,5-Trimethoxy-*N*-(2-methyl-3-oxopropyl)benzamide (122b)



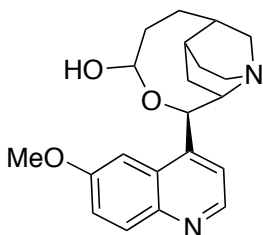
The title compound was obtained following general Method B, starting from **108n** and using 10 N NaOH during the work-up. Purification: 2% MeOH in CH_2Cl_2 (57 mg, 0.20 mmol, 9% yield). ^1H NMR (600 MHz, CDCl_3): δ 9.68 (s, 1H), 7.05 (s, 2H), 3.91 (s, 6H), 3.88 (s, 3H), 1.99 (ddt, $J = 169.1, 14.3, 7.6$ Hz, 2H), 2.05 – 1.91 (m, 1H), 1.02 (d, $J = 7.4$ Hz, 3H). ^{13}C NMR (151 MHz, CDCl_3): δ 199.3, 167.1, 153.3, 141.3, 129.2, 104.6, 60.9, 60.3, 56.4, 29.7, 14.1, 9.5. Elemental analysis calcd. for $\text{C}_{14}\text{H}_{19}\text{NO}_5$: C, 59.78; H, 6.81; N, 4.98; O, 28.44. Found: C, 59.83; H, 6.84; N, 4.90.

2,4-Difluoro-*N*-(4-oxobutyl)benzamide (124a)



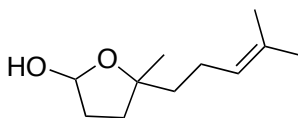
The title compound was obtained following general Method A, starting from **108p** and using 10 N NaOH during the work-up. Purification: 50% EtAOc in petroleum ether (332 mg, 1.46 mmol, 65% yield). ^1H NMR (600 MHz, CDCl_3): δ 9.83 (s, 1H), 8.17 – 8.07 (m, 1H), 7.47 (q, $J = 7.5$ Hz, 1H), 6.92 – 6.85 (m, 1H), 6.77 (bs, 1H), 3.52 (t, $J = 6.5$ Hz, 2H), 2.60 (t, $J = 7.0$ Hz, 2H), 1.98 (q, $J = 7.1$ Hz, 2H). ^{13}C NMR (151 MHz, CDCl_3): δ 202.0, 151.9, 133.8, 130.7, 112.5, 112.0, 104.6, 104.1, 39.5, 23.4, 22.0. Elemental analysis calcd. for $\text{C}_{11}\text{H}_{11}\text{F}_2\text{NO}_2$: C, 58.15; H, 4.88; F, 16.72; N, 6.16; O, 14.08. Found: C, 58.20; H, 4.93; N, 6.17.

(8*R*)-8-(6-Methoxyquinolin-4-yl)-7-oxa-1-azatricyclo[7.4.0.0^{3,11}]tridecan-6-ol (126)



The title compound was obtained following general Method B, starting from quinine **125** and using 10 N NaOH during the work-up (422 mg, 1.19 mmol, 53% yield). **¹H NMR** (600 MHz, CD₃OD): δ 8.63 (d, *J* = 4.5 Hz, 1H), 7.91 (d, *J* = 9.0 Hz, 1H), 7.65 (d, *J* = 4.4 Hz, 1H), 7.40 (s, 1H), 7.38 (d, *J* = 7.5 Hz, 1H), 5.59 (d, *J* = 7.4 Hz, 1H), 4.35 (t, *J* = 6.91 Hz, 1H), 3.94 (s, 3H), 3.10 (dq, *J* = 13.0, 9.3, 7.0 Hz, 2H), 2.73 – 2.62 (m, 1H), 2.45 – 2.35 (m, 2H), 1.86 (ddd, *J* = 26.4, 12.6, 7.2 Hz, 2H), 1.59 (d, *J* = 8.2 Hz, 1H), 1.53 – 1.37 (m, 4H), 1.27 (dt, *J* = 11.0, 5.8 Hz, 3H). **¹³C NMR** (151 MHz, CD₃OD): δ 158.4, 149.1, 146.8, 143.4, 130.0, 126.7, 122.0, 118.7, 101.1, 98.4, 70.7, 59.5, 57.9, 55.1, 42.8, 35.0, 34.4, 29.3, 27.2, 25.8, 19.9.

5-Methyl-5-(4-methylpent-3-en-1-yl)tetrahydrofuran-2-ol (128)



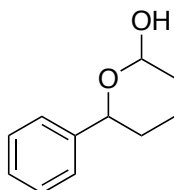
The title compound was obtained following general Method A, starting from linalool **127** and using 10 N NaOH during the work-up (323 mg, 1.76 mmol, 78% yield). **GC/MS** (*m/z*): 184; *R*_t = 13.887 min (Method A). **¹H NMR** (600 MHz, CDCl₃): δ 5.49 (bs, 1H), 5.40 (t, *J* = 6.9 Hz, 1H), 5.11 (t, *J* = 7.0 Hz, 1H), 3.64 (s, 3H), 2.10 – 1.95 (m, 4H), 1.91 (dq, *J* = 17.1, 7.2, 5.8 Hz, 2H), 1.68 (s, 3H), 1.61 (s, 3H), 1.46 (ddt, *J* = 10.6, 7.2, 4.2 Hz, 2H). **¹³C NMR** (151 MHz, CDCl₃): δ 124.6, 99.9, 84.2, 70.6, 42.8, 41.9, 34.8, 28.2, 25.7, 23.6, 17.6. Elemental analysis calcd. for C₁₁H₂₀O₂: C, 71.70; H, 10.94; O, 17.36. Found: C, 71.75; H, 10.89.

4.2.3 General method for the synthesis of cyclic hemiacetals

The following hemiacetalic compounds were all synthesized following general Method A, using 10 N NaOH in the work-up. The crude compounds were purified by means of

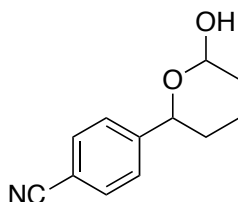
chromatography on silica gel eluting with a very slow 5-75% gradient of EtAOc in petroleum ether, if not otherwise specified. The yields are referred to the isolated 6-membered hemiacetals, obtained as 1:1 diastereoisomeric mixtures. The branched products, leading to the substituted 5-membered hemiacetals, were not isolated from the crude materials.

6-Phenyltetrahydro-2*H*-pyran-2-ol (130a)



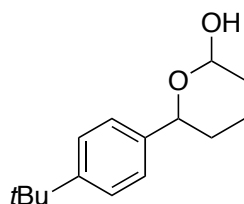
Prepared starting from allylalcohol **129a** (344 mg, 1.94 mmol, 86% yield). **GC/MS** (*m/z*): 178.5, *R*_t = 16.457 min (Method B). **¹H NMR** (600 MHz, CDCl₃): δ 7.38-7.26 (m, 10H), 5.44 (s, 1H), 5.02 (dd, *J* = 12.0, 2.0 Hz, 1H), 4.88-4.85 (m, 1H), 4.48 (d, *J* = 11.5, 1H), 3.29 (s, 1H), 2.84 (bs, 1H), 2.08-1.39 (m, 12H); **¹³C NMR** (151 MHz, CDCl₃): δ 142.9, 142.0, 128.3, 127.5, 127.4, 126.0, 125.9, 96.9, 92.4, 78.6, 71.1, 33.6, 32.7, 32.3, 29.4, 22.5, 17.9.

4-(6-Hydroxytetrahydro-2*H*-pyran-2-yl)benzonitrile (131a)



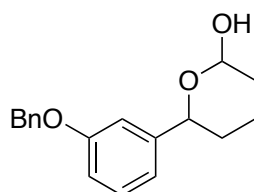
Prepared starting from allylalcohol **129b** (260 mg, 1.28 mmol, 57% yield). **GC/MS** (*m/z*): 203.6, *R*_t = 20.845 min (Method A). **¹H NMR** (400 MHz, CDCl₃) δ 7.56 (dd, *J* = 8.1, 3.0 Hz, 4H), 7.41 (dd, *J* = 13.9, 8.1 Hz, 4H), 5.40 (s, 1H), 5.02 (d, *J* = 11.6 Hz, 1H), 4.83 (d, *J* = 9.2 Hz, 1H), 4.48 (d, *J* = 11.1 Hz, 1H), 3.61 (bs, 1H), 3.17 (bs, 1H), 2.15 – 1.98 (m, 1H), 1.91 (t, *J* = 11.6 Hz, 2H), 1.86 – 1.56 (m, 5H), 1.56 – 1.30 (m, 4H). **¹³C NMR** (101 MHz, CDCl₃) δ 148.5, 147.4, 132.2, 126.6, 126.5, 118.9, 111.1, 110.9, 96.9, 92.3, 77.5, 70.3, 33.7, 32.7, 32.2, 29.4, 22.4, 17.7.

6-(4-(*tert*-Butyl)phenyl)tetrahydro-2*H*-pyran-2-ol (132a)



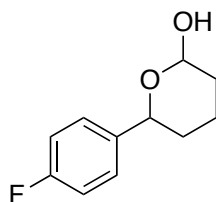
Prepared starting from allyl alcohol **129c** (433 mg, 1.85 mmol, 82% yield). **GC-MS** (m/z): 234.7, R_t = 20.368 min (Method B). **^1H NMR** (600 MHz, CDCl_3) δ 7.38 (dd, J = 8.3, 2.4 Hz, 4H), 7.35 – 7.28 (m, 4H), 5.44 (s, 1H), 5.01 (d, J = 11.3 Hz, 1H), 4.86 (d, J = 9.5 Hz, 1H), 4.46 (d, J = 11.2 Hz, 1H), 3.33 (bs, 1H), 2.88 (bs, 1H), 2.11 – 2.01 (m, 1H), 1.94 (t, J = 15.7 Hz, 2H), 1.85 (d, J = 13.0 Hz, 1H), 1.80 – 1.73 (m, 2H), 1.73 – 1.62 (m, 4H), 1.55 (qd, J = 13.0, 3.7 Hz, 1H), 1.48 – 1.38 (m, 1H), 1.32 (s, 18H). **^{13}C NMR** (151 MHz, CDCl_3) δ 143.7, 141.4, 126.2, 125.9, 125.8, 125.3, 125.2, 125.0, 96.9, 94.4, 71.2, 34.5, 33.1, 32.7, 31.5, 29.6, 28.69, 22.4, 17.8. Elemental analysis calcd. for $\text{C}_{15}\text{H}_{22}\text{O}_2$: C, 76.88; H, 9.46; O, 13.65. Found: C, 76.89; H, 9.48.

6-(3-(Benzyloxy)phenyl)tetrahydro-2H-pyran-2-ol (**133a**)



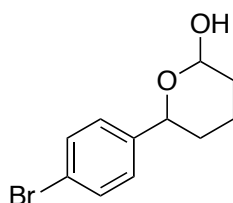
Prepared starting from allyl alcohol **129d** (447 mg, 1.58 mmol, 70% yield). **GC-MS** (m/z): 284.5 R_t = 25.353 min (Method B). **^1H NMR** (600 MHz, CDCl_3) δ 7.47 – 7.43 (m, 4H), 7.39 (t, J = 7.5 Hz, 4H), 7.34 (d, J = 7.2 Hz, 2H), 7.28 – 7.24 (m, 2H), 7.07 (s, 1H), 7.04 (s, 1H), 6.99 – 6.95 (m, 2H), 6.89 (dd, J = 6.7, 3.7 Hz, 2H), 5.47 (s, 1H), 5.08 (s, 4H), 5.01 (d, J = 10.2 Hz, 1H), 4.90 (d, J = 8.2 Hz, 1H), 4.49 (d, J = 10.0 Hz, 1H), 2.95 (bs, 1H), 2.58 (bs, 1H), 2.11 – 2.03 (m, 2H), 1.97 (d, J = 9.2 Hz, 2H), 1.89 – 1.67 (m, 4H), 1.62 (dd, J = 13.2, 3.5 Hz, 2H), 1.52 (dd, J = 12.8, 3.4 Hz, 1H), 1.49 – 1.39 (m, 1H). **^{13}C NMR** (151 MHz, CDCl_3) δ 143.2, 142.1, 129.4, 128.6, 127.9, 127.6, 127.5, 118.7, 118.6, 113.9, 113.7, 112.8, 112.5, 97.5, 94.2, 70.0, 33.6, 32.7, 31.1, 29.4, 22.3, 18.3. Elemental analysis calcd. for $\text{C}_{18}\text{H}_{20}\text{O}_3$: C, 76.03; H, 7.09; O, 16.88. Found: C, 76.07; H, 7.12.

6-(4-Fluorophenyl)tetrahydro-2H-pyran-2-ol (134a)



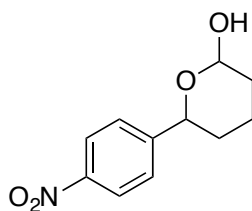
Prepared starting from allyl alcohol **129e** (374 mg, 1.91 mmol, 85% yield). **GC/MS** (m/z): 196.3, R_t = 16.523 min (Method A). **^1H NMR** (400 MHz, CDCl_3) δ 7.30 (dt, J = 8.9, 8.0 Hz, 4H), 6.99 (t, J = 7.8 Hz, 4H), 5.42 (s, 1H), 4.97 (d, J = 11.6 Hz, 1H), 4.85 (dd, J = 8.4, 6.9 Hz, 1H), 4.44 (d, J = 11.3 Hz, 1H), 3.02 (d, J = 5.9 Hz, 1H), 2.62 (s, 1H), 2.01 (t, J = 12.1 Hz, 1H), 1.98 – 1.85 (m, 2H), 1.84 – 1.62 (m, 6H), 1.51 – 1.31 (m, 3H). **^{13}C NMR** (151 MHz, CDCl_3) δ 162.9, 161.3, 138.8, 137.9, 127.8, 127.7, 127.6, 115.2, 115.1, 96.9, 92.4, 77.9, 70.5, 33.8, 32.8, 32.3, 29.4, 22.4, 17.8. Elemental analysis calcd. for $\text{C}_{11}\text{H}_{13}\text{FO}_2$: C, 67.33; H, 6.68; F, 9.68; O, 16.31. Found: C, 67.40; H, 6.73.

6-(4-Bromophenyl)tetrahydro-2H-pyran-2-ol (135a)



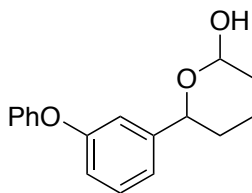
Prepared starting from allyl alcohol **129f** (231 mg, 0.90 mmol, 40% yield). **GC/MS** (m/z): 256.8-258.2 (Br isotopes), R_t = 20.251 min (Method A). **^1H NMR** (400 MHz, CDCl_3) δ 7.43 (dd, J = 8.4, 2.2 Hz, 4H), 7.22 (dd, J = 8.6, 2.1 Hz, 4H), 5.42 (s, 1H), 4.95 (d, J = 11.5 Hz, 1H), 4.88 – 4.78 (m, 1H), 4.43 (d, J = 11.1 Hz, 1H), 2.90 (d, J = 5.9 Hz, 1H), 2.51 (s, 1H), 2.06 – 1.99 (m, 1H), 1.93 (d, J = 11.4 Hz, 2H), 1.83 – 1.61 (m, 4H), 1.58 – 1.49 (m, 3H), 1.48 – 1.34 (m, 2H). **^{13}C NMR** (101 MHz, CDCl_3) δ 142.1, 141.1, 131.4, 128.0, 127.8, 127.6, 121.3, 121.1, 97.0, 92.4, 77.8, 70.5, 33.7, 32.7, 32.4, 29.4, 22.4, 17.8. Elemental analysis calcd. for $\text{C}_{11}\text{H}_{13}\text{BrO}_2$: C, 51.38; H, 5.10; Br, 31.08; O, 12.44. Found: C, 51.39; H, 5.10.

6-(4-Nitrophenyl)tetrahydro-2H-pyran-2-ol (136a)



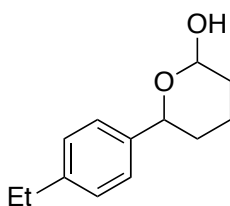
Prepared starting from allyl alcohol **129g** (205 mg, 0.92 mmol, 41% yield). **GC/MS** (m/z): 223.6 R_t = 19.357 min (Method A). **^1H NMR** (400 MHz, CDCl_3) δ 8.22-8.16 (m, 4H), 7.60-7.45 (m, 4H), 5.50 (s, 1H), 5.13 (dd, J = 12, 2.4 Hz, 1H), 4.95-4.90 (m, 1H), 4.61 (dd, J = 11.4, 2.2 Hz, 1H), 3.02 (bs, 1H), 2.62 (bs, 1H), 1.38-1.62 (m, 2H), 1.66-2.20 (m, 4H), 2.12-1.92 (m, 2H), 1.91-1.72 (m, 6H), 1.58-1.41 (m, 4H). **^{13}C NMR** (101 MHz, CDCl_3) δ 150.4, 149.2, 147.1, 147.0, 126.5, 123.5, 96.9, 92.2, 70.1, 33.8, 32.8, 32.1, 29.3, 22.3, 17.6.

1-(3-Phenoxyphenyl)tetrahydro-2H-pyran-2-ol (**137a**)



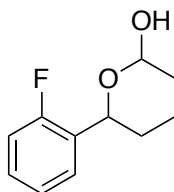
Prepared starting from allyl alcohol **129h** (474 mg, 1.76 mmol, 78% yield). **GC-MS** (m/z): 270.0, R_t = 22.205 min (Method B). **^1H NMR** (600 MHz, CDCl_3) δ 7.37 – 7.24 (m, 6H), 7.16 – 6.98 (m, 10H), 6.98 – 6.85 (m, 2H), 5.46 (s, 1H), 4.94 (d, J = 9.4 Hz, 1H), 4.80 (d, J = 10.4 Hz, 1H), 4.43 (d, J = 11.1 Hz, 1H), 3.76 (s, 1H), 2.55 (bs, 1H), 2.12 – 2.00 (m, 2H), 1.96 (s, 2H), 1.91 – 1.55 (m, 6H), 1.55 – 1.38 (m, 2H). **^{13}C NMR** (151 MHz, CDCl_3) δ 145.4, 144.4, 129.7, 123.2, 123.1, 120.9, 119.0, 118.8, 117.8, 117.8, 117.7, 116.8, 97.6, 94.2, 71.1 33.3, 32.6, 31.0, 29.5, 22.7, 18.2. Elemental analysis calcd. for $\text{C}_{17}\text{H}_{18}\text{O}_3$: C, 75.53; H, 6.71; O, 17.76. Found: C, 75.52; H, 6.67.

6-(4-Ethylphenyl)tetrahydro-2H-pyran-2-ol (**138a**)



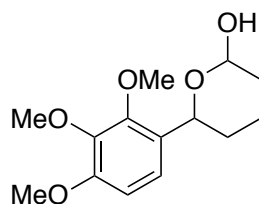
Prepared starting from allyl alcohol **129i** (338 mg, 1.64 mmol, 73% yield). **GC-MS** (m/z): 206.5, R_t = 18.824 min (Method B). **^1H NMR** (600 MHz, CDCl_3) δ 7.28 (dd, J = 12.8, 6.0 Hz, 4H), 7.22 – 7.14 (m, 4H), 5.47 (s, 1H), 4.93 (d, J = 9.3 Hz, 1H), 4.81 (d, J = 11.3 Hz, 1H), 4.44 (d, J = 11.0 Hz, 1H), 3.11 – 3.00 (m, 1H), 2.72 (dd, J = 15.0, 7.4 Hz, 1H), 2.65 (q, J = 6.8 Hz, 2H), 2.13 – 2.05 (m, 2H), 1.97 (d, J = 10.1 Hz, 2H), 1.92 – 1.59 (m, 6H), 1.59 – 1.41 (m, 2H), 1.24 (t, J = 7.7 Hz, 3H). **^{13}C NMR** (151 MHz, CDCl_3) δ 143.6, 141.3, 129.1, 128.2, 127.9 (2C), 125.9, 125.3, 97.6, 93.1, 70.9, 33.7, 32.7, 29.4, 28.6, 22.4, 17.7. Elemental analysis calcd. for $\text{C}_{13}\text{H}_{18}\text{O}_2$: C, 75.69; H, 8.80; O, 15.51. Found: C, 75.68; H, 8.78.

6-(2-Fluorophenyl)tetrahydro-2H-pyran-2-ol (**139a**)



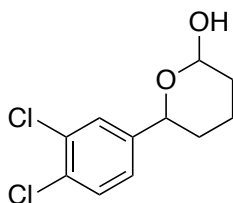
Prepared starting from allyl alcohol **129j** (229 mg, 1.17 mmol, 76% yield). **GC/MS** (m/z): 196.4, R_t = 16.242 min (Method A). **^1H NMR** (400 MHz, CDCl_3) δ 7.48 (dt, J = 30.3, 7.5 Hz, 2H), 7.25 – 7.15 (m, 2H), 7.10 (td, J = 6.9, 4.4 Hz, 2H), 7.03 – 6.93 (m, 2H), 5.41 (s, 1H), 5.35 (d, J = 11.6 Hz, 1H), 4.87 – 4.80 (m, 1H), 4.77 (d, J = 11.2 Hz, 1H), 3.57 (d, J = 5.7 Hz, 1H), 3.07 (s, 1H), 2.08 – 2.02 (m, 1H), 1.94 – 1.84 (m, 3H), 1.65 (m, 4H), 1.55 (dd, J = 11.8, 3.6 Hz, 1H), 1.48 – 1.35 (m, 3H). **^{13}C NMR** (151 MHz, CDCl_3) δ 160.6, 158.5, 130.1, 129.8, 128.8, 128.7, 127.4, 124.3, 123.9, 115.2, 115.1, 102.0, 97.7, 97.1, 93.1, 92.5, 71.8, 64.8, 32.4, 32.4, 31.8, 31.7, 29.7, 29.6, 29.5, 29.3, 22.7, 22.5, 18.4, 17.8. Elemental analysis calcd. for $\text{C}_{11}\text{H}_{13}\text{FO}_2$: C, 67.33; H, 6.68; F, 9.68; O, 16.31. Found: C, 67.37; H, 6.70.

6-(2,3,4-Trimethoxyphenyl)tetrahydro-2H-pyran-2-ol (**140a**)



Prepared starting from allyl alcohol **129k** (390 mg, 1.46 mmol, 65% yield). **GC-MS** (m/z): 267.9, R_t = 20.540 min (Method B). **^1H NMR** (600 MHz, CDCl_3) δ 7.18 (d, J = 8.7 Hz, 1H), 7.11 (d, J = 8.6 Hz, 1H), 6.69 (d, J = 8.6 Hz, 2H), 5.43 (s, 1H), 5.31 (d, J = 11.6 Hz, 1H), 4.89 (d, J = 9.3 Hz, 1H), 4.76 (d, J = 11.0 Hz, 1H), 3.89 (s, 6H), 3.85 (d, J = 4.7 Hz, 12H), 3.28 (bs, 1H), 2.85 (bs, 1H), 2.11 – 2.05 (m, 1H), 1.93 (d, J = 11.1 Hz, 2H), 1.85 (s, 2H), 1.83 – 1.65 (m, 3H), 1.65 – 1.53 (m, 2H), 1.51 – 1.37 (m, 2H). **^{13}C NMR** (151 MHz, CDCl_3) δ 141.9, 141.7, 129.1, 128.9, 128.6, 127.6, 125.3, 121.5, 121.3, 107.6, 107.5, 97.7, 93.2, 72.5, 65.2, 60.7, 56.0, 32.6, 31.2, 29.6, 25.9, 23.0, 18.7. Elemental analysis calcd. for $\text{C}_{14}\text{H}_{20}\text{O}$: C, 62.67; H, 7.51; O, 29.81. Found: C, 62.66; H, 7.46.

1-(3,4-Dichlorophenyl)tetrahydro-2H-pyran-2-ol (141a)



Prepared starting from allyl alcohol **129l** (138 mg, 0.56 mmol, 25% yield). **GC/MS** (m/z): 246.0 (246.9) -247.6 (248.5) (Cl isotopes), R_t = 18.550 min (Method B). **^1H NMR** (600 MHz, CDCl_3) δ 7.47 (d, J = 22.1 Hz, 2H), 7.42 – 7.36 (m, 2H), 7.17 (dd, J = 16.8, 8.2 Hz, 2H), 5.43 (s, 1H), 4.97 (d, J = 11.6 Hz, 1H), 4.85 (d, J = 9.6 Hz, 1H), 4.44 (d, J = 11.4 Hz, 1H), 2.77 (bs, 2H), 2.11 – 2.01 (m, 2H), 1.95 (t, J = 13.1 Hz, 2H), 1.87 – 1.63 (m, 4H), 1.55 – 1.48 (m, 2H), 1.46 – 1.38 (m, 2H). **^{13}C NMR** (151 MHz, CDCl_3) δ 143.4, 142.3, 132.4, 131.3, 131.1, 130.3, 128.1, 128.0, 125.4, 125.2, 96.9, 92.4, 69.9, 33.7, 32.7, 32.3, 29.4, 22.3, 17.7. Elemental analysis calcd. for $\text{C}_{11}\text{H}_{12}\text{Cl}_2\text{O}_2$: C, 53.47; H, 4.89; Cl, 28.69; O, 12.95. Found: C, 53.40; H, 4.85.

SECTION C - Bibliography

- [1] G. D. Lianos, K. Vlachos, O. Zoras, C. Katsios, W. C. Cho, D. H. Roukos, *Onco. Targets. Ther.* **2014**, *7*, 491–500.
- [2] B. Vogelstein, N. Papadopoulos, V. E. Velculescu, S. Zhou, L. A. Diaz, K. W. Kinzler, *Science* **2013**, *339*, 1546–1558.
- [3] N. Krall, J. Scheuermann, D. Neri, *Angew. Chem. Int. Ed.* **2013**, *52*, 1384–1402.
- [4] C. A. Klein, *Nature* **2013**, *501*, 365–372.
- [5] K. S. Bhullar, N. O. Lagarón, E. M. McGowan, I. Parmar, A. Jha, B. P. Hubbard, H. P. V. Rupasinghe, *Mol. Cancer* **2018**, *17*, 48–67.
- [6] N. Berndt, R. Karim, E. Schonbrunn, *Curr. Opin. Chem. Biol.* **2017**, *39*, 126–132.
- [7] R. Roskoski Jr., *Pharmacological Research* **2021**, *165*, 105463.
- [8] P. N. Nelson, G. M. Reynolds, E. E. Waldron, E. Ward, K. Giannopoulos, P. G. Murray, *Mol. Pathol.* **2000**, *53*, 111–117.
- [9] A. M. Scott, J. D. Wolchok, L. J. Old, *Nat. Rev. Cancer* **2012**, *12*, 278–287.
- [10] R. V. J. Chari, M. L. Miller, W. C. Widdison, *Angew. Chem. Int. Ed.* **2014**, *53*, 3796–3827.
- [11] A. Mullard, *Nat. Rev. Drug Discov.* **2021**, *20*(7), 491–495.
- [12] A. M. Scott, J. P. Allison, J. D. Wolchok, *Cancer Immun.* **2012**, *12*, 14–23.
- [13] G. J. Weiner, *Immunol. Res.* **2007**, *39*(1–3), 271–278.
- [14] M. Sadelain, I. Rivière, S. Riddell, *Nature* **2017**, *545*, 423–431.
- [15] T. Lammers, F. Kiessling, W. E. Hennink, G. Storm, *J. Control. Release* **2012**, *161*, 175–187.
- [16] C. Lee Ventola, *P&T* **2017**, *42*(12), 742–755.
- [17] G. Casi, D. Neri, *Mol. Pharmaceutics* **2015**, *12*, 1880–1884.
- [18] D. Neri, C. T. Supuran, *Nat. Rev. Drug Discov.* **2011**, *10*, 767–777.
- [19] V. Chudasama, A. Maruani, S. Caddick, *Nat. Chem.* **2016**, *8*, 114–119.
- [20] E. Cini, V. Faltoni, E. Petricci, M. Taddei, G. Giannini, L. Vesci, F. M. Milazzo, A. M. Anastasi, G. Battistuzzi, R. De Santis, *Chem. Sci.*, **2018**, *9*, 6490–6496.
- [21] P. A. Trail, *Antibodies* **2013**, *2*, 113–129.
- [22] A. H. Staudacher, M. P. Brown, *Br. J. Cancer* **2017**, *117*, 1736–1742.
- [23] P. D. Senter, E. L. Sievers, *Nat. Biotechnol.* **2012**, *30*, 631–637.
- [24] E. Perrino, M. Steiner, N. Krall, G. J. L. Bernardes, F. Pretto, G. Casi, D. Neri, *Cancer Res.* **2014**, *74*, 2569–2578.
- [25] A. Q. Dean, S. Luo, J. D. Twomey, B. Zhang, *mAbs* **2021**, *13*(1), e1951427–23.

- [26] A. Younes, U. Yasothan, P. Kirkpatrick, *Nat. Rev. Drug Discov.* **2012**, *11*, 19–20.
- [27] P. D. Senter, E. L. Sievers, *Nat. Biotechnol.* **2012**, *30*, 631–637.
- [28] J. M. Lambert, R. V. J. Chari, *J. Med. Chem.* **2014**, *57*, 6949–6964.
- [29] Y. N. Lamb, *Drugs* **2017**, *77*, 1603–1610.
- [30] A. D. Ricart, *Clin. Cancer Res.* **2011**, *17*, 6417–6427.
- [31] F. Fauteux, J. J. Hill, M. L. Jaramillo, Y. Pan, S. Phan, F. Famili, M. O'Connor-McCourt, *Oncotarget* **2016**, *7*, 2555–2571.
- [32] T. H. Han, B. Zhao, S. Centrx, S. S. Francisco, S. Genetics, *Drug Metab. Dispos.* **2014**, *42*, 1914–1920.
- [33] T. T. Junttila, G. Li, K. Parsons, G. L. Phillips, M. X. Sliwkowski, *Breast Cancer Res. Treat.* **2011**, *128*, 347–356.
- [34] G. Vidarsson, G. Dekkers, T. Rispens, *Front. Immunol.* **2014**, *5*, 520–536.
- [35] Y. T. Tai, et al., *Blood* **2014**, *123*, 3128–3138.
- [36] J. R. McCombs, S. C. Owen, *AAPS J.* **2015**, *17*, 339–351.
- [37] H. K. Erickson, W. C. Widdison, M. F. Mayo, K. Whiteman, C. Audette, S. D. Wilhelm, R. Singh, *Bioconjug. Chem.* **2010**, *21*, 84–92.
- [38] C. Chalouni, S. Doll, *J. Exp. Clin. Cancer Res.* **2018**, *37*, 20–21.
- [39] S. O. Doronina, et al., *Bioconjug. Chem.* **2006**, *17*, 114–124.
- [40] X. Zhang, X. Li, Z. Li, X. Wu, Y. Wu, Q. You, X. Zhang, *Org. Lett.* **2018**, *20*, 3635–3638.
- [41] S. O. Doronina, et al., *Nat. Biotechnol.* **2003**, *21*, 778–784.
- [42] J. Kalia, R. T. Raines, *Angew. Chem. Int. Ed.* **2008**, *47*(39), 7523–7526.
- [43] R. Tong, L. Tang, L. Ma, C. Tu, R. Baumgartner, J. Cheng, *Chem. Soc. Rev.* **2014**, *43*(20), 6982–7012.
- [44] R. Patil, et al., *Int. J. Mol. Sci.* **2012**, *13* (9), 11681–11693.
- [45] Y. Ruan, et al., *Kidney Int.* **2014**, *86* (3), 525–537.
- [46] P. R. Hamann, et al., *Bioconjug. Chem.* **2002**, *13*(1), 47–58.
- [47] A. Paci, A. Desnoyer, J. Delahousse, L. Blondel, C. Maritaz, N. Chaput, O. Mir, S. Broutin, *Eur. J. Cancer.* **2020**, *128*, 107–118.
- [48] Y. Jin, L. Song, Y. Su, L. Zhu, Y. Pang, F. Qiu, G. Tong, D. Yan, B. Zhu, X. Zhu, *Biomacromolecules* **2011**, *12*(10), 3460–3468.
- [49] Y. Zheng, J. Ren, Y. Wu, X. Meng, Y. Zhao, C. Wu, *Bioconjug. Chem.* **2017**, *28*(10), 2620–2626.

- [50] X. Yang, Z. Pan, M. R. Choudhury, Z. Yuan, A. Anifowose, B. Yu, W. Wang, B. Wang, *Med. Res. Rev.* **2020**, *40*, 2682–2713.
- [51] C. J. Choy, J. J. Geruntho, A. L. Davis, C. E. Berkman, *Bioconjug. Chem.* **2016**, *27*(3), 824-830.
- [52] S. A. Jacques, G. Leriche, M. Mosser, M. Nothisen, C. D. Muller, J.-S. Remy, A. Wagner, *Org. Biomol. Chem.* **2016**, *14*(21), 4794-4803.
- [53] P. Deslongchamps, Y. L. Dory, S. Li, *Tetrahedron* **2000**, *56*(22), 3533-3537.
- [54] G. Leriche, M. Nothisen, N. Baumlin, C. D. Muller, D. Bagnard, J. S. Remy, S. A. Jacques, A. Wagner, *Bioconjug. Chem.* **2015**, *26*(8), 1461-1465.
- [55] E. Dinand, M. Zloh, S. Brocchini, *Aust. J. Chem.* **2002**, *55*(7), 467-474.
- [56] A. Zhang, L. Yao, M. An, *Chem. Commun.* **2017**, *53*(95), 12826-12829.
- [57] A. J. Kirby, P. W. Lancaster, *J. Chem. Soc. Perkin Trans.* **1972**, *2*(9), 1206-1214.
- [58] A. Godwin, A. Meister, P. J. Odwyer, C. S. Huang, T. C. Hamilton, M. E. Anderson, *Proc. Natl. Acad. Sci. USA* **1992**, *89*(7), 3070-3074.
- [59] J. Lu, F. Jiang, A. Lu, G. Zhang, *Int. J. Mol. Sci.* **2016**, *17*, 561–584.
- [60] B. A. Kellogg, et al., *Bioconjug. Chem.* **2011**, *22*, 717–727.
- [61] P. G. Lewis, et al., *Cancer Res.* **2008**, *68*(22), 9280-9290.
- [62] P. Ray, B. Huang, Y. Tsuji, *Cell. Signal.* **2012**, *24*(5), 981-990.
- [63] G. Liou, P. Storz, *Free Radical Res.* **2010**, *44*(5), 479-496.
- [64] G. Saravanakumar, J. Kim, W. Kim, *Adv. Sci.* **2017**, *4*(1), 1600124.
- [65] X. Peng, V. Gandhi, *Ther. Deliv.* **2012**, *3*(7), 823-833.
- [66] G. D. Heggie, J. P. Sommadossi, D. S. Cross, W. J. Huster, R. B. Diasio, *Cancer Res.* **1987**, *47*(8), 2203-2206.
- [67] M. Koh, K. Makoto, I. Kazuyuki, F. Wataru, N. Takeshi, O. Hitoshi, A. Toshinori, Y. Nobuki, W. Kazuhiro, H. Sho, S. Chikashi, S. Iwao, *Cancers (Basel)* **2010**, *2*(3), 1717-1730.
- [68] Y. Ai, O. N. Obianom, M. Kuser, Y. Li, Y. Shu, F. T. Xue, *ACS Med. Chem. Lett.* **2019**, *10*(1), 127-131.
- [69] Y. Kuang, K. Balakrishnan, V. Gandhi, X. Peng, *J. Am. Chem. Soc.* **2011**, *133*(48), 19278-19281.
- [70] X. Peng, V. Gandhi, *Ther. Delivery* **2012**, *3*(7), 823-833.
- [71] S. A. Nuñez, K. Yeung, N. S. Fox, S. T. Phillips, *J. Org. Chem.* **2011**, *76*, 10099–10113.
- [72] Q. H. Xu, C. L. He, C. S. Xiao, X. S. Chen, *Macromol. Biosci.* **2016**, *16*(5), 635-646.

- [73] M. S. Shim, Y. Xia, *Angew. Chem. Int. Ed.* **2013**, 52(27), 6926-6929.
- [74] P. Pei, C. Sun, W. Tao, J. Li, X. Yang, J. Wang, *Biomaterials* **2019**, 188, 74-82.
- [75] V. Taresco, C. Alexander, N. Singh, A. K. Pearce, *Adv. Ther.* **2018**, 1, 4.
- [76] B. Liu, D. L. Wang, Y. K. Liu, Q. Zhang, L. Meng, H. Chi, J. Shi, G. Li, J. Li, X. Zhu, *Polym. Chem-Uk* **2015**, 6(18), 3460-3471.
- [77] J. Noh, B. Kwon, E. Han, M. Park, W. Yang, W. Cho, W. Yoo, G. Khang, D. Lee, *Nat. Commun.* **2015**, 6, 6907.
- [78] T. L. Andresen, D. H. Thompson, T. Kaasgaard, *Mol. Membr. Biol.* **2010**, 27(7), 353-363.
- [79] C. S. Gondi, J. S. Rao, *Expert Opin. Ther. Targets* **2013**, 17(3), 281-291.
- [80] S. R. Denmeade, A. Nagy, J. Gao, H. Lilja, A. V. Schally, J. T. Isaacs, *Cancer Res.* **1998**, 58(12), 2537-2540.
- [81] J. A. Richard, Y. Meyer, V. Jolivel, M. Massonneau, R. Dumeunier, D. Vaudry, H. Vaudry, P. Y. Renard, A. Romieu, *Bioconjug. Chem.* **2008**, 19(8), 1707-1718.
- [82] J. Katz, J. E. Janik, A. Younes, *Clin. Cancer Res.* **2011**, 17(20), 6428-6436.
- [83] R. J. Sanderson, M. A. Hering, S. F. James, M. M. C. Sun, S. O. Doronina, A. W. Siadak, P. D. Senter, A. F. Wahlln, *Clin. Cancer Res.* **2005**, 11(2), 843-852.
- [84] G. G. Bornstein, *AAPS J.* **2015**, 17(3), 525-534.
- [85] G. M. Dubowchik, R. A. Firestone, L. Padilla, D. Willner, S. J. Hofstead, K. Mosure, J. O. Knipe, S. J. Lasch, P. A. Trail, *Bioconjug. Chem.* **2002**, 13(4), 855-869.
- [86] R. M. Sharkey, S. V. Govindan, T. M. Cardillo, D. M. Goldenberg, *Mol. Cancer Ther.* **2012**, 11, 224-234.
- [87] Y. Anami, C. M. Yamazaki, W. Xiong, X. Gui, N. Zhang, Z. An, K. Tsuchikama, *Nat. Commun.* **2018**, 9(1), 2512.
- [88] Y. Wang, S. Fan, W. Zhong, X. Zhou, S. Li, *Int. J. Mol. Sci.* **2017**, 18, 1860.
- [89] Y. Y. Di, S. P. Ji, P. Wolf, E. S. Krol, J. Alcorn, *AAPS PharmSciTech* **2017**, 18(6), 2336-2345.
- [90] S. C. Jeffrey, J. B. Andreyka, S. X. Bernhardt, K. M. Kissler, T. Kline, J. S. Lenox, R. F. Moser, M. T. Nguyen, N. M. Okeley, I. J. Stone, X. Zhang, P. D. Senter, *Bioconjug. Chem.* **2006**, 17, 831-840.
- [91] P. J. Burke, P. D. Senter, D. W. Meyer, J. B. Miyamoto, M. Anderson, B. E. Toki, G. Manikumar, M. C. Wani, D. J. Kroll, S. C. Jeffrey, *Bioconjug. Chem.* **2009**, 20, 1242-1250.
- [92] S. C. Jeffrey, J. De Brabander, J. Miyamoto, P. D. Senter, *ACS Med. Chem. Lett.* **2010**,

1(6), 277-280.

- [93] N. K. Devaraj, R. Upadhyay, J. B. Hatin, S. A. Hilderbrand, R. Weissleder, *Angew. Chem. Int. Ed.* **2009**, 48(38), 7013-7016.
- [94] R. Rossin, S. M. van Duijnhoven, T. Lappchen, S. M. van den Bosch, M. S. Robillard, *Mol. Pharm.* **2014**, 11(9), 3090-3096.
- [95] X. Ji, Z. Pan, B. Yu, L. K. De La Cruz, Y. Zheng, B. Ke, B. Wang, *Chem. Soc. Rev.* **2019**, 48(4), 1077-1094.
- [96] M. De Geus, et al., *Synlett.* **2018**, 29(18), A180-A184.
- [97] P. Wang, et al., *Int. J. Biol. Sci.* **2016**, 12, 1000-1009.
- [98] S. Matikonda, D. Orsi, V. Staudacher, I. A. Jenkins, F. Fiedler, J. Chen, A. B. Gamble, *Chem. Sci.* **2015**, 6(2), 1212-1218.
- [99] P. Sustmann, D. Trill, *Angew. Chem. Int. Ed.* **1972**, 11(9), 838-840.
- [100] R. Versteegen, R. Rossin, W. Ten Hoeve, H. Janssen, M. Robillard, *Angew. Chem. Int. Ed.* **2013**, 52(52), 14112-14116.
- [101] R. Rossin, S. van Duijnhoven, W. Ten Hoeve, H. M. Janssen, L. H. J. Kleijn, F. J. M. Hoeben, R. M. Versteegen, M. S. Robillard, *Bioconjug. Chem.* **2016**, 27(7), 1697-1706.
- [102] X. Fan, Y. Ge, F. Lin, Y. Yang, G. Zhang, W. S. C. Ngai, Z. Lin, S. Zheng, J. Wang, J. Zhao, J. Li, P. R. Chen, *Angew. Chem. Int. Ed.* **2016**, 55(45), 14046-14050.
- [103] M. Peplow, *Nat. Biotechnol.* **2019**, 37, 829-841.
- [104] A. Alouane, R. Labruère, T. Le Saux, F. Schmidt, L. Jullien, *Angew. Chemie Int. Ed.* **2015**, 54, 7492-7509.
- [105] R. Walther, J. Rautio, A. N. Zelikin, *Adv. Drug Deliv. Rev.* **2017**, 118, 65-77.
- [106] M. Gisbert-Garzarán, M. Manzano, M. Vallet-Regí, *Chem. Eng. J.* **2017**, 340, 24-31.
- [107] J. S. Robbins, K. M. Schmid, S. T. Phillips, *J. Org. Chem.* **2013**, 78, 3159-3169.
- [108] E. E. Weinert, R. Dondi, S. Colloredo-Melz, K. N. Frankenfield, C. H. Mitchell, M. Freccero, S. E. Rokita, *J. Am. Chem. Soc.* **2006**, 128, 11940-11947.
- [109] M. Shamis, H. N. Lode, D. Shabat, *J. Am. Chem. Soc.* **2004**, 126, 1726-1731.
- [110] V. Kostova, P. Désos, J. B. Starck, A. Kotschy, *Pharmaceuticals* **2021**, 14, 442.
- [111] S. V. Govindan, T. M. Cardillo, R. M. Sharkey, F. Tat, D. V. Gold, D. M. Goldenberg, *Mol. Cancer Ther.* **2013**, 12, 968-978.
- [112] B. E. Toki, C. G. Cervený, A. F. Wahl, P. D. Senter, *J. Org. Chem.* **2002**, 67, 1866-1872.

- [113] M. M. C. van der Lee, et al., *Mol. Cancer Ther.* **2015**, *14*, 692–703.
- [114] R. V. Kolakowski, K. T. Haelsig, K. K. Emmerton, C. I. Leiske, J. B. Miyamoto, J. H. Cochran, R. P. Lyon, P. D. Senter, S. C. Jeffrey, *Angew. Chemie Int. Ed.* **2016**, *55*, 7948–7951.
- [115] A. Dal Corso, L. Pignataro, L. Belvisi, C. Gennari, *Chem. Eur. J.* **2019**, *25*, 14740–14757.
- [116] Y. Ogitani, et al., *Clin. Cancer Res.* **2016**, *22*, 5097–5108.
- [117] A. Dal Corso, V. Borlandelli, C. Corno, P. Perego, L. Belvisi, L. Pignataro, C. Gennari, *Angew. Chem.* **2020**, *132*, 4205 – 4210.
- [118] W. Feng, C. Gao, W. Liu, H. Ren, C. Wang, K. Ge, S. Li, G. Zhou, H. Li, S. Wang, G. Jia, Z. Liab, J. Zhang, *Chem. Commun.* **2016**, *52*, 9434–9437.
- [119] Y. Meyer, J. A. Richard, B. Delest, P. Noack, P. Y. Renard, A. Romieu, *Org. Biomol. Chem.* **2010**, *8*(8), 1777–1780.
- [120] R. P. Lyon, T. D. Bovee, S. O. Doronina, P. J. Burke, J. H. Hunter, H. D. Neff- LaFord, M. Jonas, M. E. Anderson, J. R. Setter, P. D. Senter, *Nat. Biotechnol.* **2015**, *33*, 733–735.
- [121] R. Y. Zhao, S. D. Wilhelm, C. Audette, G. Jones, B. A. Leece, A. C. Lazar, V. S. Goldmacher, R. Singh, Y. Kovtun, W. C. Widdison, J. M. Lambert, R. V. J. Chari, *J. Med. Chem.* **2011**, *54*, 3606–3623.
- [122] Y. Kovtun, et al., *Mol. Cancer Ther.* **2018**, *17*, 1271– 1279.
- [123] J. C. Kern, et al., *J. Am. Chem. Soc.* **2016**, *138*, 1430–1445.
- [124] D. K. Shah, A. M. Betts, *MAbs* **2013**, *5*, 297–305.
- [125] H. Bouchard, C. Viskov, C. Garcia-Echeverria, *Bioorg. Med. Chem. Lett.* **2014**, *24*, 5357–5363.
- [126] S. M. Kupchan, Y. Komoda, W. A. Court, G. J. Thomas, R. M. Smith, A. Karim, C. J. Gilmore, R. C. Haitiwanger, R. F. Bryan, *J. Am. Chem. Soc.* **1972**, *94*, 1354–1356.
- [127] W. C. Widdison, et al., *J. Med. Chem.* **2006**, *49*, 4392–4408.
- [128] M. P. Johansson, H. Maaheimo, F. S. Ekholm, *Sci. Rep.* **2017**, *7*, 15920–15929.
- [129] G. R. Pettit, Y. Kamano, C. L. Herald, A. A. Tuinman, F. E. Boettner, H. Kizu, J. M. Schmidt, L. Baczynskyi, K. B. Tomer, R. J. Bontems, *J. Am. Chem. Soc.* **1987**, *109*, 6883–6885.
- [130] S. O. Doronina, B. A. Mendelsohn, T. D. Bovee, C. G. Cervený, S. C. Alley, D. L. Meyer, E. Oflazoglu, B. E. Toki, R. J. Sanderson, R. F. Zabinski, A. F. Wahl, P. D. Senter, *Bioconjug. Chem.* **2006**, *17*, 114–124.
- [131] A. Maderna, C. A. Leverett, *Mol. Pharm.* **2015**, *12*, 1798–1812.

- [132] W. M. Maiese, M. P. Lechevalier, H. A. Lechevalier, J. Korshalla, N. Kuck, A. Fantini, M. J. Wildey, J. Thomas, M. Greenstein, *J. Antibiot.* **1989**, *42*, 558–563.
- [133] G. A. Ellestad, *Chirality* **2011**, *23*, 660–671.
- [134] B. Shen, X. Yan, T. Huang, H. Ge, D. Yang, Q. Teng, J. D. Rudolf, J. R. Lohman, *Bioorganic Med. Chem. Lett.* **2015**, *25*, 9–15.
- [135] Z. Pei, et al., *Mol. Pharm.* **2018**, *51*, 3979–3996.
- [136] W. Leimgruber, V. Stefanovic, F. Schenker, A. Karr, J. Berger, *J. Am. Chem. Soc.* **1965**, *87*, 5791–5793.
- [137] M. L. Miller, et al., *Mol. Cancer Ther.* **2016**, *15*, 1870–1878.
- [138] J. Mantaj, P. J. M. Jackson, K. M. Rahman, D. E. Thurston, *Angew. Chemie Int. Ed.* **2017**, *56*, 462–488.
- [139] U. Y. Lau, L. T. Benoit, N. S. Stevens, K. K. Emmerton, M. Zaval, J. H. Cochran, P. Senter, *Mol. Pharm.* **2018**, *15*, 4063–4072.
- [140] T. Yasuzawa, T. Iida, K. Muroi, M. Ichimura, K. Takahashi, H. Sano, *Chem. Pharm. Bull.* **1988**, *36*, 3728–3731.
- [141] L. Nathan Tumey, et al., *ACS Med. Chem. Lett.* **2016**, *7*, 977–982.
- [142] J. Y. Li, et al., *Cancer Cell* **2016**, *29*, 117–129.
- [143] Y. Liu, et al., *Nature* **2015**, *520*, 697–701.
- [144] S. V. Govindan, T. M. Cardillo, R. M. Sharkey, F. Tat, D. V. Gold, D. M. Goldenberg, *Mol. Cancer Ther.* **2013**, *12*, 968–978.
- [145] S. C. N. Queiroz, M. R. Assalin, S. Nobre, I. S. Melo, R. M. Moraes, V. L. Ferracini, A. L. Cerdeira, *Planta Med.* **2012**, *76*, 53.
- [146] G. M. Cragg, D. J. Newman, D. G. I. Kingston, *Chem. Biol.* **2010**, *2*, 5–39.
- [147] R. R. Nani, A. P. Gorka, T. Nagaya, H. Kobayashi, M. J. Schenermann, *Angew. Chem. Int. Ed.* **2015**, *54*, 13635–13638.
- [148] B. E. Toki, C. G. Cervený, A. F. Wahl, P. D. Senter, *J. Org. Chem.* **2002**, *67*, 866–1872.
- [149] R. Huang, Y. Sheng, Z. Xu, D. Wei, X. Song, B. Jiang, H. Chen, *Eur. J. Med. Chem.* **2021**, *216*, 113355.
- [150] E. E. Hull, M. R. Montgomery, K. J. Leyva, *Biomed Res. Int.* **2016**, 1–15.
- [151] H. J. Kim, S. C. Bae, *Am. J. Transl. Res.* **2011**, *3*(2), 166–179.
- [152] C. Zagni, G. Floresta, G. Monciino, A. Rescifina, *Med. Res. Rev.* **2017**, *37*, 1373–1428.
- [153] S. Yoon, G. Eom, *Chonnam Med. J.* **2016**, *52*, 1–11.
- [154] G. Giannini, et al., *J. Med. Chem.* **2014**, *57*, 8358–8377.
- [155] L. Vesci, E. Bernasconi, F. M. Milazzo, R. De Santis, E. Gaudio, I. Kwee, A. Rinaldi,

- S. Pace, V. Carollo, G. Giannini, F. Bertoni, *Oncotarget* **2015**, *6*, 5735–5748.
- [156] R. Badia, J. Grau, E. Riveira-Muñoz, E. Ballana, G. Giannini, J. A. Esté, *Antiviral Res.* **2015**, *123*, 62–69.
- [157] C. Cianferotti, V. Faltoni, E. Cini, E. Ermini, F. Migliorini, E. Petricci, M. Taddei, L. Salvini, G. Battistuzzi, F. M. Milazzo, A. M. Anastasi, C. Chiapparino, R. De Santis, G. Giannini, *Chem. Commun.* **2021**, *57*, 867–870.
- [158] R. Liu, R. E. Wang, F. Wang, *Expert Opin. Biol. Ther.* **2016**, *16*, 591–593.
- [159] P. E. Brandish, et al., *Bioconjug. Chem.* **2018**, *29*, 2357–2369.
- [160] J. H. Graversen, P. Svendsen, F. Dagnæs-Hansen, J. Dal, G. Anton, A. Etzerodt, M. D. Petersen, P. A. Christensen, H. J. Møller, S. K. Moestrup, *Mol. Ther.* **2012**, *20*, 1550–1558.
- [161] R. E. Wang, T. Liu, Y. Wang, Y. Cao, J. Du, X. Luo, V. Deshmukh, C. H. Kim, B. R. Lawson, M. S. Tremblay, T. S. Young, S. A. Kazane, F. Wang, P. G. Schultz, *J. Am. Chem. Soc.* **2015**, *137*, 3229–3232.
- [162] S. M. Lehar, et al., *Nature* **2015**, *527*, 323–332.
- [163] F. Li, K. K. Emmerton, M. Jonas, X. Zhang, J. B. Miyamoto, J. R. Setter, N. D. Nicholas, N. M. Okeley, R. P. Lyon, D. R. Benjamin, C. L. Law, *Cancer Res.* **2016**, *76*, 2710–2719.
- [164] A. P. Singh, S. Sharma, D. K. Shah, *J. Pharmacokinet. Pharmacodyn.* **2016**, *43*, 567–582.
- [165] S. M. Horwitz, R. H. Advani, N. L. Bartlett, E. D. Jacobsen, J. P. Sharman, O. A. O'Connor, T. Siddiqi, D. A. Kennedy, Y. Oki, *Blood* **2014**, *123*, 3095–3100.
- [166] S. Masuda, S. Miyagawa, N. Sougawa, Y. Sawa, *Nat. Rev. Clin. Oncol.* **2015**, *12*, 245.
- [167] S. Golfier, et al., *Mol. Cancer Ther.* **2014**, *13*, 1537–1548.
- [168] R. M. Sharkey, H. Karacay, S. V. Govindan, D. M. Goldenberg, *Mol. Cancer Ther.* **2011**, *10*, 1072–1081.
- [169] G. J. L. Bernardes, G. Casi, S. Trüssel, I. Hartmann, K. Schwager, J. Scheuermann, D. Neri, *Angew. Chemie Int. Ed.* **2012**, *51*, 941–944.
- [170] R. Gébleux, M. Stringhini, R. Casanova, A. Soltermann, D. Neri, *Int. J. Cancer* **2017**, *140*, 1670–1679.
- [171] A. Dal Corso, S. Cazzamalli, R. Gébleux, M. Mattarella, D. Neri, *Bioconjug. Chem.* **2017**, *28*, 1826–1833.
- [172] H. Fuchigami, S. Manabe, M. Yasunaga, Y. Matsumura, *Sci. Rep.* **2018**, *8*, 14211–14219.
- [173] T. Kline, A. R. Steiner, K. Penta, A. K. Sato, T. J. Hallam, G. Yin, *Pharm. Res.* **2015**, *32*, 3480–3493.

- [174] M. Dorywalska, et al., *Bioconjug. Chem.* **2015**, 26, 650–659.
- [175] F. Hillenkamp, M. Karas, R. C. Beavis, B. T. Chait, *Anal. Chem.* **1991**, 63, 1193–1202.
- [176] S. Quiles, K. P. Raisch, L. L. Sanford, J. A. Bonner, A. Safavy, *J. Med. Chem.* **2010**, 53, 586–594.
- [177] K. Tsuchikama, Z. An, *Protein Cell.* **2018**, 9, 33–46.
- [178] B. Q. Shen, et al., *Nat. Biotechnol.* **2012**, 30, 184–189.
- [179] R. P. Lyon, J. R. Setter, T. D. Bovee, S. O. Doronina, J. H. Hunter, M. E. Anderson, C. L. Balasubramanian, S. M. Duniho, C. I. Leiske, F. Li, P. D. Senter, *Nat. Biotechnol.* **2014**, 32, 1059–1062.
- [180] L. N. Tumey, M. Charati, T. He, E. Sousa, D. Ma, X. Han, T. Clark, J. Casavant, F. Loganzo, F. Barletta, J. Lucas, E. I. Graziani, *Bioconjug. Chem.* **2014**, 25, 1871–1880.
- [181] D. Shinmi, E. Taguchi, J. Iwano, T. Yamaguchi, K. Masuda, J. Enokizono, Y. Shiraishi, *Bioconjug. Chem.* **2016**, 27, 1324–1331.
- [182] I. Dovgan, S. Kolodych, O. Koniev, A. Wagner, *Sci. Rep.* **2016**, 6, 30835–30840.
- [183] C. Nusslein-Volhard, E. Wieschaus, *Nature* **1987**, 287, 795–801.
- [184] D. Jenkins, *Cell. Sign.* **2009**, 21, 1023–1034.
- [185] G. S. van den Brink, *Physiol. Rev.* **2007**, 87, 1343–1375.
- [186] Y. Echelard, D. J. Epstein, B. St-Jacques, L. Shen, J. Mohler, J. A. McMahon, A. P. McMahon, *Cell* **1993**, 75, 1417–1430.
- [187] D. Huangfu, K. V. Anderson, *Development* **2006**, 133(1), 3–14.
- [188] K. L. Ayers, P. P. Therond, *Trends Cell Biol.* **2010**, 20, 287–298.
- [189] R. Rohatgi, L. Milenkovic, M. P. Scott *Science* **2007**, 317, 372 – 376.
- [190] A. Liu, B. Wang, L. A. Niswander, *Development* **2005**, 132, 3103–3111.
- [191] K. D. Marini, B. J. Payne, D. Neilwatkins, G. Martellotto, *Growth Factor* **2011**, 29, 221–234.
- [192] S. Y. Cheng, S. Yue, *Adv. Cancer Res.* **2008**, 101, 29–43.
- [193] S. J. Scales, F. J. De Sauvage, *Rev. Pharmacol. Sci.* **2009**, 30, 303–312.
- [194] D. Jenkins, *Cell. Sign.* **2009**, 21, 1023–1034.
- [195] S. Pandolfi, B. Stecca, *Expert Rev. Mol. Med.* **2015**, 17, 1–36.
- [196] Q. Bai, Y. Shen, N. Jin, H. Liu, X. Yao, *Biochim. Biophys. Acta* **2014**, 1840, 2128–2138.
- [197] C. Wang, H. Wu, V. Katritch, G. W. Han, X. Huang, W. Liu, F. Y. Siu, B. L. Roth, V. Cherezov, R. C. Stevens, *Nature* **2013**, 497, 338–343.

- [198] J. K. Winkler, A. Isaacs, L. Holderbaum, V. Tatard, N. Dahmane, *Org. Lett.* **2009**, *11*, 2824-2827.
- [199] P. Sanchez, A. R. i Albata, *Mech. Dev.* **2005**, *122*, 223-230.
- [200] R. Nagata, K. Izumi, *Jpn. J. Pharmacol.* **1991**, *55*, 129– 137.
- [201] E. Petricci, F. Manetti, *Curr. Med. Chem.* **2015**, *22*, 1-34.
- [202] https://www.accessdata.fda.gov/drugsatfda_docs/label/2012/203388lbl.pdf
- [203] S. Sandhiya, G. Melvin, S. S. Kumar, S. A. Dkhar, *Rev. J. Pharmacol. Pharmacother.* **2013**, *4*, 4-7.
- [204] A. Samkari, J. White, R. Packer, *Expert Rev. Neurother* **2015**, 1-8.
- [205] https://www.accessdata.fda.gov/drugsatfda_docs/label/2016/205266s002lbl.pdf
- [206] S. Pan, X. Wu, J. Jiang, W. Gao, Y. Wan, D. Cheng, D. Han, J. Liu, N. P. Englund, Y. Wang, *ACS Med. Chem. Lett.* **2010**, *1*, 130-134.
- [207] C. D'Amato, R. Rosa, R. Marciano, V. D'Amato, L. Formisano, L. Nappi, L. Raimondo, C. Di Mauro, A. Servetto, F. Fulciniti, *Br. J. Cancer* **2014**, *111*, 1168-1179.
- [208] T. K. Rimkus, R. L. Carpenter, S. Qasem, M. Chan, H. W. Lo, *Cancers* **2015**, *8*, 22.
- [209] Y. Minami, F. Hayakawa, H. Kiyoi, A. Sadarangani, C. H. Jamieson, T. Naoe, *Blood* **2013**, *122*, 1649.
- [210] M. J. Munchhof, Q. Li, A. Shavnya, G. V. Borzillo, T. L. Boyden, C. S. Jones, S. D. LaGreca, L. Martinez-Alsina, N. Patel, K. Pelletier, *ACS Med. Chem. Lett.* **2012**, *3*, 106-111.
- [211] W. Lu, et al., *ACS Chem. Neurosci.* **2017**, A-O.
- [212] D. Amakye, Z. Jagani, M. Dorsch, *Rev. Nat. Med.* **2013**, *11*, 1410-1422.
- [213] S. Pietrobono, B. Stecca, *Cells* **2018**, *7*, 272.
- [214] A. Solinas, H. Faure, H. Roudaut, E. Traffort, A. Schoenfelder, A. Mann, F. Manetti, M. Taddei, M. Ruat, *J. Med. Chem.* **2012**, *55*, 1559-1571.
- [215] H. Roudaut, E. Traffort, T. Goropankina, L. Vincent, H. Faure, A. Schoenfelder, A. Mann, F. Manetti, A. Solinas, M. Taddei, M. Ruat, *Mol. Pharmacol.* **2011**, *79*, 453-460.
- [216] L. Hoch, H. Faure, H. Roudaut, A. Schoenfelder, A. Mann, N. Girard, L. Bihannic, O. Ayrault, E. Petricci, M. Taddei, D. Rognan, M. Ruat, *FASEB J*, **2015**, *29*, 1817-1829.
- [217] A. Chiarenza, F. Manetti, E. Petricci, M. Ruat, A. Naldini, M. Taddei, F. Carraro, *PLoS One* **2016**, *11*(3), e0149919/1-e0149919/19.
- [218] S. Pietrobono, R. Santini, S. Gagliardi, F. Dapporto, D. Colecchia, M. Chiariello, C. Leone, M. Valoti, F. Manetti, E. Petricci, M. Taddei, B. Stecca, *Cell Death and Disease* **2018**, *9*(2), 142.

- [219] S. Pietrobono, E. Gaudio, S. Gagliardi, M. Zitani, L. Carrassa, F. Migliorini, E. Petricci, F. Manetti, N. Makukhin, A. G. Bond, B. D. Paradise, A. Ciulli, M. E. Fernandez-Zapico, F. Bertoni, B. Stecca, *Oncogene*, **2021**, *40*, 3799-3814.
- [220] J. D. Bargh, A. Isidro-Llobet, J. S. Parker, D. R. Spring, *Chemical Society reviews* **2019**, *48*, 4361-4374.
- [221] C. J. Choy, J. J. Geruntho, A. L. Davis, C. E. Berkman, *Bioconjugate chemistry* **2016**, *27*, 824-830.
- [222] C. Fattorusso, et al., *J. Med. Chem.* **2008**, *51*(5), 1333–1343.
- [223] S. A. Adediran, D. Cabaret, B. Drouillat, R. F. Pratta, M. Wakselmanb, *Bioorg. Med. Chem.* **2001**, *9*, 1175-1183.
- [224] B. Kemper, M. Von Gröning, V. Lewe, D. Spitzer, T. Otremba, N. Stergiou, D. Schollmeyer, E. Schmitt, B. J. Ravoo, P. Besenius, *Chem. Eur. J.* **2017**, *23*, 6048-6055.
- [225] R. M. Stolz, B. H. Northrop, *J. Org. Chem.* **2013**, *78*(16), 8105–8116.
- [226] Q. Xie, C. Ni, R. Zhang, L. Li, J. Rong, J. Hu, *Angew. Chemie Int. Ed.* **2017**, *56*, 3206–3210.
- [227] W. Feng, Z. Mao, L. Liu, Z. Liu, *Talanta* **2017**, *167*, 134-142.
- [228] R. Wombacher, A. Jäschke, *J. Am. Chem. Soc.* **2008**, *130*(27), 8594–8595.
- [229] S. Cunha, M. B. Costa, H. B. Napolitano, C. Lariucci, I. Vencato, *Tetrahedron* **2001**, *57*, 1671-1675.
- [230] S. Takaoka, N. Takaoka, Y. Minoshima, J. M. Huang, M. Kubo, K. Harada, H. Hioki, Y. Fukuyama, *Tetrahedron* **2009**, *65*(40), 8354–8361.
- [231] P. H. J. Kouwer, C. J. Welch, G. McRobbie, B. J. Dodds, L. Priest, G. H. Mehl, *J. Mater. Chem.* **2004**, *14*(12), 1798–1803.
- [232] E. Orłowska, A. Roller, H. Wiesinger, M. Pignitter, F. Jirsa, R. Krachler, W. Kandioller, B. K. Keppler, *RSC Adv.* **2016**, *6*(46), 40238–40249.
- [233] B. E. Gryder, M. J. Akbashev, M. K. Rood, E. D. Raftery, W. M. Meyers, P. Dillard, S. Khan, A. K. Oyelere, *ACS Chem. Biol.* **2013**, *8*(11), 2550–2560.
- [234] R. Srinivasan, L. P. Tan, H. Wu, P.-Y. Yang, K. A. Kalesh, S. Q. Yao, *Org. Biomol. Chem.* **2009**, *7*(9), 1821–1828.
- [235] M. M. Bradford, *Anal. Biochem.* **1976**, *72*, 248–254.
- [236] B. L. Barthel, D. L. Rudnicki, T. P. Kirby, S. M. Colvin, D. J. Burkhart, T. H. Koch, *J. Med. Chem.* **2012**, *55*, 6595–6607.
- [237] P. T. Anastas, M. M. Kirchhoff, *Acc. Chem. Res.* **2002**, *35*(9), 686–694.

- [238] P. T. Anastas, J. C. Warner, “Green Chemistry: Theory and Practice”, Green Chem. Theory Pract. Oxford University Press, **1998**.
- [239] P. T. Anastas, T. C. Williamson, “Green Chemistry: Frontiers in Chemical Synthesis and Processes”, Oxford University Press, **1998**.
- [240] P. T. Anastas, L. G. Heine, T. C. Williamson, “Green Chemical Synthesis and Processes”, Vol. 767, ACS Symposium Series, **2000**.
- [241] P. T. Anastas, N. Eghbali, *Chem. Soc. Rev.* **2010**, 39, 301–312.
- [242] H. C. Erythropel, et al., *Green Chem.* **2018**, 20, 1929–1961.
- [243] J. Andraos, *Org. Process Res. Dev.* **2005**, 9, 149–163.
- [244] R. A. Sheldon, *Chem. Ind.* **1992**, 903–906.
- [245] R. A. Sheldon, *ACS Sustain. Chem. Eng.* **2018**, 6, 32–48.
- [246] C. Jimenez-Gonzalez, C. S. Ponder, Q. B. Broxterman, J. B. Manley, *Org. Process Res. Dev.* **2011**, 15, 912–917.
- [247] R. A. Sheldon, *Curr. Opin. Green Sustain. Chem.* **2019**, 18, 13–19.
- [248] K. Alfonsi, J. Colberg, P. J. Dunn, T. Fevig, S. Jennings, T. A. Johnson, H. P. Kleine, C. Knight, M. A. Nagy, D. A. Perry, M. Stefaniak, *Green Chem.* **2008**, 10, 31–36.
- [249] D. Prat, J. Hayler, A. Wells, *Green Chem.* **2014**, 16, 4546–4551.
- [250] D. Prat, A. Wells, J. Hayler, H. Sneddon, C. R. McElroy, S. Abou-Shehada, P. J. Dunn, *Green Chem.* **2016**, 18, 288–296.
- [251] R. A. Sheldon, *Green Chem.* **2017**, 19, 18–43.
- [252] R. A. Sheldon, *Green Chem.* **2016**, 18, 3180–3183.
- [253] V. Polshettiwar, R. S. Varma, *Green Chem.* **2010**, 12, 743–754.
- [254] U. T. Bornscheuer, G. W. Huisman, R. J. Kazlauskas, S. Lutz, J. C. Moore, K. Robins, *Nature* **2012**, 485, 185–194.
- [255] A. Illanes, A. Cauerhff, L. Wilson, G. R. Castro, *Bioresour. Technol.* **2012**, 115, 48–57.
- [256] N. Ran, L. Zhao, Z. Chen, J. Tao, *Green Chem.* **2008**, 10, 361–372.
- [257] J. L. Tucker, *Org. Process Res. Dev.* **2006**, 10(2), 315–319.
- [258] A. Behr, M. Urschey, V. A. Brehme, *Green Chem.* **2003**, 5, 198–204.
- [259] G. Papadogianakis, R. A. Sheldon, *Catal. Today* **2015**, 247, 1–190.
- [260] B. H. Lipshutz, F. Gallou, S. Handa, *ACS Sustain. Chem. Eng.* **2016**, 4, 5838–5849.
- [261] B. H. Lipshutz, *Curr. Opin. Green Sustain. Chem.* **2018**, 11, 1–8.
- [262] B. H. Lipshutz, *J. Org. Chem.* **2017**, 82, 2806–2816.
- [263] N. A. Isley, Y. Wang, F. Gallou, S. Handa, D. H. Aue, B. H. Lipshutz, *ACS Catal.* **2017**, 7, 8331–8337.

- [264] B. H. Lipshutz, S. Ghorai, *Green Chem.* **2014**, *16*, 3660–3679.
- [265] F. Gallou, *Green Chem.* **2016**, *18*, 14–19.
- [266] B. H. Lipshutz, S. Ghorai, A. R. Abela, R. Moser, T. Nishikata, C. Duplais, A. Krasovskiy, *J. Org. Chem.* **2011**, *76*, 4379–4391.
- [267] B. H. Lipshutz, S. Ghorai, *Aldrichimica Acta* **2012**, *45*, 3–16.
- [268] B. H. Lipshutz, S. Ghorai, *Acta* **2008**, *41*, 59–72.
- [269] B. H. Lipshutz, B. R. Taft, *Org. Lett.* **2008**, *10*, 1329–1332.
- [270] B. H. Lipshutz, S. Ghorai, G. T. Aguinaldo, *Adv. Synth. Catal.* **2008**, *350*, 953–956.
- [271] G. La Sorella, G. Strukul, A. Scarso, *Green Chem.* **2015**, *17*, 644–683.
- [272] N. A. Isley, F. Gallou, B. H. Lipshutz, *J. Am. Chem. Soc.* **2013**, *135*, 17707–17710.
- [273] S. Handa, E. D. Slack, B. H. Lipshutz, *Angew. Chem. Int. Ed.* **2015**, *54*, 11994–11998.
- [274] P. Guo, H. Zhang, J. Zhou, F. Gallou, M. Parmentier, H. Wang, *J. Org. Chem.* **2018**, *83*, 7523–7527.
- [275] P. Wagner, M. Bollenbach, C. Doebelin, F. Bihel, J. J. Bourguignon, C. Salomé, M. Schmitt, *Green Chem.* **2014**, *16*, 4170–4178.
- [276] C. Salomé, P. Wagner, M. Bollenbach, F. Bihel, J. J. Bourguignon, M. Schmitt, *Tetrahedron* **2014**, *70*, 3413–3421.
- [277] C. E. Brocklehurst, F. Gallou, J. C. D. Hartweg, M. Palmieri, D. Ruffe, *Org. Process Res. Dev.* **2018**, *22*, 1453–1457.
- [278] B. H. Lipshutz, Z. Bošković, C. S. Crowe, V. K. Davis, H. C. Whittemore, D. A. Vosburg, A. G. Wenzel, *J. Chem. Educ.* **2013**, *90*, 1514–1517.
- [279] M. Parmentier, M. K. Wagner, K. Magra, F. Gallou, *Org. Process Res. Dev.* **2016**, *20*, 1104–1107.
- [280] C. M. Gabriel, M. Parmentier, C. Riegert, M. Lanz, S. Handa, B. H. Lipshutz, F. Gallou, *Org. Process Res. Dev.* **2017**, *21*, 247–252.
- [281] Y. Zhang, C. S. Lim, D. S. Boon Sim, H. J. Pan, Y. Zhao, *Angew. Chem. Int. Ed.* **2014**, *53*, 1399–1403.
- [282] M. Bollenbach, P. G. V. Aquino, J. X. De Araújo-Júnior, J. J. Bourguignon, F. Bihel, C. Salomé, P. Wagner, M. Schmitt, *J. Eur. Chem.* **2017**, *23*, 13676–13683.
- [283] Q. Feng, D. Chen, M. Hong, F. Wang, S. J. Huang, *Org. Chem.* **2018**, *83*, 7553–7558.
- [284] S. M. Kelly, B. H. Lipshutz, *Org. Lett.* **2014**, *16*, 98–101.
- [285] N. R. Lee, A. A. Bikovtseva, M. Cortes-Clerget, F. Gallou, B. H. Lipshutz, *Org. Lett.* **2017**, *19*, 6518–6521.
- [286] N. R. Lee, F. Gallou, B. H. Lipshutz, *Org. Process Res. Dev.* **2017**, *21*, 218–221.

- [287] O. Roelen, *Angew. Chem.* **1948**, *60*, 213.
- [288] M. Taddei, A. Mann, "Hydroformylation for Organic Synthesis", Springer-Verlag, **2013**.
- [289] R. Franke, D. Selent, A. Börner, *Chem. Rev.* **2012**, *112*, 5675-5732.
- [290] P. J. Dunn, *Chem. Soc. Rev.* **2012**, *41*, 1452.
- [291] C. G. Vieira, E. N. Dos Santos, E. V. Gusevskaya, *Appl. Catal. A-Gen.* **2013**, *446*, 208-215.
- [292] U. Ritte, N. Winkhofer, H. G. Schmidt, H. W. Roesky, *Angew. Chem. Int. Ed. Engl.* **1996**, *35*, 524-526.
- [293] D. M. Hood, R. A. Johnson, A. E. Carpenter, J. M. Younker, D. J. Vinyard, G. G. Stanley, *Science* **2020**, *367*, 542-548.
- [294] R. A. Sanchez-Delgado, J. S. Bradley, G. Wilkinson, *J. Chem. Soc., Dalton Trans.* **1976**, 399-404.
- [295] I. Schwager, J. F. Knifton, *J. Catal.* **1976**, *45*, 256-267.
- [296] S. Pandey, K. V. Raj, D. R. Shinde, K. Vanka, V. Kashyap, S. Kurungot, C. P. Vinod, S. H. Chikkali, *J. Am. Chem. Soc.* **2018**, *140*, 4430-4439.
- [297] J. A. Osborn, G. Wilkinson, J. F. Young, *Chem. Comm.* **1965**, *2*, 17.
- [298] I. Ojima, C. Y. Tsai, M. Tzamarioudaki, D. Bonafoux, *Org. Reac.* **2000**, *56*, 1-354.
- [299] M. Beller, B. Cornils, C. D. Frohning, C. W. Kohlpaintner, *J. Mol. Catal. A: Chem.* **1995**, *104*, 17-85.
- [300] B. Breit, W. Seiche, *Synthesis* **2001**, 1-36.
- [301] D. Evans, J. A. Osborn, G. Wilkinson, *J. Chem. Soc. A* **1968**, 3134-3146.
- [302] Y. Wu, Y. Shi, J. You, *Angew. Chem. Int. Ed. Engl.* **2019**, *58*, 1-6.
- [303] G. Wilkinson, US3501531, **1970**.
- [304] D. S. Breslow, R. F. Heck, *Chem. Ind.* **1960**, *17*, 467-467.
- [305] F. Piacenti, P. Pino, R. Lazzaroni, M. Bianchi, *J. Chem. Soc. C* **1966**, 488-492.
- [306] C. R. Landis, J. Uddin, *J. Chem. Soc., Dalton Trans.* **2002**, 729-742.
- [307] W. Seiche, A. Schuschkowski, B. Breit, *Adv. Synth. Catal.* **2005**, *347*, 1488-1494.
- [308] E. Petricci, A. Mann, A. Schoenfelder, A. Rota, M. Taddei, *Org. Lett.* **2006**, *8*, 3725-3727.
- [309] E. Petricci, E. Cini, M. Taddei, *Eur. J. Org. Chem.* **2020**, 4435-4446.
- [310] E. G. Kuntz, FR Pat. 2.349.562.1976, **1976**.
- [311] B. Cornils, J. Hibbel, W. Konkol, B. Lieder, J. Much, V. Schmidt, E. Wiebus (Ruhrchemie AG, Oberhausen), DE3234701, **1982**.
- [312] M. J. Hayling, B. A. Murrer, GB2085874A, **1982**.

- [313] M. Schwarze, T. Pogrzeba, K. Seifert, T. Hamerla, R. Schomäcker, *Catal. Today* **2015**, *247*, 55-63.
- [314] M. Illner, D. Müller, E. Esche, T. Pogrzeba, M. Schmidt, R. Schomaäcker, G. Wozny, J.-U. Repke, *Ind. Eng. Chem. Res.* **2016**, *55*, 8616-8626.
- [315] T. Pogrzeba, M. Schmidt, L. Hohl, A. Weber, G. Buchner, J. Schulz, M. Schwarze, M. Kraume, R. Schomaäcker, *Ind. Eng. Chem. Res.* **2016**, *55*(50), 12765-12775.
- [316] T. Pogrzeba, D. Müller, T. Hamerla, E. Esche, N. Paul, G. Wozny, R. Schomäcker, *Ind. Eng. Chem. Res.* **2015**, *54*(48), 11953-11960.
- [317] T. Pogrzeba, M. Schmidt, N. Milojevic, C. Urban, M. Illner, J.-U. Repke, R. Schomäcker, *Ind. Eng. Chem. Res.* **2017**, *56*, 9934-9941.
- [318] B. Bibouche, D. Peral, D. Stehl, V. Söderholm, R. Schomäcker, R. von Klitzing, D. Vogt, *RSC Adv.* **2018**, *8*, 23332-23338.
- [319] A. T. Straub, M. Otto, I. Usui, B. Breit, *Adv. Synth. Catal.* **2013**, *355*, 2071-2075.
- [320] L. Obrecht, P. C. J. Kamer, W. Laan, *Catal. Sci. Technol.* **2013**, *3*, 541-551.
- [321] L. Vaccaro, "Sustainable Flow Chemistry: Methods and Applications", Wiley-VCH, **2017**.
- [322] C. Gabriel, S. Gabriel, E. H. Grant, B. S. J. Halstead, D. M. P. Mingos, *Chem. Soc. Rev.* **1998**, *27*(3), 213-223.
- [323] D. M. P. Mingos, D. R. Baghurst, *Chem. Soc. Rev.* **1991**, *20*, 1-47.
- [324] C. O. Kappe, A. Stadler, "Microwaves in Organic and Medicinal Chemistry", Wiley-VCH Verlag GmbH & Co. KGaA, **2005**.
- [325] C. O. Kappe, *Angew. Chem. Int. Ed.* **2004**, *43*, 6250-6284.
- [326] C. O. Kappe, D. Dallinger, S. S. Murphree, "Practical Microwave Synthesis for Organic Chemists", Wiley-VCH Verlag GmbH & Co. KGaA, **2009**.
- [327] B. L. Hayes, "Microwave Synthesis: Chemistry at the Speed of Light", CEM Publishing, **2002**.
- [328] B. H. Lipshutz, *Johnson Matthey Technol. Rev.* **2017**, *61*, 196-202.
- [329] M. P. Andersson, F. Gallou, P. Klumphu, B. S. Takale, B. H. Lipshutz, *Chem. Eur. J.* **2018**, *24*, 6778-6786.
- [330] D. J. Lippincott, et al., *Org. Process Res. Dev.* **2020**, *24*, 841-849.
- [331] T. Hamerla, A. Rost, Y. Kasaka, R. Schomäcker, *ChemCatChem* **2013**, *5*, 1854-1862.
- [332] G. Papeo, M. Pulici, *Molecules* **2013**, *18*, 10870-10900.
- [333] S. Sharma, J. Das, W. M Braje, A. K. Dash, S. Handa, *ChemSusChem* **2020**, *13*, 2859-2875.

- [334] P. P. Bora, M. B. Bihani, S. Plummer, F. Gallou, S. Handa, *ChemSusChem* **2019**, *12*, 3037-3042.
- [335] K. W. Anderson, S. L. Buchwald, *Angew. Chem. Int. Ed. Engl.* **2005**, *44*, 6173-6177.
- [336] M. Mondal, U. Bora, *Green Chem.* **2012**, *14*, 1873-1876.
- [337] F. Migliorini, F. Dei, M. Calamante, S. Maramai, E. Petricci, *ChemCatChem* **2021**, *13*, 2794-2806.